

APPLICATIONS OF ALUMINOSILICATE AND ZINCOSILICATE MATERIALS:
AQUEOUS PHASE ION EXCHANGE AND GAS PHASE ADSORPTION

by

TYLER J. SELBE

B.S., Kansas State University, 2005

AN ABSTRACT OF A DISSERTATION

submitted in partial fulfillment of the requirements for the degree

DOCTOR OF PHILOSOPHY

Department of Chemical Engineering
College of Engineering

KANSAS STATE UNIVERSITY
Manhattan, Kansas

2010

Abstract

Zeolites and zeolite-like materials have well-ordered structures and pores creating varying capacities for molecules based upon size, functional groups, polarity, and intermolecular forces making the materials useful for molecular sensing as well for molecules that are considered hazardous at very low concentrations with reproducible results because of these properties. This study will identify and characterize applications for zeolite and zeolite-like materials in gas and liquid phases based upon the dominating physical and chemical properties of the materials. The properties of interest include liquid phase ion exchange capacities, selectivities, gas/vapor phase adsorption capacity, and initial adsorption uptake rate.

Zincosilicates have similar framework structures to aluminosilicate zeolites; however, they have distinct advantages over traditional zeolites. Zincosilicates typically have a higher ion density, lack “cages” in their structure which leads to all the cations being accessible for ion exchange, and have the ability to form three-membered rings which lead to large void spaces in their structure. These features lead to high capture capacities for divalent heavy metal mercury ions. In this work, the potential to use zincosilicates as ion exchangers such as VPI-7, VPI-9 and VPI-10 is presented. Results have shown that zincosilicates have capture capacities greater than traditional zeolites, even greater than those that have been synthesized with functional groups intended to increase metal sorption capacities. The selectivity coefficients in a binary ion exchange system were successfully modeled using the Gibbs-Donnan selectivity model. The selectivities for the zincosilicates were $Pb > Na > Hg > K > Ca$.

Zeolites are also able to adsorb chemical species and therefore can be used as the recognition element in sensing devices. The sorption capacity of 2-chloroethyl ethyl sulfide, dimethyl methanephosphonate, ethanol, and n-butanethiol were examined with zeolites 13X, 4A, MCM-41, VPI-7, VPI-9, and ZSM-5. The zeolites selected provided very different framework composition, counteraction, and surface area features for determining the most significant properties in adsorption. Zeolite 13X had the highest equilibrium and initial uptake rate for most compounds tested, whereas the low surface area zincosilicates, VPI-7 and VPI-9, had the lowest capacity. Based on these results, a piezoelectric device with an array of zeolites can be successfully employed as a sensor.

APPLICATIONS OF ALUMINOSILICATE AND ZINCOSILICATE MATERIALS:
AQUEOUS PHASE ION EXCHANGE AND GAS PHASE ADSORPTION

by

TYLER J. SELBE

B.S., Kansas State University, 2005

A DISSERTATION

submitted in partial fulfillment of the requirements for the degree

DOCTOR OF PHILOSOPHY

Department of Chemical Engineering
College of Engineering

KANSAS STATE UNIVERSITY
Manhattan, Kansas

2010

Approved by:

Major Professor
Dr. Jennifer L. Anthony

Abstract

Zeolites and zeolite-like materials have well-ordered structures and pores creating varying capacities for molecules based upon size, functional groups, polarity, and intermolecular forces making the materials useful for molecular sensing as well for molecules that are considered hazardous at very low concentrations with reproducible results because of these properties. This study will identify and characterize applications for zeolite and zeolite-like materials in gas and liquid phases based upon the dominating physical and chemical properties of the materials. The properties of interest include liquid phase ion exchange capacities, selectivities, gas/vapor phase adsorption capacity, and initial adsorption uptake rate.

Zincosilicates have similar framework structures to aluminosilicate zeolites; however, they have distinct advantages over traditional zeolites. Zincosilicates typically have a higher ion density, lack “cages” in their structure which leads to all the cations being accessible for ion exchange, and have the ability to form three-membered rings which lead to large void spaces in their structure. These features lead to high capture capacities for divalent heavy metal mercury ions. In this work, the potential to use zincosilicates as ion exchangers such as VPI-7, VPI-9 and VPI-10 is presented. Results have shown that zincosilicates have capture capacities greater than traditional zeolites, even greater than those that have been synthesized with functional groups intended to increase metal sorption capacities. The selectivity coefficients in a binary ion exchange system were successfully modeled using the Gibbs-Donnan selectivity model. The selectivities for the zincosilicates were $Pb > Na > Hg > K > Ca$.

Zeolites are also able to adsorb chemical species and therefore can be used as the recognition element in sensing devices. The sorption capacity of 2-chloroethyl ethyl sulfide, dimethyl methanephosphonate, ethanol, and n-butanethiol were examined with zeolites 13X, 4A, MCM-41, VPI-7, VPI-9, and ZSM-5. The zeolites selected provided very different framework composition, counteraction, and surface area features for determining the most significant properties in adsorption. Zeolite 13X had the highest equilibrium and initial uptake rate for most compounds tested, whereas the low surface area zincosilicates, VPI-7 and VPI-9, had the lowest capacity. Based on these results, a piezoelectric device with an array of zeolites can be successfully employed as a sensor.

Table of Contents

List of Figures	ix
List of Tables	xiii
Acknowledgements	xv
CHAPTER 1 - Introduction and Background	1
Introduction	1
Zeolites	1
Zincosilicates: Potential for Heavy Metal Capture	2
Zeolites in Sensing Devices: Molecular Identification Through Adsorption	4
Functionalization	5
Other Sorbents and Heavy Metal Ion Exchanging Materials	5
Carbon-based sorbents	5
Natural Zeolites and Minerals	6
Silica-based sorbents	7
Metal Oxides	7
Cationic Ion Exchange	8
Cationic Dissolved Species	10
Solubilities	10
Valencies	11
Hydrolysis	11
Complexes	12
Molecular Interactions and Anions	12
Adsorption	12
Chemical Warfare Agents and Simulants	13
Ethanol	13
2-Chloroethyl Ethyl Sulfide	13
Dimethyl methanephosphonate	14
n-Butanethiol	14
Detection Methods	14

M-256 Detection Kit	15
Detection paper	15
Gas detection tube.....	16
Flame photometric detector	16
Ion mobility spectrometer	17
Surface acoustic wavelength detector	18
Gas chromatograph–mass spectrometer	19
Objective of Dissertation	20
Outline of Chapters	20
CHAPTER 2 - Materials, Methodology, and Equipment	22
Materials	22
Zincosilicates and Zeolites.....	22
VPI-9 Synthesis	23
VPI-10 Synthesis	24
Zeolite 13X	25
Zeolite 4A	25
MCM-41	26
Zeolite Properties	26
Cationic Species	27
Chemical Warfare and Explosive Agent Simulants.....	28
Methods for Measuring Exchange Capacity.....	29
Atomic Absorption Spectroscopy	29
Atomic Absorption Experimental Setup.....	31
Energy Dispersion Spectroscopy	34
Energy Dispersion Spectrometer Experimental Setup.....	36
X-Ray Diffraction	37
X-Ray Diffractometer	39
Other Techniques	40
Cationic Exchange Mass Balances	40
Exchange Energies.....	41
Methods for Measuring Adsorption.....	41

BET Surface Area Analyzer	42
BET Surface Area Apparatus.....	42
Gravimetric Microbalance	44
Gravimetric Microbalance Apparatus.....	46
Equilibrium Measurements.....	47
Initial Uptake Rate Measurements.....	49
Quartz Crystal Microbalance	49
Quartz Crystal Microbalance Apparatus.....	51
Experimental Setup.....	53
Thermogravimetric Analyzer.....	54
Other Techniques	55
CHAPTER 3 - Results – Aqueous Phase Ion Exchange.....	56
Capture Capacities of Metals Using Zincosilicates	56
Experimental Procedure.....	56
Single Dissolved Species Cationic Exchange Results	57
Mercury and VPI-7	57
Mercury and VPI-9	58
Mercury and VPI-10	58
Comparison of Zincosilicates	58
As-made Countercation Influence on Capture Capacity	63
Comparison to Mercury Capture by Other Sorbents	68
Comparison to Capture of Lead by the Zincosilicates.....	68
Mercury vs. Lead	69
Structure.....	69
Regeneration.....	69
Selectivities Between Cationic Species	70
Cationic Selectivity.....	70
Gibbs-Donnan Selectivity Model	70
Selectivity Results.....	72
Mercury-Zincosilicate Exchange Energies.....	75
CHAPTER 4 - Results – Gas Phase Adsorption.....	78

Adsorption of Chemical Warfare and Explosive Simulants	78
Gravimetric Microbalance Results	78
Equilibrium Capacities.....	78
Initial Uptake Rates.....	79
Quartz Crystal Microbalance Results	80
Equilibrium Capacities.....	80
Initial Uptake Rates.....	81
Ethanol Capacity.....	82
DMMP capacity	84
2-CEES capacity.....	86
n-Butanethiol capacity	88
Discussion.....	90
Initial Uptake Rates.....	91
Ethanol initial uptake rate	91
DMMP initial uptake rate	93
2-CEES initial uptake rate	95
n-Butanethiol initial uptake rate	97
Discussion.....	99
Influence of Sorbent and Sorbate Structure	100
Influence of Humidity/Water on Measurements	101
Water Uptake onto Zeolites	101
Molecular Sensing/Identification.....	102
Zeolite Array with Gas Mixture.....	103
CHAPTER 5 - Conclusions and Recommendations.....	106
Capture of Mercury Summary and Conclusions.....	106
Detection of Warfare Agents Summary and Conclusions	107
Recommendations.....	108
References.....	110
Appendix A - Ion Exchange Data.....	120
Appendix B - Adsorption Data	134

List of Figures

Figure 1 Schematic of VPI-7 along (010) showing only tetrahedral atoms	2
Figure 2 (a) Calculated XRD pattern of VPI-7. ¹⁴⁹ (b) XRD pattern for synthesized VPI-7.....	23
Figure 3 (a) Calculated XRD pattern of VPI-9. ¹⁴⁹ (b) XRD pattern for synthesized VPI-9.....	24
Figure 4 (a) Calculated XRD pattern of VPI-10. ¹⁵⁰ (b) XRD pattern for synthesized VPI-10.....	24
Figure 5 Calculated XRD pattern of zeolite 13X. ¹⁴⁹	25
Figure 6 Calculated XRD pattern of zeolite 4A. ¹⁴⁹	26
Figure 7 Varian Model AA240 apparatus with PSD 120 attached	32
Figure 8 Varian VGA-77 cold vapor accessory.....	33
Figure 9 Atomic level interactions required for EDS: a high energy electron from the source ejects a high energy electron from the sample atom, then being replaced by other electrons in the sample atom resulting in an emitted x-ray. Adapted from Goldstein. ¹⁶³	34
Figure 10 SEM-EDS apparatus.....	36
Figure 11 X-ray diffraction technique measures the path length difference between two incident x-rays. The angle of incidence allows for determining the distance between two adjacent atoms.	38
Figure 12 Setup used for XRD analysis.....	39
Figure 13 Bruker AXS D8 Advance apparatus.....	40
Figure 14 AUTOSORB-1 BET surface area analyzer	43
Figure 15 Schematic of buoyancy correction in gravimetric microbalance. Relevant forces and directions of the sample and counterweight side are shown. Adapted from Anthony. ¹⁶⁸	44
Figure 16 Hiden ISO-200 gravimetric microbalance setup	46
Figure 17 Schematic of gravimetric microbalance. Adapted from Anthony. ¹⁶⁸	47
Figure 18 Inficon, Inc. quartz crystal electrode configuration.....	52
Figure 19 Setup used for QCM measurements.....	53
Figure 20 RQCM-200 apparatus.....	54
Figure 21 (a) Percentage of divalent mercury captured using zincosilicate VPI-7. (b) Mercury to zinc ratio as function of initial concentration of mercury for VPI-7. The vertical line at 5025 ppm represents the concentration of mercury in solution that is equal to the number of zinc sites.....	59

Figure 22 Ion Exchange Isotherm of Mercury onto VPI-7.....	60
Figure 23 (a) Percentage of divalent mercury captured using zincosilicate VPI-9. (b) Mercury to Zinc ratio as function of initial concentration of mercury for VPI-9. The vertical line at 3730 ppm represents the concentration of mercury in solution that is equal to the number of zinc sites.....	60
Figure 24 Ion Exchange Isotherm of Mercury onto VPI-9.....	61
Figure 25 Percentage of divalent mercury captured using VPI-10.....	62
Figure 26 Average percentage mercury captured as function of initial concentration with each zincosilicate.....	63
Figure 27 VPI-7 structure viewed along [001] ¹⁷⁵	64
Figure 28 VPI-9 structure viewed along [110] ¹⁷⁵	65
Figure 29 Mercury to zinc capture quantities for zincosilicates at initial concentrations above and below the maximum theoretical capture capacity.....	66
Figure 30 Heavy metal capture quantities with the presence of sodium at an initial mercury concentration of 200 ppm.	67
Figure 31 Linearized plot to determine exchange energy in VPI-7.....	76
Figure 32 Linearized plot to determine the exchange energy of VPI-9.....	76
Figure 33 Method for determining initial uptake rate using gravimetric microbalance.....	80
Figure 34 Method for determining the initial uptake rate using the QCM.....	82
Figure 35 Equilibrium adsorption capacity of ethanol onto zeolites with respect to zeolite mass.....	83
Figure 36 Equilibrium adsorption capacity of ethanol onto zeolites with respect to zeolite surface area.....	84
Figure 37 Equilibrium adsorption capacity of DMMP onto zeolites with respect to zeolite mass.....	85
Figure 38 Equilibrium adsorption capacity of DMMP onto zeolites with respect to zeolite surface area.....	86
Figure 39 Equilibrium adsorption capacity of 2-CEES onto zeolites with respect to zeolite mass.....	87
Figure 40 Equilibrium adsorption capacity of 2-CEES onto zeolites with respect to zeolite surface area.....	88

Figure 41 Equilibrium adsorption capacity of n-Butanethiol onto zeolites with respect to zeolite mass.....	89
Figure 42 Equilibrium adsorption capacity of n-Butanethiol onto zeolites with respect to zeolite surface area	90
Figure 43 Initial uptake rate of ethanol onto zeolites with respect to zeolite mass	92
Figure 44 Initial uptake rate of ethanol onto zeolites with respect to zeolite surface area	93
Figure 45 Initial uptake rate of DMMP onto zeolites with respect to zeolite mass.....	94
Figure 46 Initial uptake rate of DMMP onto zeolites with respect to zeolite surface area.....	95
Figure 47 Initial uptake rate of 2-CEES onto zeolites with respect to zeolite mass	96
Figure 48 Initial uptake rate of 2-CEES onto zeolites with respect to zeolite surface area.....	97
Figure 49 Initial uptake rate of n-Butanethiol onto zeolites with respect to zeolite mass	98
Figure 50 Initial uptake rate of n-Butanethiol onto zeolites with respect to zeolite surface area.	99
Figure 51 Influence of water on the initial uptake rate of ethanol onto zeolites	102
Figure 52 Change in uptake rate with vapor mixture	104
Figure 53 VPI-7 Mercury Ion Exchange Percent Removal as Function of Time.....	123
Figure 54 VPI-7 Ion Exchange Mercury:Zinc as Function of Time.....	124
Figure 55 VPI-9 Mercury Ion Exchange Percent Removal as Function of Time.....	128
Figure 56 VPI-9 Ion Exchange Mercury:Zinc as Function of Time.....	129
Figure 57 VPI-10 Mercury Ion Exchange Percent Removal as Function of Time.....	130
Figure 58 Kinetic Data for Ethanol Uptake onto Zeolite 4A.....	138
Figure 59 Kinetic Data for Ethanol Uptake onto ZSM-5	138
Figure 60 Kinetic Data for Ethanol Uptake onto Zeolite 13X.....	139
Figure 61 Kinetic Data for Ethanol Uptake onto Zeolite VPI-7.....	139
Figure 62 Kinetic Data for Ethanol Uptake onto Zeolite VPI-9.....	140
Figure 63 Kinetic Data for Ethanol Uptake onto MCM-41	140
Figure 64 Kinetic Data for DMMP Uptake onto Zeolite 4A	141
Figure 65 Kinetic Data for DMMP Uptake onto Zeolite 13X.....	141
Figure 66 Kinetic Data for DMMP Uptake onto Zeolite ZSM-5	142
Figure 67 Kinetic Data for DMMP Uptake onto MCM-41	142
Figure 68 Kinetic Data for 2-CEES Uptake onto ZSM-5.....	143
Figure 69 Kinetic Data for 2-CEES Uptake onto MCM-41	143

Figure 70 Kinetic Data for n-butanethiol Uptake onto Zeolite 4A.....	144
Figure 71 Kinetic Data for n-butanethiol Uptake onto Zeolite VPI-9	144
Figure 72 Kinetic Data for n-butanethiol Uptake onto MCM-41	145
Figure 73 Equilibrium adsorption isotherm of ethanol onto zeolite 4A	145
Figure 74 Equilibrium adsorption isotherm of ethanol onto zeolite 13X.....	146
Figure 75 Equilibrium adsorption isotherm of ethanol onto zeolite ZSM-5	146
Figure 76 Equilibrium adsorption isotherm of ethanol onto zeolite VPI-7	147
Figure 77 Equilibrium adsorption isotherm of ethanol onto zeolite VPI-9	147
Figure 78 Equilibrium adsorption isotherm of ethanol onto MCM-41.....	148
Figure 79 Equilibrium adsorption of DMMP onto zeolite 4A.....	148
Figure 80 Equilibrium adsorption of DMMP onto zeolite 13X.....	149
Figure 81 Equilibrium adsorption of DMMP onto zeolite ZSM-5	149
Figure 82 Equilibrium adsorption of DMMP onto zeolite MCM-41	150
Figure 83 Equilibrium adsorption of 2-CEES onto zeolite ZSM-5	150
Figure 84 Equilibrium adsorption of 2-CEES onto zeolite MCM-41.....	151
Figure 85 Equilibrium adsorption of n-butanethiol onto zeolite 4A.....	151
Figure 86 Equilibrium adsorption of n-butanethiol onto zeolite VPI-9.....	152
Figure 87 Equilibrium adsorption of n-butanethiol onto zeolite MCM-41	152

List of Tables

Table 1 Physical properties of selected zeolites	27
Table 2 Metal salts and their single component solubilities in water	28
Table 3 Target compounds used in adsorption	29
Table 4 Lamp and standard settings used for AAS.....	33
Table 5 Activity coefficients of selected ions at 0.025 M.	72
Table 6 Selectivity coefficients of cationic species with VPI-7	74
Table 7 Selectivity coefficients of cationic species with VPI-9	74
Table 8 List of simulants, simulant vapor pressure, and maximum experimental pressure used in order to avoid condensation of the simulant within the experimental chamber during adsorption.....	78
Table 9 VPI-7 Mercury Ion Exchange Data and Calculations Part I.....	120
Table 10 VPI-7 Mercury Ion Exchange Data and Calculations Part II	121
Table 11 VPI-7 Mercury Ion Exchange Data and Calculations Part III.....	122
Table 12 VPI-9 Mercury Ion Exchange Data and Calculations Part I.....	125
Table 13 VPI-9 Mercury Ion Exchange Data and Calculations Part II	126
Table 14 VPI-9 Mercury Ion Exchange Data and Calculations Part III.....	127
Table 15 VPI-10 Mercury Ion Exchange Data and Calculations Part I.....	129
Table 16 VPI-10 Mercury Ion Exchange Data and Calculations Part II	130
Table 17 Zincosilicate Temperature Exchange Experimental Results Part I	131
Table 18 Zincosilicate Temperature Exchange Experimental Results Part II	131
Table 19 Binary Selectivity Experimental Results Part I	131
Table 20 Binary Selectivity Experimental Results Part II	132
Table 21 Binary Selectivity Coefficient Calculations for VPI-7 Part I	132
Table 22 Binary Selectivity Coefficient Calculations for VPI-7 Part II.....	132
Table 23 Binary Selectivity Coefficient Calculations for VPI-9 Part I	133
Table 24 Binary Selectivity Coefficient Calculations for VPI-9 Part II.....	133
Table 25 Loading of Selected Zeolite-Sorbate Systems on Gravimetric Microbalance Calculations Part I.....	134

Table 26 Loading of Selected Zeolite-Sorbate Systems on Gravimetric Microbalance Calculations Part II	135
Table 27 Loading of Selected Zeolite-Sorbate Systems on QCM Calculations Part I.....	136
Table 28 Loading of Selected Zeolite-Sorbate Systems on QCM Calculations Part II.....	137

Acknowledgements

I would like to thank my primary advisor Dr. Jennifer Anthony. Her guidance and knowledge were most helpful in the completion of my graduate studies. Dr. Anthony's mentoring encouraged me to continue on and complete my Doctoral Degree instead of stopping at a Master's Degree. Dr. Keith Hohn was also very helpful with my project. He was very willing to give guidance on the project whenever needed. I feel grateful to have the opportunity to have learned from two such brilliant minds and mentors. I hope that I will carry at least some of their characteristics into my career in chemical engineering.

I would also like to thank Dr. Larry Glasgow. Whether we were discussing professional or personal matters, the time spent together was truly enjoyable. Your instruction, insight, and candor were of great benefit to my development and encouraged me to continue into graduate school.

I would like to thank all the graduate students I have met and worked with along the way. Whether it was teaching me how to use a piece of equipment, working on homework, or spending recreational time together, I have been extremely blessed to have had such a wonderful time during my graduate studies due to experiences with all these people. Ty McGown, Nathan Keiser, Kyle Taggart, and Tarl Vetter all made the first two years of graduate school fly by with all the fun we had together. Clinton Whiteley has been down the hall throughout my entire tenure as a K-State graduate student; it has been nice to have such a good friend so nearby. Paul Schoenecker made the latter stages of my education fun; he taught me how to have fun outside the laboratory setting in graduate school.

Finally, I would like to thank my family. It is truly a blessing to know you have the steadfast support of so many people that love you.

CHAPTER 1 - Introduction and Background

Introduction

Zeolite and zeolite-like materials have been known for over 200 years.¹ Zeolites have been identified; and, using specific experimental conditions, zeolites have been synthesized in a laboratory setting while others are found naturally occurring on earth. These materials are useful in both gas and liquid media for use as: catalysts, additives in adhesives, coatings, ion exchangers, and adsorbents.

While there are over 180,000 potential zeolite frameworks, at present there are currently only 176 known synthesized zeolites.² With the vast amount of potential growth and development of new materials in this microporous and nanoporous class, materials' physical properties and uses will be sought. In this work, focus will be given to understand and evaluate the gas phase adsorption and aqueous phase ion exchange characteristics of zeolites, specifically, VPI-7, VPI-9, VPI-10, 13X, 4A, ZSM-5, and MCM-41.

Zeolites

Zeolites, by definition, are aluminosilicate materials.³ This means that they are comprised primarily of aluminum tetrahedrally coordinated within a silica framework. The replacement of the silicon with aluminum results in a charge being associated to the framework. In order to achieve a neutrally charged material, the framework has countercations that are bound to the structure. This means that zeolites have countercations associated with their framework to maintain charge neutrality. The framework may contain any positively charged cation, but the most common cations are either alkali or alkaline metal cations.

Zeolites have repeating structures and this results in having uniform micropores (pores <10nm) and have uniform bulk properties.⁴ Zeolites are classified as molecular sieves. This term was introduced by McBain when he described materials that were capable of selective separations based upon size or shape constraints.⁵ Zeolites can be found naturally in a wide range of geographic locations or can be synthesized in a laboratory.⁴ Natural zeolites are typically formed when ash and volcanic rocks react with a basic water solution (pH>7).⁶ There are around

50 known naturally occurring zeolites that have been discovered. Both aluminosilicate and zincosilicate materials have been synthetically produced.

Zincosilicates: Potential for Heavy Metal Capture

The discovery of zincosilicates occurred when researchers were trying to develop other molecular sieves with framework densities lower than 12.5. Framework density is defined as the number of tetrahedral atoms per 1000 cubic Angstroms.² At that time, 12.5 was the minimum framework density prior to the development of any zincosilicate materials. The molecular sieve CoAPO-50, also known as AFY, was the only zeolite with a framework density this low.⁷ Interestingly, a framework density of 12.5 corresponds to a void space of about one half of the total volume of the structure. Brunner and Meier discovered that there is a correlation between the smallest ring size in a zeolite and its framework density.⁷ They proposed structures needed to contain three-membered rings (3MR) in order to create porosities greater than 50%.⁷ Figure 1 below depicts the 3MR which are part of the Spiro-5 unit in VPI-7.⁸

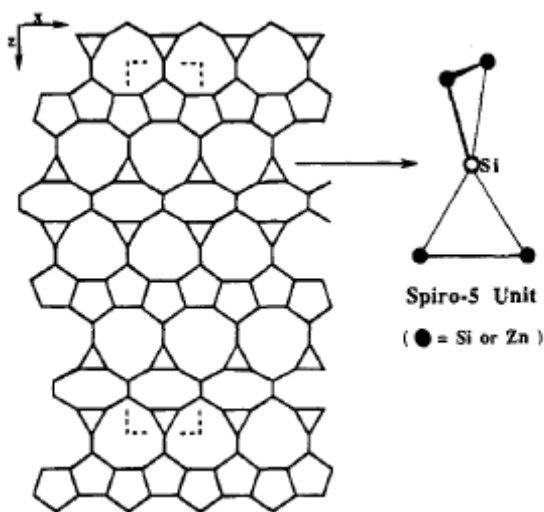


Figure 1 Schematic of VPI-7 along (010) showing only tetrahedral atoms

With the conclusion that zeolites with 3MRs were needed, beryllsilicates were found to promote formation of 3MRs. Beryllsilicates are beryllium-containing zeolites. Dense materials like euclase and phenakite and the mineral lovdarite contain 3MRs.⁷ However, beryllium-containing compounds are very toxic, making it difficult to work with their reagents and products.⁷ ZSM-18, an aluminosilicate, was shown to contain 3MRs; however, aluminosilicate bond angles generally do not prefer the narrow angles that are needed to form 3MRs.⁷ It was

then that zincosilicate analogues of euclase and phenakite, two materials that promoted 3MR formation, were successfully synthesized.⁷ Upon this discovery, zinc was found to be a suitable replacement for beryllium to create zeolites with 3MRs thus reducing the hazardous nature of synthesizing the materials but also resulting in lower framework densities.

Zincosilicate materials differ from the ‘true’ definition of a zeolite because of the replacement of the aluminum in the framework with zinc. This results in a tetrahedrally, covalently bound zinc instead of aluminum and also increases the negative charge on the framework. As previously stated, the aluminum results in a single negative charge associated with the framework for every aluminum. A zinc atom in the framework results in twice the charge of that of an aluminum atom. This leads to an increase in the charge density of the material if each aluminum were to be replaced. As is the case with aluminum in aluminosilicates, a certain maximum amount of zinc in the zincosilicate framework is achievable. The maximum amount of aluminum or zinc associated with the framework is governed by Loewenstein’s rule.⁹ Loewenstein’s rule states that the framework cannot consist of alternating zinc-oxygen-zinc bonds; whenever two tetrahedral atoms are linked by one oxygen bridge, the center of only one can be occupied by zinc, the other center must be occupied by silicon. The zinc atoms are bonded to oxygen atoms, which are then bonded to silicon atoms to produce the resulting framework. Zincosilicates also have no ‘cages’ associated with their structure. Cages are areas within the framework that contain countercations that cannot move through the framework and are not available for ion exchange or reaction with other species. In effect, these cations are bound to the framework reducing or inhibiting the cation exchange capacity. These properties of a higher charge density and lack of framework cages are expected to be beneficial in heavy metal ion exchange.

Mercury and lead are highly toxic heavy metals that are regularly introduced into water, soil, and air in the environment. Trace amounts of mercury and lead can produce adverse health effects and potentially result in death. The threat of mercury and lead contamination in water, soil, and air requires that new materials be developed that are capable of capturing or retaining mercury and lead from exposure to the environment.

Meeting current government regulations on heavy metals released into the environment require more advanced materials for meeting more stringent standards. The EPA currently requires that no more than 15 ppb and 2 ppb of lead and mercury, respectively, may be found in

drinking water under the Safe Drinking Water Act (SDWA). The EPA's upper exposure limits (UEL) in air for lead and mercury are 0.05 mg/m^3 and 0.1 mg/m^3 for lead and mercury, respectively.¹⁰

Lead and mercury are found in various forms. Lead can be found in a cationic (1^+ , 2^+) state, as agglomerates, or as metal complexes while mercury can be found in a cationic (2^+) state, in elemental form, as agglomerates, or as metal complexes. This aspect poses many challenges for any sorbent or capture agent used in environmental cleanup.

Due to the previously stated unique properties of zincosilicates, the potential uses for zincosilicates are great and has not been previously examined for the ion exchange of heavy metals specifically for environmental purposes. An investigation was conducted to quantify and qualitatively understand the process or processes involved to capture heavy metals using zeolite-like materials. Understanding the influences by which these materials capture and retain heavy metals can be very important for many environmental applications and could also indicate or show other uses for these materials. The structural stability and regeneration of these materials will be of importance in order to develop industrial and commercial uses.

Zeolites in Sensing Devices: Molecular Identification Through Adsorption

Zeolites have certain physical properties allowing for specific, quantitative reactions/sorptions to occur. Their hydrophobicity/hydrophilicity, surface area, composition, and counterions all play a critical role in the amount or rate of uptake of a particular species or mixture of species. This ability to tailor adsorption properties can be harnessed for use in identifying certain species or certain atoms or functional groups within molecules. This is known as molecular identification. Molecular identification can lead to advances in selective reactions, ion exchanges, and adsorptions, as well as separation with chemical enantiomers.

In this work a small array of zeolites was developed to indicate that zeolites are capable of molecular sensing. Due to slow diffusion within the pore, the overall adsorption capacity was not the primary focus, but rather the rate with which certain species interact with a monolayer of zeolites should allow for quick identification of molecules or functional groups. Diffusion into particles of varying size will change the rate of adsorption, but by requiring standard conditions with initial deposition layers, results can be reproduced and errors can be eliminated.

Larger arrays of zeolites and more adsorbate compounds and mixtures will further demonstrate the utility of zeolites as chemical sensors or molecular identifiers. With an almost limitless amount of zeolite frameworks, these materials should be able to selectively adsorb and thereby identify any molecule, functional group, or even chemical bonding arrangement.

Functionalization

Zeolite adsorption, catalysis, and ion exchange properties can be tailored to specific species and materials. This is generally defined as functionalization. Functionalized materials allow for selective reactions or processes to occur. This can be very advantageous for complex systems or systems where some processes may be undesirable to occur.

Sorbents such as activated carbons and silicas have been functionalized to remove specific species such as mercury through the introduction of a thiol or sulfur-containing group which is known to create a strong bond with mercuric species. While functionalization has clear benefits when implemented, there is one significant drawback. The cost of functionalization either through the development of a material with a functional group or the time and monetary cost of determining the best-suited species for selective reaction/sorption can make diminish the benefit of functionalization. The materials used in this study are not functionalized but will be compared to other functionalized sorbents reported in literature.

Other Sorbents and Heavy Metal Ion Exchanging Materials

Besides zeolites, other materials are used for adsorption, ion exchange, catalysis, and a variety of other needed chemical processes. The following section will describe some other major sorbents and ion exchanging materials and list their advantages and disadvantages. The primary focus of this section will be aimed at sorbents capable of heavy metal capture of lead and mercury.

Carbon-based sorbents

Carbon-based sorbents are the most prevalent and widely used category of sorbents. Materials in this group of sorbents include: biomass, cellulose, and activated carbons. This group of sorbents has the widest and broadest definition of any category of sorbent.

Extensive investigations of mercury adsorption on naturally occurring sorbent materials have been reported.¹¹⁻⁴⁶ Biomass and cellulose can be byproducts or waste materials from other

processes and research has been done to reduce waste and find alternative uses. This means that these types of carbon sorbents are widely available and cost effective, an advantageous feature. They typically have high chemical and mechanical stability and are biodegradable.¹¹ The high chemical and mechanical stability allows a wide range of operating conditions. The materials also allow desorption, meaning the materials can be used repeatedly.¹²

There are some drawbacks to using carbon-based sorbents though. Activated carbon can be costly to use and regenerate and can also degrade at higher temperatures. Biosorbents are typically less efficient at capturing heavy metals. Activated carbons and biosorbents are the two least efficient adsorbent materials reviewed; but, while this may be categorically accurate, each material's efficiency varies.^{13, 14}

Natural Zeolites and Minerals

Natural zeolites and minerals are another class of sorbents. These materials are not as widely researched as carbon-based sorbents, but they can be effective heavy metal sorbents with unique properties.^{13, 45, 47-69} Naturally-occurring zeolites, such as clinoptilolite and zeolite tuff, and minerals, such as dolomite, kaolinitic clays, and vermiculite are materials that fit within this category of sorbents. Clinoptilolite is the most naturally occurring zeolite; it has a broad geographic distribution.⁴⁷ Zeolite tuff has shown to have larger heavy metal uptake capacities than that of clinoptilolite.⁴⁷

Natural minerals can come from a variety of sources. Most comprise parts of subsurface soils while others are found from specific sources. Dolomite is a major component of shallow groundwater aquifers while vermiculite is commonly used with asbestos insulation.⁴⁸

The biggest advantage of this category of sorbents is that they have the highest efficiency in sorbing heavy metals compared to other categories of sorbents.^{13, 45, 47-69} Zeolites have a negative charge associated with their framework and this charge must be offset by counterions.⁴⁹ Natural zeolites have a higher resistance to acidic conditions than synthetic zeolites and can be used as pH buffers.^{50, 70} Natural zeolites are also compatible with biological species. The materials are naturally occurring, so no environmental steps are necessary in order to use them.⁵¹ These materials can be found in a host of geographic regions making them widely available.

A significant disadvantage of zeolites and minerals is the readiness for use. While the materials can be found in a wide geographic distribution, the mineral or zeolite must be extracted

or mined then isolated before they can be used as sorbents. This makes turning the zeolite or mineral into a sorbent a costly and time intensive process.

Silica-based sorbents

Another category of sorbents is silica-based sorbents. Like naturally-occurring zeolites, they are silica-based structures but need not be naturally occurring. Materials in this category include: quartz, silica gels, titanosilicates, and synthetic zeolites. Silica gels are the most different of all the previously listed materials in this category, because instead of capturing through ion exchange, they capture materials through adsorption.^{71, 72} Materials in this category have a number of ways to sorb other materials.

Silica-based sorbents are somewhat similar to naturally occurring zeolites, so it should not be surprising that there are some similar advantages when using these materials.^{13, 38, 45, 57, 71-92} One major advantage is that synthetic zeolites also offer a very high sorption efficiency of heavy metals compared to all other sorbents. This is similar to naturally occurring zeolites. Silica-based sorbents can also have a negative framework charge allowing the possibility of ion exchange with its counterions.⁷³ Titanosilicates also have frameworks like naturally occurring zeolites. These materials have well-defined structures and pores.⁷⁴ The well-defined structures and pores give rise to efficient ion exchange properties like other zeolites and minerals.⁷⁵ Many of the materials in this group have a tetrahedrally-bound silicon atom in their structure which leads to them having a weakly acidic silanol group. The silanol group can then be exchanged and affords easy uptake of metal cations.^{76, 77}

These materials have disadvantages also. They must be synthesized. Synthesis routes are often poorly understood, so making these materials can be an expensive and/or a time-consuming process. They also lack uniform pores and microstructures which can lead to discontinuity in material properties.

Metal Oxides

Metal oxide sorbents are one final category of heavy metal sorbents.^{13, 38, 80, 85, 93-102} These materials often come from industrial waste processes or byproducts and can be reused as sorbents. Fly ash contains metal oxides such as aluminum oxide, calcium oxide, and iron oxide and furnace slag and red mud are another kind of industrial byproducts. The materials in this category are similar to naturally-occurring minerals in that they are similar to constituents in soil.

For example, hydrating aluminum oxide leads to the formation of aluminum hydroxides, which is similar to bayerite, boehmite, and gibbsite.⁹³

A distinct advantage of using metal oxide sorbents is their availability. They come from industrial processes and are either waste or byproducts. This makes their use affordable in many cases. These materials also are able to remove heavy metals from aqueous solutions with a very high efficiency.¹³ They also have negatively charged surfaces. This allows for precipitation of materials under basic conditions or can lead to electrostatic adsorption.¹⁰³ Metal oxides also have functional hydroxyl groups. The hydroxyl groups are capable of reacting with metal cations, leading to capture.

With the advantages of metal oxide come some disadvantages with their use. Electrostatic adsorption can lead to a build up of charge on the surface thereby decreasing the heavy metal capturing efficiency. These materials can also increase the amount of waste generated with their usage. While they are typically materials that are being reused, the end result after heavy metal capture is the need for disposal of the materials. This leads to disposal of a waste material and heavy metal that often times must be treated before disposal.⁷⁰

Cationic Ion Exchange

Ion exchange is a process in which quantities of charged particles are replaced by an equal amount of another species of charged particles. The species can vary in their specific charges, but the aggregate charge remains the same for the overall exchange. Thompson and Way identified ion exchange occurring in soils and coined the term ‘base exchange’.¹⁰⁴⁻¹⁰⁶ Lemberg and Wiegner later identified the materials that were accomplishing the ion exchange in the soils.¹⁰⁷⁻¹⁰⁹ These materials were zeolites, clays, glauconites, and humic acids. The first industrial ion exchanger was introduced in 1903 by Harm and Rumpler.¹¹⁰⁻¹¹² Ion exchange resins were discovered in 1935 and now are prevalent in almost all industrial and laboratory ion exchange process.¹¹³ After 1950, the theory behind ion exchange began to catch up with the technology to accurately describe the mechanisms and model the specific conditions in ion exchange experiments.¹¹³

Ion exchangers are solid, insoluble materials that allow cations or anions to be exchanged. Ion exchange is the redistribution of ions until charge neutrality is achieved. The charged species will be exchanged for an equivalent amount of another charged species. The

exchange occurs when the solid phase is contacted with an electrolytic solution of the exchanging species. Ion exchange is, typically, a reversible process.

Ion exchange is and can be coupled with sorption processes as the two are hard to isolate and distinguish in experimental conditions. Ion exchange and sorption are fundamentally different processes however. Ion exchange is a stoichiometric process, sorption need not be. Ion exchange requires that for every ionic charge removed from solution, another ionic charge must replace it. Sorption processes have a solute species removed without replacement. Though the fundamental difference is quite apparent, separating the two processes can be rather challenging in practice.¹¹³

Ion exchangers' properties are usually determined by their structure. Most ion exchangers consist of a framework that is held together through covalent bonds or lattice energy. This framework has an inherent charge associated with it and is countered by ions of the opposite charge. If the material is a cationic exchanger, the material is referred to as a polyanion. If the material exchanges anions, the material is known as a polycation.¹¹³

Ion exchangers are thought of as structures with counter ions moving about their pores. The total amount of counter ions in the pores is known as the ion exchange capacity. This is a constant value and is determined only by the framework charge. When an ion exchanger is placed in an electrolyte solution, ions will diffuse from the framework into the solution, and ions in solution will diffuse into the pores of the framework. This process occurs until kinetic or thermodynamic equilibrium is achieved along with charge neutrality. The solution and exchanger will contain both species of ions. The distribution may not be even between the two phases. This means that one species may be more prevalent in the ion exchanger than what is in solution. Also, the solution will also be contained within the pores of the exchanger. This is where ion exchange and sorption become coupled. Sorption of the solution must occur prior to ion exchange. The solution facilitates ion exchange. The solution that remains in the framework is considered sorbed.¹¹³

Ion exchange is usually thought of as a physical process but has also been referred to as a chemical process. The physical process is described by electrostatic interactions. That is, the charges on the species and the attraction of ions and their ionic strengths determine the outcome of the process. In a chemical process, the determining factor is the formation of the bonds, in this case ionic bonds, between the framework and the exchange species. While ion exchange can

have some similarities to chemical processes, the ion exchange kinetics typically have no resemblance to chemical kinetics. Chemical influences are usually rather small as shown by their minimal heat evolved from the processes.¹¹³

Distribution of ions is typically uneven in ion exchange. This is due to the species preferences between phases. The determination of the preference can be rather obvious or subtle in some cases. The first reason for a preference can be simple electrostatic forces. A higher charge species can be preferred by an exchanger. Another reason for preference between species is size. A larger species may not be able to diffuse or even fit into the pores of an exchanger thereby excluding it from the ion exchange process. Finally, steric hindrances can play a role in ion exchange. A larger species may be already contained in the pores and does not allow other species to diffuse. All of these factors play a role in determining the preference of one ionic species over another, also known as the selectivity of the ion exchanger.¹¹³

Cationic Dissolved Species

The cationic species chosen for ion exchange have unique properties. The solubility of each salt, the hydrolysis of the cation, and intermolecular interactions will play a role in determining the cationic exchange capacity. Hydrolysis can affect the charge density of the cation, solubility will determine how much of a species can be present in the aqueous phase, and the anion can reduce access to the exchanger or produce precipitates upon ion exchange.

Solubilities

A popular way of remembering solubility is described by “like dissolves like”. While this may be an oversimplification, the trend is generally followed. This means that a polar solvent will readily dissolve a polar solute and vice versa for nonpolar solvents and solutes.

In aqueous solutions, solubilities of metal salts are widely known. Sodium chloride, potassium chloride, mercury chloride, and lead chloride are readily dissolved in water. The solubility of ionic species in water arises from electrostatic interactions of the species. The positive cation is attracted to the electronegative oxygen in the water molecule and the anion is attracted to the partially-positive charged hydrogens in water.

The solubility of the salt is a function of temperature and pressure as well as the solvating solution and the phase of the dissolving species. For example, the solubility of aragonite and calcite differ even though the chemical formula is identical. The two structures are polymorphs

of calcium carbonate. The pressure dependence of solubility for an ideal solution is described thermodynamically by Equation 1 below.

$$\left(\frac{\partial \ln N}{\partial P}\right)_T = -\frac{V_{aq} - V_{cr}}{RT} \quad \text{Equation 1}$$

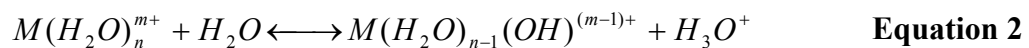
where N is the mole fraction of the component in solution, P is pressure, V_{aq} is the partial molar volume of the component in solution, V_{cr} is the partial molar volume of the component in the dissolving solid, R is the universal gas constant, and T is the temperature. The pressure dependence of solubility is weak and usually neglected in solid and liquid phases.

Valencies

The charge on the dissolved cationic species will play an important role in ion exchange processes. The higher the charge on a cation, the stronger the electrostatic forces will be in the interaction. Alkali metals are monovalent, while alkaline metals are divalent, and transition metals have a range of potential valencies between 1 to 6. A specific transition metal may have multiple discrete valencies associated with it. Most transition metals have valencies of 1 to 3 when given proper charge values.

Hydrolysis

Metal ions are considered Lewis acids. In aqueous solutions they form what are referred to as aqua ions.¹¹⁴ The aqua ions undergo hydrolysis and this is explained by Bronsted-Lowry acid-base theory. The first hydrolysis step is:



Hydrolysis can proceed beyond the first step. This often results in the formation of many hydroxo species. For ions with oxidation states higher than four, the concentration of the aqua ion is negligible.¹¹⁴

The metal ion weakens the OH bond of a water molecule making the deprotonation step possible.¹¹⁴ Sodium is a very weak acid and almost has no discernable hydrolysis while larger cations like calcium and lead are not normally classed as acids due to their large pK_a values. Hydrolysis can be suppressed by making the solution acidic such as adding nitric acid.¹¹⁴ Hydrolysis tends to increase as pH rises (increased basicity) and can lead to the precipitation of a hydroxide compound. Nonetheless, hydrolysis can play a factor in the ion exchange process, but its influence is determined by the cationic species present.

Complexes

When molecular species are dissolved in water, other species or complexes can form besides hydrolysis. The species can partially dissolve leading to a multitude of complexes if the molecule is comprised of many atoms. When dissolving HgCl_2 into water, the most likely mercury species formed are: Hg^{2+} , Hg_2^{2+} , Hg^0 , HgCl^+ , HgCl_2 , HgCl_3^- , HgCl_4^{2-} , HgClOH , $\text{Hg}(\text{OH})_2$, and HgOH^+ .¹¹⁵ Complexation of mercury species can be controlled by varying the pH or by introducing a stabilizing matrix or buffer.¹¹⁶

Molecular Interactions and Anions

Molecular interactions between multiple dissolved species will affect the physical properties of the solution in much the same ways as changing the temperature does. While no general trend is followed for dissolving multiple species in solution, the presence of other species should reduce the maximum of each species being dissolved. This is extremely important to note when dealing with ionic salts that have low or even moderate solubilities in water. Silver chloride has a rather low solubility when it is dissolved as a single species in water. One would then expect its solubility to decrease even more with the presence of other dissolving salts with like anions.

The anion in solution can also play a crucial role in determining the solubility and other important factors when investigating ion exchange. Multiple anions can drastically affect the solubility of dissolved ionic species and in certain cases can make an otherwise soluble species precipitate from solution when introduced to the presence of another anion in solution.

Adsorption

Adsorption is adhesion of a species to the surface of another. The adsorbent, or solid phase, has a thin layer or film of the adsorbate species attracted to its surface. Desorption is the reversal of this process. Adsorption occurs due to a thermodynamic surface energy difference between the adsorbent and adsorbate species. Atoms attracted to the adsorbent surface can also attract other adsorbate species resulting in multilayer adsorption. Adsorbed species can facilitate or then undergo chemical reaction while adsorbed to the surface of an adsorbent. Generally speaking, the surface area of an adsorbent is determined by its structure. Typically, the more porous the structure, the greater the surface area will be. Large surface areas have a large influence on the reactivity of the surface. Since reactivity and adsorption rates between

chemicals can vary, adsorption can be used to separate certain chemical species or functional groups or chemical sensing/detection.

Chemical Warfare Agents and Simulants

Chemical warfare agents (CWAs) are very toxic substances to humans. They can cause serious injury or death at very low concentrations and with short exposure times. These materials can attack the skin, mucous membranes, the nervous system, or the respiratory system. Chemical warfare simulants are chemicals that have similar molecular sizes and functional groups but lack or have reduced toxicity.

Ethanol

Ethanol is a straight chain alcohol. Its chemical formula is $\text{CH}_3\text{CH}_2\text{OH}$. Ethanol has an estimated molecular volume of 71.8 \AA^3 . It can be toxic to humans when ingested or inhaled.¹¹⁷ It can have both long and short-term effects on humans. Ethanol can affect the human nervous system, metabolism, can cause birth defects, and can intensify the effects other drugs and chemicals have on the body.¹¹⁷

Ethanol is considered a chemical warfare simulant according to the United States Army and has a single functional group and small molecular size compared to other listed warfare agents. Its smaller molecular size will allow for sorption into smaller pore zeolites.

2-Chloroethyl Ethyl Sulfide

2-Chloroethyl Ethyl Sulfide is a compound similar to sulfur mustard gas. It is commonly referred to as 2-CEES. The chemical formula is $\text{CH}_2\text{ClCH}_2\text{SCH}_2\text{CH}_3$. 2-CEES has an estimated molecular volume of 143 \AA^3 . It is a flammable liquid and vapor; it is a slightly yellow, clear liquid. 2-CEES is a vesicant or blister agent. This means that it causes skin and respiratory tract irritation and blistering.^{118, 119} The compound can also cause central nervous system depression, pulmonary edema, and cyanosis of the extremities.¹²⁰

2-CEES is also called half mustard due to the only difference between sulfur mustard and itself is the loss of one chloride at its opposing end. Sulfur mustard has two chlorides, one at each end, whereas 2-CEES has only one chloride.¹¹⁹ Since there is a limited difference between the two compounds, the size, physical, and chemical properties should be nearly identical. The diffusion properties into the pores of microporous and mesoporous materials are likely to be the

same as sulfur mustard. This would mean 2-CEES will be well-suited to appropriately model the adsorbant properties of sulfur mustard while remaining more safely to handle.

Dimethyl methanephosphonate

Dimethyl methanephosphonate (DMMP) is a colorless liquid with chemical formula $\text{CH}_3\text{PO}(\text{OCH}_3)_2$. DMMP has an estimated molecular volume of 133 \AA^3 . It has a distinct odor and it can be used as a flame retardant.¹²¹ In contact with water it slowly undergoes hydrolysis.¹²¹

Dimethyl methanephosphonate is harmful if inhaled, swallowed or absorbed through the skin.^{122, 123} It is used in the synthesis of sarin nerve gas and is a simulant of sarin nerve gas. It has a centrally-located phosphonate group and is considered a chemical warfare simulant according to the United States Army and Marine Corps. DMMP should mimic sorption characteristics of sarin nerve gas.

n-Butanethiol

Butanethiol is a volatile, clear to yellowish liquid with a foul odor.¹²⁴ The human nose can easily detect it in the air at concentrations as low as 10 parts per billion.¹²⁴ The molecular formula is $\text{C}_4\text{H}_9\text{SH}$. N-Butanethiol has an estimated molecular volume of 131 \AA^3 . Butanethiol is a thiol of low molecular weight, and it is highly flammable.¹²⁴ Butanethiol is used as an industrial solvent and as an odorant in natural gas.

Butanethiol is a very noxious and caustic chemical compound, and at sufficiently high concentrations, it produces serious health effects in both humans and animals, especially as a result of prolonged exposure.¹²⁴ Sufficiently high concentrations of the foul-smelling, volatile substance causes eye irritation, headaches, nausea and vomiting, dizziness, and irritation of the respiratory tract.¹²⁵ Even higher concentrations can lead to unconsciousness and coma after prolonged exposure. Contact with the skin and mucous membranes causes burns, and contact with the eyes can lead to blurred vision or complete blindness.¹²⁵ It is not considered a chemical warfare simulant by the United States military but has similar size and functional groups to 2-CEES to investigate the different adsorption properties between the two species.

Detection Methods

With the presence of many chemical warfare agents, many methods and devices have been developed to detect, capture, or destroy the substances to save human lives. The United

States military has a variety of detection methods that will allow for identification of the target compound or compounds so proper safety precautions can be implemented. The following sections describes the most commonly used devices to identify CWAs. These methods all have certain features that are advantageous, but have disadvantages to their use as well. The development of a new technique or device that has as few or no disadvantages to its use would clearly be preferred.

M-256 Detection Kit

The M-256 setup utilizes a variety of wet chemistries, each specific for a class of agent. These different tests are grouped together on a detector card and one simply breaks a series of vials to detect the presence of the agent vapor.¹²⁶ Detection works within 15 minutes for blood, nerve, or blister agents.^{126, 127} This device requires a 10 minute period for exposure to vapors and five minute analysis. After testing is complete, the spots are compared to positive and negative examples printed on cards and vapor-sampler body for operator comparison.¹²⁶ The setup is primarily used only in military situations and is used within close proximity to a known chemical attack to determine if chemical levels are sufficiently low for unmasked troops to enter. The device is portable and is considered the one of the most sensitive devices currently employed by the U.S. military.¹²⁸

This setup requires a significant amount of background knowledge for the user to identify the substance. An educated guess must be made as to what type of agent is most likely present leading to specific choices in further experimentation.¹²⁸ This can lead to human error. The device can also produce false positives but has yet to produce a known false negative.¹²⁸

Detection paper

Detection paper enables the detection of a droplet of CWA, and the detection limit is said to be in the $\mu\text{g cm}^{-2}$ level. Detection paper is used for military defense and in chemical terrorism countermeasures.¹²⁹⁻¹³¹ This technique is the least expensive and most simplistic way to determine the presence of a CWA.¹³⁰ The paper contains two dyes and a pH indicator which are integrated in to the cellulose fibers of the paper. When a drop of the CWA is presented onto the paper, a color change occurs.¹²⁹⁻¹³¹ It can detect blister and nerve agents and can distinguish between specific nerve agents due to changes in its pH indicator as well.

The paper does lack some specificity in that it cannot distinguish between all types of CWAs.¹³⁰ Common household chemicals can result in color changes as well resulting in a high number of occurrences of false positives. The US military uses this device in conjunction with other techniques to increase reliability of results.¹³²

Gas detection tube

A gas detection tube enables the detection of CWA vapors using the respective gas-specific tubes, and the detection limit is said to be lower than mg m^{-3} level. It is used for military and civil defense.^{131, 132} The colorimetric tubes monitor one substance per tube and detect CWAs in gas or vapor form.^{131, 133} The tubes have a sorbent material that has had a reagent solution applied to the sorbent. The end of the glass tube is broken off and the sample is pumped into the glass chamber. Upon detection of the CWA, the sorbent changes color.

The device is primarily used for qualitative detection of CWAs. The color change response usually occurs within a few minutes but is dependent upon the flow rate of the sample through the chamber as well as the concentration of the CWA.¹³² The tubes are single use tubes and are designed to detect one CWA per tube.¹³⁰ This can result in the use of up to 160 tubes per analysis or require some prior knowledge about what CWA is most likely present in order to avoid false negative readings. The device does work well under a broad range of temperatures and is not affected by humidity in reporting results.¹³⁴

Flame photometric detector

Flame photometric detectors (FPD) are an atomic spectroscopy technique based upon light emission properties. The device works by pumping air into a reaction chamber and then burning the sample in a hydrogen-rich flame.¹³⁵ The substances present will produce light of specific wavelengths.¹³⁶ This produces a characteristic emission spectrum of the sample.^{130, 132, 135, 137} An optical filter in the device allows certain wavelengths to pass through and a photodetector produces a signal. Since elements produce characteristic wavelengths, detection of specific elements can be achieved.^{132, 135, 136}

These devices work well for detecting blister agents (vesicants) and nerve agents due to the typically low concentration of organosulfur and organophosphorus containing compounds in the atmosphere and can detect them simultaneously.^{135, 136} The device works within seconds or near real-time due to the continual flow of sample being pumped into the reaction chamber.¹³⁸

Also, the device produces no toxic waste, since the sample is destroyed under a hydrogen flame.¹³⁸ The device suffers no memory effects and samples do not need to be prepared for analysis.¹³⁶

The major shortcoming of FPDs is that they only work well for detecting sulfur and phosphorus-containing CWAs.¹³⁷ Many CWAs have functional groups that do not contain these elements making the device useless under these circumstances. The device can also produce false positives since the FPD detects for only sulfur and phosphorus. Nontoxic compounds can contain these elements but the device would not be able to distinguish between nontoxic and CWAs.¹³⁹ The use of a gas chromatograph (GC) can improve the selectivity of the device but makes analysis much longer, more expensive, and reduces overall portability of the collective system.¹³⁵

Ion mobility spectrometer

Ion mobility spectrometer (IMS) is a device that analyses ions based upon their mass, charge, and mobility.^{136, 139-142} IMS is able to quantitatively detect and identify a CWA vapor and their degradation products. The device draws in a sample under clean, dry air.^{136, 143} Membranes and molecular sieves are used to remove moisture/humidity upon sample entry while allowing for the CWA to pass through.¹³⁶ Once the sample reaches the analysis chamber, the chemical is ionized under atmospheric conditions. Various ionization sources can be used, however, most commonly β -emitters such as Ni-63 are selected due to low noise production, high stability, lack of power requirements, and safe operation in explosive environments.^{136, 140, 141, 144} The high energy beta particles react with nitrogen and oxygen in the ionization chamber creating reactant ionic species.¹³⁶ The reactant ionic species interact with the sample making product ions for detection. Reagent ions or dopants may be added to the dry air flow to increase the selectivity of the device.^{136, 142} Dopants reduce the formation of ions from some species that would interfere with the detection process while still allowing the CWAs to ionize.¹³⁶ The created ions then pass through an electric field drift tube where they are separated based upon their mobility.¹⁴⁰ At the end of the drift tube is a collector that detects the ions as a current.^{133, 136, 143} Larger ions take longer to pass through the drift tube since they will collide more frequently with other species in the tube. The resulting spectrum shows the relative intensity of the ionic species indicating the concentration of the CWA.^{133, 143}

The IMS device is simple and sensitive.¹⁴⁵ They also provide results very quickly and the devices are considered portable and inexpensive.^{136, 145} The device uses few moving parts and have limited power requirements.¹³⁶

The device does have some disadvantages. The device must be calibrated once turned on clearly increasing setup time and require some foreknowledge of likely species CWAs present.¹³⁶ Since clean, dry air is required in the sample chamber, the use of membranes and molecular sieves can reduce the sensitivity of the device too.¹³⁶ Also, the device may exhibit peak interferences from compounds that are not of interest, that is a false positive.¹⁴⁰ Short drift tubes may also exhibit peak overlap producing incoherent results or require the use of other peaks in order to determine species present.^{136, 146} While the detectors work well at low concentrations, they can become saturated if the concentrations are too high.¹³⁶ This may contaminate the device for future use.¹⁴⁵ Finally, temperature, pressure, and humidity can affect the performance of the device resulting in peak shift and the formation of hydrated ionic species.^{136, 145}

Surface acoustic wavelength detector

Chemical detectors based on surface area wavelength (SAW) technology are now appearing, and have been introduced into the military and civil defense.^{137, 139} Available technology is portable and automated. These devices work by detecting changes in the acoustic wave properties traveling at ultrasonic frequencies as they pass through piezoelectric materials.¹⁴³ The device requires the change of surface waves and the sorption of CWAs onto a polymer-coated piezoelectric surface to occur in order for the device to work.¹³⁶ When sample vapor enters the SAW device, molecules in the vapor come into contact with the coating at a certain rate, based upon the vapor flow rate.¹³⁶ When a CWA comes into contact with the surface of the coating, the CWA can either sorb or deflect off the surface.¹³⁶ Several polymer coatings are chosen for use in the SAW device based upon certain affinity for specific functional groups and molecules.^{132, 136, 143, 147}

Generally, the SAW device requires a preconcentrator which will release the test vapors over a shorter time span allowing initial concentrations to be increased.^{136, 148} The CWAs enter the SAW array and any sorption onto the polymers results in a frequency change that can be converted to a mass change signal. The process is assumed to reach equilibrium to calculate the vapor concentration.¹³⁶ The detector is then heated to purge the system of all sorbed species onto the polymer coating to reuse the device.¹³⁶

This device can be made at low cost with high sensitivity.¹³⁶ The response time is very short and the device can be made very lightweight.

The device, theoretically, should have a very low false positive rate.¹³⁶ However, when coated with polymers, each polymer can sorb multiple species of chemicals resulting in a potential false positive. This shortcoming can be overcome by using an array of polymers that will identify a host of functional groups and chemical species.^{132, 136, 143, 147} The device can also be affected by humidity and temperature variations.^{132, 148} Highly reactive vapors may also damage the device or produce memory effects onto the polymers especially if operating outside the necessary temperature range.¹³⁶

Gas chromatograph–mass spectrometer

Gas chromatography–mass spectrometry is a standard laboratory technology used in CWA identification, and portable types of such instruments are now commercially available for the environmental monitoring of volatile organic compounds.¹³⁶ When vapor is absorbed, the components in the vapor are separated by GC using an apolar capillary column and elevated temperature control, and the separated peaks are electron-ionized and analyzed by a quadrupole mass spectrometer.^{135, 136} CWAs can be identified by their GC retention times and a comparison of the mass spectrum with a mass spectral library.¹³⁹ Moderately volatile compounds, those with boiling points between 100-250°C, can be detected.¹³⁶

Blister, nerve, and blood agents can be detected and identified within about 10 minutes after sample has been presented.^{135, 139} CNCl vapor can be detected using the direct (no GC separation) mode.¹³⁵ The operation is easy, but it is necessary to use a personal computer with a rather professional procedure for the data analysis.¹³⁶ This limits portability and requires large power requirements relative to other methods.¹³⁶ The user must also be trained in order for successful operation of the device.^{135, 139}

The development of a new device or technique will require the development of a simple-to-use, lightweight, portable apparatus with low power requirements that will be able to detect all classes and species of CWAs at varying concentrations within a short timeframe. Also desired, is the lack of false positives and false negatives resulting from the analysis.

Objective of Dissertation

The objective of this thesis is to identify and characterize applications and potential uses for zeolite and zeolite-like materials in gas and liquid phases based upon the dominating physical and chemical properties of the materials. The properties of interest include liquid phase ion exchange capacities, selectivities, gas/vapor phase adsorption capacity, and initial adsorption uptake rate.

Outline of Chapters

Chapter 2 will cover the theory behind measuring ion exchange and adsorption capacity. This theory includes a description of the various techniques employed to measure either ion exchange or adsorption capacities with the primary focus being the techniques used in this work. Also described are the experimental procedures and apparatuses used in this work, including an atomic absorption spectrometer (AAS), an x-ray diffractometer (XRD), an energy dispersion x-ray spectrometer (EDX), a BET surface area analyzer, a gravimetric microbalance, a quartz crystal microbalance (QCM), and a thermogravimetric analyzer (TGA). This chapter also lists the zeolite, zeolite-like materials, ion exchangers, and adsorbents used and their origins.

Chapter 3 presents the results from the liquid phase ion exchange and selectivity measurements using zincosilicate materials. The zincosilicates vary in framework structure, pore size, silicon-to-zinc ratio, and initial countercation species in the framework. The cationic dissolved species vary in charge and size for the selectivity experiments. The ion exchange metals were chosen to be divalent due to the unique properties of zincosilicates compared to traditional zeolites, the discrepancy between lead and mercury uptake in other ion exchangers (lead is much easier to capture than mercury), and the utility in capturing materials that are regarded as hazardous to the humans and the environment. The results of the selectivity experiments are also modeled.

Chapter 4 presents the results from the gas phase adsorption experiments. These results include the equilibrium adsorption capacities and initial uptake rates of chemical warfare and explosive stimulants onto a broader range of zeolites and zeolite-like materials for use in a handheld device. This chapter addresses the impact of pore size, framework composition, framework countercations, and surface area have on the adsorption of compounds with various

molecular sizes and functional groups. The results will also study the effect of mixtures of chemicals and humidity will have on the adsorption uptake of the selected zeolites.

Chapter 5 will summarize the conclusions and recommendations for areas of future work.

CHAPTER 2 - Materials, Methodology, and Equipment

This chapter will describe the zincosilicate materials used in the ion exchange of heavy metals, the zeolite materials used in adsorption, the metals used in the ion exchange processes, and the agents used in adsorption. The physical basis or phenomenon for the measurement techniques and the specific apparatuses used for describing the cationic exchange and adsorption properties of aluminosilicate and zincosilicate materials will also be detailed.

Materials

Zincosilicates and Zeolites

A variety of aluminosilicate and zincosilicate materials were used in this work. Aluminosilicates 13X, 4A, MCM-41, and ZSM-5 and zincosilicates VPI-7, VPI-9, and VPI-10 were used. The zincosilicate materials were chosen for their distinct features they offer from conventional zeolites. While they have uniform micropores, long-range ordering frameworks, and bulk properties like their aluminosilicate counterparts, they have a tetrahedrally bound zinc in place of the aluminum, thereby increasing the charge density of the framework. This may allow for larger ion exchange capacities and/or ion exchange with higher valency ions. Also, zincosilicates do not have cages in their framework. This allows for all counteranions associated with the framework to be accessible for ion exchange. The other aluminosilicates were chosen due to their distinct features between each other. They have different surface areas, pore sizes, counteranions, and frameworks. These varying features will allow for comparison and determination of the physical properties that determine adsorption capabilities.

VPI-7 was synthesized in the laboratory using zinc oxide (ZnO), sodium hydroxide (NaOH), and potassium hydroxide (KOH) purchased from Fisher Scientific and tetraethylammonium hydroxide (TEAOH) and Ludox HS-40 colloidal silica from Sigma-Aldrich. The molar ratio of the reagents used in making this material was 0.88 NaOH: 0.3 KOH: 0.32 TEAOH: 0.039 ZnO: 1 SiO₂: 26 H₂O. The reagents were mixed and the resulting solution was then placed in Teflon-lined autoclaves. The autoclaves were then heated for four days at 200°C. After synthesis, the material was washed several times with deionized water, dried in an

oven at 50°C for a period no less than 24 hours, then crushed and analyzed using powder x-ray diffraction to confirm crystallinity. The calculated XRD pattern of VPI-7 is shown in Figure 2. Once crystallinity was confirmed using x-ray diffraction, the material was used in either the as-made form as described above or was heat treated at 400°C for at least 2 hours to calcine the material, which removed any remaining structure-directing agent from its interior.

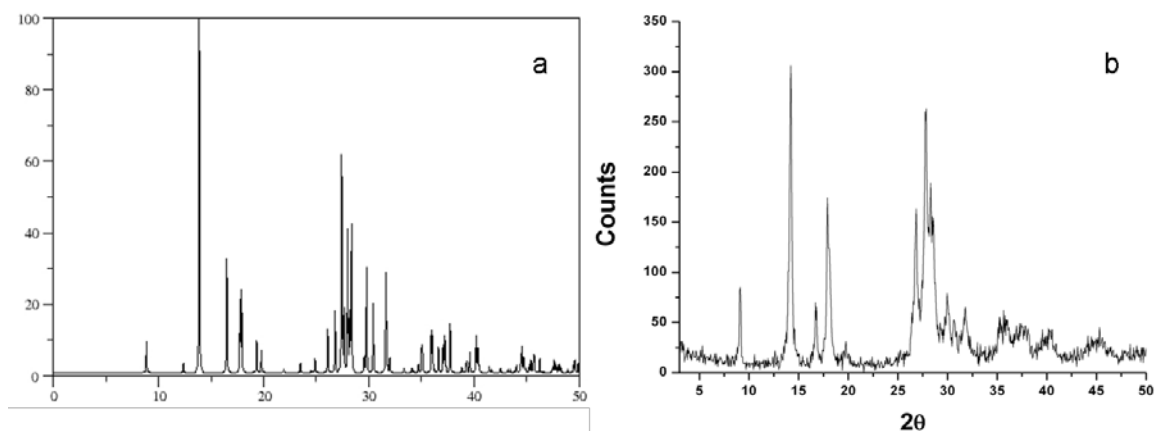


Figure 2 (a) Calculated XRD pattern of VPI-7.¹⁴⁹
(b) XRD pattern for synthesized VPI-7.

VPI-9 Synthesis

VPI-9 was synthesized in the laboratory using rubidium hydroxide, potassium hydroxide, and zinc oxide reagents purchased from Fisher Scientific. Tetraethylammonium hydroxide was purchased from Sigma-Aldrich, and Syloid 63 was used as the silica source. The molar ratio of reagents was 0.6 RbOH: 0.3 KOH: 0.08 TEAOH: 0.037 ZnO: 1 SiO₂: 23 H₂O. The material was synthesized by mixing the reagents and then placing the resulting mixture into Teflon-lined autoclaves while being heated at 200°C for four days. The solid product was then washed with deionized water, crushed into powder, and analyzed using XRD. The material was then used either ‘as-made’ or calcined similar to VPI-7 described above. The calculated XRD pattern of VPI-9 is shown below in Figure 3.

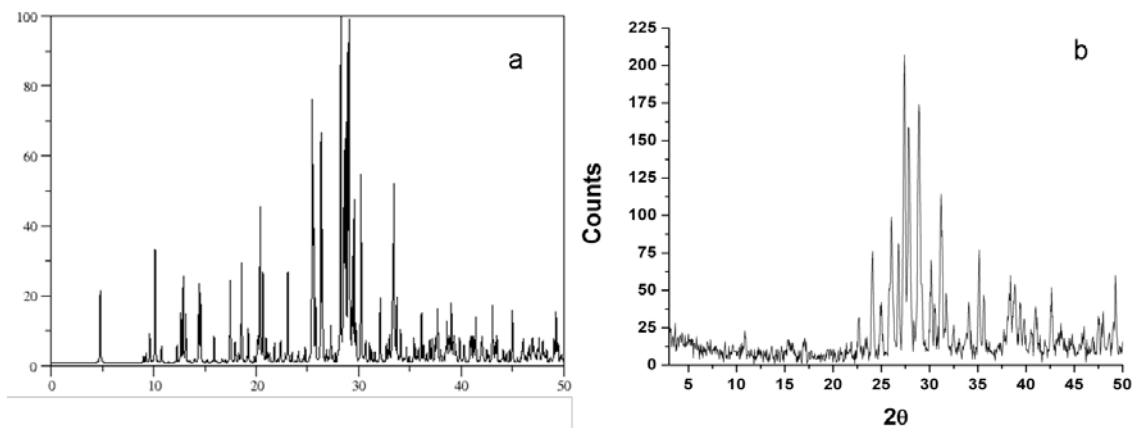


Figure 3 (a) Calculated XRD pattern of VPI-9.¹⁴⁹
(b) XRD pattern for synthesized VPI-9.

VPI-10 Synthesis

VPI-10 was also synthesized in the laboratory using the same reagents as VPI-9 from the same vendors in different proportions. The molar ratios of the reagents used for synthesizing VPI-10 are 0.6 RbOH: 0.6 KOH: 0.08 TEAOH: 0.037 ZnO: 1 SiO₂: 23 H₂O. The reagents were mixed and then placed in Teflon-lined autoclaves for a period of five days under autogeneous pressure and heated at 200°C. The solid product was then vacuum-filtered and washed with deionized water, dried, crushed, and then analyzed under x-ray diffraction to confirm crystallinity. The proposed XRD pattern is shown below in Figure 4.⁵

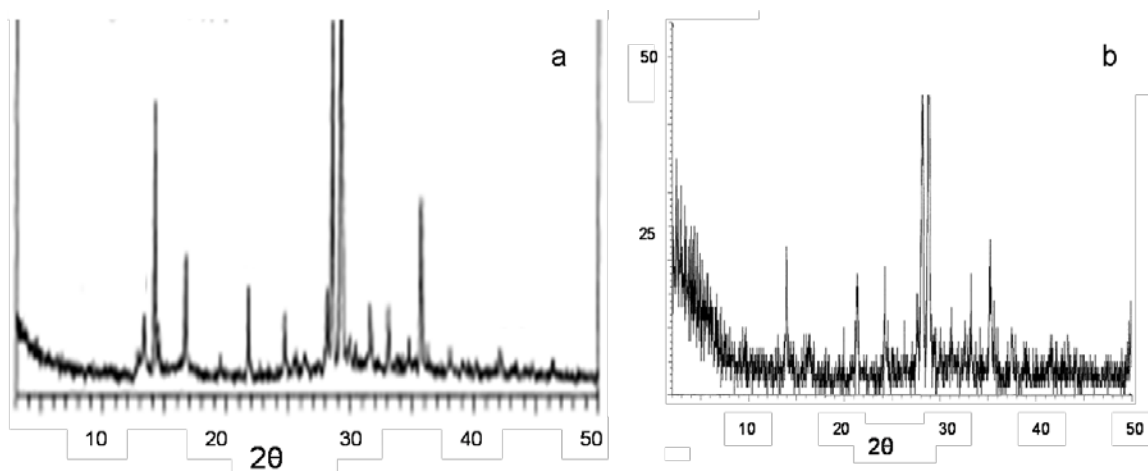


Figure 4 (a) Calculated XRD pattern of VPI-10.¹⁵⁰
(b) XRD pattern for synthesized VPI-10.

Zeolite 13X

Zeolite 13X was purchased from Fisher Scientific and was used as received. The chemical formula for the hydrated form of zeolite 13X is $\text{Na}_{88}(\text{H}_2\text{O})_{220}[\text{Si}_{104}\text{Al}_{88}\text{O}_{384}]$. The calculated XRD pattern of 13X is shown in Figure 5.

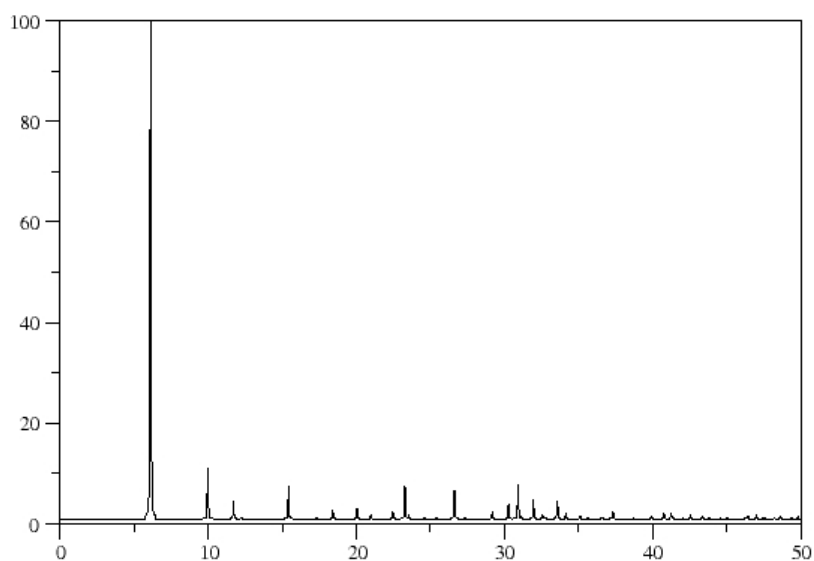


Figure 5 Calculated XRD pattern of zeolite 13X.¹⁴⁹

Zeolite 4A

Zeolite 4A was also purchased from Fisher Scientific and was used as received. The molecular formula for the hydrated form of zeolite 4A is $\text{Na}_{96}(\text{H}_2\text{O})_{216}[\text{Si}_{96}\text{Al}_{96}\text{O}_{384}]$. The calculated x-ray diffraction pattern is shown below in Figure 6.

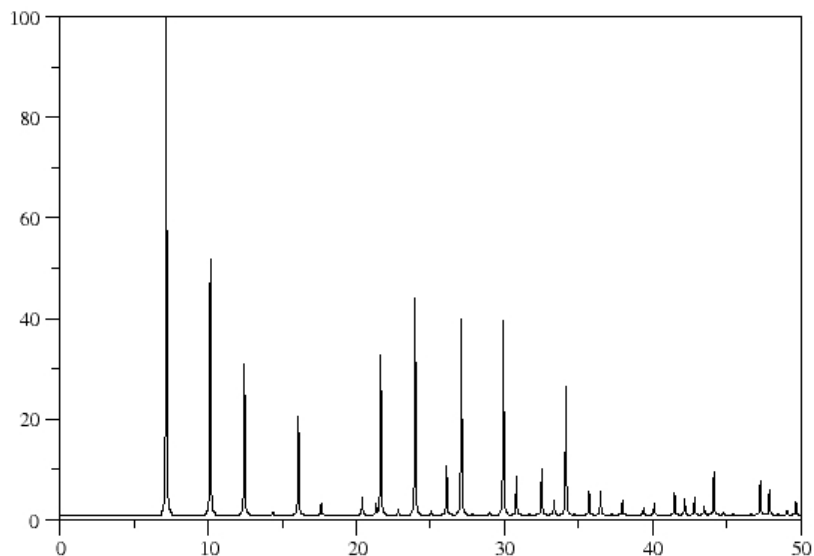


Figure 6 Calculated XRD pattern of zeolite 4A.¹⁴⁹

MCM-41

MCM-41 was synthesized in the laboratory from the prescribed route of Beck et al.¹⁵¹ The reagents were purchased from Fisher Scientific and Sigma-Aldrich. After synthesis, the material was washed with deionized water and then analyzed under x-ray diffraction to confirm structure formation. The resulting material had pores of about 10 nm in cross-section.

Zeolite Properties

Table 1 shows some of the physical characteristics and properties of the selected zeolites. The size, location, and charge on the counteractions can change intermolecular forces and accessibility into the pores thereby affecting sorption properties. The Si:Al ratio value conveys the counteraction charge density of the material as well as the hydrophobicity/hydrophilicity of the framework. If the ratio is large in magnitude, the framework has a low counteraction charge density and is hydrophobic; the opposite holds as the ratio approaches unity. MCM-41 has a pure silica framework with ionic species contained within its pores. It does not have a charge density associated with its framework making it the most hydrophobic framework of the selected materials. The pore size of the zeolite will affect the rate of diffusion into the pores. Larger pores will allow for faster diffusion. Surface area will also affect sorption. Larger surface areas

allow the potential for more molecules to sorb onto the surface of the zeolite. Finally, the particle diameter will affect the time needed to reach equilibrium. Larger particles require more time than smaller particles for molecules to diffuse into the interior. These physical properties will influence the sorption capacity and uptake rate of a molecule onto the zeolite.

Table 1 Physical properties of selected zeolites

Sorbent	Native Cations	Si:Al Si:Zn*	Pore Size (Å)	BET Surface Area (m ² /g)	Particle Diameter (µm)
4A	Na ⁺ ¹⁷⁴	1:1 ¹⁷⁴	4.1x4.1 ¹⁷⁴	120	50
13X	Na ⁺ , Mg ²⁺ ¹⁷⁴	2.31:1 ¹⁷⁴	7.4x7.4 ¹⁷⁴	156	50
MCM-41	R ₄ N ⁺	-	100x100 ¹⁵¹	700 ¹⁵¹	50
VPI-7	Na ⁺ , K ⁺	3.5:1* ¹⁷⁴	3.8x4.0 ¹⁷⁴	17	500
VPI-9	K ⁺ , Rb ⁺	4:1* ¹⁷⁴	3.5x3.6 ¹⁷⁴	41	75
ZSM-5	H ⁺ ¹⁷⁴	~75:1 ¹⁷⁴	5.1x5.5 ¹⁷⁴	116	50

Cationic Species

The sources used for cationic exchange were: lead chloride, mercury chloride, sodium chloride, potassium chloride, and calcium chloride. All metal salts were purchased from Fisher Scientific and used as received. The dissolving of mercury chloride in water results in a divalent mercury cation in solution. Although many complexes of mercury can form when dissolving mercury chloride, a 5 wt% addition of nitric acid was added to the water solution to stabilize and ensure divalent mercury was the primary cationic species present.¹¹⁶ This will stabilize all concentrations of mercury between 20-20000 ppm. When a 5 v/v% nitric acid was used to stabilize the divalent mercury in systems, the pH was 2. If nitric acid was not used the pH was as high as 6.1 The mercury cations were run at room temperature varying between 20-23°C for ion exchange and selectivity coefficient experiments also a stable regime with a nitric acid matrix and deionized water solution.

Mercury is considered a more difficult element to ion exchange when compared to other common elements dissolved in water.¹⁵² Lead chloride is considered much easier to capture from wastewater streams and the like when compared to mercury. Both elements in even small quantities are considered dangerous to human health.¹⁵³ Examination and comparison of the capture capacity of these cations onto zincosilicate materials will give a broader understanding of the potential uses of the zincosilicates for gathering other dissolved species and their selectivities.

The solubilities of the dissolved metal salts are desired for developing ion exchange criteria. The solubilities of the selected metal salts in water are shown in Table 2.

Table 2 Metal salts and their single component solubilities in water.

Metal Salt	Solubility in water at 20°C (g/100cm³)
PbCl ₂	0.99
HgCl ₂	7.4
NaCl	35.8
KCl	34.4
CaCl ₂	74.5

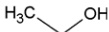
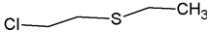
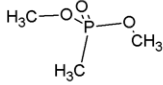
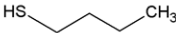
Chemical Warfare and Explosive Agent Simulants

Chemical warfare agents (CWAs) are extremely dangerous to expose to humans. The materials can target the human respiratory system (choking agents), the nervous system (nerve agents), the skin (blister agents), or mucous membranes and circulatory system (blood agents).¹⁵⁴

CWAs have analogs, or compounds that mimic the physical and chemical properties of a particular CWA but with a reduced or negligible toxicity in some cases.¹⁵⁵ These analogs are a useful starting point for determining adsorption characteristics from the actual CWA, but the analogs limit the inherent dangers that go along with the CWA and makes handling the chemical safer.¹⁵⁵

The nerve agents and their analogs selected for evaluation in this investigation are shown in Table 3. The chemical name, structure, chemical formula, main functional group or groups, and type of simulant or analog are listed. The two main simulants are 2-CEES, 2-chloroethyl ethyl sulfide, and DMMP, dimethyl methanephosphonate. 2-CEES is also known as half mustard due to its similar structure and analogous nature to mustard gas.¹⁵⁴ DMMP is a simulant or analog that has similar properties to VX nerve gas.¹⁵⁴ All of the chemicals in this table were purchased from Fisher Scientific and used as received.

Table 3 Target compounds used in adsorption

Target Compound	Chemical Structure	Chemical Formula	Functional Group(s)	Agent Type
Ethanol		C ₂ H ₆ O	OH	Polar organic
2-CEES		C ₄ H ₉ ClS	Cl, S	Blister
DMMP		C ₃ H ₉ O ₃ P	PO ₃	Nerve
N-Butyl Mercaptan		C ₄ H ₁₀ S	S	Similar to 2-CEES

Methods for Measuring Exchange Capacity

Atomic Absorption Spectroscopy

The first steps towards developing atomic absorption spectroscopy was when Herschel and Talbot discovered that when certain atoms were placed in a flame, atomic emission occurred.¹⁵⁶ Kirchoff noted that ‘Matter absorbs light at the same wavelength at which it emits light’.¹⁵⁶ These two principles lead to the development of Atomic Absorption Spectroscopy (AAS) by Alan Walsh at the Commonwealth Science and Industry Research Organization in the Division of Chemical Physics in the 1950s.¹⁵⁷

AAS is a quantitative elemental analysis technique.¹⁵⁸ Elements will absorb specific wavelengths of light in order to excite its valence electrons. Each element has its own characteristics wavelength that it will absorb. The AAS detects specific elements by sending a beam of UV light at the characteristic wavelength for that element through a high temperature flame and vaporized sample and then into a detector.¹⁵⁸ If the element is present, it will absorb some of the light and reduce the beam’s intensity.¹⁵⁸ The detector then measures remaining light intensity and determines the concentration of the element based upon the difference in light intensity of the vaporized sample.¹⁵⁸

The specific behavior that is observed through atomic absorption is the excitation of electrons to higher orbitals, a property of quantum mechanics. Although there is no absolute energy level, (i.e. no zero energy), energy changes can be measured. Electrons have specific energy states that they can occupy leading to an integral number of transitions that can occur

through absorption.¹⁵⁸ The change in energy is determined by knowing difference in the energy input through the flame source and what is detected at the detector.¹⁵⁸ The concentration of the element is determined by knowing the total energy difference and the transition energy change of the element reducing to a specific integral number of transitions which can then be deduced to a concentration based upon calibration. According to the Beer-Lambert law, the absorption of light is directly proportional to the concentration of the element being analyzed. The relationship is as follows:

$$\Delta E = n \cdot \frac{h}{\lambda} \qquad \text{Equation 3}$$

where ΔE is the overall energy difference in the absorption, n is the number of transitions that occur, h is Planck's constant and λ is the wavelength of the incident UV beam.¹⁵⁹

This technique is simple in principle and is very accurate. It does however, have some disadvantages. Sample preparation can be an involved process. If a sample is not readily soluble in solution or is not readily vaporized, it must be pretreated in order to make it compatible with the system. Contaminants must also be carefully monitored and avoided. The apparatus setup also allows only for the analysis of one element at a time. This can greatly increase the amount of time needed in order to analyze multiple elements. One also must take care in avoiding evaporation of solvent from sample. If the element under consideration is in a volatile solution, over time, the concentration of the element will increase as the solution evaporates. This will cause results to be higher than actual and misleading. Finally, the AAS system will destroy the sample. Since the sample cannot be recovered, other analytic techniques cannot be completed after AAS has been performed.¹⁶⁰

The analysis of liquids occurs in three steps. The first is desolvation, the liquid solvent is evaporated leaving only the dry sample behind. The second step is vaporization or ashing. This involves turning the dry sample to a gas. The final step is atomization where the compound making up the sample are broken into free atoms.¹⁵⁷ Once the sample is vaporized, a beam of light is focused onto the vaporized sample and read by a detector.

Each element must be analyzed by a specific hollow cathode lamp. The lamp contains an anode and a cylindrical metal cathode that contains the metal being analyzed. A high voltage is then applied across the anode and cathode thereby exciting the metal atoms. The excited atoms

produce a certain emission spectra, which travels through the center of the sample chamber area and into the detector. If not properly aligned, the result will be diminished beam intensity.

Once the beam passes through the sample it is usually sent through a monochromator. The monochromator filters background light and other interferences that may be present. A monochromator separates light by using either optical dispersion in a prism or diffraction using a diffraction grating. A monochromator can be replaced by a bandpass interference filter in certain circumstances.¹⁵⁷

After the light passes through the monochromator, it goes into the detector, which is typically a photomultiplier tube. Photomultiplier tubes detect light in the infrared, ultraviolet, and visible light spectra. They are made of a glass vacuum tube containing a photocathode, anode, and several dynodes. The incident beam strikes the photocathode at the entrance of the device. Electrons are given off due to the photoelectric effect. The electrons are sent by a focusing electrode to an electron multiplier. The electron multiplier increases the amount of electrons by a process known as secondary emission. Eventually, the electrons reach the anode where the accumulation of charge creates a sharp current pulse indicating the arrival of a photon at the photocathode.¹⁶¹ The information from the photomultiplier tube is then transferred to a data processor and reported as a concentration based upon a calibration curve.

Atomic Absorption Experimental Setup

There were two basic setups for gathering data from the AAS. A graphite furnace method was used for determining concentrations of calcium, lead, potassium, and sodium while a cold vapor technique was used for determining mercury concentrations.

The graphite furnace uses a graphite tube with an electric current to heat the sample. This method is especially useful when handling samples of small size, with low concentrations (<50 ppb), or can easily be oxidized.¹⁵⁷

The cold vapor technique used for analyzing mercury takes a small liquid sample and digests it with a potassium permanganate solution. This step can be ignored if all forms of mercury in the sample are known to be Hg(II) as the potassium permanganate oxidizes all forms of mercury to Hg(II). The mercury is then reduced with a stannous chloride-hydrochloric acid solution to elemental mercury. The elemental mercury is sparged through a chamber where it is then detected by the AAS.

The AAS used in these procedures was a Varian Model AA240 which employs a Varian graphite tube atomizer model GTA120 for analyzing Ca, K, Na, and Pb elements and cold vapor generation accessory Varian Model VGA 65. A programmable sample dispenser was also used at times, for completing multiple analyses with the graphite tube furnace Varian Model PSD 120.

Prior to analysis, samples were diluted prior to being introduced to the PSD, GTA, or VGA. This dilution was dependent upon the initial concentration of the analyte in solution and the prescribed analytic range of the instrument. Using the PSD, if a sample was outside the calibration range of the standards, the PSD would dilute the sample until an acceptable absorbance was found or dilution was no longer possible. The maximum dilution allowable by the PSD was reducing the sample by a factor of 15. If the sample was still outside the calibration range after the maximum dilution, another manual dilution was needed and performed. A picture of the Varian AA240 with PSD 120 installed is shown below.

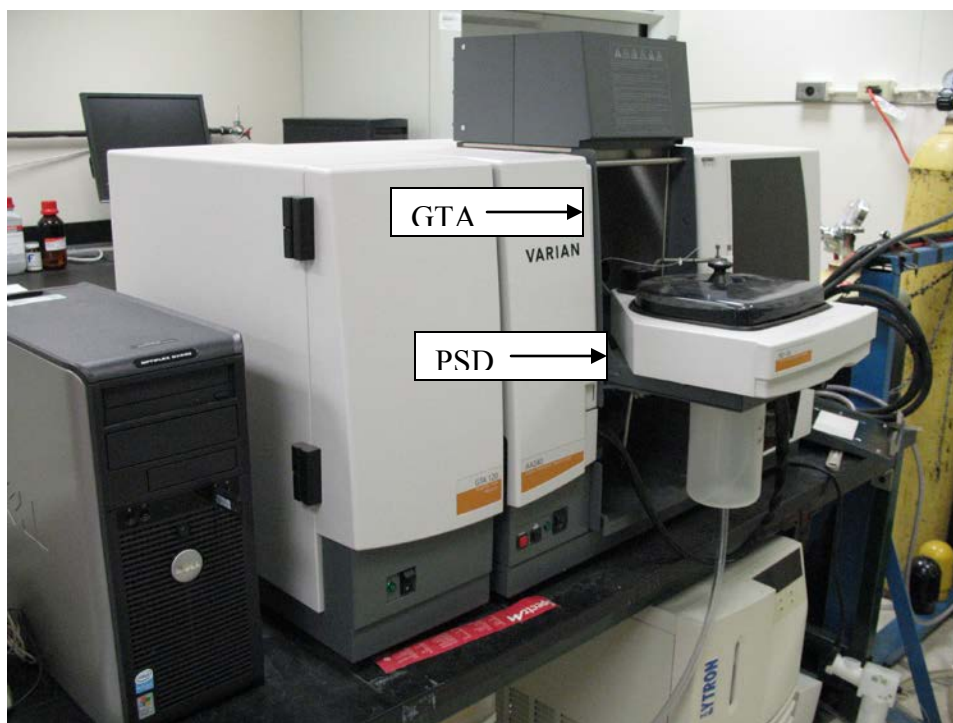


Figure 7 Varian Model AA240 apparatus with PSD 120 attached

Using the GTA, each element has certain instrument parameters that are required for successful analysis. The following table lists the element, lamp wavelength, slit size, and upper recommended concentration for a standard. For all elements, the default settings on the instrument were used for the calibration algorithm, recalibration rate, and reslope rates which were linear, 0, and 0, respectively. For wavelengths less than 325 nm, the deuterium background

correction lamp was turned on. This feature reduces the effects of background interferences on the analysis. The calibration curve was completed using three standard concentrations and one blank for all elements.

Table 4 Lamp and standard settings used for AAS

Element	Wavelength (nm)	Current (mA)	Slit	Concentration (ppb)
Ca	422.7	10.0	0.5R	1.0
Hg	253.7	4.0	0.5	5.0
K	766.5	5.0	1.0	2.0
Na	589.6	5.0	0.5R	40.0
Pb	217.0	10.0	1.0	6.0

When analyzing mercury, the VGA 77 accessory was used. The VGA is a continuous flow device that uses a peristaltic pump to mix the reagent streams of water and stannous chloride-hydrochloric acid solution with an ultra high purity argon carrier gas. The inert gas and volatiles are stripped from the liquid in a gas liquid separator where they are then sent through a flow cell through the path of the hollow cathode beam where absorbance is measured. Three mercury standards and a blank were made for calibration. Samples were diluted manually. Figure 8 shows the VGA-77 accessory.

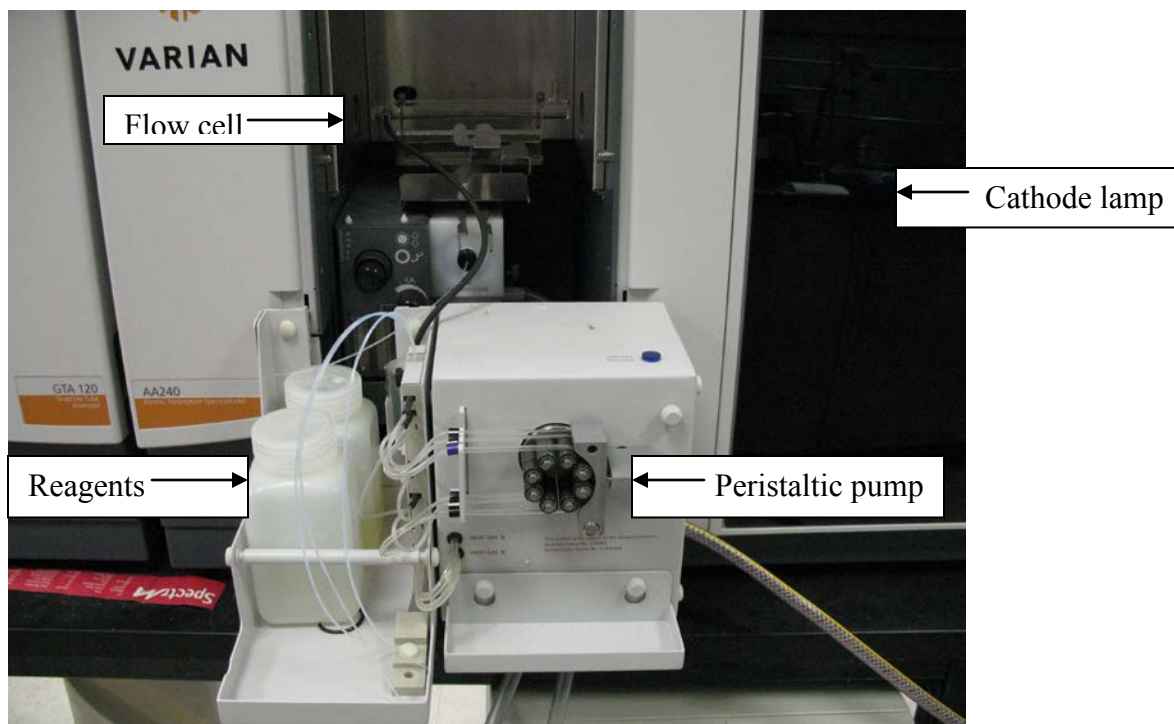


Figure 8 Varian VGA-77 cold vapor accessory

Energy Dispersion Spectroscopy

Energy dispersion X-ray spectroscopy (EDS) is an elemental analysis or chemical characterization technique. It is a type of x-ray fluorescence.¹⁶² The system detects x-rays that are emitted from a sample after the sample is bombarded with an electron beam. When the sample is bombarded with electrons, electrons are ejected from the sample's surface. The sample's electron vacancies that result are filled by electrons from a higher state. An x-ray is then emitted to balance the energy difference between the two electron states.¹⁶² Each element has its own characteristic x-rays that are emitted and thus elemental analysis can be accomplished by determining the energy of the emitted x-ray. Figure 9 below shows the fundamental principle for EDS.

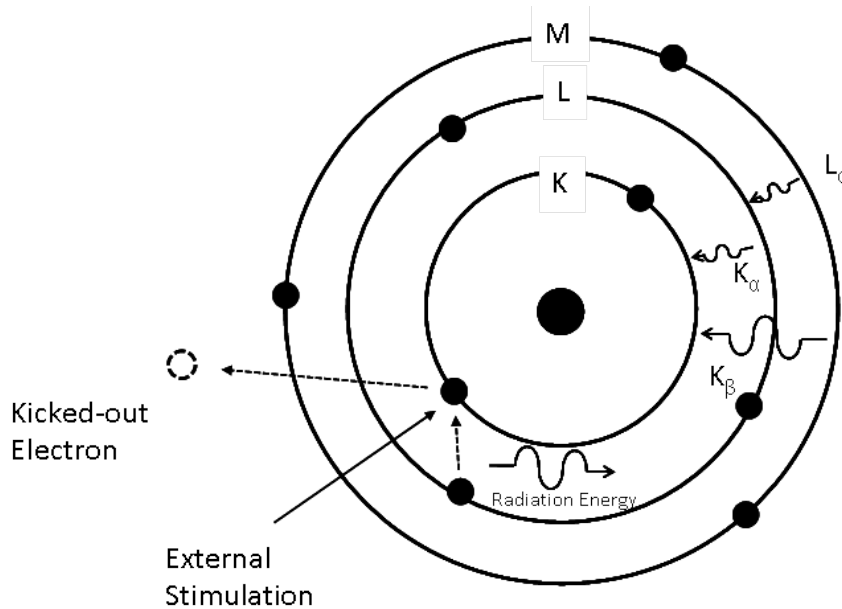


Figure 9 Atomic level interactions required for EDS: a high energy electron from the source ejects a high energy electron from the sample atom, then being replaced by other electrons in the sample atom resulting in an emitted x-ray. Adapted from Goldstein.¹⁶³

There are four primary components to an EDS system: a beam source, an x-ray detector, a pulse processor, and analyzer. Although stand-alone systems do exist, most EDS systems are coupled with an scanning electron microscope (SEM). SEMs are equipped with a cathode and magnetic lenses to create and focus a beam of electrons. Since the 1960s, most SEMs have been equipped with elemental analysis capabilities.¹⁶³

The EDS setup bombards a sample of a small area with focused, high energy electrons.¹⁶³ The electrons strike the sample ejecting electrons and x-rays. The EDS x-ray detector measures the relative abundance of emitted x-rays and their energy.¹⁶³ When an x-ray strikes the detector, it creates a charge pulse that is proportional to the x-ray energy. The charge pulse is converted to a voltage pulse where a multichannel analyzer sorts out the voltages. Software usually is used to deconvolute the voltages acquired and thus determines the elements present in a sample.

There are several advantages to using EDS analysis. The analysis can be accomplished in very short time spans. The analysis can also be completed with very little sample. Most systems can analyze a 'spot' of sample as small as $1 \mu\text{m}^2$. A semi-quantitative feature also allows for determination of chemical composition by comparing peak-height ratio relative to a standard. Also, EDS allows and analyzes many elements simultaneously. This allows for chemical compositions to be determined very rapidly.

There are some disadvantages to the use of EDS. First, there are some x-ray spectrum energy overlaps between a few elements.¹⁶³ These overlaps are most prevalent in x-rays generated by emission from different energy level shells (K, L, and M) in different elements. Examples include the overlap of the Mn- K_{α} and Cr- K_{β} or the overlap between Ti- K_{α} and various L lines in Ba.¹⁶³ Peak overlaps particularly occur at higher energies and may correspond to several elements leading to the user making judicious selection about which elements are most appropriate for the given sample. This selection process clearly can be problematic if chemical composition is unknown. EDS also has difficulty detecting the lightest elements due to the presence of the Si-Li window equipped on the apparatus. This means that elements lighter than sodium may not be properly identified or even recognized due to the emission lines of these elements. Elements lighter than boron cannot be analyzed at all due to the low energy x-rays emitted from these elements that are absorbed by the Si-Li window on the apparatus, referred to as a Beryllium window.¹⁶³ Another situation that must be accounted for when using EDS is charge storage. A sample that is very conductive must be treated differently than one that is insulating. An insulating sample will build up charge due to the bombardment of electrons from the electron beam. The potential difference between the surface of the sample holder and the electron source can result in the sample being electrostatically attracted to the source. If enough charge is stored in the sample, it can move to the electron source. Care must be taken in selecting the appropriate potential and beam current. Finally, EDS has difficulty or is not even

capable in most cases of detecting liquid or gas samples or biologically ‘living’ samples, making solid samples analyses practical.

Energy Dispersion Spectrometer Experimental Setup

The Energy Dispersion Spectrometer (EDS) used for analysis of zincosilicate samples before and after cationic ion exchange was the IXRF Systems SEM-2004. This system also has a Scanning Electron Microscope (SEM) attached. As stated previously, the EDS has a beryllium window (cannot analyze elements lighter than beryllium) and may have difficulty in identifying elements lighter than sodium. Sodium was the lightest element analyzed in this study using EDS. The EDS-SEM system used in shown in Figure 10.



Figure 10 SEM-EDS apparatus

EDS analysis was used to verify results received from the AAS. Specifically, the technique analyzed the solid zincosilicate samples after ion exchange in order to account for all the heavy metal captured in an ion exchange. This was a heavy metal mass balance of the ion exchange process.

A sample was prepared by placing a small amount (<20 mg) of zincosilicate onto a sample platform that had a small portion of carbon tape attached. The carbon tape was used to

adhere the sample to the platform and leave carbon as the primary component of external influences on the results of the analysis.

The sample was then loaded into the sample chamber and a vacuum environment was imposed. From that point, the EDS-SEM software was used to focus on specific areas of the sample using the SEM. The x-ray analysis portion of the EDS was then used with specific criteria in order for the analysis to be performed. The incident counts required were 2000 counts/min with an acquisition time of 120 seconds. This was sufficient data for the EDS deconvolution software to successfully analyze the data. Other user imposed criteria were judicious selection of elements to be examined. Since the EDS has the capability of analyzing all elements heavier than sodium successfully and can analyze any elements with heavier than that of beryllium, the user only analyzed for elements that were assumed present in the sample. Since the samples were synthesized in the laboratory, the zincosilicates themselves should have only been composed of silicon, oxygen, zinc, potassium, rubidium, and sodium. If the structure-directing agent is present, the system may also contain carbon, nitrogen, and hydrogen. The ion exchanges presented lead or mercury and chlorine. It must be noted that although carbon might be present in the sample due its presence in the structure-directing agent, tetraethylammonium hydroxide, it was neglected in the analysis specifically for two reasons: 1. Carbon was present in carbon tape and would inflate the carbon signal received. 2. Carbon is lighter than sodium resulting in reduced accuracy of any number reported by the apparatus. Hydrogen was neglected due to the beryllium window, being too light of an element to detect. Nitrogen was also neglected in the analysis since it was determine that no structure-directing agent was present in the framework. With these criteria, the elements examined using the EDS were: chlorine, lead, mercury, potassium, rubidium, silicon, sodium, and zinc.

X-Ray Diffraction

X-ray diffraction (XRD) is a technique used to qualitatively analyze the crystalline structure of a material. In x-ray diffraction, a sample is exposed to a source of x-rays with wavelengths between 5 and 25 nm.¹⁶⁴ This range of wavelengths is close to the length of many chemical bonds and is the reason why XRD is a useful qualitative analysis technique. Incident x-rays onto a sample can produce one of two results: the x-ray can eject electrons from the atom and be absorbed or the beam can be scattered. With XRD, x-rays incident in a crystalline

structure will diffract the x-rays at different angles of incidence.¹⁶⁵ At most angles, the subsequent diffraction will result in destructive interference of the wavelengths, but at particular angles the result will be constructive interference of the wavelengths resulting in a sharp intensity at that angle.¹⁶⁶ This is described via Bragg's law. The requirement for constructive interference is determined by the path difference between the two x-rays and is described by Equation 7.

$$2 \cdot d \cdot \sin(\theta) = n \cdot \lambda \quad \text{Equation 4}$$

Where d is the crystal lattice spacing, θ is the angle of incidence, n is an integer number of wavelengths and λ is the wavelength of the x-ray. This concept is depicted in Figure 11 below.

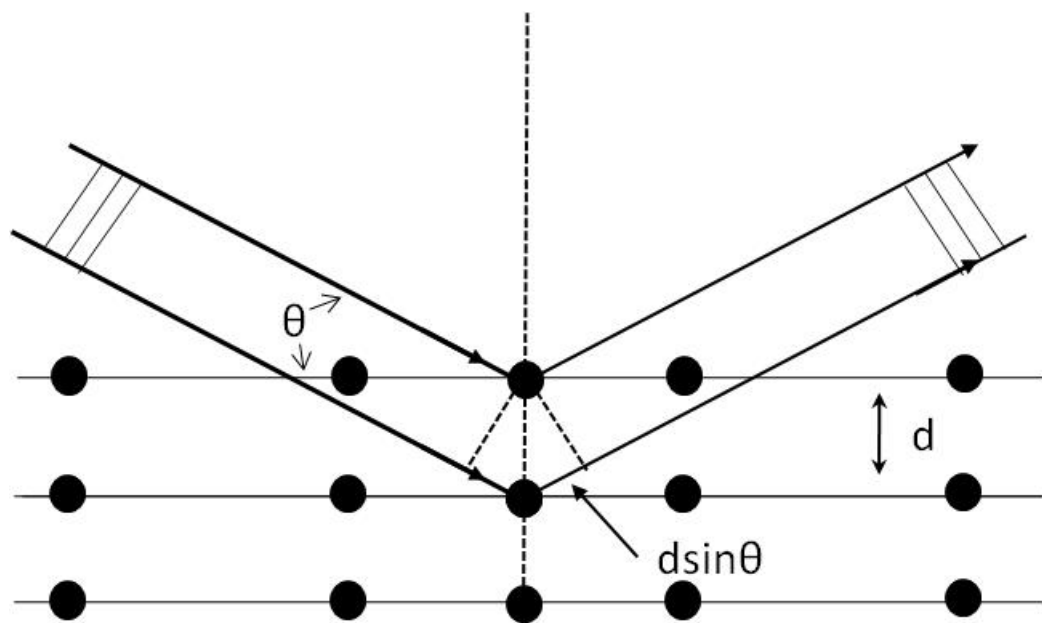


Figure 11 X-ray diffraction technique measures the path length difference between two incident x-rays. The angle of incidence allows for determining the distance between two adjacent atoms.

An x-ray diffractor consists of an x-ray source, a detector and a variety of slits and spacing between slits. The source side is usually referred to as the tube side and x-rays are generally produced using Cu-K_α source of wavelength 1.5418 \AA . When the incident beam strikes a powder crystalline sample, diffraction occurs at all angles and orientations.¹⁶⁶ In order to filter and reduce the effects of radiation noise and background, filters are used on both sides of

the setup. The more filters that are used and the smaller the filter size, the longer the analysis will take but will achieve a better resolution diffractogram.

X-ray diffraction works well for determining the crystal structure of compounds with long-range ordering. As stated before, it is a qualitative technique and determines the positioning of atoms in the crystal structure. It will not determine the elements present in the sample or the bonding of the atoms in the structure.

X-Ray Diffractometer

The x-ray diffractometer used for analyzing the resulting zincosilicate was a Bruker AXS D8 Advance model. Scans were taken from a 2θ angle range of $2-50^\circ$ in increments of 0.05° at a scanning rate of $2^\circ/\text{minute}$. The voltage was set at 40kV and the current was set at 40mA . There were five slots located on the equipment to place filter slits. One filter was on the detector or ‘tube’ side, while four slit slots were located on the detector side. The tube side slot had a 1 mm slit while the four other slits were as follows: 0.6 mm , no slit, 0.6 mm and 1 mm , listed in order of the slit nearest to furthest from the sample. The following schematic shows the setup used with the instrument involving filter slits and their location. These setup parameters were used for analyzing all synthesized zeolite samples. The Bruker AXS D8 Advance apparatus is shown in Figure 13.

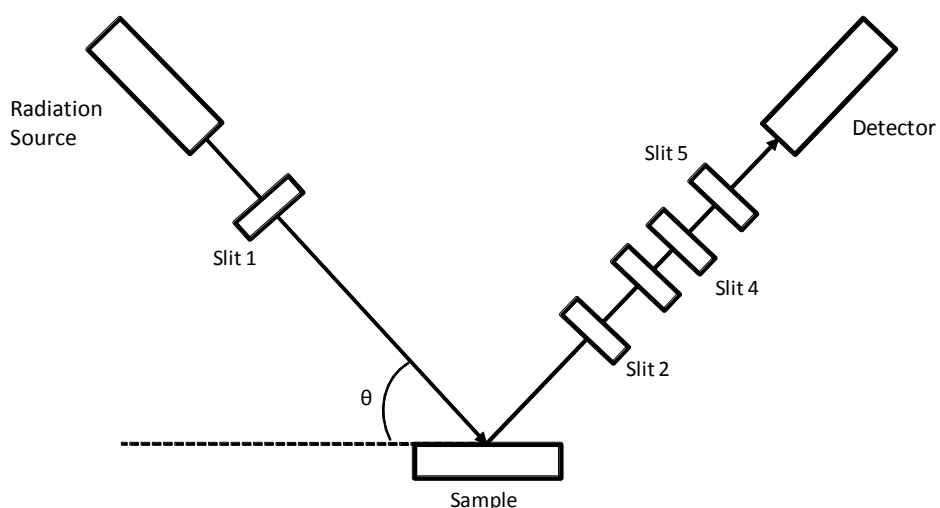


Figure 12 Setup used for XRD analysis



Figure 13 Bruker AXS D8 Advance apparatus

Other Techniques

Other techniques are available for qualitative and quantitative chemical analysis. Gravimetric techniques are available that will measure the amount of a particular element or compound by precipitating the compound or element out of a dissolved sample or by volatilizing the element of interest and measuring the mass loss. Gravimetric analyzers and Differential Scanning Calorimeters (DSC) are techniques available for providing information regarding adsorbed species, structural changes, or structural deterioration. Inductively coupled plasma atomic emission (ICP) can also be used for chemical analysis. It is very similar to AAS but is significantly more expensive to provide similar results. ICP was used in analysis of solid zincosilicate samples. Samples were sent to Galbraith Laboratories, Inc. where the ICP analysis was completed.

Cationic Exchange Mass Balances

The techniques of AAS and EDS described in the above sections were used for determining the ion exchange capacities of the zincosilicate materials. In a batch exchange

process, a known initial concentration of exchanging ions is presented in an electrolyte solution. The ion exchanger zirconosilicate initially contains no ions of interest in the exchange. Their frameworks contain either potassium and sodium or potassium and rubidium. Using AAS, the final concentration of the exchanging ion can be determined. The volume of solution is assumed to remain constant and therefore a quantifiable amount of exchanging ions in solution can be evaluated. Using EDS, the amount of the ion exchanging element of interest present in the solid phase can be determined. This allows for a complete mass balance on the ion exchange batch process. The mass balance of the system is shown in Equation 8 below.

$$\overline{M}_{initial} + M_{initial} = \overline{M}_{final} + M_{final} \quad \text{Equation 5}$$

where $\overline{M}_{initial}$ is amount of the ion initially present in the solid zeolite phase, $M_{initial}$ is the amount of the ion of interest initially in the aqueous solution phase, \overline{M}_{final} is the amount of the ion of interest exchanged into the zirconosilicate material, and M_{final} is the amount of the ion of interest that remains in the aqueous solution phase after ion exchange. Typically, the ionic species of interest is not present initially in the zirconosilicate solid phase, so this term can be neglected.

Exchange Energies

The energy associated with ion exchange can be determined by measuring the heat evolved from solution when the ion exchange takes place. Ion exchange energy can be determined using the van't Hoff equation when the system involves only one cationic exchanging species in solution assuming the ion exchange is a chemical process for modeling the batch system. The energy of exchange can be calculated from the ion exchange capacity at several temperatures. The determination of the exchange energy can be identified by making a plot of the natural logarithm value of ion exchange capacity versus the inverse of the ion exchange solution temperature. This approach is limited to single component exchanges and a modest temperature range as determined by the solvent properties. The temperature range used was 25-70°C, which is considered reasonable for aqueous systems.

Methods for Measuring Adsorption

BET Surface Area Analyzer

In 1938, Brunauer, Emmett, and Teller developed a theory regarding the measurement of the specific surface area of a material. This theory was based upon an extension of the Langmuir theory for monolayer adsorption.¹⁶⁷ The theory included three hypotheses: gas molecules physically adsorb to the surface of a solid in layers infinitely, there is no interaction between each adsorption layer, and the Langmuir model can be applied to each layer.¹⁶⁷ With these criteria, the resulting equation was developed:

$$\frac{1}{v[(P_0/P)-1]} = \frac{c-1}{v_m c} \left(\frac{P}{P_0} \right) + \frac{1}{v_m c} \quad \text{Equation 6}$$

where P is the equilibrium pressure, P₀ is the saturation pressure of the gas at the adsorption temperature, v is the amount of gas adsorbed, v_m is the monolayer amount of gas adsorbed, and c is a BET constant defined by:

$$c = \exp\left(\frac{E_1 - E_L}{RT}\right) \quad \text{Equation 7}$$

in which E₁ is the heat of adsorption of the first layer and E_L is the heat of liquefaction of the gas molecule.

The total surface area of a solid can be determined by:

$$S_T = \frac{v_m N A_{cs}}{V} \quad \text{Equation 8}$$

where N is Avogadro's number, A_{cs} is the cross-sectional area of the adsorbed gas molecule, and V is the volume of the adsorbent gas.

The BET method works well for determining adsorption isotherms of gases and surface area of solids. The technique is performed at isothermal conditions with liquid nitrogen used for controlling the temperature, nitrogen as the adsorbing gas species, and partial pressures between 0-0.35 torr typically.

BET Surface Area Apparatus

The BET analyzer used for measuring the BET surface area of the selected zeolites was an AUTOSORB-1, shown in Figure 14. This device measure the quantity of gas adsorbed onto the solid surface at a specified equilibrium vapor pressure by the static volumetric method. The

data are obtained by admitting a known quantity of nitrogen gas into the sample cell with the sample maintained at a temperature below the critical temperature of the nitrogen.

The sample cell was initially weighed without a sample. The sample was loaded into the sample cell and the cell was weighed again. Since zeolites can be hygroscopic, the sample cell was loaded into an outgassing station. The outgassing station heated the sample at low pressure to remove and previously adsorbed molecules. Outgassing was done at 200°C at 0.05 mmHg for a minimum of two hours. After allowing the sample to cool back to room temperature, the sample was reweighed. The difference between the empty cell and the currently measured weight is the weight of the outgassed sample. The sample was then ready to be analyzed using the AUTOSORB-1.

Nitrogen was used as the adsorbing gas. The sample chamber and reference cell were cooled by liquid nitrogen to a constant temperature. The multipoint 11 point BET method was selected for the analysis in the AUTOSORB-1 software. The sample weight was entered and the process was automated from that point forward.

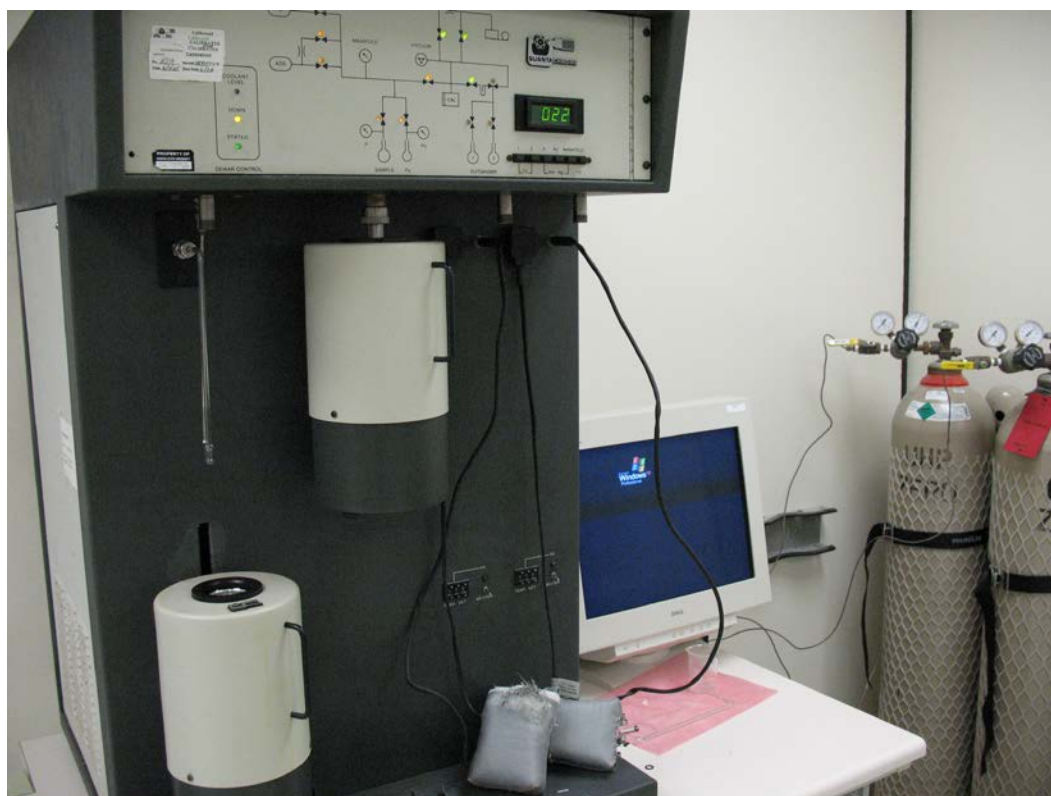


Figure 14 AUTOSORB-1 BET surface area analyzer

Gravimetric Microbalance

A gravimetric microbalance is a device for sensitively detecting mass changes. The basic technique is rather simple in nature. A sample is loaded onto a sample holder. The mass of the sample is then weighed. Then an adsorbing or absorbing species is introduced to the sample ideally in a pressure and temperature controlled environment. The weight of the sample will change as adsorption or absorption occurs with the solid phase.

Buoyancy corrections are taken into account when using a gravimetric microbalance. Buoyancy effects are often minimal, but can be particularly significant for measuring low adsorbing species. One method is to use a counterweight to offset the effects of the buoyancy of the sample and sorbing species may have. The counterweight is symmetric to the sample side.

Figure 15 below shows a schematic for how to account for buoyancy effects

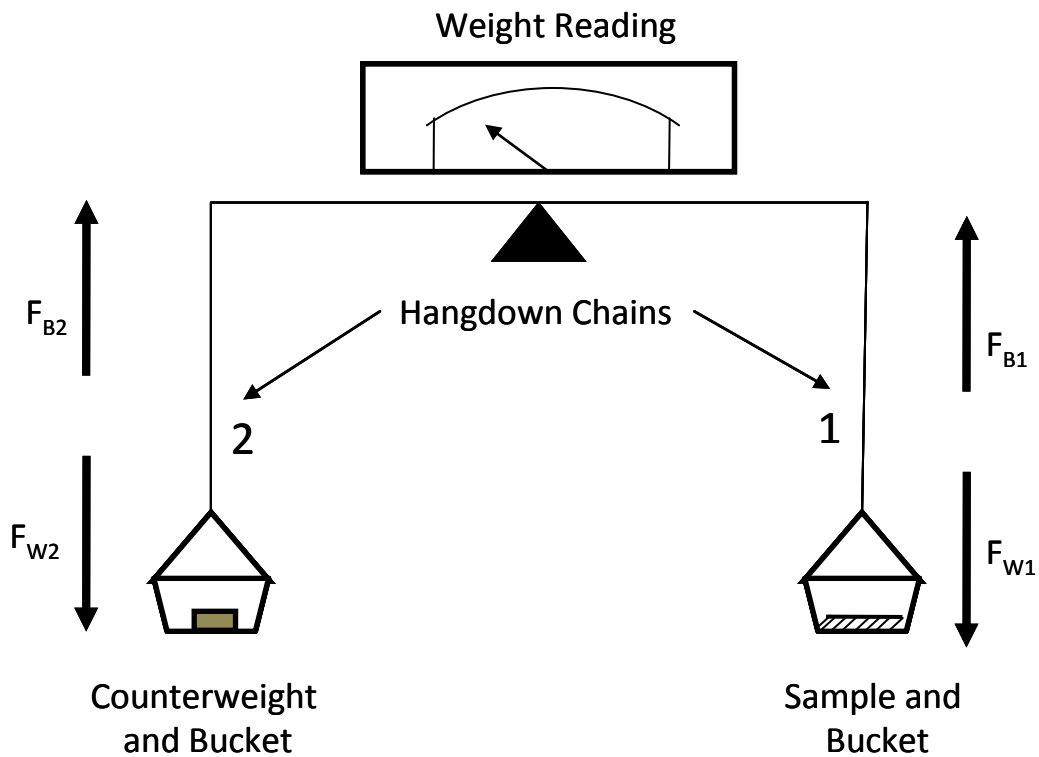


Figure 15 Schematic of buoyancy correction in gravimetric microbalance. Relevant forces and directions of the sample and counterweight side are shown. Adapted from Anthony.¹⁶⁸

Mathematically, the forces involved in the weight measurement are described by:

$$\Delta W = [F_{W1} - F_{W2}] - [F_{B1} - F_{B2}] \quad \text{Equation 9}$$

where the subscripts W denote the weight, the subscripts B denote the buoyancy, the subscripts 1 denote the sample side, 2 denotes the counterweight side, and ΔW is the overall weight change. Substituting in the appropriate relationships for the forces involved, Equation 12 can be rewritten as:

$$\Delta W = g(m_S + m_A + m_1 - m_C - m_2 - \rho_B(V_S + V_A + V_1 - V_C - V_2)) \quad \text{Equation 10}$$

where g is the gravitational constant, m_S is the sample mass, m_A is the mass adsorbed, m_1 is the mass of the sample holder components, m_C is the mass of the counterweight, m_2 is the mass of the counterweight components, ρ_B is the bulk gas density, V_S is the sample volume, V_A is the volume of gas adsorbed, V_1 is the volume of the sample balance components, V_C is the volume of the counterweight, and V_2 is the volume of the counterweight components. Before adding samples to the chamber, the instrument is tared, or zeroed. Assuming that the sample does not expand during adsorption and the volume of gas adsorbed has an insignificant role in buoyancy, the prior equation simplifies to:

$$\frac{\Delta W}{g} = m_A - \rho_B(V_S + V_1 - V_C - V_2) \quad \text{Equation 11}$$

Noting that the volume of the counterweight, the sample components, and counterweight components will remain constant regardless of the sample, the buoyancy term can be rewritten to solve for the mass adsorbed as:

$$m_A = \frac{\Delta W}{g} + \rho_B(V_S + V_0) \quad \text{Equation 12}$$

where V_0 is the combined volumes of the counterweight, counterweight components, and sample components.

The gravimetric microbalance can measure adsorption capacity by allowing equilibrium to be reached by monitoring the mass change over time. When the mass ceases to change, equilibrium has been reached at that point. Pressure and temperature regulation are also available. Proper outgassing of the sample is needed to ensure other molecules are not already adsorbed to the sample prior to analysis. This technique allows for monitoring of mass changes during outgassing as well.

This apparatus allows for one sample to be run at a time within the sample chamber. In order for a gas mixture to be introduced, the gas must be premixed or else the equipment will not be able to deliver the gas due to its valve setup. The user must also be aware of condensation

points of the adsorbing species. If at any point condensation occurs, measurements will be invalid. Finally, the equilibrium process may take an extended period of time to be reached. Some gases slowly adsorb onto solids, meaning that equilibrium will take multiple days or weeks in some cases to be reached.

Gravimetric Microbalance Apparatus

The instrument used in the adsorption equilibrium and initial uptake rate measurements was the Intelligent Gravimetric Analyser from Hiden Analytical. This device is a gravimetric microbalance which is capable of measuring adsorption isotherms using either vapors or gases. This equipment has been used to measure adsorption isotherms in previous work and a more detailed description of the device can be found elsewhere.¹⁶⁹ The gravimetric microbalance used is shown in Figure 16. This specific apparatus has temperature capabilities of -15 to 80°C (varies depending on bath fluid) using the water bath jacket and room temperature to 500°C using the furnace. There are three pressure transducers available 0 to 1 bar, 0 to 10 bar, and 0 to 20 bar.



Figure 16 Hiden ISO-200 gravimetric microbalance setup

Equilibrium Measurements

A schematic of the gravimetric microbalance apparatus is shown in Figure 17. The microbalance consists of a weighing mechanism with sample pan and counterweight which have been configured to minimize buoyancy effects in the system. A $1\mu\text{g}$ resolution is achieved with this device.

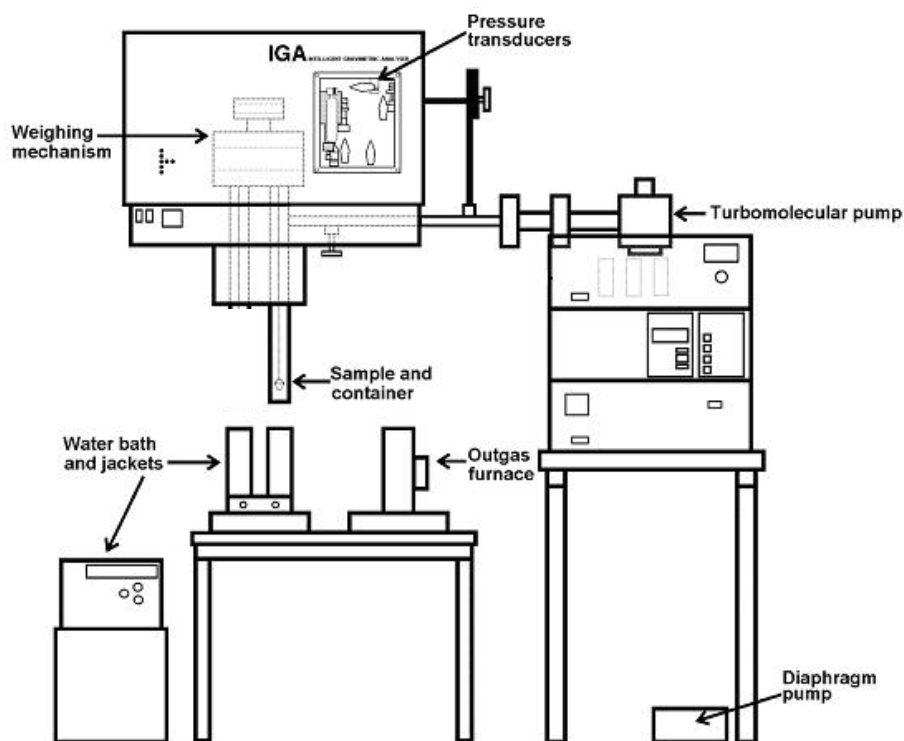


Figure 17 Schematic of gravimetric microbalance. Adapted from Anthony.¹⁶⁸

The sample buckets are attached to the weighing mechanism with gold hang down chains. The bucket used is conically-shaped and made of stainless steel. The same type of bucket is used on both the sample side and counterweight side of the apparatus. Samples were approximately 50 mg in weight.

After hanging the loaded sample bucket on the chain, the chamber was sealed using a copper gasket. The sample was dried and degassed under vacuum by using a diaphragm pump then evacuating the chamber with a turbomolecular pump to 10^{-8} bar. Samples were often heated to 100°C using an external furnace during the degassing/vacuum process. Once the mass

readings stabilized, the sample was considered fully degassed, and the adsorption experiments were ready to proceed. Adsorption experiments were completed at temperatures between 25-45°C.

During experiments, the sample chamber temperature was controlled using a water jacket and constant temperature bath. Once the set temperature was reached, vapor was introduced into the sample chamber through a leak valve until a specified pressure was reached. Pressures were maintained using a manometer. The pressure was maintained within 0.06% of the setpoint through control of the leak valve and exhaust valve. As the vapor entered the chamber, the sample mass increased as adsorption occurred into the sample. The weight change was monitored until the mass did not change appreciably for 30 minutes, after which the sample was considered to have reached equilibrium. This process was repeated to a set number of pressures until a maximum pressure was reached (90% of the saturation pressure at the given temperature) to produce an isotherm or if a single equilibrium point was desired the procedure was only run once. Although multiple pressure transducers were available to control the vapor pressure in the sample chamber, the pressures used were no greater than 200 mbar. This pressure was low enough to only require the use of a single transducer operating between 0-1 bar. After the completion of the adsorption, the sample was degassed and the initial mass was compared to the final mass to ensure desorption completion and no losses to the system had occurred.

Buoyancy corrections were also taken into consideration in these experiments. Accuracy in these measurements is important for vapors with low adsorption capacities. Buoyancy can be a large contributor in the measured weight change in the system at low sorption capacities. Buoyancy calculations are dependent on the volume of the balance components, volume of the sample, and density of the bulk vapor.

Since the density of all the vapors at the temperatures chosen is extremely low, the buoyancy correction term for the adsorption experiments is negligible as the influence was less than 1% of the error in the measurement.

Another important factor for making equilibrium measurements, was ensuring equilibrium had been reached. Sufficient time must be given for the vapor to diffuse into the pores of the zeolites. Since some molecules diffuse more slowly due to steric hindrances, molecular size, functional groups, and other inter/intramolecular forces, ample time must be given to reach equilibrium. The molecule 2-CEES requires over 300 hours to reach equilibrium

with zeolite 13X. So measuring an entire adsorption isotherm with this system, could take several months. Monitoring the weight change over time allows for determination of the time necessary to reach equilibrium by noting when the mass ceases to change by less than 1 μg .

Initial Uptake Rate Measurements

Initial uptake rate measurements were taken using the same equipment as in the previous section but examining the short-term kinetics of the system instead of the long-term equilibrium.

A sample was placed in the sample chamber, degassed, and brought to isothermal conditions as described in the previous section. Once the initial mass reached equilibrium, vapor was introduced into the sample chamber. Ideally, the vapor would be introduced into the sample chamber and would reach the specified pressure setpoint immediately. As this was not the case, the chamber was brought to its equilibrium pressure as quickly as possible by selection of thermodynamic equation of state in the equipment's software that properly described the vapor being introduced into the chamber. This feature in the software would communicate with controllers in the equipment allowing for timely volatilization of the vapor being used. In many cases, the desired pressure was around 10 mbar making the time necessary to reach a steady pressure rather short. Nonetheless, this was an important facet in making the initial uptake rate measurements.

Initial uptake rates were evaluated by examining the kinetic data received once an outgassed sample was introduced to a vapor. The outer surface area of the zeolite was exposed to the vapor an adsorption occurred at the surface limiting diffusion effects that would be seen later in equilibrium measurements. The amount of vapor adsorbed per mass of zeolite over time determined the initial uptake rate.

Quartz Crystal Microbalance

A quartz crystal microbalance (QCM) is a device that measures the mass of a deposited species onto the surface of a quartz crystal surface. The mass change is determined through a relationship between the frequency change in the crystal. This relationship was first recognized by Sauerbrey.¹⁷⁰ The simple equation has been used for many years and in many applications. Though some necessary modifications have been made for larger loadings specifically, the general form of the equation is shown below

$$\Delta f = -C_f \cdot \Delta m$$

Equation 13

where Δf is the frequency change of the crystal, C_f is the sensitivity factor of the crystal, and Δm is the mass change. The Sauerbrey equation assumed that the additional mass deposited on the crystal has the same acousto-elastic properties as quartz.¹⁷⁰ This assumption resulted in the sensitivity factor being a fundamental property of the QCM crystal. The sensitivity factor is defined as:

$$C_f = \frac{2n \cdot f^2}{\sqrt{\rho_q \cdot \mu_q}} \quad \text{Equation 14}$$

Where n is the number of the harmonic at which the crystal is driven, f is the fundamental resonant frequency of the crystal, ρ_q is the density of quartz, and μ_q is the piezoelectrically stiffened effective shear modulus of quartz. Inserting equation 17 into equation 16 and solving for the mass change results in:

$$\Delta m = \frac{(f_q - f) \cdot \sqrt{\rho_q \cdot \mu_q}}{2n \cdot f^2} \quad \text{Equation 15}$$

Where f_q is the resonant frequency of the unloaded crystal, f is the frequency of the loaded crystal, and all other symbols are as previously defined. Under the Sauerbrey assumptions, the change in frequency is a function of mass per unit area only. This means that the QCM does not require calibration. This does require that the Sauerbrey equation be only applied to uniform, rigid, thin films.¹⁷¹ Vacuum and gas phase thin film depositions which fail to fulfill these conditions exhibit a more complicated frequency-mass relationship and could require calibration in order to achieve accurate results.

The underlying assumptions with the Sauerbrey equation require specific conditions that must be strictly adhered to in order to achieve reliable results. Modifications to the Sauerbrey equation have been made to allow more flexibility to determining mass loadings onto a QCM. Lu and Lewis analyzed the loaded crystal as a one-dimensional composite resonator of quartz and the deposited film.¹⁷² The Z-Match equation accounts for situations where heavy loading onto the crystal occurs and significant deviations from the Sauerbrey equation arise. The Z-Match equation is shown below in Equation 19.

$$\Delta m = \left(\frac{N_q \cdot \rho_q}{\pi \cdot \sqrt{\frac{\rho_q \cdot \mu_q}{\rho_f \cdot \mu_f}} \cdot f} \right) \cdot \tan^{-1} \left[\sqrt{\frac{\rho_q \cdot \mu_q}{\rho_f \cdot \mu_f}} \cdot \tan \left[\pi \cdot \left(\frac{f_q - f}{f} \right) \right] \right] \quad \text{Equation 16}$$

where N_q is the frequency constant for an AT-cut quartz crystal, ρ_f is the density of the material, μ_q is the shear modulus of the film material, and all other constants are as previously defined. If the density and the shear modulus are identical to quartz, the Z-Match equation reduces back to the Sauerbrey equation.

The QCM apparatus consists of a quartz crystal resonator, a piezoelectric controller device, and processor. The quartz crystal resonator provides the frequency change as loading changes. The piezoelectric controller detects the frequency and resistance changes due to loading of the sample and the processor with software converts and outputs the results in terms of mass change.

The QCM is a very sensitive detector for measuring mass changes. It can detect mass changes to less than 10 ng/cm² under optimal conditions. Damaging the quartz crystal resonator and its electrodes and other hardware will reduce the sensitivity of the device. The electrodes cannot be scratched or measurements will be faulty. Washing with water is the only recommended procedure for cleaning crystals for reuse. One other limitation of this device is the operating temperature range. Temperature has a significant influence on the behavior of quartz resonant frequency, this requires the device to be used at room temperature ideally, with a recommended temperature range of 25-90°C only.

Quartz Crystal Microbalance Apparatus

The Quartz Crystal Microbalance (QCM) used in gas adsorption onto zeolites was a RQCM-200 from Inficon, Inc. This device has a software package for configuration of the RQCM-200, setup of multiple experiments, log data with real-time graphing, and review results from previous experiments.

The device has the ability to attach three detectors for gathering data from three crystals simultaneously. The system also has a phase lock oscillator circuit that provides measurement stability over a frequency range of 3.8 to 6.0 MHz. The circuit also incorporates adjustable crystal capacitance cancellation reducing the error caused by the capacitance of the crystal,

cable, and fixture. Capacitance cancellation is critical for accurate measurement involving soft films.

The essential components for accurate data collection are the crystals, the holders, and the flow cells. The AT-cut, 5 MHz, 1 inch diameter quartz crystal is used for its excellent mechanical and piezoelectric properties. The cut and size were chosen to allow for desired operating properties involving temperature and reducing frequency change due to mounting stress.

The electrodes on the quartz crystal enable frequency changes from the quartz crystal to be sent as electrical signals and converted to output. The electrodes are made of polished gold and the average surface roughness is less than 50 Å. High surface roughness can increase the apparent mass loading onto the crystal due to materials becoming trapped in surface pores. The figure below shows the electrode configuration on the crystals. The front electrode has an oversized diameter of ½ inch to ensure a more consistent deposition of material across the active area of the crystal. The back or rear electrode has ¼ inch diameter electrode. The exposed area of the front electrode is 137 mm² but the active oscillation region is limited to the overlapping area of the front and rear electrodes of 34.19 mm².

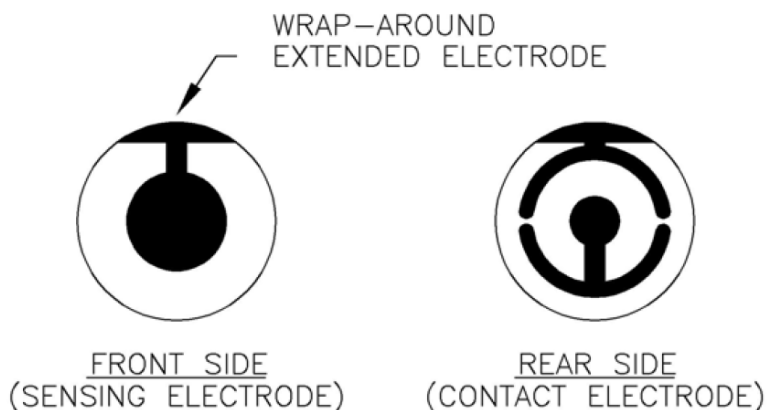


Figure 18 Inficon, Inc. quartz crystal electrode configuration

Proper handling of the crystals was essential to avoid damage and measurement errors. The crystals were only handled while wearing nitrile gloves. The crystals were cleaned with deionized water and dried using an air line, since it was recommended to not wipe of the crystals to avoid scratching the surface.

The crystal holders used had a cavity specifically designed for a 1 inch diameter crystal. Inside the cavity were two Pogo pins providing connections to the crystal's front and rear

electrodes. The Pogo pins are internally connected to a BNC connector via an internal coaxial cable.

Finally, the flow cell used was designed specifically for the Inficon series crystal holders. The FC-550 flow cell was made of Kynar®. The cell has two stainless steel inlet and outlet tubes with a 0.047" I.D. x 0.062" O.D. compatible with 0.062" I.D. tubing. A Viton® O-ring provided sealing between the cell and the face of the sensor crystal. Once installed in a probe, it created a flow chamber of approximately 0.1 mL.

Experimental Setup

For all adsorption experiments, the setup involved the use of the RQCM-200, data acquisition PC, one to three crystals, holders, and flow cells, a flow meter, a carrier gas, and sample injection port with appropriate connecting lines and tubes. A schematic of the overall system is shown in Figure 19.

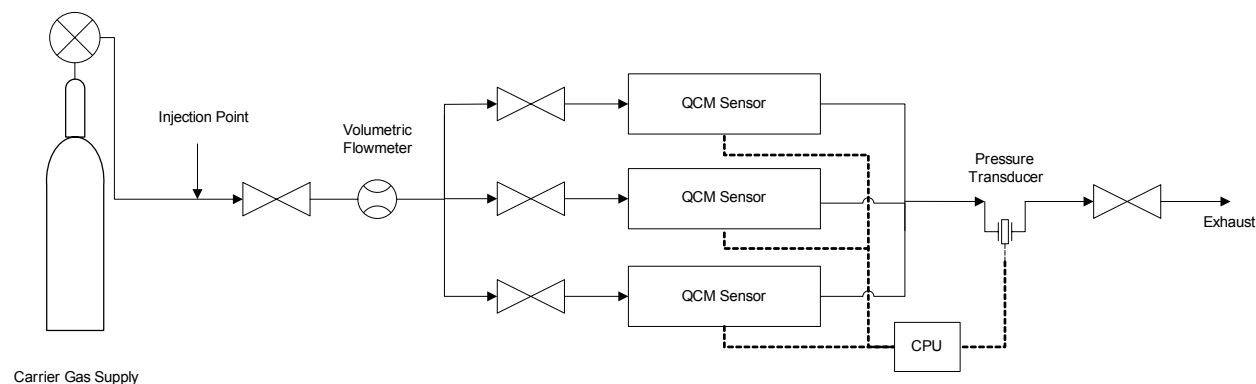


Figure 19 Setup used for QCM measurements

The carrier gas used was nitrogen. A sample injection port was located downstream from the carrier gas outlet. Samples were introduced using a syringe pump. A needle valve was used to regulate flow which was monitored by a volumetric flow meter. Stainless steel tubing was then split at a junction into three lines that could be opened or closed by individual ball valves. As the sample moved past the ball valves, it then entered the QCM sensor where measurements were taken and then exited the sample chamber where the gas or vapor exited the system. The pressure in the system was never greater than 5 psig due to crystal sensitivity requirements and system recommendations from Inficon, Inc.

Figure 20 shows the RQCM-200 used for adsorption measurements.

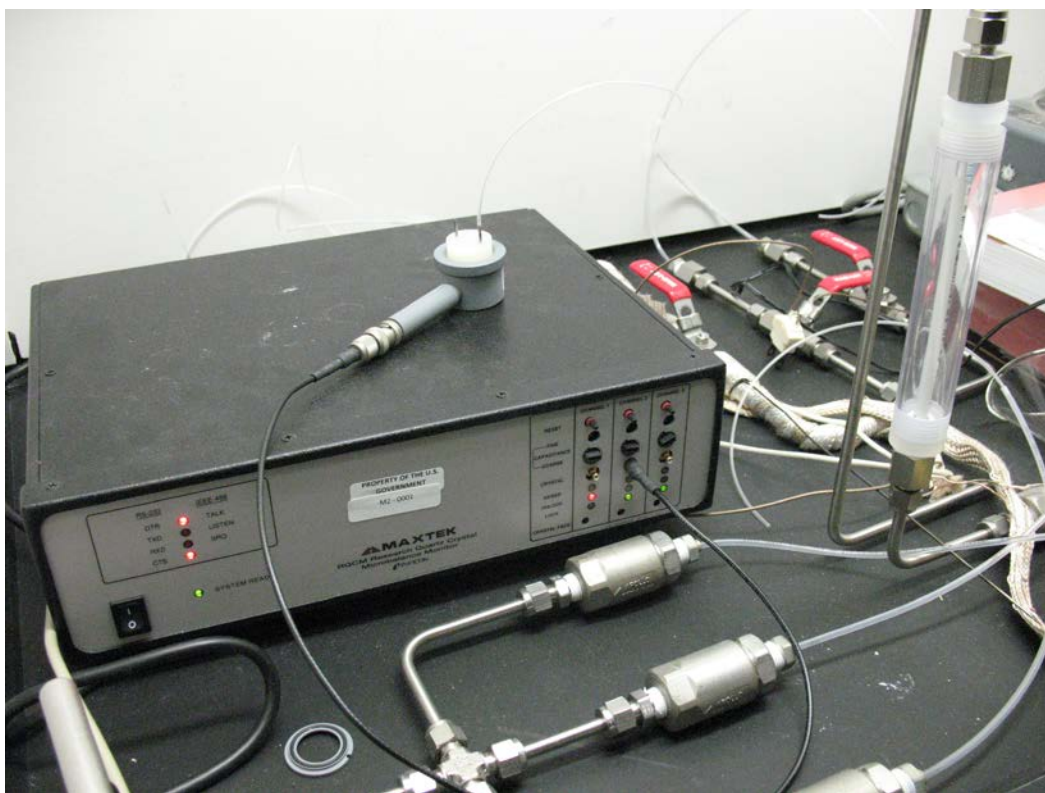


Figure 20 RQCM-200 apparatus

Thermogravimetric Analyzer

A thermogravimetric analyzer (TGA) is an instrument that measures mass changes of a sample with changing temperature. This means it is capable of determining the thermal stability of the sample as well as when sorbed materials begin to degrade or desorb.

The analysis is very dependent upon the precision of the weight, temperature, and temperature change measurements. The device will gradually raise the temperature of the sample and measure the change in weight. Commonly, weight loss curves appear very similar so additional analyses or transformations may be required before complete interpretation. Deconvolution software can be employed to determine when multiple compounds, molecules, and the like begin desorbing simultaneously. Derivative weight loss curves are typically helpful in determining the point at which weight loss is most apparent.

The analyzer usually consists of a sample pan made of platinum. The sample is loaded into electrically heated, well-insulated oven with a thermocouple to monitor the temperature

while a computer is used to control the heating. The system can be placed in an inert atmosphere limiting the oxidation effects or other undesired reactions.

The output from this device is a plot of the weight versus temperature curve. Software may be capable of curve smoothing to identify peak/troughs and points of inflection.

Other Techniques

Differential Scanning Calorimetry and Differential Thermal Analyzers (DTA) are often employed to study sorption and thermal stability of materials. DTA uses an inert reference with the sample and treats them to identical thermal cycles. The temperature differences between the sample and the reference are recorded. The differential temperature is plotted against temperature yielding a thermogram. Exothermic and endothermic changes can then be detected from the sample. DSC is similar to DTA. This analyzer uses a reference and sample and measure the amount of heat required to change the temperature of the sample and reference. The end result is similar to DTA in that a plot of heat input versus temperature results in a thermogram where exothermic and endothermic changes in the sample are noted. This technique works well when the reference has a very stable heat capacity over the range of temperatures studied. DSC is especially successful in determining phase transitions in samples.

CHAPTER 3 - Results – Aqueous Phase Ion Exchange

This chapter will explain the results from the aqueous phase ion exchange properties of zincosilicates VPI-7, VPI-9, and VPI-10. The capture capacities of single dissolved cationic species and the selectivity coefficients of the zincosilicates will also be examined.

Capture Capacities of Metals Using Zincosilicates

Experimental Procedure

The crystalline structure of the as-made or calcined zincosilicate was verified using x-ray diffraction, ensuring that the pore and channel structure of the material were still intact allowing for ion exchange to occur. Once crystallinity of the zincosilicate was verified, standard synthetic stock concentrations of mercury were prepared ranging between 20 and 20,000 ppm. The selected concentration range was based upon previously studied mercury-zeolite ion exchange systems. Previous mercury-zeolite systems have had concentrations ranging from 0-25,000 ppm with a pH range between 1-12.^{13, 45, 47-69} Mercury solutions were at pH of either 6 or contained a 5 wt% solution of nitric acid lowering the pH to less than 2. This was to ensure that complexes of mercury did not form and the divalent form of mercury was primarily present. The aqueous metal solution (approximately 15 mL) was added to a small sample (on the order of 0.15 g) of a zincosilicate, which yielded a volumetric ratio of zincosilicate to liquid of 0.1 g: 10 mL that was determined to be optimal in previous work.¹⁷³ The aqueous metal solution in contact with the zincosilicate sample was mixed under batch conditions for 2 to 12 hours.

After ion exchange, the zincosilicate sample was separated from solution using vacuum filtration. The solid sample was placed in a 50 °C oven for drying. The post-exchanged aqueous phase was analyzed for lead or mercury concentration within 24 hours using an atomic absorption spectrometer (Varian AA240). Mercury analysis was conducted using the VGA280 cold vapor generation accessory, and lead analysis was conducted using the GTA120 graphite furnace accessory. All solutions and reagents (lead (II) nitrate, mercury (II) chloride, nitric acid, stannous chloride, and hydrochloric acid) needed for atomic absorption analyses were purchased from Fisher Scientific. The structures of the dried solid samples following ion-exchange were

reexamined using an x-ray diffractor (Bruker AXS D8 Advance). A scanning electron microscope with an energy dispersion spectrometer (SEM-EDS) was used to analyze the heavy metal content in the post-exchanged zincosilicates (solid phase). This technique was used to confirm a mass balance for the heavy metal after ion exchange. Samples of the post-exchanged solid phase zincosilicates were also sent to Galbraith Laboratories, Inc. for elemental analysis of mercury, silicon, and zinc to confirm reliability in our experimental procedure.

Single Dissolved Species Cationic Exchange Results

The three tested zincosilicates VPI-7, VPI-9, and VPI-10 all successfully captured the heavy metals. Mercury concentrations were varied from 20 to 20,000 ppm and exchanges were performed at room temperature. Previous work from our group has reported lead capture capacities with VPI-7, VPI-9, and VPI-10.¹⁷³ In these studies, lead initial concentrations ranged between 100 to 20,000 ppm and exchanges were performed at 25 °C and 80 °C. In general, as the concentration of lead and mercury in the initial solution increased, the amount of ion exchange also increased. The two pH values tested on all zincosilicates yielded similar mercury capture capacity results with the tested zincosilicates, indicating that a deionized water solution or 5 wt% nitric acid solution does not significantly effect the mercury ion capture capacity.

Mercury and VPI-7

Figure 21 summarizes the results of mercury capture using VPI-7. As the initial concentration of mercury in solution increases, the amount of mercury removed by the zincosilicates increases. Up to 75% of available mercury was removed using VPI-7 and 2000 ppm HgCl₂ solution. Lesser amounts of available mercury were removed as the initial concentration of the heavy metal decreased.

The mercury to zinc ratio in VPI-7 was also determined. The results can be seen in Figure 21b. As mercury concentration increases the mercury to zinc ratio increases. One must note that at concentrations above 5025 ppm Hg, more mercury was in solution than what could theoretically be exchanged with the zincosilicate. A vertical line in Figure 21 is given for the maximum mercury concentration for which the zincosilicates could capture all mercury in solution in an ideal ion exchange in the VPI-7 and VPI-9 systems. This concentration was calculated so that the number of mercury atoms in equaled the number of zinc atoms in the zeolites, since an ideal and complete ion exchange would result in a Hg to Zn ratio of 1. At

concentrations of 20,000 ppm, a ratio of 0.8 Hg: 1 Zn was achieved. The calcined samples typically had slightly lower ratios than the as-made samples for each concentration. This is likely due to the contraction of the pores with the removal of water, since it was confirmed that there was no structure-directing agent remaining in the as-made samples prior to calcination. The calcined and as-made samples have apparent overlap in Figure 21.

After the ion exchange, the structure of VPI-7 was examined using XRD. The structure of VPI-7 was unchanged after ion exchange with mercury.

Mercury and VPI-9

Figure 23a shows the exchange capacity of mercury with VPI-9. At lower concentrations of mercury, nearly all the mercury was removed. An average of 98.6% of all mercury was removed when concentration was 20 ppm, 96.9% of all mercury was removed at 200 ppm, and 88.5% of 2000 ppm mercury was removed using VPI-9.

The mercury to zinc ratio was also considered in VPI-9. With increasing concentration, the mercury to zinc ratio increases and is presented in Figure 23b. The vertical line at 3730 ppm Hg indicates that more mercury was in solution than what could be theoretically ion exchanged with VPI-9. A ratio of 0.8:1 Hg:Zn is achieved with a theoretically supersaturated system of mercury. This indicates an equilibrium threshold for mercury/VPI-9 at room temperature. Calcined VPI-9, like VPI-7, also has a slightly lower exchange capability than its as-made structure. Many of the calcined and as-made sample points have very similar values in Figure 23 and appear to coincide.

Mercury and VPI-10

VPI-10 also has capacity for ion exchange with mercury as shown in Figure 25. For concentrations between 2000 and 20 ppm, 80-85% of available mercury was exchanged. Higher concentrations removed slightly less than the lower concentrations. VPI-10 typically became x-ray amorphous during ion exchange. Its framework is more open than either VPI-7 or VPI-9 making a structural collapse more likely than in the VPI-7 or VPI-9.

Comparison of Zincosilicates

Figure 26 shows the mean amount of mercury removed by each zincosilicate. VPI-9 has the highest capacity for mercury exchange followed by VPI-10 and VPI-7, respectively. VPI-9

captured greater than 90% of the ionic mercury available in an unsaturated solution. VPI-9 and VPI-10 typically captured greater than 80% and 70%, respectively. As concentration increases for each zincosilicate, the percentage of ionic mercury removed tended to decrease slightly.

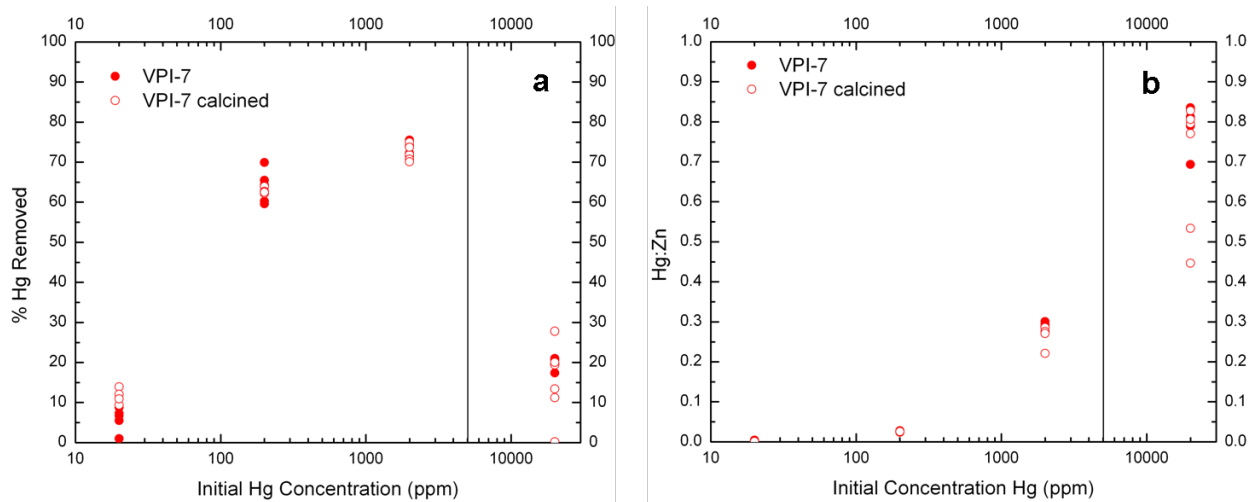


Figure 21 (a) Percentage of divalent mercury captured using zincosilicate VPI-7.
(b) Mercury to zinc ratio as function of initial concentration of mercury for VPI-7.
The vertical line at 5025 ppm represents the concentration of mercury in solution that is equal to the number of zinc sites.

Figure 22 shows a common form, known as a Barrer plot, for analyzing ion exchange isotherms. The isotherm represents the interdependence between ionic composition of two phases: the ion exchange material and the solution. The equivalent fraction is plotted on both axes and results in a dimensionless comparison between the phases. The 45° line denotes the preference for ion exchange. If points are above the 45°, the plot indicates that the exchanger has a preference for the ion of interest, in this case mercury. If the points lie below the 45° line, this means that ion of interest is most likely to be found in solution and not ion exchanged readily. Since the points mostly lie below the 45° line, VPI-7 is likely to ion exchange poorly and much of the mercury will remain in solution.

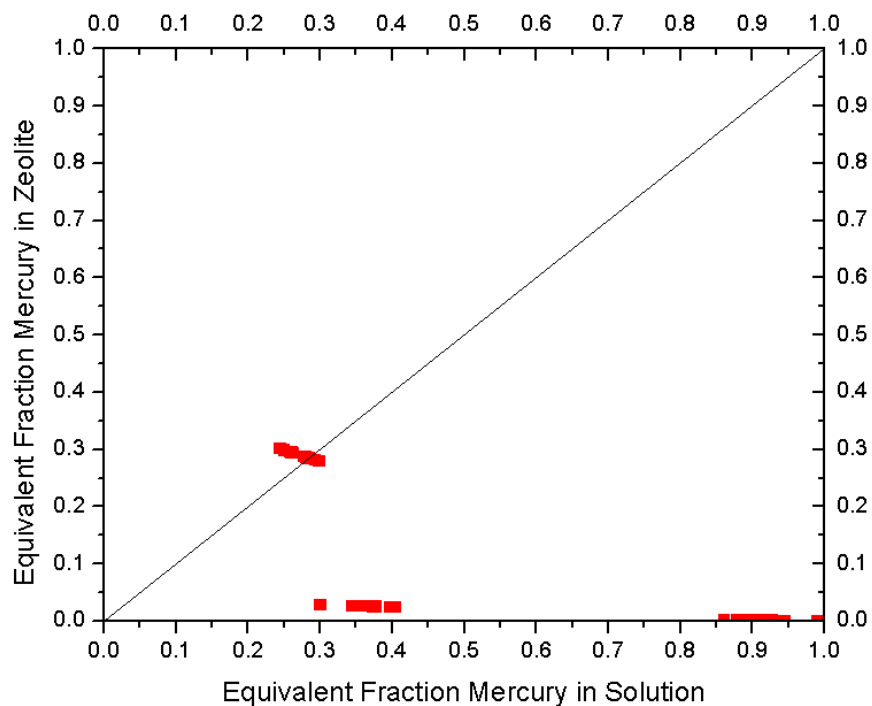


Figure 22 Ion Exchange Isotherm of Mercury onto VPI-7

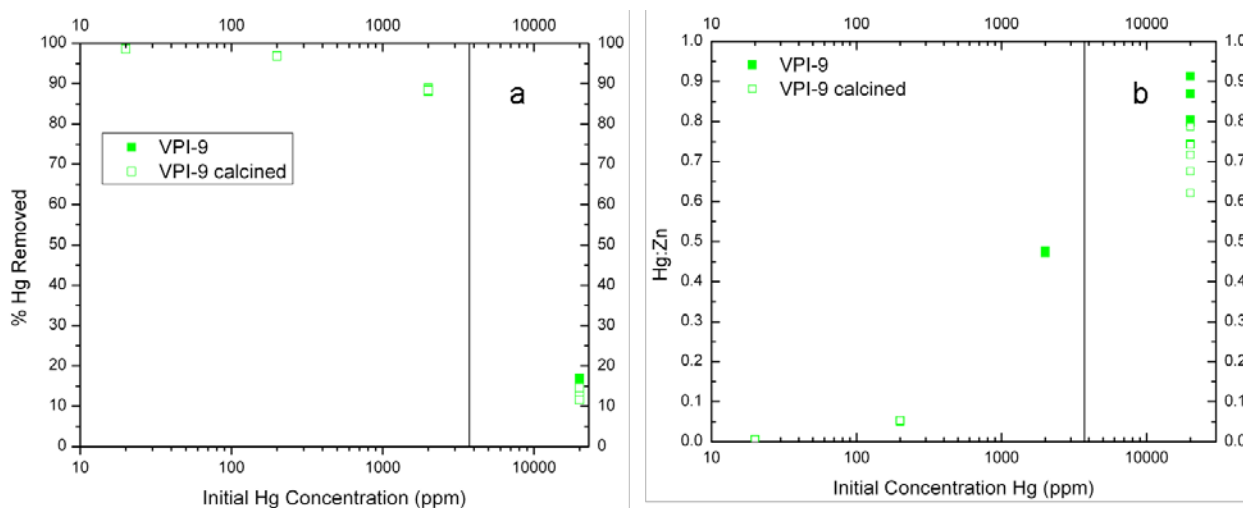


Figure 23 (a) Percentage of divalent mercury captured using zincosilicate VPI-9.
(b) Mercury to Zinc ratio as function of initial concentration of mercury for VPI-9.
The vertical line at 3730 ppm represents the concentration of mercury in solution that is equal to the number of zinc sites.

Figure 24 depicts a common ion exchange isotherm as previously described. Since the points lie above the 45° line, VPI-9 has a preference for exchanging mercury for the counterions in the zeolite, Rb^+ and K^+ .

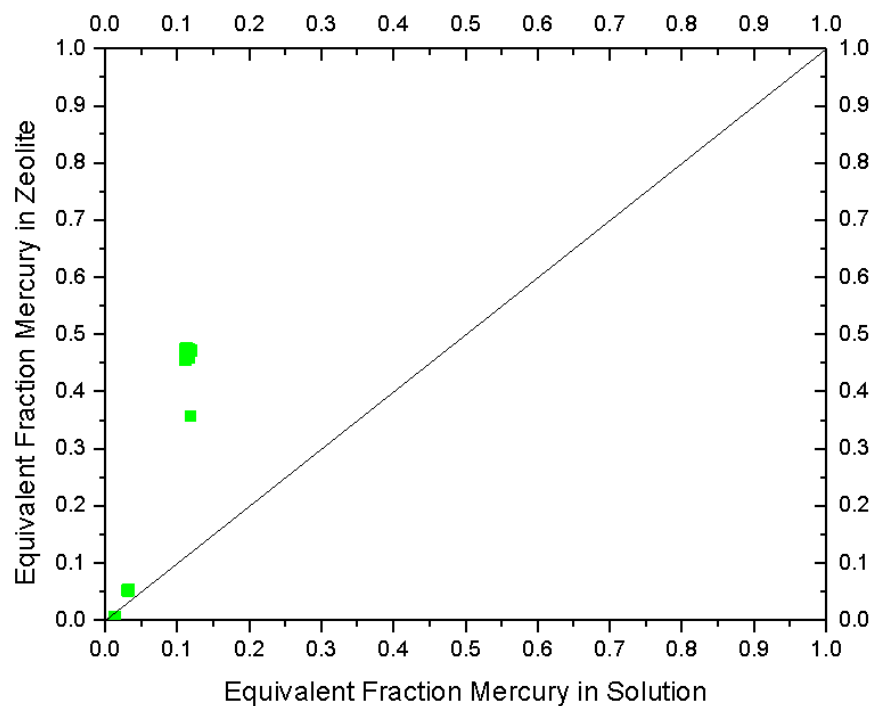


Figure 24 Ion Exchange Isotherm of Mercury onto VPI-9

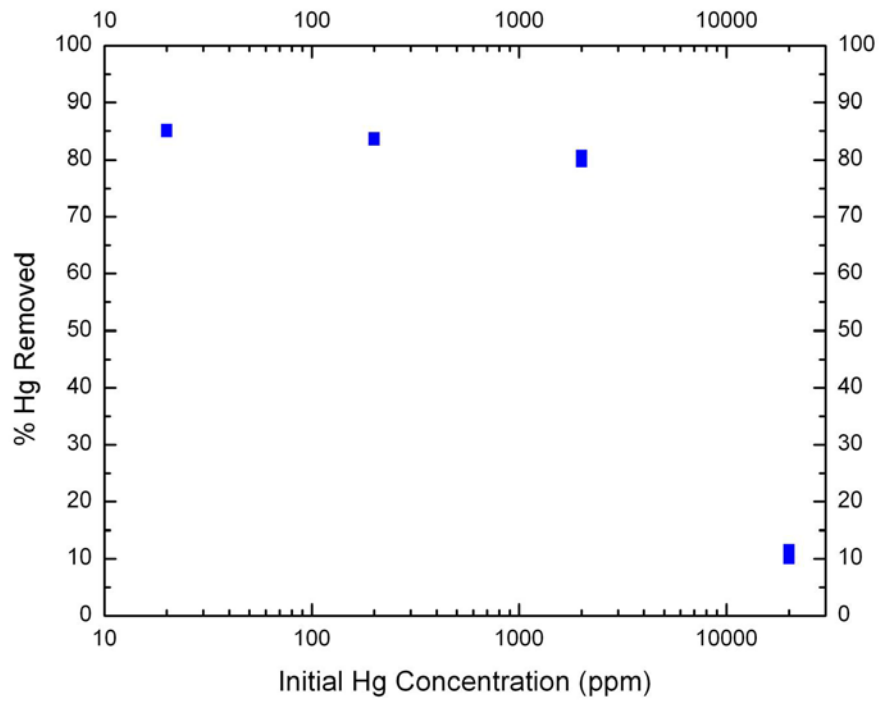


Figure 25 Percentage of divalent mercury captured using VPI-10.

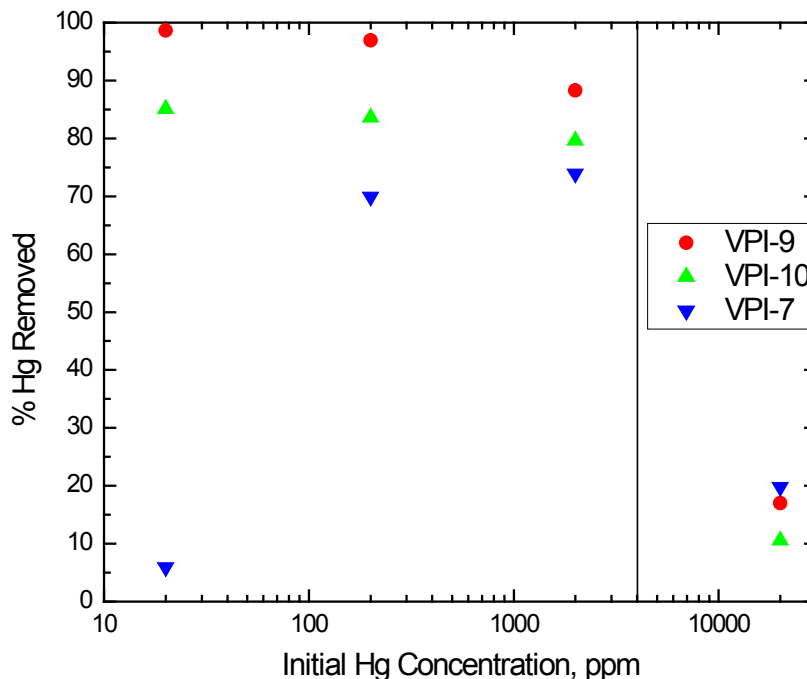


Figure 26 Average percentage mercury captured as function of initial concentration with each zincosilicate.

As-made Counteraction Influence on Capture Capacity

While VPI-7 has a simpler framework structure than VPI-9, VPI-9 has a higher capture capacity for mercury than VPI-7. There are several structural reasons why the higher capture of mercury by VPI-9 than VPI-7 seems counterintuitive. The pore channel network in VPI-7 is much less tortuous than in VPI-9.¹⁷⁴ The framework in VPI-9 has two periodic building units while VPI-7 has one.¹⁷⁴ VPI-7 has slightly larger pores (3.8x4.0 nm) than VPI-9 (3.5x3.6 nm). The two structures of VPI-7 and VPI-9 are shown in Figure 27 and Figure 28 for comparison. The composition of the hydrated sodium form of VPI-7 is $[\text{Na}_{32}(\text{H}_2\text{O})_{40}] [\text{Si}_{56}\text{Zn}_{16}\text{O}_{144}]$ while the composition of VPI-9 is $[\text{Rb}_{44}\text{K}_4(\text{H}_2\text{O})_{48}] [\text{Si}_{96}\text{Zn}_{24}\text{O}_{240}]$.¹⁷⁵ VPI-7 also has a slightly higher amount of zinc in its framework than VPI-9 as well, meaning that a relatively larger amount of cations are available for ion exchange with VPI-7 than in VPI-9. As stated previously, both zincosilicates lack cages around their counteractions allowing accessibility to all cations associated with the framework for ion exchange.

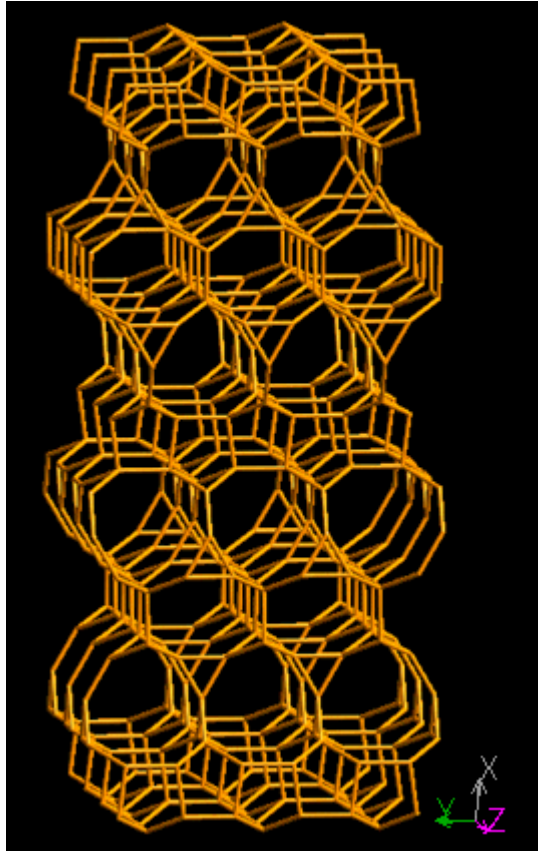


Figure 27 VPI-7 structure viewed along $[001]^{1/5}$

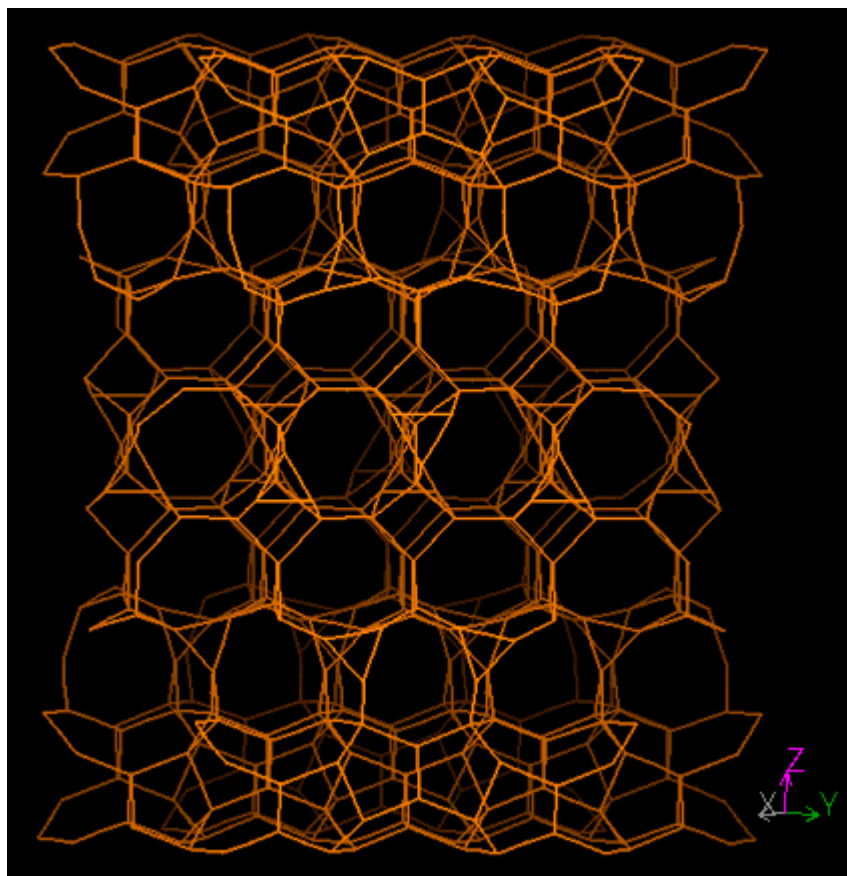


Figure 28 VPI-9 structure viewed along [110]¹⁷⁵

The framework, structure, pore sizes, higher zinc content were characteristics that all indicate a more favorable ion exchange in VPI-7 was likely. However, since VPI-9 had a higher uptake than VPI-7, the only major characteristic that favored ion exchange in VPI-9 was the different countercationic species. It was then hypothesized that the countercation presence in the as-made structure played the most crucial role in determining capture capacities between VPI-7 and VPI-9.

As-made VPI-7 contains countercations sodium and potassium within its framework whereas VPI-9 contains potassium and rubidium. As-made VPI-9 has nearly twice the capture capacity of as-made VPI-7. Sodium is present only in the as-made VPI-7, and the electronegativity on this cation is lower than that of potassium and rubidium. The energy required to separate two ionic species decreases as the ionic radius increases.¹⁷⁶ Since the cations are associated with the negatively charged zinc of the framework, sodium forms a stronger bond with the crystalline framework than does potassium or rubidium, making ion

exchange with sodium more difficult than with potassium than with rubidium. The influence of the counterions on ion exchange was further evaluated to evaluate the hypothesis.

An ion exchange with a high concentration sodium solution was performed with VPI-7 and VPI-9. This was an effort to ion exchange the potassium and rubidium from the interior of the zeolitic framework. Upon introducing the zincosilicates to sodium concentrations of 30,000 ppm, the zincosilicates, VPI-7 and VPI-9 were analyzed under EDS to determine the change in sodium within the framework. VPI-7 had its sodium concentration increase by 28% making 74% of its framework cations sodium. VPI-9 had sodium constitute 53% of its framework cations after the exchange. Once the ion exchange was completed, a second ion exchange was performed with mercury in conditions similar to those previously explained.

The mercury removal was then compared. The results from this can be seen in Figure 29 and Figure 30. The first figure shows the mercury to zinc ratio found after an ion exchange with mercury. The second figure shows the mercury to zinc ratio with the presence of sodium.

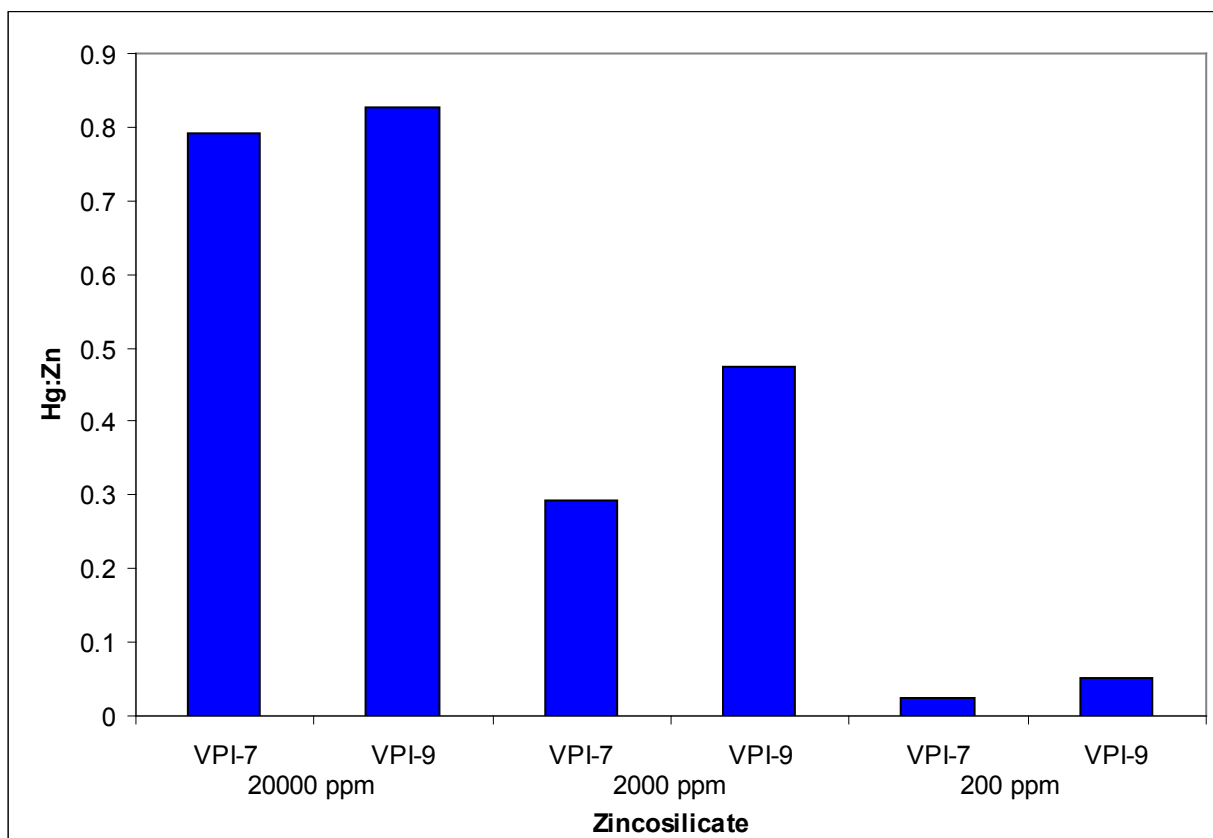


Figure 29 Mercury to zinc capture quantities for zincosilicates at initial concentrations above and below the maximum theoretical capture capacity

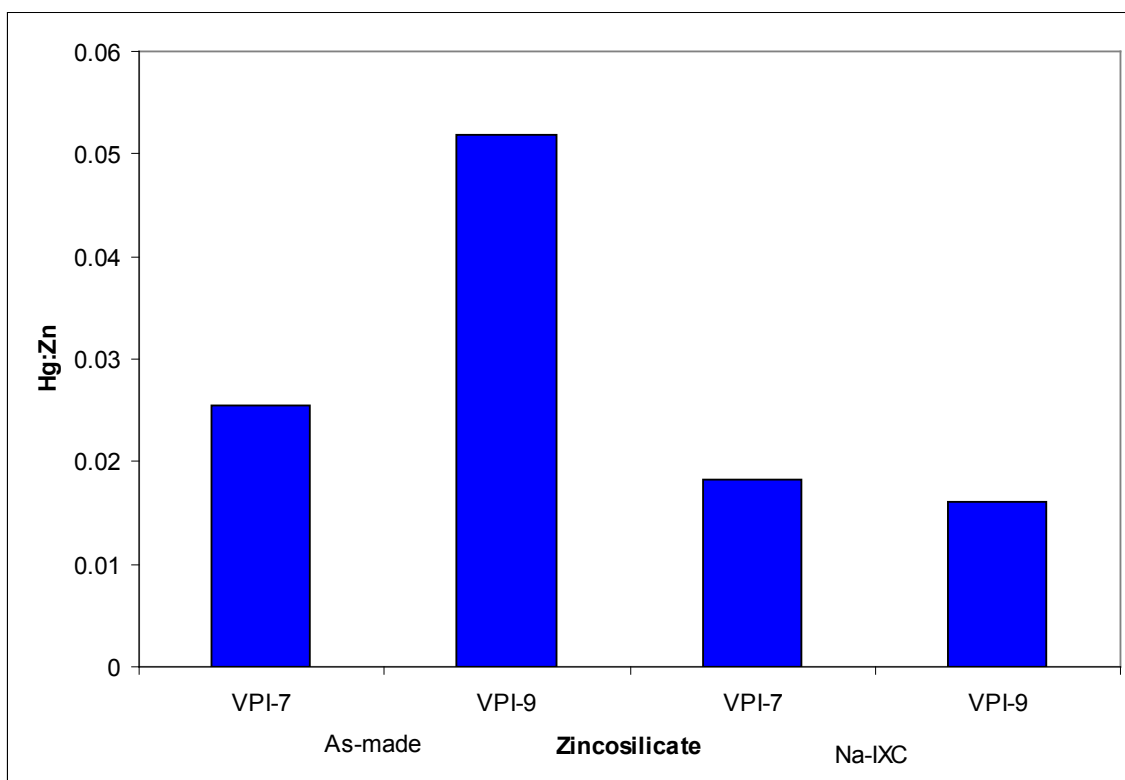


Figure 30 Heavy metal capture quantities with the presence of sodium at an initial mercury concentration of 200 ppm.

There is significant decrease in the amount of mercury taken up by VPI-9 after sodium has replaced the potassium and rubidium initially associated with its framework. Comparing mercury to zinc ratios found in the framework with initial concentrations of 200 ppm, the Hg :Zn ratio with VPI-7 was initially 0.0254. After the ion exchange with sodium, then following ion exchanging with mercury at 200 ppm, the Hg :Zn ratio reduces to 0.0182. Even more dramatic results are seen when evaluating VPI-9. VPI-9 initially has a Hg :Zn ratio of 0.0519; after exchanging with sodium then reevaluating the mercury capture capacity this value decreases to less than 0.016, clear evidence confirming that the larger pore, less tortuous pore channel network, and higher zinc content in VPI-7 would favor a higher capacity for exchange than VPI-9 if the initial counteranions were the same. However, the exchange capacity depends significantly on the properties of the framework counteranions.

Comparison to Mercury Capture by Other Sorbents

The mercury removal capacity of zincosilicates is higher than other common sorbents and exchangers reported in the literature. Typical mercury removal capacity for functionalized carbon sorbents ranged from 0.12-0.14 $\text{g}_{\text{Hg}}/\text{g}_{\text{sorbent}}$.⁴⁴⁻⁴⁶ These carbon sorbents were activated carbons or carbon fibers functionalized specifically for mercury removal impregnated with sulfur.

Mercury removal for zeolites ranges from 0.14-0.17 $\text{g}_{\text{Hg}}/\text{g}_{\text{zeolite}}$.⁶⁶⁻⁶⁹ Natural or unmodified zeolites captured between 0.14-0.15 $\text{g}_{\text{Hg}}/\text{g}_{\text{zeolite}}$ while modified or functionalized zeolites captured between 0.15-0.17 $\text{g}_{\text{Hg}}/\text{g}_{\text{zeolite}}$. The modified zeolites were functionalized through insertion of metals or by adding organic compounds into the pore framework to increase mercury removal.

Functionalized silicas can remove 0.13-0.17 $\text{g}_{\text{Hg}}/\text{g}_{\text{sorbent}}$.^{86-92, 177} The silica materials used were amorphous mesoporous to microporous silica. The silica was functionalized with an organic compound containing either a mercapto, thiol, or sulfur functional group to specifically remove mercury. In one study, multiple functional groups were available in the functionalized additive in order to increase mercury uptake.⁸⁹

VPI-7, VPI-9, and VPI-10 can remove 0.31, 0.38, and 0.21 $\text{g}_{\text{Hg}}/\text{g}_{\text{zincosilicate}}$, respectively. These zincosilicates, VPI-7, VPI-9, and VPI-10, were non-functionalized and were able to capture significantly more mercury than other sorbents that were functionalized specifically for mercury removal.

Comparison to Capture of Lead by the Zincosilicates

The results from McGown examined lead capture using VPI-7, VPI-9, and VPI-10.¹⁷³ As the initial lead concentration increases from ~300 ppm to 1000 ppm, the percent of lead exchanged tends to decrease. This is expected as either equilibrium is achieved in higher concentrations or accessibility to remaining ions is nearly or completely impeded. VPI-7 removed no less than 60% of lead in 1000 ppm initial concentration of lead.

A theoretically complete exchange would involve one (1) lead ion per one (1) zinc anion in the zincosilicate framework. As the initial concentration of lead increases, the ratio of lead to zinc increases.

For concentrations between 300 and 1000 ppm of lead, 9.5 to 17.5% of the lead in solution was removed using VPI-9.¹⁷³

7.5 to 17.5% of the lead in solution was removed using VPI-10. An x-ray amorphous VPI-10 structure was observed in 25% of the lead ion exchanges.

Mercury vs. Lead

While the zincosilicates, VPI-7, VPI-9, and VPI-10 successfully captured both lead and mercury, one significant difference in the results were observed. The primary difference between the capture of mercury and lead in the zincosilicates is the amount of heavy metal captured. Mercury is typically captured in greater percentage amounts than lead in VPI-7, VPI-9, and VPI-10.

Structure

The VPI-9 structure may have collapsed during ion exchange implied by its amorphous x-ray diffraction pattern, but its structural framework has been shown to contract and expand under various conditions. If contraction occurred, its structure would be regenerable as stated by Annen 1992.¹⁵⁰ McGown showed that although the x-ray pattern indicated an amorphous structure, IR data showed the structure to still be intact. This indicates that the lead introduced into the structure was absorbing x-rays leading to the amorphous x-ray pattern.

Regeneration

A secondary ion exchange was completed in order to regenerate the structure of the zincosilicates and reverse the initial ion exchange of the heavy metals. Attempts were made to reintroduce potassium ions back into the structure of VPI-7 and VPI-9. High concentrations (20,000ppm) of KCl were added to lead-zincosilicate structures that had become x-ray amorphous. After exposing the lead-zincosilicate amorphous structures to the KCl solution for up to ten hours at room temperature, the solid phase was recollected and examined under both XRD and EDS techniques described previously. It was found that the amount of lead did not decrease in the solid phase to regenerate the initial zincosilicate structure. This indicates that the binding of the heavy metal to the framework is quite strong. The concentration of KCl could be further increased to regenerate the materials.

Selectivities Between Cationic Species

While zincosilicates have a capture capability for single species in aqueous systems, practical systems will have multiple competing ions present. This leads to an investigation involving the understanding of the preferences the zincosilicates have for one ionic species over another. A study was performed to quantify the selectivity of some common ionic species with lead and mercury with zincosilicates VPI-7 and VPI-9.

Cationic Selectivity

The previous results examine the capture capacity of zincosilicates in the presence of a single ion in each ion exchange, practical systems will have multiple cationic species present. The following section examines the development of a model for determining the selectivity coefficient of cationic species when using zincosilicates VPI-7 and VPI-9.

Gibbs-Donnan Selectivity Model

While there have been a number of attempts and successes to model ion exchange equilibria, Helfferich thoroughly explains the theoretical approach to modeling ion exchange. One such model that successfully explains and predicts ion exchange equilibria in zeolitic materials is the Gibbs-Donnan Selectivity model.¹¹³ This model requires the treatment of the ion exchange resin to be a charged matrix that is permeable to dissolved electrolytes and its solvent. When equilibrated with solvent, the solvent moves into the resin, or charged matrix, in this case, the zincosilicate. Theoretically, the matrix is thought of as a flexible matrix comprised of a network of elastic springs which exert pressure on the inner pore liquid of the matrix until the chemical potential of the solvent in both the liquid and solid resin matrix is equal. In order to simplify this requirement, it is assumed that the chemical potential in an isothermal system can be split into two additive terms, one that is pressure dependent and the other is composition dependent.¹¹³

With the assumptions comes the mathematical development of the model. Thermodynamically speaking, the equations listed below are the conditions that are required and assumed. The chemical potential and activity expressions are:

$$\bar{\mu}_s = \mu_s$$

Equation 17

and

$$RT \cdot \ln \bar{a}_s + \bar{P} \cdot \bar{V}_s = RT \cdot \ln a_s + P \cdot V_s \quad \text{Equation 18}$$

where α_s and V_s represent the activity and partial molal volume of the solvent, P is the pressure exerted on the solvent and the bar above denotes the solid phase while symbols without the bar denote the liquid phase. Since V can be assumed to be independent of pressure without introduction of serious error, Equation 21 can be rewritten as:

$$RT \cdot \ln \bar{a}_s + \pi \cdot \bar{V}_s = RT \cdot \ln a_s \quad \text{Equation 19}$$

where π is pressure difference between the interior solid phase and the external solution.

The ion exchange process is described by:



leading to the following expression derived for the concentration distribution of monovalent-monovalent ions at equilibrium.

$$RT \frac{\bar{m}_N m_M}{m_M m_N} = RT \cdot \ln K_M^N = \pi(V_M - V_N) + RT \cdot \ln \frac{\bar{\gamma}_M}{\gamma_N} - 2RT \cdot \ln \frac{\gamma_{\pm MX}}{\gamma_{\pm NX}} \quad \text{Equation 21}$$

For monovalent-divalent and divalent-divalent systems, the equations are,

$$RT \frac{(\bar{m}_N)^2 m_M}{m_M (m_N)^2} = RT \cdot \ln K_M^N = \pi(V_M - 2V_N) + RT \cdot \ln \frac{\bar{\gamma}_M}{(\gamma_N)^2} - RT \cdot \ln \frac{(\gamma_{\pm MX2})^3}{(\gamma_{\pm NX})^4} \quad \text{Equation 22}$$

and

$$RT \frac{\bar{m}_N m_M}{m_M m_N} = RT \cdot \ln K_M^N = \pi(V_M - V_N) + RT \cdot \ln \frac{\bar{\gamma}_M}{\gamma_N} - 3RT \cdot \ln \frac{(\gamma_{\pm MX2})}{(\gamma_{\pm NX})} \quad \text{Equation 23}$$

respectively. In these equations K is the experimentally determined selectivity coefficient, N is the cationic species going into the solid phase, M represents the cationic species being

exchanged from the solid phase, m is the molal concentration of the species, $\bar{\gamma}$ is the activity coefficient of the ion in the solid phase and γ_{\pm} is the mean molal activity coefficient of the

electrolyte in the external solution. In these expressions, only π and $\frac{\bar{\gamma}_M}{\gamma_N}$ are not readily

available in literature. The partial molal volume of the ions at infinite dilution and the mean

molal activity coefficients of the simple electrolytes can be obtained from literature while the selectivity coefficient is determined experimentally. However, due to the rigidity of the zeolite material and the constant solvent uptake over the activity range the activity coefficient ratio of the solid phase will remain constant and independent of the ionic strength of the external solution. The pressure difference term, π , is calculable as a function of solvent activity with Equation 22 since the activity of water in the solid phase is a constant in the system.

Selectivity Results

ASPEN software was used to approximate the ionic activity coefficients of the dissolved metal salts in water using an NRTL model. The ratio of these numbers almost always approached identical values for metal salts with the same valency ratio since the ionic strength of the dissolved salts was rather low (<0.05 total molality). Another method that can be employed is the use of the Debye-Huckel equation for approximating this value and that works well at low ionic strengths. The Debye-Huckel equation is:

$$-\log_{10} \gamma_{\pm} = \frac{A \cdot z^2 \cdot \sqrt{I}}{1 + \sqrt{I}} \quad \text{Equation 24}$$

where γ_{\pm} is the mean activity coefficient, A is a solvent constant, z is the charge on the cation, and I is the ionic strength of the solution.

Table 5 Activity coefficients of selected ions at 0.025 M.

System	ASPEN activity coefficient first cation	ASPEN activity coefficient second cation	Debye-Huckel activity coefficient first cation	Debye-Huckel activity coefficient second cation	ASPEN activity coefficient ratio	Debye-Huckel activity coefficient ratio
Pb:Hg	0.2900	0.2899	0.3229	0.3229	1.0003	1.0000
Pb:Na	0.3435	0.7683	0.3903	0.7904	0.4471	0.4938
Pb:K	0.3436	0.7666	0.3903	0.7904	0.4482	0.4938
Pb:Ca	0.2799	0.2719	0.3229	0.3229	1.0294	1.0000
Hg:Na	0.3436	0.7684	0.3903	0.7904	0.4472	0.4938
Hg:K	0.3438	0.7667	0.3903	0.7904	0.4484	0.4938
Hg:Ca	0.2800	0.2720	0.3229	0.3229	1.0294	1.0000

The Gibbs-Donnan Model allows for the determination of the $\frac{\gamma_M}{\gamma_N}$ term without resorting to finding the activity of H₂O in the solid zeolite phase. By measuring the selectivity of the system at one point with one metal in trace amounts, the determination of the

$\pi(V_M - V_N) + RT \cdot \ln \frac{\gamma_M}{\gamma_N}$ terms can be found with application of the Harned-Cooke relationship.

This relationship finds the activity of a metal at trace concentrations in the presence of another metal at much higher concentrations while being dependent only on the concentration of the second metal and the activity of the pure metal that is in present in trace amounts. Other physical constants in the Harned-Cooke equation are available in the literature.¹⁷⁸ It must be noted that as the ionic molar volume of the species coincide, the pressure term disappears. But it also must be noted that the pressure difference has been found to influence this calculation by no more than 2% in most cases when modeling ion exchange with zeolites.¹⁷⁹

The following conditions were applied while taking into consideration the selected governing Gibbs-Donnan model and its underlying assumptions and criteria. The solubility of lead chloride played an important role in the total achievable molarity in the solution. Although other forms of lead salts are available, the chloride form was chosen to reduce effects and possible precipitation and reaction of other species in the selectivity experiments. While investigating the selectivity of lead compared to other species, the initial molarity was not higher than 0.025 M for either species resulting in a total molarity of 0.05 for the solution. Salts were dissolved in 1:1 ratio for the experimental conditions. Higher concentrations of salts can be used for salts with higher solubilities. For example, mercury chloride has a solubility of 7.4 g/100 mL whereas lead chloride is only 0.99 g/100 mL. Zincosilicates, VPI-7 and VPI-9, were chosen as the ion exchange resins to be studied. The electrolyte solution was added to zincosilicates at a ratio of 0.1 g_{zeolite}/10 mL_{solution}. This ratio was constant for all trials. In most trials, the amount of zincosilicate used was approximately 0.15 g and the amount of solution used was approximately 15 mL.

The table below shows the experimental results and Gibbs-Donnan predicted values for selectivity coefficients for divalent heavy metals lead and mercury, common monovalent metals found in water such as sodium and potassium, and one divalent metal, calcium between zincosilicate materials as-made VPI-7 and as-made VPI-9. Calcium, lead, potassium, and sodium concentrations of the liquid phase were determined using the AAS graphite furnace using conditions as previously described in Chapter 2; the mercury concentration of the liquid phase was analyzed with the cold vapor generation accessory on the AAS.

Table 6 Selectivity coefficients of cationic species with VPI-7

Cations	Experimental Selectivity	Model Selectivity
Pb:Hg	2.31	2.57
Pb:Na	2.07	1.99
Pb:K	3.82	3.77
Pb:Ca	4.02	3.88
Hg:Na	0.79	0.89
Hg:K	1.46	1.67
Hg:Ca	1.13	1.10

Table 7 Selectivity coefficients of cationic species with VPI-9

Cations	Experimental Selectivity	Model Selectivity
Pb:Hg	3.40	3.58
Pb:Na	2.91	2.86
Pb:K	4.27	4.19
Pb:Ca	4.45	4.33
Hg:Na	0.08	0.11
Hg:K	1.88	2.06
Hg:Ca	1.08	1.15

Based upon the results found from the binary cationic exchange systems examined using zincosilicates VPI-7 and VPI-9, the Gibbs-Donnan model works well for describing the selectivity coefficients in the process. The experimental values and theoretical values are all within 12.5% agreement. The model accurately predicts the selectivity coefficients of binary cationic systems in zincosilicates, indicating the assumptions incorporated in the development of the model are applicable for describing ion exchange selectivity in zincosilicates VPI-7 and VPI-9.

For the zincosilicates examined and modeled, the preference or selectivity of the cations studied is $Pb > Na > Hg > K > Ca$. Other zeolite systems have seen similar results when examining the selectivity coefficient of the alkali and alkaline metals.¹⁸⁰ Selectivity in these systems were $Na > K > Ca$; a trend followed in this study as well. Selectivity coefficients with heavy metals have been examined as well. Other studies have shown that the selectivity trend is $Pb > Hg$ and with selectivity coefficients of similar magnitude, consistent with these results.¹⁵² While the selectivity coefficients between the two zincosilicates is different for each species, the overall trend for each cation is the same in both VPI-7 and VPI-9.

Mercury-Zincosilicate Exchange Energies

Ion exchange energies of mercury were examined using as-made zincosilicates, VPI-7 and VPI-9. The ion exchange energies for these materials were calculated using the van't Hoff equation which relates the change in equilibrium of a process as temperature changes.

$$\ln\left(\frac{K_2}{K_1}\right) = \frac{\Delta H}{R} \cdot \left(\frac{1}{T_1} - \frac{1}{T_2}\right) \quad \text{Equation 25}$$

where K_2 is the amount of mercury removed at absolute temperature T_2 , K_1 is the amount of mercury removed at absolute temperature T_1 , ΔH is the enthalpy of the process and R is the universal gas constant.

The previously described procedure for mercury ion exchange was used at several system temperatures to find the exchange energies of VPI-7 and VPI-9. The amount of mercury exchanged was evaluated at 25, 40, 50, and 70°C. A plot of the natural logarithm of the amount exchanged versus the inverse of the absolute temperature of the exchange is shown in Figure 31 and Figure 32. A linear regression technique was employed to linearize the data points in order to determine the slope, which according to the van't Hoff model yields the value of the exchange energy divided by the universal gas constant.

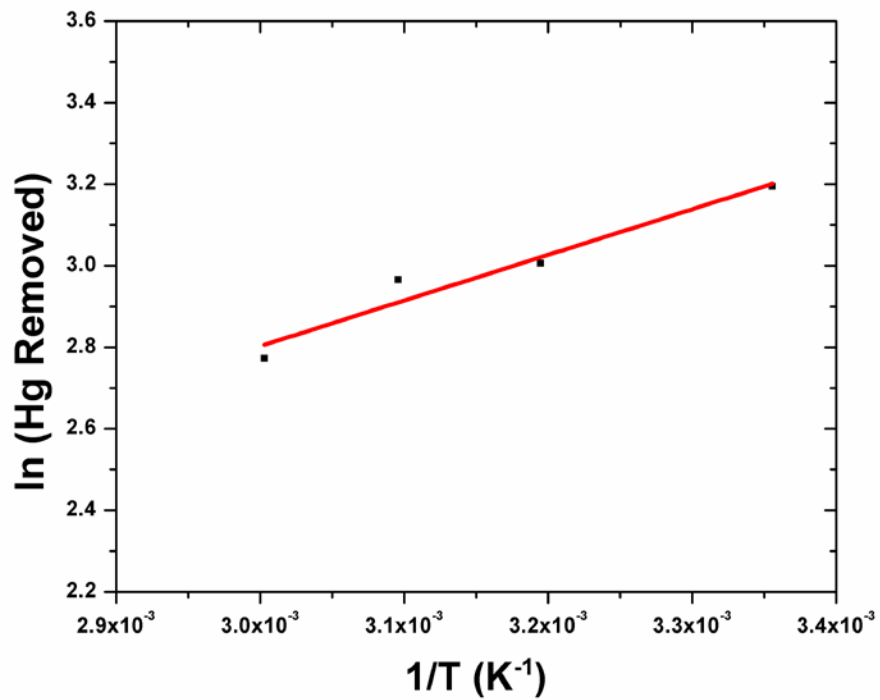


Figure 31 Linearized plot to determine exchange energy in VPI-7

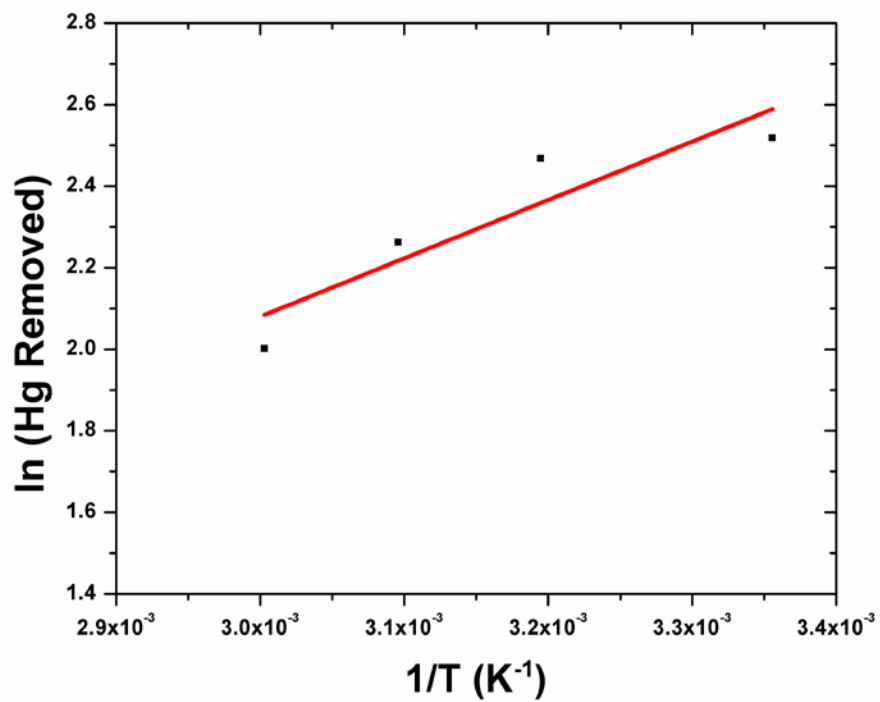


Figure 32 Linearized plot to determine the exchange energy of VPI-9

The exchange energy of VPI-7 and VPI-9 with divalent mercury are 271 and 693 J/mol, respectively. These values are lower than exchange energies for other zeolitic materials and divalent ions. A zinc ion exchange with zeolite 4A was reported to have an ion exchange energy of 2340 J/mol.¹⁸¹ A lead exchange with 13X reported 1070 J/mol exchange energy.⁵⁷ While the exchange energy for mercury was lower than other reported values for zeolites, this value seems appropriate. Mercury is typically rather difficult to capture, making the energy release for exchange lower. Functionalization of materials will increase the exchange energy, which indicates a more thermodynamically favorable process. The zincosilicates examined still have a higher capacity for mercury than other sorbents that are functionalized specifically to capture mercury meaning that VPI-7 and VPI-9 have a more thermodynamically favorable process in comparison to those mercury exchange systems. However, the values found were lower than some systems with other non-mercuric cationic species, indicating that the mercury exchange is a thermodynamically less favorable process in comparison to ion exchange with those cationic metals.

Ion exchange is the primary process occurring in the zincosilicates to capture the heavy metals. This was determined because the experiments do not capture more than the theoretical maximum for ion exchange. While this does not exclude adsorption from occurring, it does support the ion exchange process. A decrease in the native countercationic species is noticed when analyzing the solid sample after experimentation, indicating that sodium, potassium, or rubidium species have been removed, meaning ion exchange is occurring. Also, the post-exchanged x-ray diffraction patterns suggest that a slight structural change has occurred due to the exchange. Typically the peaks in the post-exchange patterns are shifted with no extra peaks in our system.

CHAPTER 4 - Results – Gas Phase Adsorption

This chapter describes the results from the adsorption of chemical warfare simulants onto zeolites. The results from both a gravimetric microbalance and QCM are compared in order to evaluate the viability of using a QCM with multiple zeolites and sorbates as a molecular sensing device

Adsorption of Chemical Warfare and Explosive Simulants

Gravimetric Microbalance Results

Equilibrium Capacities

Equilibrium adsorption measurements were taken using selected zeolite-simulant mixtures. The vapor generation chamber was loaded with an adsorbate liquid, and the sample bucket loaded with a sample of zeolite (~50 mg). The sample chamber was then evacuated and heated for a period of time to remove anything adsorbed to zeolite surface and the contents in the sample bucket were recorded as the initial adsorbent weight. The software was then initiated for the sample chamber to begin to become pressurized with the vapor to the specified value. Vapor pressures were chosen not to exceed 90% of the expected saturation pressure at the experimental temperature to ensure that no condensation would occur during the measurement. For example, the vapor pressure of ethanol at 45°C is 231 mbar, so an adsorption vapor pressure of 208 mbar or less was used in order to avoid condensation of ethanol in the sample chamber.

Table 8 shows the chosen adsorbates, the calculated vapor pressure of the target adsorbate, and the chosen adsorption vapor pressure for all equilibrium.

Table 8 List of simulants, simulant vapor pressure, and maximum experimental pressure used in order to avoid condensation of the simulant within the experimental chamber during adsorption

Simulant	Vapor Pressure @45C (mbar)	Maximum Experimental Pressure (mbar)
n-butanethiol	152.5	125
2-CEES	17.3	14
DMMP	114.6	100
ethanol	267.9	200

Equilibrium times vary according to molecular sizes, vapor pressures, pore sizes, steric hindrances, molecular interactions, and other system properties. The particle size will also play a role in both uptake rate and time needed to reach equilibrium. Smaller particles will result allow diffusion to occur more rapidly into pores. Zeolite 13X, 4A, ZSM-5, and MCM-41 all had particle sizes of less than 50 μm . VPI-7 and VPI-9 had 500 μm and 75 μm particle sizes, respectively. 2-CEES requires over 300 hours for equilibrium to be reached on multilayer samples, whereas ethanol requires less than five hours to reach equilibrium with the zeolite investigated. Equilibrium is determined by monitoring the weight change over time; once the weight ceases to change, uptake has stopped ergo equilibrium has been reached.

Initial Uptake Rates

Initial uptake rates of target compounds were investigated. Due to the extensive equilibrium times needed for some of the target compounds, another method was examined to make a more direct, quicker comparison of the capacity of the target compounds onto zeolites. This was chosen by monitoring the kinetics of the uptake over time at the initial presence of the adsorbate. Since the sample chamber was initially evacuated, the initial pressurization of the sample chamber to the adsorbate would create the largest rate of uptake. This value was likely to change based upon the adsorbate vapor pressure and the equilibrium capacity of the adsorbate-adsorbent system.

The initial uptake rate was evaluated as the limiting slope of the uptake of the target compound upon initial pressurization of the sample chamber. More clearly, the uptake rate is the amount of mass adsorbed into the zeolite over time. The initial uptake rate could be considered as the uptake of adsorbate onto only the exposed area of zeolite in the sample bucket. Diffusion into the interior of the sample does not occur as rapidly, making the system act as if only a monolayer of zeolite is present. Figure 33 depicts how the initial uptake rate was evaluated using the gravimetric microbalance data.

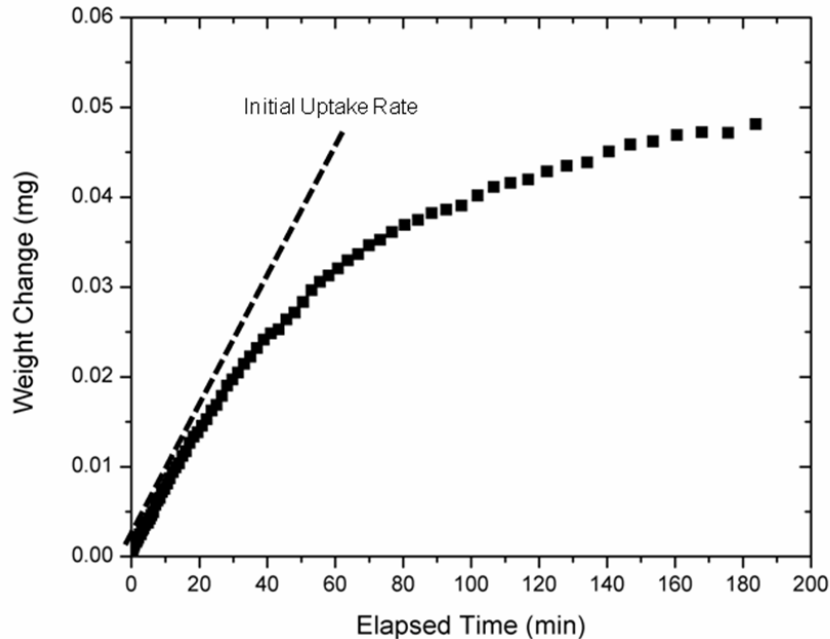


Figure 33 Method for determining initial uptake rate using gravimetric microbalance

Quartz Crystal Microbalance Results

Equilibrium Capacities

Using the RQCM-200, a 1 mL aliquot of 5 wt% zeolite solution was deposited onto the front face of the quartz crystal. The zeolite was allowed to begin to settle onto the crystal for a period of 30 seconds after which the zeolite was spin-coated at 2000 rpm for two minutes. This two step process provided a more even dispersion of the zeolite along the active area of the electrode. The crystal was then placed in a 50°C oven for at least one hour to dry the zeolite. This process, however, would not be sufficient to remove all the adsorbed water in the zeolite pores.

The amount loaded onto the zeolite was determined by measuring the frequency change of the unloaded crystal to the loaded spin-coated zeolite crystal according to the Z-match equation. This is similar to the adsorption measurements except that this was done manually and not automated by the RQCM-200.

Upon determination of the zeolite loaded onto the crystal, the crystal was then placed in the flow cell and allowed to equilibrate to the system conditions. The temperature was

maintained at 22°C and flow rates of the nitrogen carrier gas and sample vapor did not exceed 5 mL/min onto a crystal. The target compound was maintained at 5 mol% while the carrier gas comprised 95 mol% of the gas mixture. After the crystal became equilibrated to the temperature and nitrogen flow, the target compound was injected into the sample port at a constant rate by a syringe pump.

The RQCM-200 device recorded the resistance, mass, and quartz crystal frequency over time. Equilibrium was determined to be reached once mass/frequency changes in the system were no longer seen.

Initial Uptake Rates

Initial uptake rates using the RQCM-200 were determined using the same approach as with the gravimetric microbalance. Once a sample began to exhibit mass changes, uptake occurred. By knowing the amount of zeolite loaded onto the crystal and noting the mass change once the adsorbate gas was present, an initial uptake rate could be evaluated. There was, however, lag time between the start of the injection and the time of injection due to the distance between the injection port and the sample crystal.

Figure 34 depicts the method for the evaluation of the initial uptake rate using the QCM. There is a slight difference in the resulting units between the gravimetric microbalance and QCM calculations. The QCM measures frequency changes and reports mass changes in units of mass/area whereas the gravimetric microbalance reports solely overall mass changes. In order to compare the two methods identical units are needed. The QCM value needs to be multiplied by the active area of oscillation in order for the mass change per area to be converted into an overall mass change. The active oscillation area was reported earlier as 34.19mm².

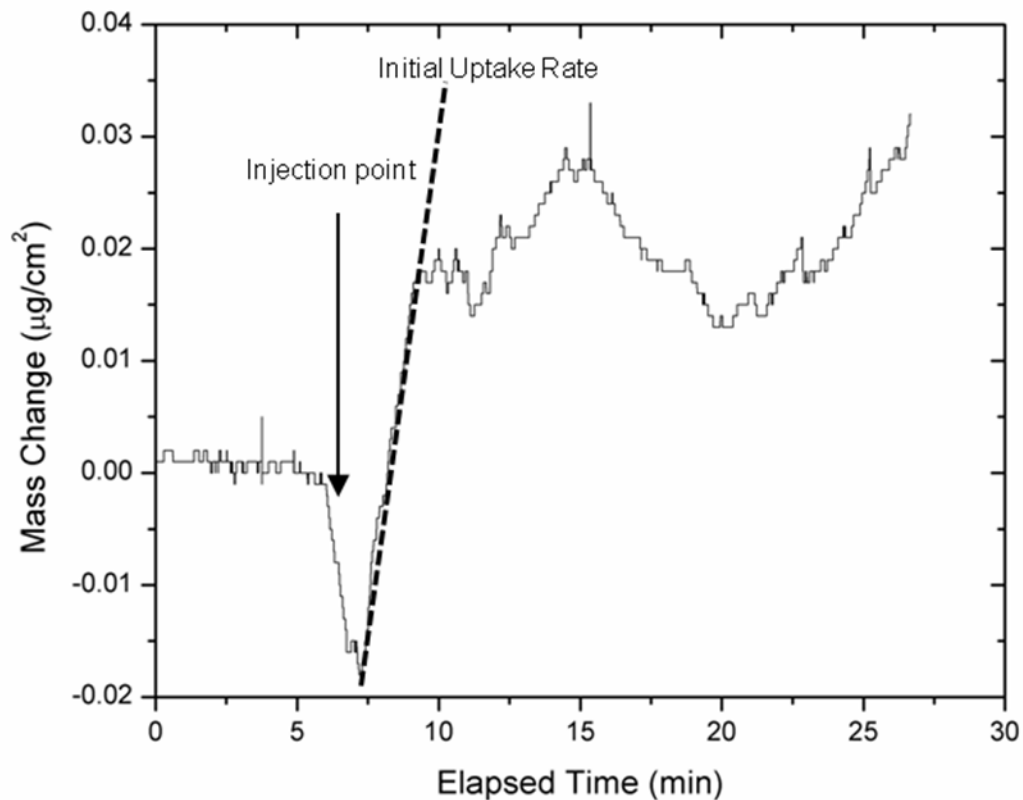


Figure 34 Method for determining the initial uptake rate using the QCM

The results for the equilibrium capacities of the target compounds and zeolites are shown in the following figures. The results from both the gravimetric microbalance and the QCM are shown for comparison between the two methods.

Ethanol Capacity

Figure 35 shows the equilibrium capacity for ethanol on the selected zeolites. There is strong agreement in the determined equilibrium capacities between the QCM and gravimetric microbalance. Zeolite 13X has the highest capacity for ethanol at $0.173 \text{ g}_{\text{ethanol}}/\text{g}_{13\text{X}}$, while the zinosilicates, VPI-7 and VPI-9, have the lowest equilibrium capacity at 0.0352 and $0.0492 \text{ g}_{\text{ethanol}}/\text{g}_{\text{VPI}}$, respectively. Reported literature values for ethanol onto 13X is $0.162 \text{ g}_{\text{ethanol}}/\text{g}_{13\text{X}}$, which is within 2.3% of the gravimetric microbalance and 6.4% of the QCM results.

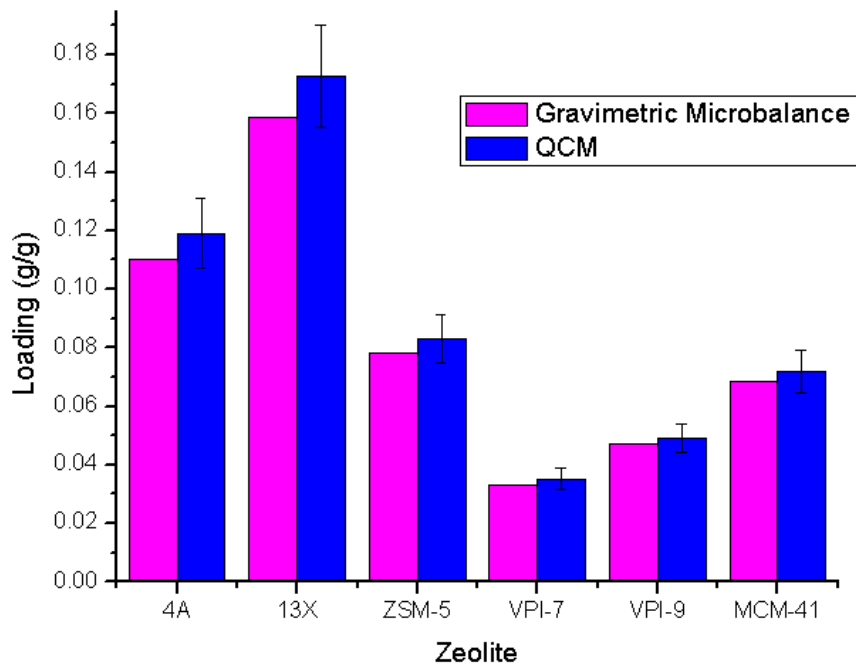


Figure 35 Equilibrium adsorption capacity of ethanol onto zeolites with respect to zeolite mass

Figure 36 shows the adsorption capacity of ethanol onto the zeolites with respect to the zeolite surface area. The zincosilicates, VPI-7 and VPI-9 which had the lowest adsorption capacity with respect to mass have the highest sorption capacity when measured by the surface area of the zeolite. MCM-41 has the lowest equilibrium loading when considered with its very high surface area.

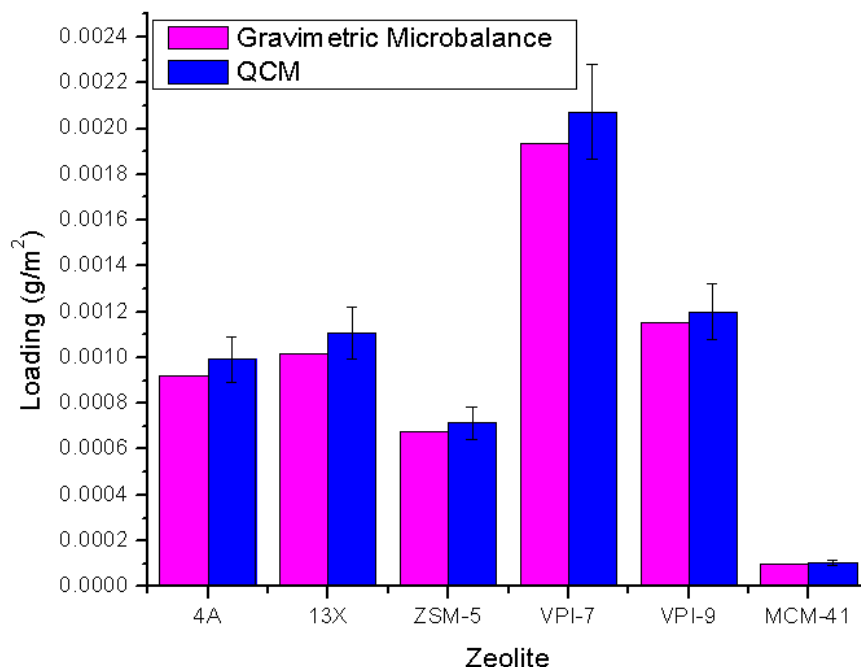


Figure 36 Equilibrium adsorption capacity of ethanol onto zeolites with respect to zeolite surface area

DMMP capacity

The adsorption capacity of DMMP onto the selected zeolites was also determined. Figure 37 shows the DMMP equilibrium adsorption capacity at 40°C onto zeolites. The gravimetric microbalance and QCM values are given for direct comparison. ZSM-5 has the lowest equilibrium loading of all tested zeolites at 0.0080 g_{ethanol}/g_{ZSM-5}. 13X has the highest loading capacity at 0.168 g_{ethanol}/g_{13X}. Once again, similar to the ethanol results, there is good agreement between the gravimetric and QCM results.

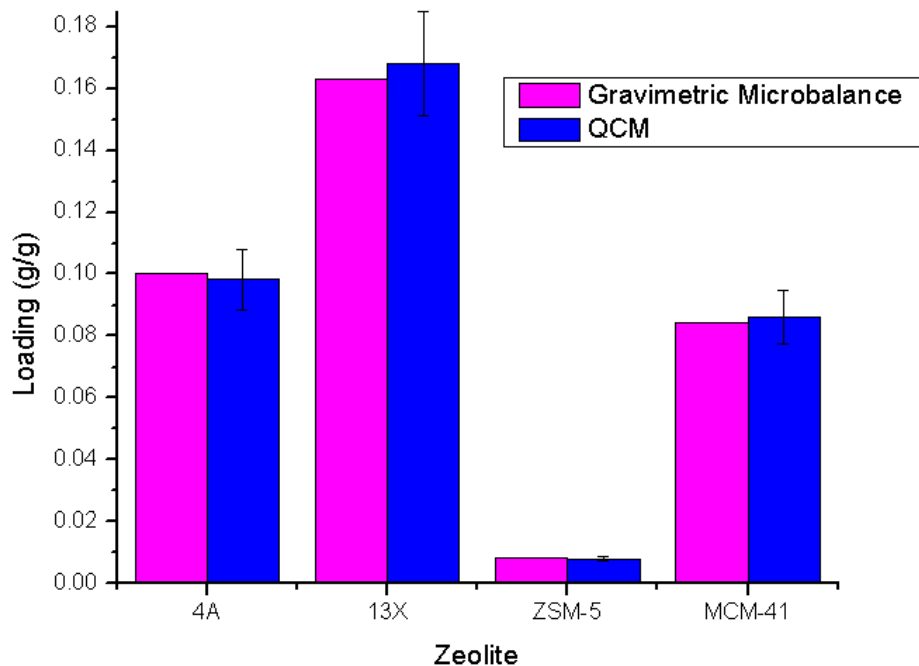


Figure 37 Equilibrium adsorption capacity of DMMP onto zeolites with respect to zeolite mass

Figure 38 shows the zeolite equilibrium capacity with respect to zeolite surface area. Zeolites 4a and 13X have the highest loading of DMMP in this comparison. MCM-41 has a very high surface area compared to the other zeolites making the loadings one of the lowest when considering it with respect to surface area. ZSM-5 has similar surface area to 4A and 13X, but ZSM-5's lower loadings leave ZSM-5 with a comparable loading as MCM-41 when making a comparison with zeolite surface area.

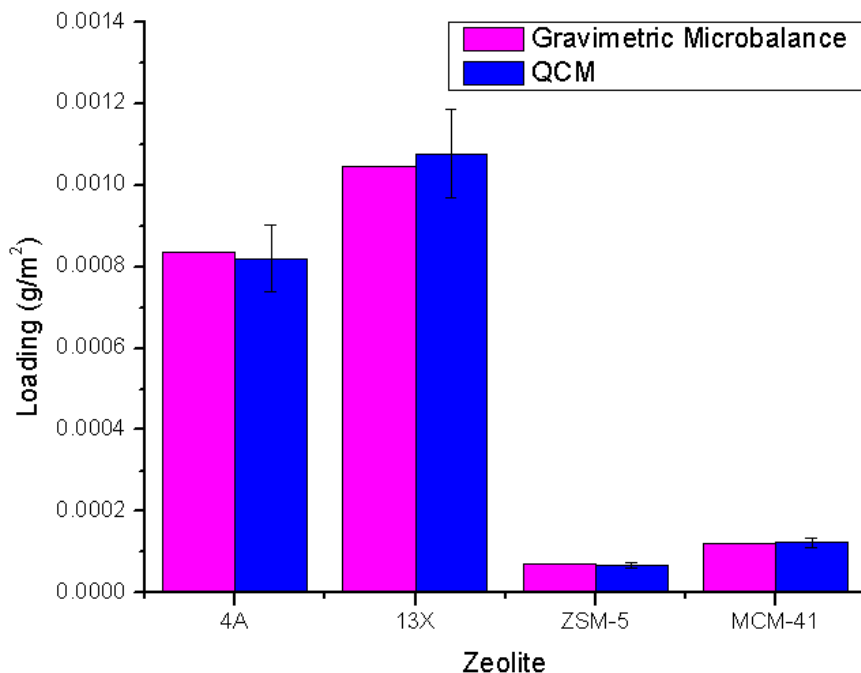


Figure 38 Equilibrium adsorption capacity of DMMP onto zeolites with respect to zeolite surface area

2-CEES capacity

Half mustard adsorption capacity was also investigated. However, as previously stated, equilibrium with the gravimetric microbalance required over 300 hours in order for one equilibrium data point to be collected. Due to the lengthy equilibrium time needed for adsorption of 2-CEES onto microporous zeolites, only two zeolites were examined. Once again there was excellent agreement between the gravimetric microbalance and the QCM. The loading of 2-CEES onto ZSM-5 was 0.5320 and 0.5852 $\text{g}_{2\text{-CEES}}/\text{g}_{\text{ZSM-5}}$ using the gravimetric microbalance and QCM, respectively. A previous equilibrium loading was reported to be 0.5603 $\text{g}_{2\text{-CEES}}/\text{g}_{\text{ZSM-5}}$.¹⁸² The results for 2-CEES-zeolites system are shown in Figure 39.

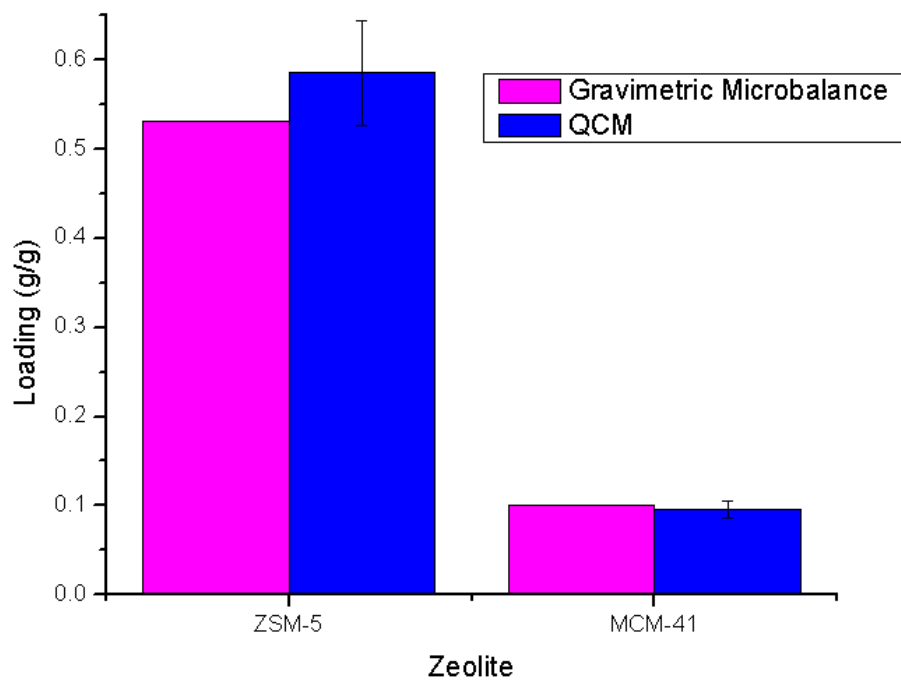


Figure 39 Equilibrium adsorption capacity of 2-CEES onto zeolites with respect to zeolite mass

Figure 40 shows the equilibrium loading capacity of 2-CEES onto ZSM-5 and MCM-41 with respect to the surface area of each zeolite. ZSM-5 has the lower surface area, 116 m²/g, than MCM-41, 700 m²/g, and has a higher loading when compared to MCM-41 with respect to both mass and surface area comparison.

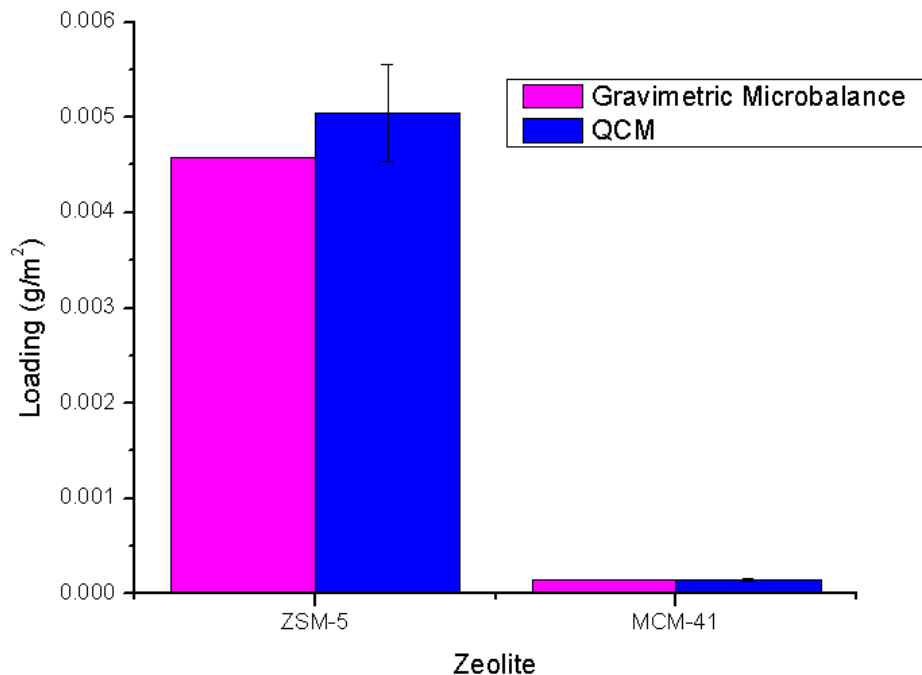


Figure 40 Equilibrium adsorption capacity of 2-CEES onto zeolites with respect to zeolite surface area

n-Butanethiol capacity

Finally, equilibrium capacities of *n*-Butanethiol were examined onto zeolites. The results from both the gravimetric microbalance and QCM are shown in Figure 41. The zincosilicate has the lowest capacity, less than 0.05 g_{*n*-Butanethiol}/g_{VPI-9}, while MCM-41 has the highest capacity of the examined zeolites at 0.095 g_{*n*-Butanethiol}/g_{MCM-41}.

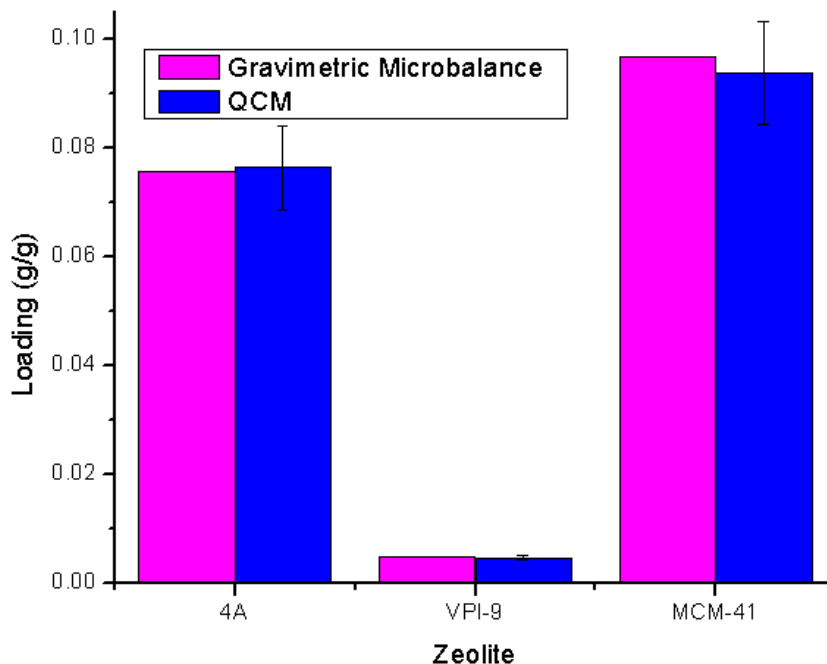


Figure 41 Equilibrium adsorption capacity of n-Butanethiol onto zeolites with respect to zeolite mass

Figure 42 depicts the equilibrium sorption capacity of n-butanethiol onto three selected zeolites with respect to the zeolite surface area. Zeolite 4A has a significantly higher sorption capacity than VPI-9 and MCM-41 when comparing the zeolites with respect to their surface area. In Figure 41, MCM-41 and VPI-9 have a large discrepancy in their loadings when comparing with respect to the zeolite mass. However, MCM-41 and VPI-9 have very similar loadings when comparing to the zeolite surface area.

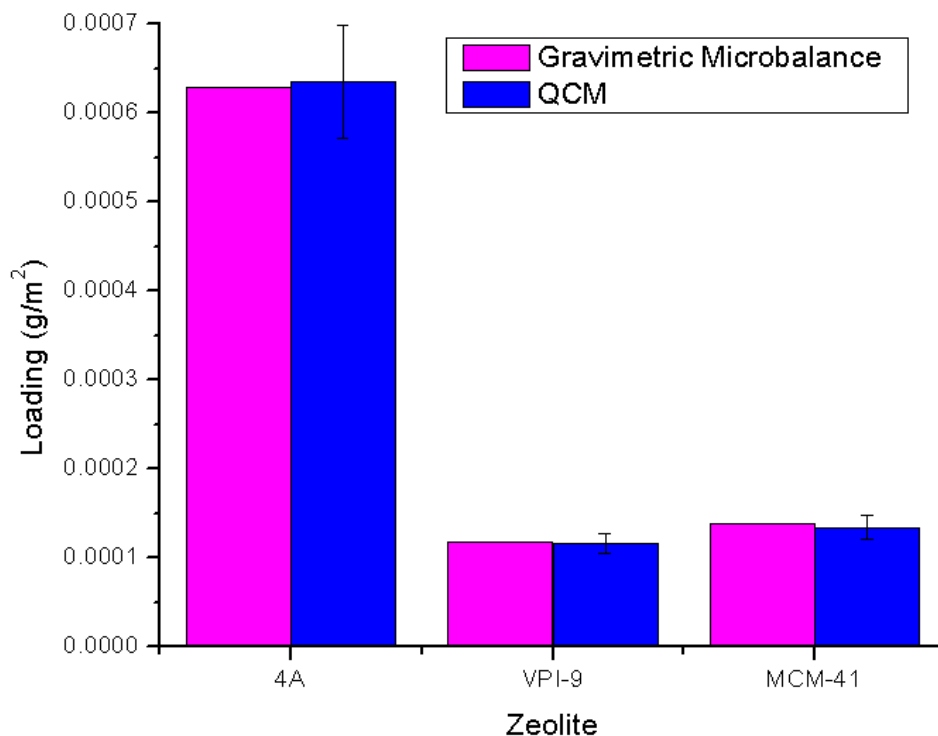


Figure 42 Equilibrium adsorption capacity of n-Butanethiol onto zeolites with respect to zeolite surface area

Discussion

The results from both the gravimetric microbalance and QCM system were consistent. The calculated loading values of these two methods were within 11% agreement or less. When comparing the results from either system to previously published values for equilibrium loading, the values differed by less than 8%. This margin of error between systems and other reported systems indicates that the methodology employed with the gravimetric microbalance and QCM is sufficient to produce accurate results.

Ethanol, dimethyl methanephosphonate, and n-butanethiol equilibrium loadings onto zeolites show that zeolites 4A and 13X have the highest capacity for the selected simulants. Zeolites 13X and 4A have higher Si:Al ratio than ZSM-5 and MCM-41 increasing the charge density on the framework leading to higher loading. The larger surface area of 13X and 4A also allows for higher equilibrium loadings with respect to mass than zincosilicates VPI-7 and VPI-9.

When considering the equilibrium loadings onto ethanol with respect to zeolite surface area, the zincosilicates have the highest capacity. The surface area of the zeolites is 1/3 or less than that of all other selected aluminosilicates frameworks. This surface area difference accounts for discrepancy between the loading per mass and the loading per surface area. Zeolites 13X and 4A have the highest loadings with respect to mass and surface area of the aluminosilicate frameworks onto ethanol, dimethyl methanephosphonate, and n-butanethiol.

Initial Uptake Rates

Using the methodology described above, the initial uptake of the target compounds onto zeolites was also calculated. The results from these calculations are shown in the following figures. Results from the QCM and gravimetric microbalance are shown together for comparison.

Ethanol initial uptake rate

The ethanol uptake rates for both the gravimetric microbalance and QCM are shown in Figure 43. There is good agreement between the two methods as all values for the zeolite-ethanol systems are within 13%. The zincosilicates have a lower uptake rate than do the aluminosilicates. Zeolite 13X has the highest uptake rate while zeolite 4A has about 70% the uptake rate of that of 13X. All other zeolites are less than half the uptake rate of 13X.

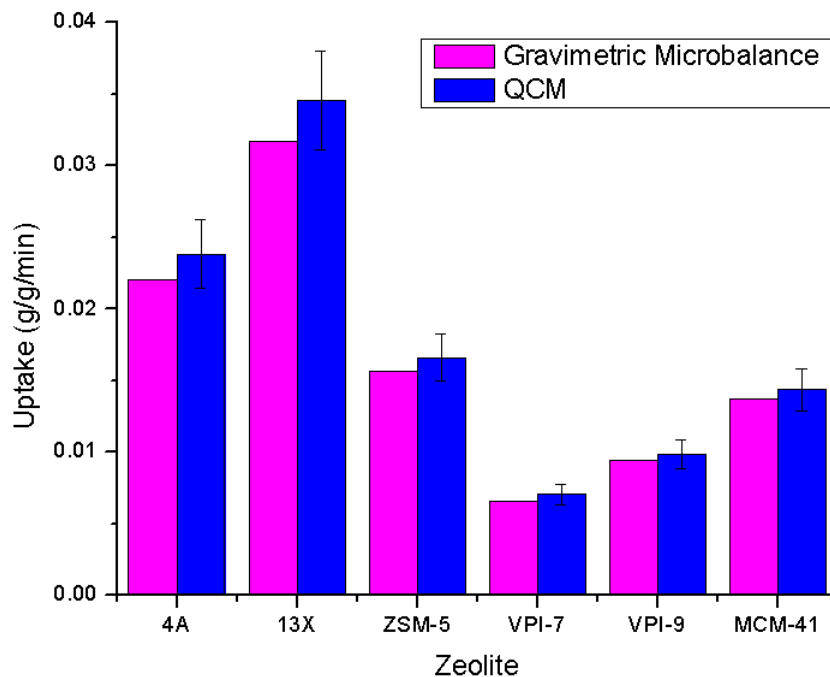


Figure 43 Initial uptake rate of ethanol onto zeolites with respect to zeolite mass

Figure 44 displays the initial uptake rate of ethanol onto zeolites when considering the surface area of the zeolite. VPI-7 which has the lowest mass uptake rate of the selected zeolites has the highest uptake rate of all selected zeolites when considering its surface area. VPI-7's lower surface area results in a larger uptake rate than other zeolites. This means that VPI-7 is able to sorb more ethanol per surface area than the other selected zeolites.

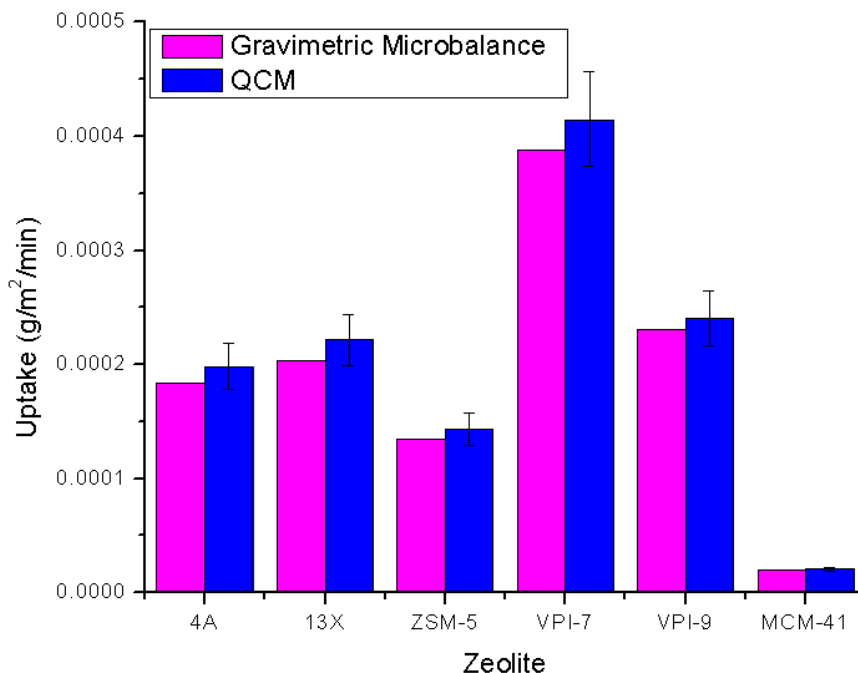


Figure 44 Initial uptake rate of ethanol onto zeolites with respect to zeolite surface area

DMMP initial uptake rate

The initial uptake rate of DMMP was also examined and is illustrated in Figure 45. DMMP has a phosphonate functional group centrally located in the molecule and is a significantly larger molecule than that of ethanol. These among other factors resulted in an uptake rate lower than that of ethanol by almost an order of magnitude. Similarly, 13X had the highest uptake rate of all the zeolites studied with DMMP followed by 4A. It should be noted that the initial uptake rate of DMMP onto zinosilicates VPI-7 and VPI-9 using the QCM device were not included due to inconsistent coating of the material onto the quartz crystal and inconsistent frequency measurements once placed in the crystal holder. Since a stable signal could not be reached prior to starting the experiment, signals were often unstable and unreliable for evaluation. VPI-7 and VPI-9 had larger particle sizes than of the other tested zeolites which contributed significantly to the inconsistent coating.

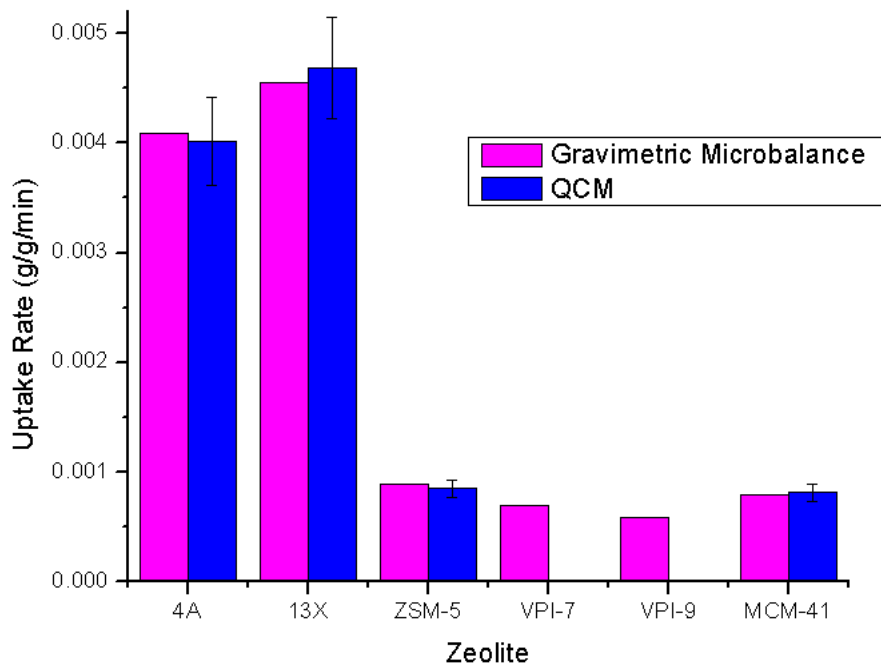


Figure 45 Initial uptake rate of DMMP onto zeolites with respect to zeolite mass

Figure 46 shows the initial uptake rate of DMMP onto zeolites with respect to surface area of the zeolite. VPI-7 which had a very low uptake rate when considered on a mass basis has the highest uptake rate on a surface area basis. ZSM-5 and MCM-41 have the lowest initial uptake rates of the selected zeolites by surface area.

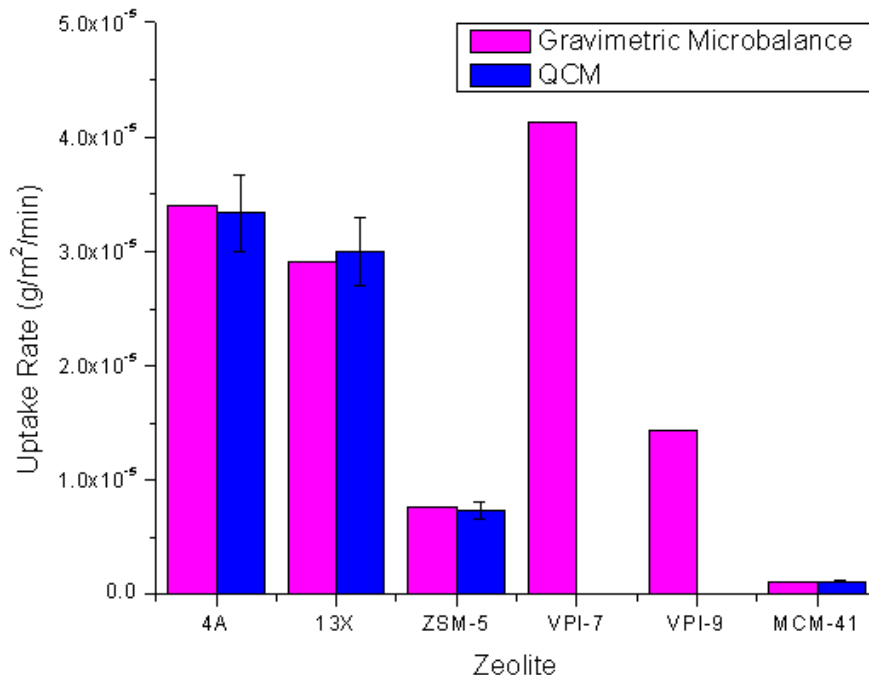


Figure 46 Initial uptake rate of DMMP onto zeolites with respect to zeolite surface area

2-CEES initial uptake rate

The initial uptake rate of the target compound 2-CEES was examined and is shown in Figure 47. 2-CEES is a molecule with two potential functional groups for adsorption. The chloride at the end of the molecule and the centrally located sulfur may potentially bind to the surface of a zeolite. Steric hindrances in this molecule are expected to play a lesser role than in DMMP.

The initial uptake rates onto the zeolitic materials are similar in magnitude to those of DMMP, which are an order of magnitude less than those seen with ethanol adsorption. ZSM-5 has the highest uptake rate of the selected zeolites at 0.004 g_{2-CEES}/g_{zeolite}/min while 13X and 4A are slightly less than ZSM-5. MCM-41 and the zincosilicates have very low uptake rates, all less than 0.0009 g_{2-CEES}/g_{zeolite}/min.

Results from the QCM and the zincosilicates have been excluded for similar reasons as mentioned in the previous section.

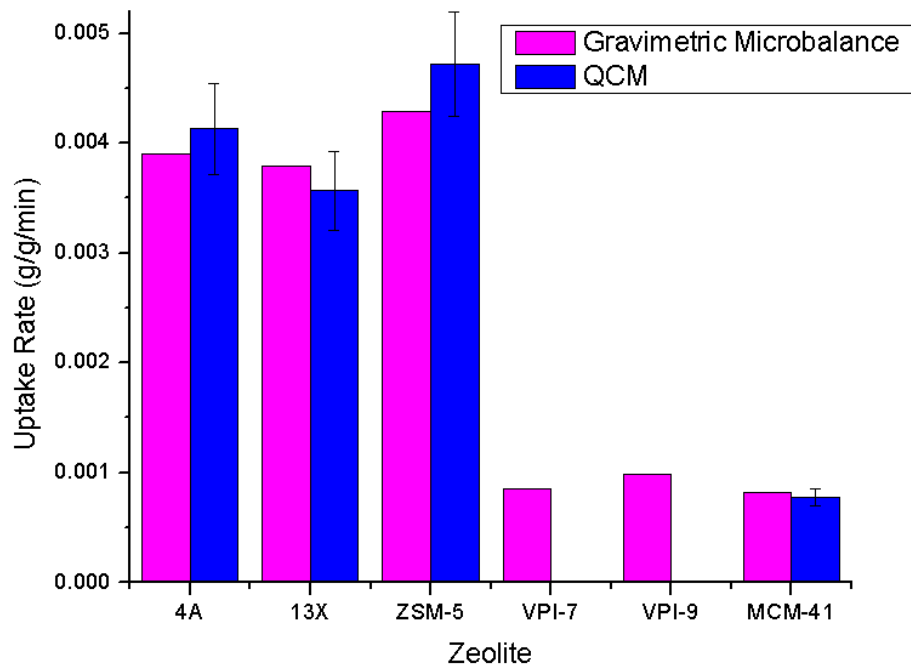


Figure 47 Initial uptake rate of 2-CEES onto zeolites with respect to zeolite mass

Figure 48 displays the initial uptake rate of 2-CEES onto selected zeolites by surface area. The zincosilicates, especially VPI-7, have a higher uptake rate when considering their lower surface area relative to the other zeolites. MCM-41 has a very high surface area and a low uptake rate on this basis.

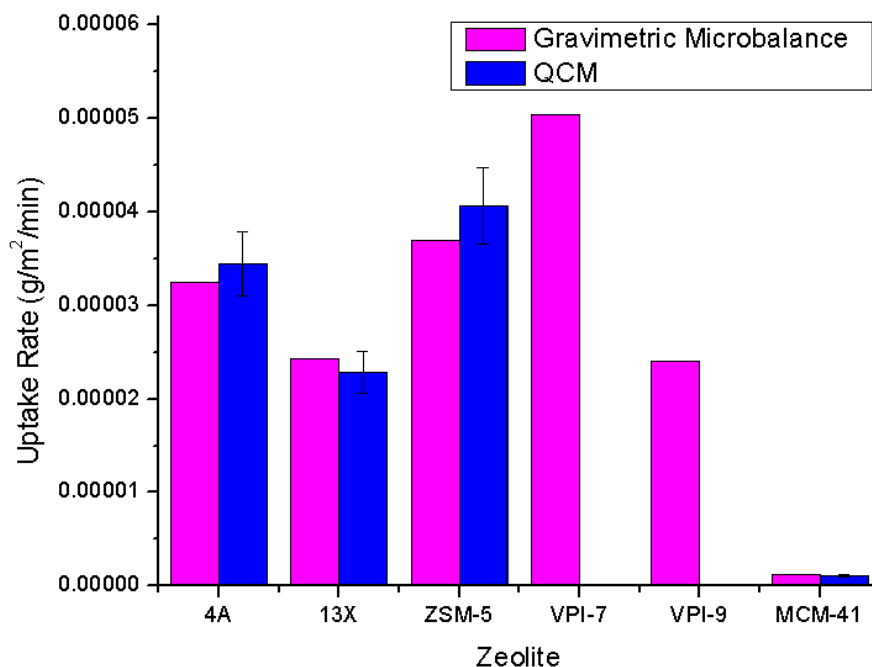


Figure 48 Initial uptake rate of 2-CEES onto zeolites with respect to zeolite surface area

n-Butanethiol initial uptake rate

Finally, the initial uptake rate of *n*-Butanethiol was examined and is shown in Figure 49. *N*-Butanethiol is a molecule with a single functional group, a sulfur end group. The steric hindrances for adsorption in this molecule are expected to play a lesser role than in DMMP and in 2-CEES. Once again, 13X has the highest initial uptake rate of all tested zeolites at $5.11 \cdot 10^{-3}$ $\text{g}_{\text{n-butanethiol}}/\text{g}_{13\text{X}}/\text{min}$. The single zincosilicate tested, VPI-9, had the lowest uptake rate at $7.70 \cdot 10^{-4}$ $\text{g}_{\text{n-butanethiol}}/\text{g}_{\text{VPI-9}}/\text{min}$

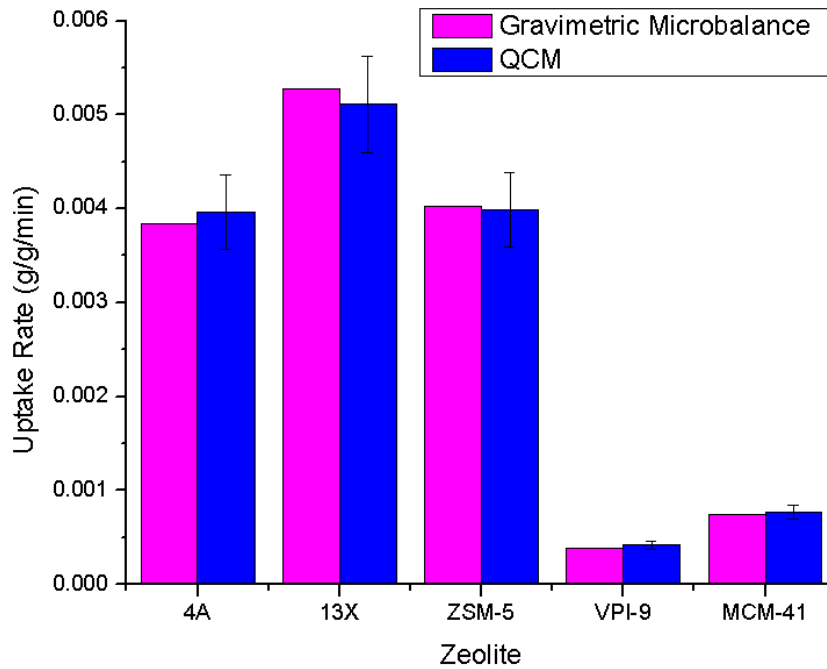


Figure 49 Initial uptake rate of n-Butanethiol onto zeolites with respect to zeolite mass

Figure 50 shows the uptake rate on n-Butanethiol onto zeolites by surface area. Zeolite 4A, 13X, and ZSM-5 have the highest uptake rate of the selected zeolites. MCM-41 has the lowest uptake rate by surface area of the selected zeolites due to its very high surface of 700 m²/g.

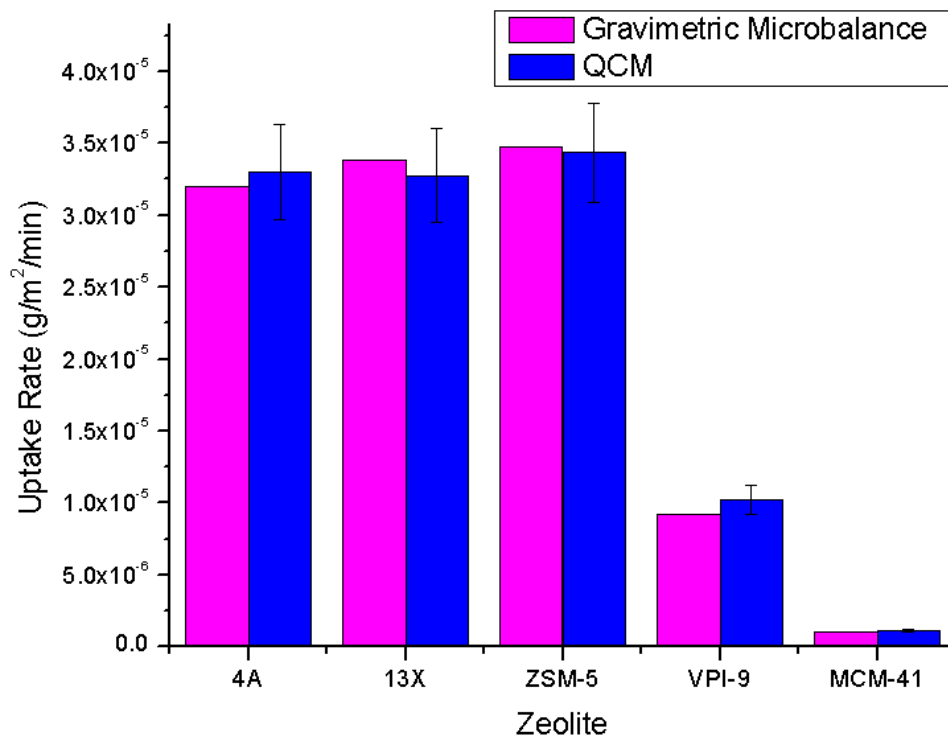


Figure 50 Initial uptake rate of n-Butanethiol onto zeolites with respect to zeolite surface area

Discussion

The use of the gravimetric microbalance to evaluate both the equilibrium capacity and initial uptake rate of the selected simulants yielded accurate results. The equilibrium capacity of ethanol onto 13X was consistent with a previously published value as was the equilibrium capacity of 2-CEES onto ZSM-5.¹⁸² The kinetics, specifically the overall amount of time required to achieve equilibrium, was also consistent when comparing these results of the two 2-CEES/ZSM-5 systems.

The equilibrium adsorption capacity of the simulant/zeolite systems of the QCM and gravimetric microbalance were reliable. All equilibrium capacity values were within 5% agreement between the QCM and gravimetric microbalance.

The gravimetric microbalance and QCM uptake rates were within good agreement as well. Although the systems slightly differed (the QCM was in a flow setup and the gravimetric microbalance was static), the calculated values of the uptake rates were within 7% to 14.8%

agreement when comparing the two systems. Since the uptake rates were evaluated within small times of the introduction of the simulant into the chamber with the gravimetric microbalance and the QCM system was very small in volume and mass when adsorption occurred, the difference between the static nature of the gravimetric microbalance and the QCM flow setup seemed to be irrelevant. The consistency in the results for both equilibrium and initial uptake rates in the two apparatuses indicates that the QCM was and can be employed successfully for determining adsorption properties in flow systems using minimal amounts of sorbents and time.

Influence of Sorbent and Sorbate Structure

The zeolite framework plays a critical role in the uptake rate of the compound as does the chemical structure of the adsorbing species. Ethanol, on average, has the highest uptake rate of all tested adsorbates. Its simple structure, small size, and very polar functional group are key contributors to its uptake rate. DMMP, 2-CEES, and n-Butanethiol all had lower uptake rates than ethanol. DMMP had the lowest average uptake rate onto all zeolites. This is likely due to its large size and single, centrally-located phosphonate functional group in the molecule. While the chemical constituents and size of 2-CEES and n-Butanethiol are similar, the sulfur functional group appears to influence adsorption the greatest. N-Butanethiol has a sulfur end group while 2-CEES has a centrally located sulfur group. 2-CEES also has a polar chloride end group, which could enhance adsorption; however, the uptake rates between the zeolites and these two compounds are very similar. The influence of the location of the functional group will be discussed in further detail with the use of a mixture and zeolite array.

The structure of the zeolite will also play an important role in the uptake of the adsorbing species. 13X and 4A structures are comprised of sodalite cages with different connection schemes between cages. A more detailed explanation of the periodic building units can be found elsewhere.¹⁷⁴ These two structures, 13X and 4A, had the highest uptake rates typically. Hydrophobic zeolites such as 13X and 4A have shown higher adsorption of organic compounds than hydrophilic zeolites. The zincosilicates had typically the lowest uptake rate of all tested adsorbents. The combination of low surface area and channel tortuosity were key contributors to the low uptake result. MCM-41 has a large pore size and high surface area but low adsorption uptake. The tertiary amine surfactant used in the synthesis has been shown to alter adsorption capacity.¹⁸³

Influence of Humidity/Water on Measurements

The utility of these materials as accurate recognition elements is likely going to be affected by the presences, or lack thereof, of adsorbed water. Zeolites can be very hygroscopic. This can have a profound influence on the material's adsorption properties with other species. Here the influence of water on the initial uptake rate measurements was examined.

Water Uptake onto Zeolites

In order to evaluate the influence of water/humidity onto the zeolites, samples of zeolites with and without water sorbed were desired. Initial zeolite samples were spin-coated onto the quartz crystals by making a 5 wt% mixture of zeolite in water. Once spin-coated onto the crystal face, the sample was dried at 50°C to remove residual water on the crystal but did not remove large amounts of water sorbed in the pores of the zeolites.

Samples lacking water in the zeolite pores were prepared by calcining the samples at 400°C for 2 hours. A 5 wt% mixture of zeolite in acetone was made to in order to carry out the spin-coating procedure. The sample was then dried at 50°C for 2 hours and considered ready for use in the QCM. This process was carried out as quickly as possible to minimize water sorption for these experimental trials. It must be noted that although water was likely to have no or reduced presence in the pores of the zeolites through the described preparation method, acetone could be present in the pores instead. Since both water and acetone are polar molecules, hydrophobic zeolites also have been shown to adsorb lesser amounts of water and acetone than other nonpolar molecules,¹⁸⁴ and the amount of adsorbed acetone has a lower heat of adsorption than water in zeolite 13X and MCM-41.^{185, 186} These two factors will lower the influence acetone has on the uptake rate onto the zeolites and also means that acetone should adsorb in significantly lesser amounts than water.

The results comparing the adsorption of ethanol onto zeolites with and without the presence of water in the pores of the zeolites is shown in the Figure 51.

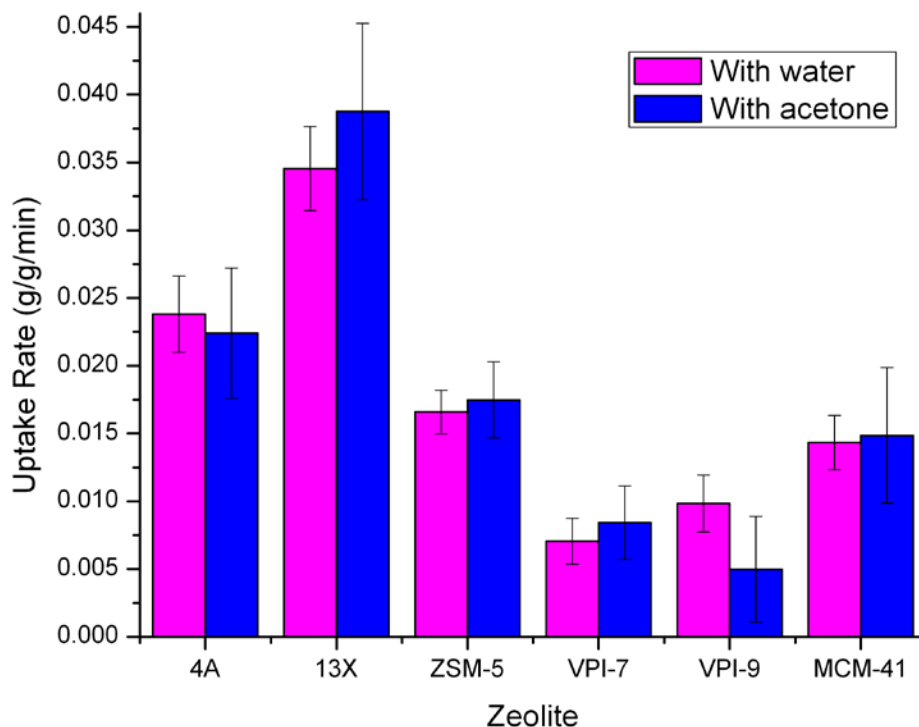


Figure 51 Influence of water on the initial uptake rate of ethanol onto zeolites

The uptake rate increases in four of the six zeolites examined when acetone is used as the solvent. This means that the presence of water does diminish the uptake rate of the zeolites, at least slightly. The increase is 12.2% in zeolite 13X and less than that for all other zeolites that saw an increase in uptake rate without water present. VPI-9 and 4A show a decrease in the uptake rate when acetone is used instead of water. Zeolite 4A's uptake rate decreased by 6.3%. VPI-9 had a rather significant amount of error associated with its trial as the material was rather difficult to spin-coat when using acetone.

Molecular Sensing/Identification

Zeolites have potential to selectively adsorb certain molecules over others. This selectivity may be due to size of the molecules and the zeolite pores, the structure of the zeolite framework, the cations associated with the zeolite framework, functional groups on the adsorbate or zeolite, the number and location of the functional groups, the presence of other sorbed molecules, and chemical ratio or makeup of the species that are being adsorbed.

Understanding zeolite sorption selectivity may help one to discern certain molecules that are being adsorbed, the relative size of the molecule, and/or its functional groups, which will be critical information for molecular sensing or identification.

Zeolite Array with Gas Mixture

Using the QCM, mixtures of vapors in a carrier gas were presented to an array of zeolites. Three quartz crystals were coated with three different zeolites and a mixture of gases was to be exposed to the each crystal simultaneously. The amount of zeolite on each crystal was determined as previously described and allowed to reach a steady mass/frequency reading before the gas mixture was introduced. The response of each crystal to the gas mixture was recorded and then evaluation made on what, if any, chemicals were sorbed and in what quantity.

An array of three zeolites were used: 4A, 13X, and ZSM-5 and two vapors: 2-CEES and n-Butanethiol. 2-CEES and n-Butanethiol were chosen due to their similar chemical structure. Both chemicals have four carbons and a sulfur group. There are two main differences between these two molecules: the positioning of the sulfur group and a chloride functional group. The sulfur group is centrally-located in 2-CEES and an end group on n-Butanethiol and 2-CEES has a chloride functional end group that is lacking in n-Butanethiol. Nitrogen was used as the carrier gas. The zeolites were coated and placed in the crystal holders using the same method described previously. After equilibrium was reached with the system, a 3 mol% mixture of n-Butanethiol and 3 mol% 2-CEES was introduced to the coated crystals. The mixture was allowed to adsorb and the initial uptake rates measured.

Figure 52 shows the results from this procedure.

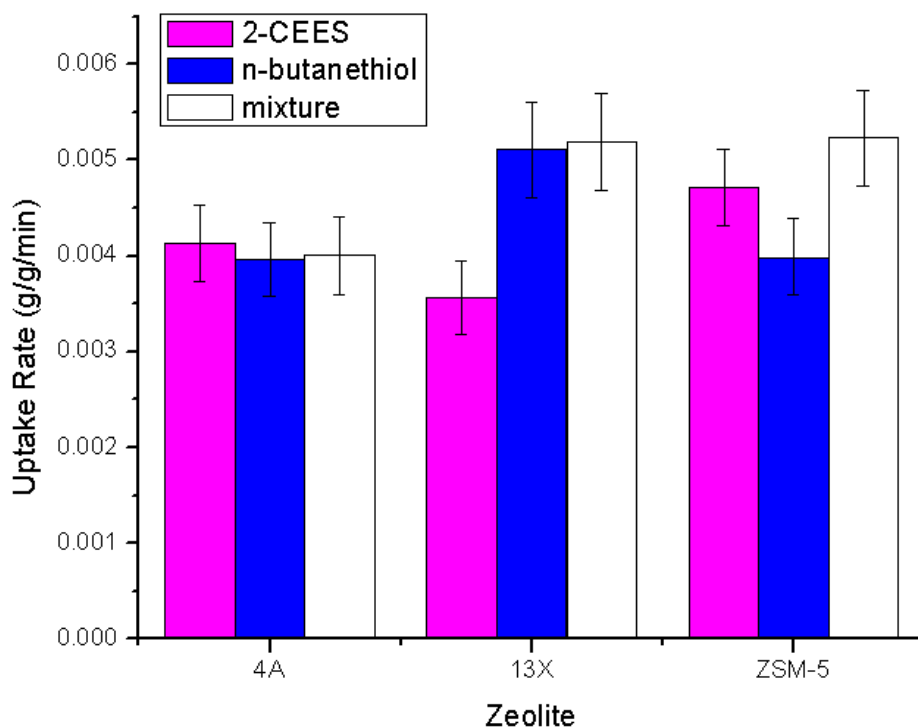


Figure 52 Change in uptake rate with vapor mixture

With the presence of a mixture the change in the uptake rate with 4A is insignificant. This means that 4A does not selectively adsorb 2-CEES over n-Butanethiol. In ZSM-5, the overall uptake rate of the mixture is greater than the uptake rate of the single component systems. Single adsorbate trials contained 5 mol% adsorbate and 95 mol% nitrogen, the relative increase in the ZSM-5 mixture trial is likely due to the overall increase in the mole fraction of adsorbate species being 6% instead of 5%. However, zeolite 13X has the same uptake rate with both the mixture and n-Butanethiol present than compared to just 2-CEES present. This means that adsorption onto zeolite 13X is likely controlled by the adsorption of the sulfur functional group and not the chloride functional group that is in 2-CEES. The location of the sulfur functional within the molecule may play a role in determining the overall capacity of adsorption, but clearly does play a critical role in the initial uptake rate of the species. With the reduced steric hindrances of a sulfur end group in n-Butanethiol, zeolite 13X can more readily adsorb the

molecule than the centrally-located sulfur group in 2-CEES. While one cannot exclude the role the chloride functional group may or may not play in determining adsorption capacity or initial uptake rate on zeolites 4A and ZSM-5, the influence of the sulfur functional group and its location on the adsorbing species plays a critical role in the initial uptake rate onto 13X.

CHAPTER 5 - Conclusions and Recommendations

Capture of Mercury Summary and Conclusions

The aqueous phase ion exchange capacities of zincosilicates VPI-7, VPI-9, and VPI-10 with mercury have been reported. VPI-9 has the highest capacity for mercury of the three zincosilicates studied. All of the zincosilicates are able to capture mercury in higher amounts than other common sorbents reported, even those that had been functionalized specifically for mercury capture. Over 90% of the divalent mercury initially in the system could be captured using VPI-9 in batch conditions. The counteraction(s) associated with the framework play an important role in determining the mercury ion exchange capacity. Specifically, the as-made VPI-9 structure contained potassium and rubidium ions for ion exchange. When this was exchanged with a sodium solution and then followed by a mercury exchange, this decreased the mercury cation exchange capacity of the material to levels similar to those in VPI-7. The zincosilicate materials are highly capable of capturing toxic cationic heavy metals from aqueous solutions.

The ion exchange energy of VPI-7 and VPI-9 was also investigated. A van't Hoff modeling procedure was used as the experimental conditions warranted. The ion exchange energy for VPI-7 and VPI-9 was 271 and 693 J/mol, respectively. These values are slightly lower than exchange energies seen with other metals and zeolites but have values of similar magnitude. The larger exchange energy value with mercury and VPI-9 indicates a more thermodynamically favorable process than the mercury exchange with VPI-7.

The selectivity coefficient of the zincosilicates VPI-7 and VPI-9, with monovalent and divalent cations was also studied. The selectivity between heavy metals, mercury and lead, alkali metals, sodium and potassium, and an alkaline metal, calcium, were examined with low ionic strengths at equimolar compositions. The highest selectivity was for lead followed by sodium. VPI-7's selectivity was $Pb > Na > Hg > K > Ca$ and VPI-9's selectivity was $Pb > Na > Hg > K > Ca$. The selectivity coefficients were successfully modeled using the Gibbs-Donnan selectivity model. The assumptions in this model and experimental conditions were ideal for selecting this model and it had been successfully employed in ion exchange previously.

The zincosilicates used in this study have a high affinity for the capture of mercury and can be used in aqueous media as ion exchangers to capture divalent heavy metals. The zincosilicates are non-functionalized and could be modified to increase the capture capacity of divalent heavy metals and other materials. The material's counteranions play a critical role in determining capture capacities; sodium reduces the capture capacity of divalent heavy metals mercury and lead. The materials are thermally and mechanically stable and show promise in being regenerable based upon the moderate exchange energies found with the capture of mercury. The selectivity coefficients of VPI-7 and VPI-9 indicate there is a strong preference for lead with very limited uptake of calcium when in the presence of other cations.

Detection of Warfare Agents Summary and Conclusions

Gas phase adsorption with zeolites 13X, 4A, MCM-41, VPI-7, VPI-9, and ZSM-5 was also studied. The zeolites selected provided very different features for determining the most significant properties in adsorption capacity among these being: framework composition, counteranion, and surface area. The sorption capacity of 2-chloroethyl ethyl sulfide, dimethyl methanephosphonate, ethanol, and n-Butanethiol were examined onto these zeolites. Equilibrium capacities and initial uptake rates were evaluated on two apparatuses: a gravimetric microbalance and QCM. There was good agreement between both methods' results. Zeolite 13X had the highest equilibrium and initial uptake rate for most compounds tested. The zincosilicates, VPI-7 and VPI-9, had the lowest equilibrium capacity and initial uptake rate for all compounds studied. Ethanol adsorption capacity was highest of all the compounds studied. Ethanol equilibrium capacity and initial uptake rate were an order of magnitude higher than that of 2-CEES and DMMP.

The influence of water sorbed into the zeolites was examined. When water was sorbed into the pores prior to adsorbing another species, the result was typically a lower sorption capacity and uptake rate than when water was not present. The results were somewhat inconsistent as the technique used to evaluate the influence of water likely needs to be modified to ensure no water was sorbed into the pores prior to experimentation, although significant efforts were made to ensure this did not occur. Placing the coated quartz crystals under vacuum to remove sorbed species would remedy this inconsistency.

Zeolites were also evaluated for their potential as molecular sensors and identifiers. By creating a small array of zeolites and a mixture of gases we were able to isolate a preference for the chlorine located in 2-CEES over the sulfur functional group in n-Butanethiol. While both molecules' functional groups are located at the end of the molecule and the molecular sizes are similar, the uptake rate of 2-CEES is appreciably different when the two molecules are introduced in 3 mole% equimolar ratios in nitrogen.

The QCM device with an array of zeolites can be successfully employed as functional group sensing device indicated through these results. It is expected that with the use of a larger array of zeolites and mixtures of simulants that a handheld, portable molecular/chemical sensing device could be developed using the initial uptake rate techniques employed in this study.

Recommendations

Further analysis involving cationic exchange with the zincosilicates should be made. This could include other transition metals specifically monovalent and divalent species. The potential for understanding the binding energy associated with these materials may lead to other uses such as in catalysis. For example, if platinum and/or palladium can be introduced in significant amounts into the interior of the zincosilicates, this could create a potentially well-ordered nanoporous sized catalyst.

Another area that should be examined with the zincosilicates is the reuse of the material. Regeneration of the material was not investigated and multiple ion exchange cycles with the material would help determine if the materials have long-term applications. Ion exchange times for equilibrium were not specifically determined either. While under batch conditions, equilibrium was reached in less than two hours when exchanging divalent mercury with all zincosilicates. A fixed bed setup to determine breakthrough times would be an appropriate choice for evaluating residence times needed to reach equilibrium in aqueous ion exchange systems.

In adsorption, further experiments need to be run using other target compounds, specifically other dangerous compounds like those found in explosives like 2,4-dinitrotoluene (2,4-DNT). There are many zeolitic structures that could potentially be used as molecular sensors. Changing the countercations within the framework, the hydration content (swelling can occur as water is taken in), and functionalizing the zeolites leave almost limitless possibilities as

to capture capacity and initial uptake rate measurements. Identifying critical physical parameters such as the role of surface area, framework type/content, and counteractions should all be evaluated in order to establish rigorous guidelines and potential modeling of systems for molecular identification.

While there may be a host of broad areas for developing adsorption criteria for molecular sensing, a very specific area involving this work should be addressed. More clear identification of the hydration content of each of the zeolites needs to be analyzed. While significant effort was made to control the water content or hydration of some zeolite samples, potential water uptake could have occurred in intermediate steps such as transfer of the crystals from the spin-coater to the oven, while in the oven, and from the transfer from the oven to the crystal holder. This could be remedied by placing the coated quartz crystal in a vacuum environment before or even after placing the crystals in the crystal holder. This would ensure removal of water from the framework and would lead to more consistent experimental results than what data that was produced under the current conditions.

Another area that should be examined is the potential for false identification of certain materials. Certain chemicals may yield similar results to some of the tested target compounds. Organic chemicals such as those in lacquers and floor polishes have been documented as giving ‘false positive’ measurements meaning that the chemical signal from these materials has a similar signal to other dangerous materials.

Finally, a larger array of zeolites will help determine molecular sensing capabilities. The QCM employed has capabilities of measuring three signals simultaneously. A practical device for molecular identification would require a larger array of zeolites with capability of making measurements of all zeolites in the array simultaneously. A different system than what is currently being used must be developed in order to develop a practical device for commercial purposes.

References

1. Flanigen, E. M., Review and New Perspectives in Zeolite Crystallization. *Advances in Chemistry Series* **1973**, (121), 119-139.
2. Commission, I. Z. A. S., Framework Density (FD). In 2006.
3. Stamires, D. N., Properties of Zeolite, Faujasite, Substitutional Series - Review with New Data. *Clays and Clay Minerals* **1973**, 21, (5), 379-389.
4. Colella, C.; Gualtieri, A. F., Cronstedt's zeolite. *Microporous and Mesoporous Materials* **2007**, 105, (3), 213-221.
5. Annen, M. J. Synthesis and Characterization of Novel Molecular Sieves Containing Three-Membered Rings. Virginia Polytechnic Institute and State University, Blacksburg, VA, 1992.
6. Hoover, D. L.; Shepard, A. O., Zeolite Zoning in Volcanic Rocks at Nevada Test Site Nye County Nevada. *American Mineralogist* **1965**, 50, (1-2), 287-&.
7. Annen, M. J., Mark E. Davis, John B. Higgins, John L. Schlenker, VPI-7: The First Zincosilicate Molecular Sieve Containing Three-membered T-Atom Rings. *Journal of the Chemical Society-Chemical Communications* **1991**, 17, 1175-1176.
8. Cambor, M. A., Mark E. Davis, 29Si MAS NMR Spectroscopy of Tectozincosilicates. *Journal of Physical Chemistry* **1994**, 98, (50), 13151-13156.
9. Pelmeshnikov, A. G. P., E.A. ; Edisherashvili, M.O. ; Zhidomirov, G.M., On the Loewenstein Rule and Mechanism of Zeolite Dealumination. *Journal of Physical Chemistry* **1992**, 96, (17), 7051-7055.
10. <http://www.nlm.nih.gov/pubs/factsheets/hsdbfs.html> (June 15, 2009),
11. Rivas, B. L., Sandra Villegas, Beatriz Ruf, Synthesis of Water-Insoluble Functional Copolymers Containing Amide, Amine, and Carboxylic Acid Groups and Their Metal-Ion-Uptake Properties. *Journal of Applied Polymer Science* **2006**, 102, (6), 5232-5239.
12. Kapoor, A., T. Viraraghavan, Removal of Heavy Metals from Aqueous Solutions Using Immobilized Fungal Biomass in Continuous Mode. *Water Research* **1998**, 32, (6), 1968-1977.
13. Sublet, R., Marie-Odile Simonnot, Alain Boireau, Michel Sardin, Selection of an Adsorbent for Lead Removal from Drinking Water by a Point-Of-Use Treatment Device. *Water Research* **2003**, 37, (20), 4904-4912.
14. Yu, Q., Jose T. Matheickal, Pinghe Yin, Pairat Kaewsarn, Heavy Metal Uptake Capacities of Common Marine Macro Algal Biomass. *Water Research* **1999**, 33, (6), 1534-1537.
15. Gardea-Torresdey, J. L., et. al., Adsorption of Toxic Metal Ions from Solution By Inactivated Cells of *Larrea Tridentata*. *Journal of Hazardous Substance Research* 1.
16. Goel, J.; Kadirvelu, K.; Rajagopal, C.; Garg, V. K., Investigation of adsorption of lead, mercury and nickel from aqueous solutions onto carbon aerogel. *Journal of Chemical Technology and Biotechnology* **2005**, 80, (4), 469-476.
17. Goel, J., K. Kadirvelu, C. Rahagopal, V.K. Garg, Removal of Lead(II) from Aqueous Solution by Adsorption on Carbon Aerogel Using a Response Surface Methodological Approach. *Industrial Engineering Chemistry Research* **2005**, 44, 1987-1994.

18. Lodeiro, P. e. a., The Marine Macroalga *Cystoseira Baccata* as Biosorbent for Cadmium (II) and Lead (II) Removal: Kinetic and Equilibrium Studies. *Environmental Pollution* **2006**, 142, 264-273.
19. Naja, G. e. a., Lead Biosorption Study with *Rhizopus Arrhizus* Using a Metal Based Titration Technique. *Journal of Colloid and Interface Science* **2005**, 292, (2).
20. Shin, D. H., et. Al., Design of High Efficiency Chelate Fibers with an Amine Group to Remove Heavy Metal Ions and pH-Related FT-IR Analysis. *Industrial Engineering Chemistry Research* **2004**, 43.
21. Zulkali, e. a., Comparative Studies of *Oryza Sativa* L. Husk and Chitosan as Lead Adsorbent. *Journal of Chemical Technology and Biotechnology* **2005**, 0268-2575.
22. Deng, S., Renbi Bai and J. Paul Chen, Aminated Polyacrylonitrile Fibers for Lead and Copper Removal. *Langmuir* **2003**, 19, 5058-5064.
23. Deng, S., and Yen-Peng Ting, , Characterization of PEI-modified Biomass and Biosorption of Cu(II), Pb(II) and Ni(II). *Water Research* **2005**, 39, 2167-2177.
24. Li, Y.-H., et. al., Adsorption Thermodynamic, Kinetic and Desorption Studies of Pb²⁺ on Carbon Nanotubes. *Water Research* **2005**, 39, 605-609.
25. Rivera-Utrilla, J., Activated Carbon Surface Modifications by Adsorption of Bacteria and Their Effect on Aqueous Lead Adsorption. *Journal of Chemical Technology and Biotechnology* **2001**, 76, 1209-1215.
26. Shekinah, P., et. al., Adsorption of Lead(II) from Aqueous Solution by Activated Carbon Prepared from *Eichhornia*. *Journal of Chemical Technology and Biotechnology* **2002**, (77), 458-464.
27. Shukla, S., and Roshan S. Pai, Removal of Pb(II) From Solution Using Cellulose-Containing Materials. *Journal of Chemical Technology and Biotechnology* **2005**, 80, 176-183.
28. Yan, G., and Thiruvengkatachari Viraraghavan, Heavy-Metal Removal From Aqueous Solution by Fungus *Mucor Rouxii*. *Water Research* **2003**, 37, 4486-4496.
29. Zhan, X.-M., and Xuan Zhao, Mechanism of Lead Adsorption From Aqueous Solutions Using an Adsorbent Synthesized From Natural Condensed Tannin. *Water Research* **2003**, 37, 3905-3912.
30. Abdel-Halim, S. H., et. al., Removal of Lead Ions from Industrial Waste Water by Different Types of Natural Materials. *Water Research* **2003**, 37, 1678-1683.
31. Ahluwalia, S. S., D. Goyal, Removal of Heavy Metals by Waste Tea Leaves from Aqueous Solution. *Engineering in Life Sciences* **2005**, 5, (2), 158-162.
32. Akhtar, N., J. Iqbal, M. Iqbal, Enhancement of Lead(II) Biosorption by Microalgal Biomass Immobilized onto Loofa (*Luffa cylindrica*) Sponge. *Engineering in Life Sciences* **2004**, 4, (2), 171-178.
33. Chang, J.-S., Jeng-Charn Huang, Selective Adsorption/Recovery of Pb, Cu and Cd with Multiple Fixed Beds Containing Immobilized Bacterial Biomass. *Biotechnology Progress* **1998**, 14, 735-741.
34. Denizli, A.; Ozkan, G.; Arica, M. Y., Preparation and characterization of magnetic polymethylmethacrylate microbeads carrying ethylene diamine for removal of Cu(II), Cd(II), Pb(II), and Hg(II) from aqueous solutions. *Journal of Applied Polymer Science* **2000**, 78, (1), 81-89.
35. Krishnan, K. A., A. Sheela, T. S. Anirudhan, Kinetic and Equilibrium Modeling of Liquid-Phase Adsorption of Lead and Lead Chelates on Activated Carbons. *Journal of Chemical Technology and Biotechnology* **2003**, 78, (6), 642-653.

36. Malik, D. J., Characterization of Novel Modified Active Carbons and Marine Algal Biomass for the Selective Adsorption of Lead. *Water Research* **2002**, 36, 1527-1538.
37. Puranik, P. R., K. M. Paknikar, Biosorption of Lead Cadmium, and Zinc by Citrobacter Strain MCM B-181: Characterization Studies. *Biotechnology Progress* **1999**, 15, 228-237.
38. Zou, W., Runping Han, Zongzhang Chen, Jie Shi, Liu Hongmin, Characterization and Properties of Manganese Oxide Coated Zeolite as Adsorbent for Removal of Copper(II) and Lead(II) Ions from Solution. *J. Chem. Eng. Data* **2006**, 51, 534-541.
39. Choi, S. B., Y.S. Yun, Lead Biosorption by Waste Biomass of Corynebacterium Glutamicum Generated from Lysine Fermentation Process. *Biotechnology Letters* **2004**, 26, 331-336.
40. Ferraz, A. I., Teixeira, J.A., The Use of Flocculating Brewer's Yeast for Cr(III) and Pb(II) Removal from Residual Wastewaters. *Bioprocess Engineering* **1999**, 21, 431-437.
41. Hamdy, A. A., Removal of Pb(2+) by Biomass of Marine Algae. *Current Microbiology* **2000**, 41, 239-245.
42. Ho, Y. S., G. McKay, Batch Sorber Design Using Equilibrium and Contact Time Data for the Removal of Lead. *Water, Air and Soil Pollution* **2000**, 124, 141-153.
43. Marques, P. A. S. S., M.F. Rosa, H.M. Pinheiro, pH Effects on the Removal of Cu(2+), Cd(2+) and Pb (2+) from Aqueous Solution by Waste Brewery Biomass. *Bioprocess Engineering* **2000**, 23, 135-141.
44. Feng, W. G.; Kwon, S.; Feng, X.; Borguet, E.; Vidic, R. D., Sulfur impregnation on activated carbon fibers through H₂S oxidation for vapor phase mercury removal. *Journal of Environmental Engineering-Asce* **2006**, 132, (3), 292-300.
45. Hsi, H. C.; Rood, M. J.; Rostam-Abadi, M.; Chen, S. G.; Chang, R., Mercury adsorption properties of sulfur-impregnated adsorbents. *Journal of Environmental Engineering-Asce* **2002**, 128, (11), 1080-1089.
46. Schroden, R. C.; Al-Daous, M.; Sokolov, S.; Melde, B. J.; Lytle, J. C.; Stein, A.; Carbajo, M. C.; Fernandez, J. T.; Rodriguez, E. E., Hybrid macroporous materials for heavy metal ion adsorption. *Journal of Materials Chemistry* **2002**, 12, (11), 3261-3267.
47. Peric, J., et. al. , Removal of Zinc, Copper and Lead by Natural Zeolite-A Comparison of Adsorption Isotherms. *Water Research* **2004**, 38, 1893-1899.
48. Lee, S.; Dyer, J. A.; Sparks, D. L.; Scrivner, N. C.; Elzinga, E. J., A Multi-Scale Assessment of Pb(II) Sorption on Dolomite. *Journal of Colloid and Interface Science* **2006**, 298, (1), 20-30.
49. Yu, D. Y., Z.R. Xu, X.G. Yang, In Vitro, In Vivo Studies of Cu(II)-Exchanged Montmorillonite for the Removal of Lead (Pb). *Animal Feed Science and Technology* **2006**, 127, 327-335.
50. Seida, Y., Yoshio Nakano, Yasuo Nakamura, Rapid Removal of Dilute Lead from Water by Pyroaurite-Like Compound. *Water Research* **2001**, 35, (10), 2341-2346.
51. Ozawa, M., S. Kanahara, Removal of Aqueous Lead by Fish-Bone Waste Hydroxyapatite Powder. *Journal of Materials Science* **2005**, 40, 1037-1038.
52. Ali, A. A.-H., and Ribhi El-Bishtawi, Removal of Lead and Nickel Ions Using Zeolite Tuff. *Journal of Chemical Technology and Biotechnology* **1997**, 69, 27-34.
53. Altin, O., et. al., Effect of pH, Flow Rate and Concentration on the Sorption of Pb and Cd on Montmorillonite: 1. Experimental. *Journal of Chemical Technology and Biotechnology* **1999**, 74, 1131-1138.

54. Bhattacharjee, S., et. Al., Removal of Lead From Contaminated Water Bodies Using Sea Nodule as an Adsorbent. *Water Research* **2003**, 37, 3954-3966.
55. Bosso, S. T., J. Enzweiler, Evaluation of Heavy Metal Removal from Aqueous Solution Onto Scolecite. *Water Research* **2002**, 36, (19), 4795-4800.
56. Chen, X., Judith V. Wright, James L. Conca, Loni M. Peurrung, Effects of pH on Heavy Metal Sorption on Mineral Apatite. *Environmental Science and Technology* **1997**, 31, (3), 624-631.
57. Curkovic, L., S. Cerjan-Stefanovic, T. Filipan, Metal Ion Exchange by natural and Modified Zeolites. *Water Research* **1997**, 31, (6), 1379-1382.
58. Das, N. C., et. al., A Design of a Vermiculite Column Adsorber for the Removal of Lead From Water. *Environmental Pollution* **1993**, 80, 129-132.
59. Naseem, R., and S.S. Tahir, Removal of Pb(II) from Aqueous/Acidic Solutions by Using Bentonite as an Adsorbent. *Water Research* **2001**, 35, 3982-3986.
60. Orumwense, F. F. O., Removal of Lead from Water by Adsorption on a Kaolinitic Clay. *Journal of Chemical Technology and Biotechnology* **1996**, 65, 363-369.
61. Prasad, M., S. Saxena, S.S. Amritphale, Navin Chandra, Kinetics and Isotherms for Aqueous Lead Adsorption by Natural Minerals. *Industrial Engineering Chemistry Research* **2000**, 39, 3034-3037.
62. Rashed, M. N., Lead Removal from Contaminated Water Using Mineral Adsorbents. *The Environmentalist* **2001**, 21, 187-195.
63. Singh, S. P., L.Q. Ma, M.J. Hendry, Characterization of Aqueous Lead Removal by Phosphatic Clay: Equilibrium and Kinetic Studies. *Journal of Hazardous Materials B* **2006**, 136, 654-662.
64. Trgo, M., J. Peric, N. Vukojevic Medvidovic, A Comparative Study of Ion Exchange Kinetics in Zinc/Lead-Modified Zeolite-Clinoptilolite Systems. *Journal of Hazardous Materials B* **2006**, 136, 938-945.
65. Wu, Z., et. al., Effects of Organic Acids on Adsorption of Lead Onto Montmorillonite, Goethite and Humic Acid. *Environmental Pollution* **2003**, 121, 469-475.
66. Ursini, O.; Lilla, E.; Montanari, R., The investigation on cationic exchange capacity of zeolites: The use as selective ion trappers in the electrokinetic soil technique. *Journal of Hazardous Materials* **2006**, 137, (2), 1079-1088.
67. Gebremedhin-Haile, T.; Olguin, M. T.; Solache-Rios, M., Removal of mercury ions from mixed aqueous metal solutions by natural and modified zeolitic minerals. *Water Air and Soil Pollution* **2003**, 148, (1-4), 179-200.
68. Haggerty, G. M.; Bowman, R. S., Sorption of Chromate and Other Inorganic Anions by Organo-Zeolite. *Environmental Science & Technology* **1994**, 28, (3), 452-458.
69. Devos, D. E.; Thibaultstarzyk, F.; Knopsgerrits, P. P.; Parton, R. F.; Jacobs, P. A., A Critical Overview of the Catalytic Potential of Zeolite-Supported Metal-Complexes. *Macromolecular Symposia* **1994**, 80, 157-184.
70. Wingenfelder, U., et. Al., Removal of Heavy Metals from Mine Waters by Natural Zeolites. *Environmental Science Technology* **2005**, 39.
71. Bowe, C. A., Robert F. Benson, Dean F. Martin, Extraction of Heavy Metals by Mercaptans Attached to Silica Gel by a Corkscrew Mechanism. *Environmental Science and Health Part A* **2002**, 37, (8), 1391-1398.

72. Bowe, C. A., Duke D. Poore, Robert F. Benson, Dean F. Martin, Extraction of Heavy Metals by Amines Adsorbed onto Silica Gel. *Journal of Environmental Science and Health* **2003**, 38, (11), 2653-2660.
73. Scott, J., Deyan Guang, Kornat Naeramitmarnsuk, Mallika Thabuot, Rose Amal, Zeolite Synthesis from Coal Fly Ash for the Removal of Lead Ions from Aqueous Solution. *Journal of Chemical Technology and Biotechnology* **2001**, 77, 63-69.
74. Xu, Y.-M., Rong-Shu Wang, Feng Wu, Surface Characters and Adsorption Behavior of Pb(II) onto a Mesoporous Titanosilicate Molecular Sieve. *Journal of Colloid and Interface Science* **1999**, 209, 380-385.
75. Lv, L., et. Al., Competitive Adsorption of Pb, Cu and Cd Ions on Microporous Titanosilicate ETS-10. *Journal of Colloid and Interface Science* **2005**, 287, (1).
76. Chiron, N., et. al., Adsorption of Cu(II) and Pb(II) Onto a Grafted Silica: Isotherms and Kinetic Models. *Water Research* **2003**, 37, 3079-3086.
77. Tran, H. H., F.A. Roddick, J.A. O'Donnell, Comparison of Chromatography and Desiccant Silica Gels for the Adsorption of Metal Ions-I. Adsorption and Kinetics. *Water Research* **1999**, 33, (13), 2992-3000.
78. Contreras, C., Guadalupe de la Rosa, Jose R. Peralta-Videa, Jorge L. Gardea-Torresdey, Lead Adsorption by Silica-immobilized Humic Under Flow and Batch Conditions: Assessment of Flow Rate and Calcium and Magnesium Interference. *Journal of Hazardous Materials B* **2006**, 133, 79-84.
79. Delacour, M. L., E. Gailliez, M. Bacquet, M. Morcellet, Poly(ethylenimine) Coated onto Silica Gels: Adsorption Capacity Toward Lead and Mercury. *Journal of Applied Polymer Science* **1998**, 73, 899-906.
80. Han, R., Weihua Zou, Zongpei Zhang, Jie Shi, Jiujun Yang, Removal of Copper(II) and Lead(II) from Aqueous Solution by Manganese Oxide Coated Sand I. Characterization and Kinetic Study. *Journal of Hazardous Materials B* **2006**, 137, 384-395.
81. Poore, D. D., Robert F. Benson, Dean F. Martin, Removal of Heavy Metal Ions From Aqueous Solutions Using Dithiooxamides Supported on Silica Gel. *Environmental Science and Health Part A* **1996**, 31, (9), 2167-2172.
82. Terada, K., Akihiko Inoue, Junko Inamura, Toshiyasu Kiba, 2-Mercaptobenzothiazole Supported on Silica Gel for the Chromatographic Concentration of Cadmium, Copper, Lead, and Zinc in Natural Water Samples. *Bulletin of the Chemical Society of Japan* **1977**, 50, (5), 1060-1065.
83. Verwilghen, C. e. a., Lead and Cadmium Uptake by Sulfur-Containing Modified Silica Gels. *Environmental Chemistry Letters* **2004**.
84. Voken, M. a. O. Y. A., Pre-Concentration of Some Trace Metals from Sea Water on a Mercapto-modified Silica Gel. *Analyst* **1987**, 112, 1409-1412.
85. Han, R., Weihua Zou, Hongkui Li, Yanhu Li, Jie Shi, Copper(II) and Lead(II) Removal from Aqueous Solution in Fixed-Bed Columns by Manganese Oxide Coated Zeolite. *Journal of Hazardous Materials B* **2006**, 137, 934-942.
86. Olkhoviyk, O.; Jaroniec, M., Adsorption characterization of ordered mesoporous silicas with mercury-specific immobilized ligands. *Adsorption-Journal of the International Adsorption Society* **2005**, 11, 685-690.
87. Venkatesan, K. A.; Srinivasan, T. G.; Rao, P. R. V., Removal of complexed mercury by dithiocarbamate grafted on mesoporous silica. *Journal of Radioanalytical and Nuclear Chemistry* **2003**, 256, (2), 213-218.

88. Aguado, J.; Arsuaga, J. M.; Arencibia, A., Adsorption of aqueous mercury(II) on propylthiol-functionalized mesoporous silica obtained by cocondensation. *Industrial & Engineering Chemistry Research* **2005**, 44, (10), 3665-3671.
89. Olkhovyk, O.; Jaroniec, M., Ordered mesoporous silicas with 2,5-dimercapto-1,3,4-thiadiazole ligand: High capacity adsorbents for mercury ions. *Adsorption-Journal of the International Adsorption Society* **2005**, 11, (3-4), 205-214.
90. Perez-Quintanilla, D.; del Hierro, I.; Carrillo-Hermosilla, F.; Fajardo, M.; Sierra, I., Adsorption of mercury ions by mercapto-functionalized amorphous silica. *Analytical and Bioanalytical Chemistry* **2006**, 384, (3), 827-838.
91. Bibby, A.; Mercier, L., Mercury(II) ion adsorption behavior in thiol-functionalized mesoporous silica microspheres. *Chemistry of Materials* **2002**, 14, (4), 1591-1597.
92. Antochshuk, V.; Jaroniec, M., 1-allyl-3-propylthiourea modified mesoporous silica for mercury removal. *Chemical Communications* **2002**, (3), 258-259.
93. Strawn, D. G., et. al., Kinetics and Mechanisms of Pb(II) Sorption and Desorption at the Aluminum Oxide-Water Interface. *Environmental Science Technology* **1998**, 32, 2596-2601.
94. Dimitrova, S. V., Use of Granular Slag Columns for Lead Removal. *Water Research* **2002**, 36, 4001-4008.
95. Curkovic, L., et. al., Batch Pb²⁺ and Cu²⁺ Removal by Electric Furnace Slag. *Water Research* **2001**, 35, 3436-3440.
96. Dong, D., et. al., Adsorption of Pb and Cd Onto Metal Oxides and Organic Material in Natural Surface Coatings as Determined by Selective Extractions: New Evidence for the Importance of Mn and Fe Oxides. *Water Research* **2000**, 34, 427-436.
97. Dong, D., et. al., Lead Adsorption to Metal Oxides and Organic Material of Freshwater Surface Coatings Determined Using a Novel Selective Extraction Method. *Environmental Pollution* **2002**, 119, 317-321.
98. Gupta, V. K., et. al., Process Development for the Removal of Lead and Chromium from Aqueous Solutions Using Red Mud-An Aluminum Industry Waste. *Water Research* **2001**, 35, 1125-1134.
99. Ozverdi, A., Mehmet Erdem, Cu²⁺, Cd²⁺ and Pb²⁺ Adsorption from Aqueous Solutions by Pyrite and Synthetic Iron Sulphide. *Journal of Hazardous Materials B* **2006**, 137, 626-632.
100. Pan, B., Bingjun Pan, Xinqing Chen, Weiming Zhang, Xiao Zhang, Qingjian Zhang, Quanxing Zhang, Jinlong Chen, Preparation and Preliminary Assessment of Polymer-Supported Zirconium Phosphate for Selective Lead Removal from Contaminated Water. *Water Research* **2006**, 40, 2938-2946.
101. Smith, E. H., Uptake of Heavy Metals in Batch Systems by a Recycled Iron-Bearing Material. *Water Research* **1996**, 30, (10), 2424-2434.
102. Xu, Y., Surface Complexation of Pb(II) on Iron Oxide and Manganese Oxide: Spectroscopic and Time Studies. *Journal of Colloid and Interface Science* **299**, 28-40.
103. Cho, H., et al., A Study on Removal Characteristics of Heavy Metals from Aqueous Solution by Fly Ash. *Journal of Hazardous Materials* **2005**, 127, (1-3).
104. Barrer, R. M.; White, E. A. D., The Hydrothermal Chemistry of Silicates .1. Synthetic Lithium Aluminosilicates. *Journal of the Chemical Society* **1951**, (MAY), 1267-&.
105. Barrer, R. M.; White, E. A. D., The Hydrothermal Chemistry of Silicates .2. Synthetic Crystalline Sodium Aluminosilicates. *Journal of the Chemical Society* **1952**, (MAY), 1561-1571.
106. Barrer, R. M.; McCallum, N., Hydrothermal Chemistry of Silicates .4. Rubidium and Cesium Aluminosilicates. *Journal of the Chemical Society* **1953**, (DEC), 4029-&.

107. Barrer, R. M., Synthesis of a Zeolitic Mineral with Chabazite-Like Sorptive Properties. *Journal of the Chemical Society* **1948**, (FEB), 127-&.
108. Barrer, R. M., Ion Exchange and Ion-Sieve Processes in Crystalline Zeolites. *Journal of the Chemical Society* **1950**, (SEP), 2342-2350.
109. Barrer, R. M.; Hinds, L., Ion-Exchange in Crystals of Analcite and Leucite. *Journal of the Chemical Society* **1953**, (JUN), 1879-&.
110. Amphlett, C. B.; McDonald, L. A.; Redman, M. J., Cation Exchange Properties of Zirconium Phosphate. *Chemistry & Industry* **1956**, (44), 1314-1315.
111. Amphlett, C. B.; McDonald, L. A.; Redman, M. J., Synthetic Inorganic Ion-Exchange Materials .1. Zirconium Phosphate. *Journal of Inorganic & Nuclear Chemistry* **1958**, 6, (3), 220-235.
112. Amphlett, C. B.; McDonald, L. A.; Redman, M. J., Synthetic Inorganic Ion-Exchange Materials .2. Hydrous Zirconium Oxide and Other Oxides. *Journal of Inorganic & Nuclear Chemistry* **1958**, 6, (3), 236-245.
113. Helfferich, F., *Ion Exchange*. McGraw-Hill Book Company, Inc.: New York, 1962.
114. Baes, C. F.; Mesmer, R. E., The Thermodynamics of Cation Hydrolysis. *American Journal of Science* **1981**, 281, (7), 935-962.
115. Reddy, M. A., G. Speciation and Fractionation Modeling Studies - Dissolved Organic Carbon (DOC)-Mercury Interaction. http://www.brr.cr.usgs.gov/projects/SW_corrosion/mercury-poster/index.html (July 15, 2010),
116. Dobb, D. E. R., G. A.; Rowan, J. T.; Butler, L. C. In *Preservation of Mercury in Environmental Aqueous Performance Evaluation Samples*, I & EC Special Symposium of the American Chemical Society, Atlanta, GA, 1993; Atlanta, GA, 1993; pp 426-429.
117. Pohorecky, L. A.; Brick, J., Pharmacology of Ethanol. *Pharmacology & Therapeutics* **1988**, 36, (2-3), 335-427.
118. Elsayed, N. M.; Omaye, S. T.; Klain, G. J.; Inase, J. L.; Dahlberg, E. T.; Wheeler, C. R.; Korte, D. W., Response of Mouse-Brain to a Single Subcutaneous Injection of the Monofunctional Sulfur Mustard, Butyl 2-Chloroethyl Sulfide (Bcs). *Toxicology* **1989**, 58, (1), 11-20.
119. Dixon, M.; Needham, D. M., Biochemical Research on Chemical Warfare Agents. *Nature* **1946**, 158, (4013), 432-438.
120. Dacre, J. C.; Goldman, M., Toxicology and pharmacology of the chemical warfare agent sulfur mustard. *Pharmacological Reviews* **1996**, 48, (2), 289-326.
121. *Dimethyl methanephosphonate*. 4 ed.; Noyes Publications: William Andrew Publishing: Norwich, NY, 2002; Vol. 1.
122. Smith, D. B.; Goldstein, S. G.; Roomet, A., A Comparison of the Toxicity Effects of the Anticonvulsant Eterobarb (Antilon, Dmmp) and Phenobarbital in Normal Human Volunteers. *Epilepsia* **1986**, 27, (2), 149-155.
123. Mattie, D. R.; Hixson, C. J.; Gaworski, C. L.; Thorson, G. R., Toxic Effects of Inhaled Dimethyl Methylphosphonate (Dmmp) on the Testes of Fischer-344 Rats. *Toxicology* **1987**, 47, (1-2), 231-232.
124. *Butyl Mercaptan*. 4 ed.; Noyes Publications: William Andrew Publishing: Norwich, NY, 2002; Vol. 1.
125. Ames, R. G.; Gregson, J., Mortality Following Cotton Defoliation - San-Joaquin Valley, California, 1970-1990. *Journal of Occupational and Environmental Medicine* **1995**, 37, (7), 812-819.

126. M256A1 Chemical Agent Detector Kit. In *U.S. Army Equipment Information*, 2005; Vol. Army Study Guide.
127. *M256A1 Chemical Agent Detector Kit*. Tradeways Ltd.: Annapolis, MD.
128. Ingles, S., *Chemical and Biological Protection, Detection and Decontamination Items*. U.A.S. a.B.C.C.: 2001.
129. In *Detection of Chemical Weapons*, Organisation for the Prohibition of Chemical Weapons.
130. Davis, G., CBRNE - Chemical Detection Equipment. In.
131. *Guide for the Selection of Chemical Agent and Toxic Industrial Material Detection Equipment for Emergency First Responders, Guide 100-04*. SAVER: 2005; Vol. I and II.
132. Kosal, M. E., *The Basics of Chemical and Biological Weapons*. Center for Non-proliferation Studies: USA, 2003.
133. Coutant, S., Chemical Warfare Agent Detection and Personal Protection. *Jane's Defence Weekly* **1999**.
134. Longworth, T. L. C., J.C.; Barnhouse, J.L.; Ong, K.Y.; Procell, S.A., Domestic Preparedness Program: Testing of Commercially Available Detectors Against Chemical Warfare Agents: Summary Report. In Ground, A. P., Ed. Maryland, 1999; pp 1-11.
135. Nieuwenhuizen, M. S., *Detection and Screening of Chemicals related to the Chemical Weapons Convention*. John Wiley and Sons, Ltd.: 2006.
136. Sun, Y. O., K. Y., *Detection Technologies for Chemical Warfare Agents and Toxic Vapors*. 1 ed.; CRC Press: Boca Raton, FL, 2005.
137. Traeger, J. C., Strategy for Incidental Detection of Chemical Warfare Agents by Australian Customs. In 2006; pp 1-8.
138. Frishman, G. A., A., Fast-GC-PFPD System for Field Analysis of Chemical Warfare Agents. *Field Analytical Chemistry and Technology* **2000**, 4, (4), 170-194.
139. Seto, Y. K.-K., M.; tsuge, K.; Ohsawa, I.; Matsushita, K.; Sekiguchi, H.; Itoi, T.; Iura, K.; Sano, T.; Yamashiro, S., sensing technology for chemical-warfare agents and its evaluation using authentic agents. *Sensors and Actuators B* **2005**, 108, 193-197.
140. Murray, G. M.; Southard, G. E., Sensors for chemical weapons detection. *Ieee Instrumentation & Measurement Magazine* **2002**, 5, (4), 12-21.
141. Eiceman, G. A. K., Z., *Ion Mobility Spectrometry*. CRC Press: Boca Raton, FL, 1994.
142. Creaser, C. S.; Griffiths, J. R.; Bramwell, C. J.; Noreen, S.; Hill, C. A.; Thomas, C. L. P., Ion mobility spectrometry: a review. Part 1. Structural analysis by mobility measurement. *Analyst* **2004**, 129, (11), 984-994.
143. Incidents, C. o. R. D. N. f. I. C. M. R. t. C. a. B. T., Detection and Measurement of Chemical Agents. In National Academy Press: Washington, D.C., 1999; pp 43-64.
144. Hill, H. H.; Martin, S. J., Conventional analytical methods for chemical warfare agents. *Pure and Applied Chemistry* **2002**, 74, (12), 2281-2291.
145. Hill, H. H.; Simpson, G., Capabilities and limitations of ion mobility spectrometry for field screening applications. *Field Analytical Chemistry and Technology* **1997**, 1, (3), 119-134.
146. *SIFT-MS: A New Method for the Rapid and Accurate Detection of Security Threats*; Syft Technologies: 2005.
147. Cajigas, J. C. L., T. L.; Davis, N.; Ong, K. Y., Testing of HAZMATCAD Detectors Against Chemical Warfare Agents: Summary Report of Evaluation Performed at Solider Biological and Chemical Command. In Ground, A. P., Ed. Maryland, 2003; pp 1-12.

148. Surface Acoustic Wave (SAW) Sensing [Technology for the Detection of Nerve and Blister Agents]. In *MSA*, Pittsburgh, PA, 2005.
149. Treacy, M. M. J. H., John B., *Collection of simulated XRD powder patterns for zeolites*. 5 ed.; Elsevier: Boston, 2007; p 485.
150. Annen, M. J. Synthesis and characterization of novel molecular sieves containing three-membered rings. Ph.D. Dissertation, Virginia Polytechnic Institute and State University, Blacksburg, VA, 1992.
151. Beck, J. S.; Vartuli, J. C.; Roth, W. J.; Leonowicz, M. E.; Kresge, C. T.; Schmitt, K. D.; Chu, C. T. W.; Olson, D. H.; Sheppard, E. W.; McCullen, S. B.; Higgins, J. B.; Schlenker, J. L., A New Family of Mesoporous Molecular-Sieves Prepared with Liquid-Crystal Templates. *Journal of the American Chemical Society* **1992**, 114, (27), 10834-10843.
152. Zamzow, M. J.; Eichbaum, B. R.; Sandgren, K. R.; Shanks, D. E., Removal of Heavy Metals and Other Cations from Wastewater Using Zeolites. *Separation Science and Technology* **1990**, 25, (13), 1555 - 1569.
153. Miller, M. W. C., Thomas W., *Mercury, mercurials, and mercaptans*. Thomas: Springfield, IL, 1973; p 386.
154. Somani, S. M. R., James A., *Chemical warfare agents : toxicity at low levels*. CRC Press: Boca Raton, 2001; p 447.
155. Bermudez, V. M., Quantum-chemical study of the adsorption of DMMP and sarin on gamma-Al₂O₃. *Journal of Physical Chemistry C* **2007**, 111, (9), 3719-3728.
156. Schrenk, W. G., *Analytical Atomic Spectroscopy*. Plenum Press: New York, 1975.
157. Smith Jr., S. B., G. M. Hieftje, A New background Correction Method for Atomic Absorption Spectroscopy. *Applied Spectroscopy* **1983**, 37, 419-424.
158. Atomic absorption spectrometry: theory, design and applications. *Atomic absorption spectrometry: theory, design and applications*. **1991**, xx + 529 pp.
159. Huff, T., *Atomic Absorption Spectroscopy*.
160. Settle, F., *Handbook of Instrumental Techniques for Analytical Chemistry* Prentice Hall: 1997.
161. Engstrom, R. W., *Photomultiplier Handbook*. RCA: 1980.
162. Balmer, V., X-Ray Analysis Via Energy Dispersion and Electron-Microscope. *Journal of Microscopy-Oxford* **1974**, 20, (1), A17-A18.
163. Goldstein, J. I.; Newbury, D. E.; Echlin, P.; Joy, D. C.; Fiori, C.; Lifshin, E., Scanning electron microscopy and X-ray microanalysis. A text for biologists, materials scientists, and geologists. *Scanning electron microscopy and X-ray microanalysis. A text for biologists, materials scientists, and geologists*. **1981**, 673 pp.
164. Guinier, A., *X-Ray Diffraction*. W.H. Freeman and Company: San Francisco, 1963.
165. Warren, B. E., *X-Ray Diffraction*. Addison-Wesley: Reading, Massachusetts, 1969.
166. Bragg, W. H., Intensity of Reflexion of X-Rays by Crystals. *Acta Crystallographica Section a-Crystal Physics Diffraction Theoretical and General Crystallography* **1969**, A 25, 3-&.
167. Emmett, P. H.; Brunauer, S.; Love, K. S., The measurement of surface areas of soils and soil colloids by the use of low temperature van der waals adsorption isotherms. *Soil Science* **1938**, 45, (1), 57-65.
168. Anthony, D. J. L. Gas Solubilities in Ionic Liquids: Experimental Measurements and Applications. Ph.D. Dissertation, University of Notre Dame, South Bend, IN, 2004.
169. Moore, D. D. Experimental Studies of Gas Adsorption on Microporous Materials. University of Notre Dame, South Bend, IN, 2000.

170. Sauerbrey, G., Verwendung Von Schwingquarzen Zur Wagung Dunner Schichten Und Zur Mikrowagung. *Zeitschrift Fur Physik* **1959**, 155, (2), 206-222.
171. Varineau, P. T.; Buttry, D. A., Applications of the Quartz Crystal Microbalance to Electrochemistry - Measurement of Ion and Solvent Populations in Thin-Films of Poly(Vinylferrocene) as Functions of Redox State. *Journal of Physical Chemistry* **1987**, 91, (6), 1292-1295.
172. Lu, *Journal of applied physics* **1972**, 43, (11), 4385.
173. McGown, T. Infrared spectroscopy for the characterization of porous zincosilicate materials and their use in lead capture. Masters Thesis, Kansas State University, Manhattan, KS, 2007.
174. Koningsveld, H. v. Schemes for Building Zeolite Framework Models. <http://www.iza-structure.org/databases/> (April 1, 2010),
175. Meier, W. M.; Olson, D. H.; Baerlocher, C., Atlas of zeolite structure types. *Zeolites* **1996**, 17, (1-2), 1-229.
176. Lange, N. A. S., J. G., *Lange's handbook of chemistry*. 16th ed. ed.; McGraw-Hill: New York 2005.
177. Antochshuk, V.; Olkhovyk, O.; Jaroniec, M.; Park, I. S.; Ryoo, R., Benzoylthiourea-modified mesoporous silica for mercury(II) removal. *Langmuir* **2003**, 19, (7), 3031-3034.
178. Robinson, R. A.; Stokes, R. H., Solutions of Electrolytes and Diffusion in Liquids. *Annual Review of Physical Chemistry* **1957**, 8, 37-54.
179. Petruzzelli, D.; Helfferich, F. G.; Liberti, L., Ion-Exchange Kinetics on Reactive Polymers and Inorganic Soil Constituents. *Rates of Soil Chemical Processes* **1991**, 27, 95-118.
180. Bukata, S.; Marinsky, J. A., Ion Exchange in Concentrated Electrolyte Solutions .3. Zeolite Systems with Salts of Group 1 + 2 Metals. *Journal of Physical Chemistry* **1964**, 68, (5), 994-&.
181. Trgo, M.; Peric, J.; Medvidovic, N. V., A comparative study of ion exchange kinetics in zinc/lead - modified zeolite-clinoptilolite systems. *Journal of Hazardous Materials* **2006**, 136, (3), 938-945.
182. Stout, S. C.; Larsen, S. C.; Grassian, V. H., Adsorption, desorption and thermal oxidation of 2-CEES on nanocrystalline zeolites. *Microporous and Mesoporous Materials* **2007**, 100, (1-3), 77-86.
183. Mangrulkar, P. A.; Kamble, S. P.; Meshram, J.; Rayalu, S. S., Adsorption of phenol and o-chlorophenol by mesoporous MCM-41. *Journal of Hazardous Materials* **2008**, 160, (2-3), 414-421.
184. Serrano, D. P.; Calleja, G.; Botas, J. A.; Gutierrez, F. J., Characterization of adsorptive and hydrophobic properties of silicalite-1, ZSM-5, TS-1 and Beta zeolites by TPD techniques. *Separation and Purification Technology* **2007**, 54, (1), 1-9.
185. Crocella, V.; Cerrato, G.; Magnacca, G.; Morterra, C., Adsorption of Acetone on Nonporous and Mesoporous Silica. *Journal of Physical Chemistry C* **2009**, 113, (37), 16517-16529.
186. Hung, C. T.; Bai, H. L.; Karthik, M., Ordered mesoporous silica particles and Si-MCM-41 for the adsorption of acetone: A comparative study. *Separation and Purification Technology* **2009**, 64, (3), 265-272.

Appendix A - Ion Exchange Data

Table 9 VPI-7 Mercury Ion Exchange Data and Calculations Part I

Sample ID	Zeolite Used	Mass Zeolite (g)	Calcined (y/n)	Volume (g)	Exchange Time (hr)
A7.8.10.4.1	VPI-7	0.1509	n	15.1033	10
A7.8.8.4.1	VPI-7	0.1506	n	15.0637	8
A7.8.6.4.1	VPI-7	0.1511	n	15.1084	6
A7.8.4.4.1	VPI-7	0.1499	n	15.0102	4
A7.9.2.4.1	VPI-7	0.1488	n	14.8925	2
A7.9.10.3.1	VPI-7	0.1503	n	15.0357	10
A7.9.8.3.1	VPI-7	0.1509	n	15.1013	8
A7.9.6.3.1	VPI-7	0.1507	n	15.0706	6
A7.10.4.3.1	VPI-7	0.1516	n	15.1674	4
A7.10.2.3.1	VPI-7	0.1512	n	15.136	2
A7.11.10.2.1	VPI-7	0.151	n	15.1041	10
A7.11.8.2.1	VPI-7	0.1501	n	15.0078	8
A7.11.6.2.1	VPI-7	0.15	n	15.0107	6
A7.11.4.2.1	VPI-7	0.1499	n	15.0046	4
A7.13.2.2.1	VPI-7	0.1506	n	15.0652	2
A7.13.10.1.1	VPI-7	0.1507	n	15.0731	10
A7.13.8.1.1.	VPI-7	0.1504	n	15.0399	8
A7.13.6.1.1	VPI-7	0.1505	n	15.0522	6
A7.13.4.1.1	VPI-7	0.1511	n	15.1111	4
A7.14.2.1.1	VPI-7	0.1504	n	15.0403	2
C7.2.10.4.1	VPI-7	0.1506	y	15.0614	10
C7.3.8.4.1	VPI-7	0.1506	y	15.0609	8
C7.3.6.4.1	VPI-7	0.1511	y	15.1121	6
C7.3.4.4.1	VPI-7	0.1512	y	15.1216	4
C7.3.2.4.1	VPI-7	0.1518	y	15.1806	2
C7.4.10.3.1	VPI-7	0.1502	y	15.0239	10
C7.4.8.3.1	VPI-7	0.1504	y	15.0429	8
C7.4.6.3.1	VPI-7	0.1508	y	15.0815	6
C7.4.4.3.1	VPI-7	0.151	y	15.1042	4
C7.4.2.3.1	VPI-7	0.1513	y	15.1351	2
C7.8.10.2.1	VPI-7	0.1507	y	15.0695	10
C7.8.8.2.1	VPI-7	0.1506	y	15.0626	8
C7.8.6.2.1	VPI-7	0.1502	y	15.0217	6
C7.8.4.2.1	VPI-7	0.1493	y	14.9328	4
C7.9.2.2.1	VPI-7	0.1492	y	14.9233	2
C7.9.10.1.1	VPI-7	0.1503	y	15.0286	10
C7.9.8.1.1	VPI-7	0.1517	y	15.1717	8
C7.6.6.1.1	VPI-7	0.1501	y	15.012	6
C7.6.4.1.1	VPI-7	0.15	y	15.0041	4
C7.6.2.1.1	VPI-7	0.1498	y	14.9805	2

Table 10 VPI-7 Mercury Ion Exchange Data and Calculations Part II

Time Error (hr)	Initial Hg conc. (ppm)	AA conc. (ppb)	Dilution Factor	Actual conc.	Hg removed
0.1	20000	3.97	4000000	15880	20.6
0.1	20000	3.95	4000000	15800	21
0.1	20000	4.01	4000000	16040	19.8
0.1	20000	4.13	4000000	16520	17.4
0.1	20000	3.96	4000000	15840	20.8
0.1	2000	2.78	200000	556	72.2
0.1	2000	2.85	200000	570	71.5
0.1	2000	2.61	200000	522	73.9
0.1	2000	2.45	200000	490	75.5
0.1	2000	2.59	200000	518	74.1
0.1	200	3.57	20000	71.4	64.3
0.1	200	3.45	20000	69	65.5
0.1	200	3.01	20000	60.2	69.9
0.1	200	3.98	20000	79.6	60.2
0.1	200	4.04	20000	80.8	59.6
0.1	20	3.3	6000	19.8	1
0.1	20	3.11	6000	18.66	6.7
0.1	20	3.04	6000	18.24	8.8
0.1	20	3.09	6000	18.54	7.3
0.1	20	3.15	6000	18.9	5.5
0.1	20000	4.03	4000000	16120	19.4
0.1	20000	4.44	4000000	17760	11.2
0.1	20000	4.33	4000000	17320	13.4
0.1	20000	4	4000000	16000	20
0.1	20000	3.61	4000000	14440	27.8
0.1	2000	2.81	200000	562	71.9
0.1	2000	2.5	200000	500	75
0.1	2000	2.63	200000	526	73.7
0.1	2000	2.93	200000	586	70.7
0.1	2000	2.99	200000	598	70.1
0.1	200	3.61	20000	72.2	63.9
0.1	200	3.78	20000	75.6	62.2
0.1	200	3.61	20000	72.2	63.9
0.1	200	3.73	20000	74.6	62.7
0.1	200	3.75	20000	75	62.5
0.1	20	3.4	6000	20.4	-2
0.1	20	3.02	6000	18.12	9.4
0.1	20	2.87	6000	17.22	13.9
0.1	20	2.93	6000	17.58	12.1
0.1	20	2.97	6000	17.82	10.9

Table 11 VPI-7 Mercury Ion Exchange Data and Calculations Part III

Hg mass (mol)	Zn (mol)	Hg:Zn
3.1224E-04	3.8442E-04	0.8122
3.1461E-04	3.7663E-04	0.8353
2.9587E-04	3.7462E-04	0.7898
2.5318E-04	3.6508E-04	0.6935
2.4123E-04	2.8970E-04	0.8327
1.0769E-04	3.7362E-04	0.2882
1.0545E-04	3.6960E-04	0.2853
1.0884E-04	3.6960E-04	0.2945
1.1482E-04	3.8191E-04	0.3006
1.1339E-04	3.8643E-04	0.2934
9.7679E-06	3.8241E-04	0.0255
9.9336E-06	3.8141E-04	0.0260
1.0658E-05	3.8367E-04	0.0278
9.1770E-06	3.8191E-04	0.0240
8.9071E-06	3.7563E-04	0.0237
1.5220E-08	3.8191E-04	0.0000
9.9511E-08	3.7261E-04	0.0003
1.3215E-07	3.7764E-04	0.0003
1.0620E-07	3.6558E-04	0.0003
8.2458E-08	3.7638E-04	0.0002
2.9156E-04	3.7839E-04	0.7705
1.6802E-04	3.7613E-04	0.4467
2.0084E-04	3.7638E-04	0.5336
3.0678E-04	3.8568E-04	0.7954
4.1629E-04	3.7462E-04	1.1112
1.0808E-04	3.7739E-04	0.2864
1.0913E-04	3.8191E-04	0.2857
8.5473E-05	3.8643E-04	0.2212
1.0545E-04	3.8241E-04	0.2758
1.0339E-04	3.8141E-04	0.2711
9.4111E-06	3.8367E-04	0.0245
9.4590E-06	3.8191E-04	0.0248
9.7781E-06	3.7563E-04	0.0260
9.5249E-06	3.8191E-04	0.0249
9.4786E-06	3.7261E-04	0.0254
-3.0494E-08	3.7764E-04	-0.0001
1.4330E-07	3.6558E-04	0.0004
2.0773E-07	3.7638E-04	0.0006
1.8416E-07	3.7839E-04	0.0005
1.6381E-07	3.7613E-04	0.0004

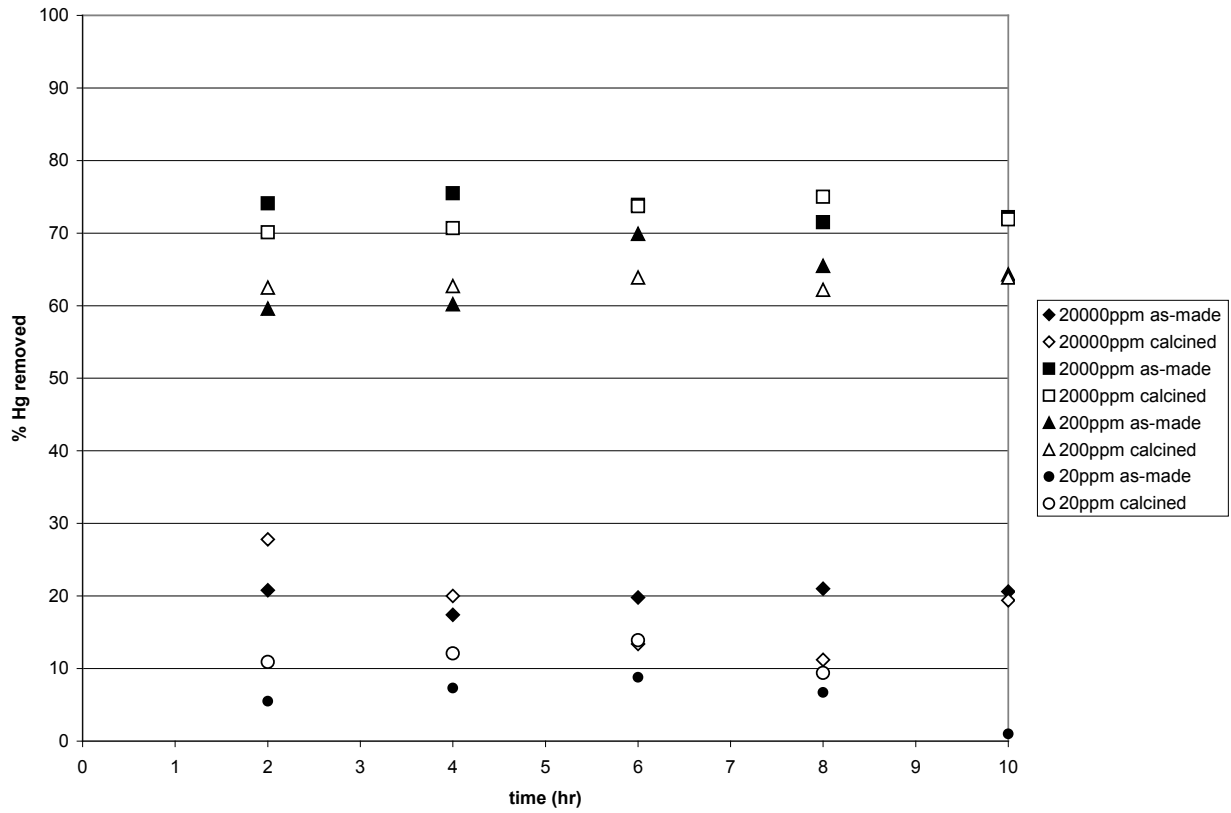


Figure 53 VPI-7 Mercury Ion Exchange Percent Removal as Function of Time

VPI-7 mercury exchanges

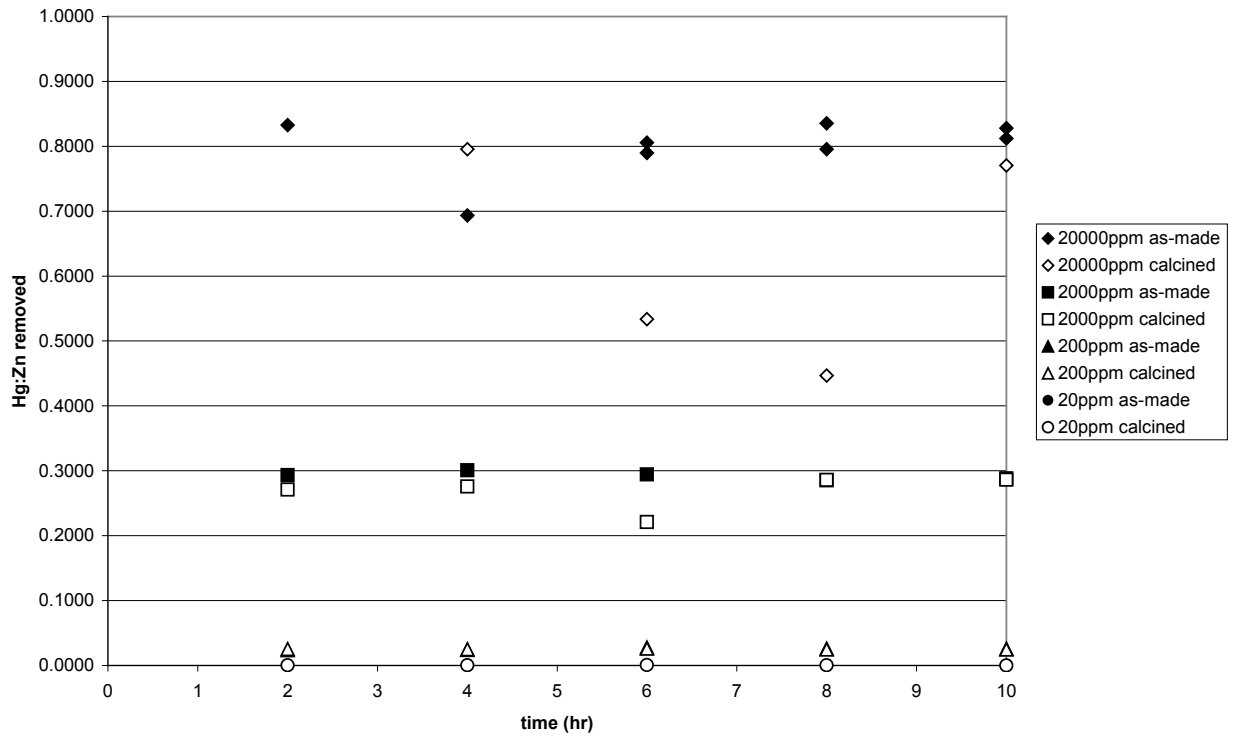


Figure 54 VPI-7 Ion Exchange Mercury:Zinc as Function of Time

Table 12 VPI-9 Mercury Ion Exchange Data and Calculations Part I

Sample ID	Zeolite Used	Mass Zeolite (g)	Calcined (y/n)	Volume (g)	Exchange Time (hr)
A9.8.10.4.1	VPI-9	0.153	n	15.1575	10
A9.8.8.4.1	VPI-9	0.1499	n	14.9815	8
A9.8.6.4.1	VPI-9	0.1491	n	14.9427	6
A9.8.4.4.1	VPI-9	0.1453	n	14.5503	4
A9.9.2.4.1	VPI-9	0.1153	n	11.5974	2
A9.9.10.3.1	VPI-9	0.1487	n	14.9157	10
A9.9.8.3.1	VPI-9	0.1471	n	14.7485	8
A9.9.6.3.1	VPI-9	0.1471	n	14.7278	6
A9.10.4.3.1	VPI-9	0.152	n	15.2074	4
A9.10.2.3.1	VPI-9	0.1538	n	15.3022	2
A9.10.10.2.1	VPI-9	0.1522	n	15.1912	10
A9.10.8.2.1	VPI-9	0.1518	n	15.1658	8
A9.10.6.2.1	VPI-9	0.1527	n	15.2468	6
A9.11.4.2.1	VPI-9	0.152	n	15.2442	4
A9.11.2.2.1	VPI-9	0.1495	n	14.9448	2
A9.11.10.1.1	VPI-9	0.152	n	15.2199	10
A9.11.8.1.1	VPI-9	0.1483	n	14.8524	8
A9.12.6.1.1	VPI-9	0.1503	n	15.0173	6
A9.12.4.1.1	VPI-9	0.1455	n	14.5474	4
A9.12.2.1.1	VPI-9	0.1498	n	14.9923	2
C9.8.10.4.1	VPI-9	0.1506	y	15.0287	10
C9.8.8.4.1	VPI-9	0.1497	y	15.0014	8
C9.8.6.4.1	VPI-9	0.1498	y	14.9879	6
C9.8.4.4.1	VPI-9	0.1535	y	15.3388	4
C9.9.2.4.1	VPI-9	0.1491	y	14.9744	2
C9.9.10.3.1	VPI-9	0.1502	y	15.0317	10
C9.9.8.3.1	VPI-9	0.152	y	14.5503	8
C9.9.6.3.1	VPI-9	0.1538	y	11.5974	6
C9.10.4.3.1	VPI-9	0.1522	y	14.9157	4
C9.10.2.3.1	VPI-9	0.1518	y	14.7485	2
C9.10.10.2.1	VPI-9	0.1527	y	14.7278	10
C9.10.8.2.1	VPI-9	0.152	y	15.2074	8
C9.10.6.2.1	VPI-9	0.1495	y	15.3022	6
C9.11.4.2.1	VPI-9	0.152	y	15.1912	4
C9.11.2.2.1	VPI-9	0.1483	y	15.1658	2
C9.11.10.1.1	VPI-9	0.1503	y	15.2468	10
C9.11.8.1.1	VPI-9	0.1455	y	15.2442	8
C9.12.6.1.1	VPI-9	0.1498	y	14.9448	6
C9.12.4.1.1	VPI-9	0.1506	y	15.2199	4
C9.12.2.1.1	VPI-9	0.1497	y	15.0287	2

Table 13 VPI-9 Mercury Ion Exchange Data and Calculations Part II

Time Error (hr)	Initial Hg conc. (ppm)	AA conc. (ppb)	Dilution Factor	Actual conc.	Hg removed
0.1	20000	4.3	4000000	17200	14
0.1	20000	4.25	4000000	17000	15
0.1	20000	4.15	4000000	16600	17
0.1	20000	4.19	4000000	16760	16.2
0.1	20000	4.26	4000000	17040	14.8
0.1	2000	2.28	100000	228	88.6
0.1	2000	2.25	100000	225	88.75
0.1	2000	2.34	100000	234	88.3
0.1	2000	2.41	100000	241	87.95
0.1	2000	2.21	100000	221	88.95
0.1	200	3.09	2000	6.18	96.91
0.1	200	3.07	2000	6.14	96.93
0.1	200	3.08	2000	6.16	96.92
0.1	200	3.15	2000	6.3	96.85
0.1	200	3.01	2000	6.02	96.99
0.1	20	2.78	100	0.278	98.61
0.1	20	2.71	100	0.271	98.645
0.1	20	2.78	100	0.278	98.61
0.1	20	2.65	100	0.265	98.675
0.1	20	2.55	100	0.255	98.725
0.1	20000	4.33	4000000	17320	13.4
0.1	20000	4.31	4000000	17240	13.8
0.1	20000	4.37	4000000	17480	12.6
0.1	20000	4.42	4000000	17680	11.6
0.1	20000	4.27	4000000	17080	14.6
0.1	2000	2.3	100000	230	88.5
0.1	2000	2.24	100000	224	88.8
0.1	2000	2.36	100000	236	88.2
0.1	2000	2.31	100000	231	88.45
0.1	2000	2.34	100000	234	88.3
0.1	200	3.15	2000	6.3	96.85
0.1	200	3.18	2000	6.36	96.82
0.1	200	3.24	2000	6.48	96.76
0.1	200	3.11	2000	6.22	96.89
0.1	200	3.14	2000	6.28	96.86
0.1	20	2.8	100	0.28	98.6
0.1	20	2.7	100	0.27	98.65
0.1	20	2.69	100	0.269	98.655
0.1	20	2.79	100	0.279	98.605
0.1	20	2.8	100	0.28	98.6

Table 14 VPI-9 Mercury Ion Exchange Data and Calculations Part III

Hg mass (mol)	Zn (mol)	Hg:Zn
3.1113E-04	3.7915E-04	0.8206
3.1634E-04	3.7839E-04	0.8360
2.9915E-04	3.7965E-04	0.7880
2.6118E-04	3.7663E-04	0.6935
3.0976E-04	3.7387E-04	0.8285
1.0856E-04	3.7764E-04	0.2875
1.0797E-04	3.7915E-04	0.2848
1.1137E-04	3.7864E-04	0.2941
1.1451E-04	3.8090E-04	0.3006
1.1216E-04	3.7990E-04	0.2952
9.7119E-06	3.7940E-04	0.0256
9.8301E-06	3.7714E-04	0.0261
1.0492E-05	3.7688E-04	0.0278
9.0328E-06	3.7663E-04	0.0240
8.9789E-06	3.7839E-04	0.0237
1.5073E-08	3.7864E-04	0.0000
1.0077E-07	3.7789E-04	0.0003
1.3246E-07	3.7814E-04	0.0004
1.1031E-07	3.7965E-04	0.0003
8.2722E-08	3.7789E-04	0.0002
2.9219E-04	3.7839E-04	0.7722
1.6868E-04	3.7839E-04	0.4458
2.0250E-04	3.7965E-04	0.5334
3.0243E-04	3.7990E-04	0.7961
4.2202E-04	3.8141E-04	1.1065
1.0802E-04	3.7739E-04	0.2862
1.1282E-04	3.7789E-04	0.2986
1.1115E-04	3.7889E-04	0.2934
1.0679E-04	3.7940E-04	0.2815
1.0610E-04	3.8015E-04	0.2791
9.6294E-06	3.7864E-04	0.0254
9.3689E-06	3.7839E-04	0.0248
9.5989E-06	3.7739E-04	0.0254
9.3629E-06	3.7513E-04	0.0250
9.3271E-06	3.7487E-04	0.0249
-3.0057E-08	3.7764E-04	-0.0001
1.4261E-07	3.8116E-04	0.0004
2.0867E-07	3.7714E-04	0.0006
1.8155E-07	3.7688E-04	0.0005
1.6329E-07	3.7638E-04	0.0004

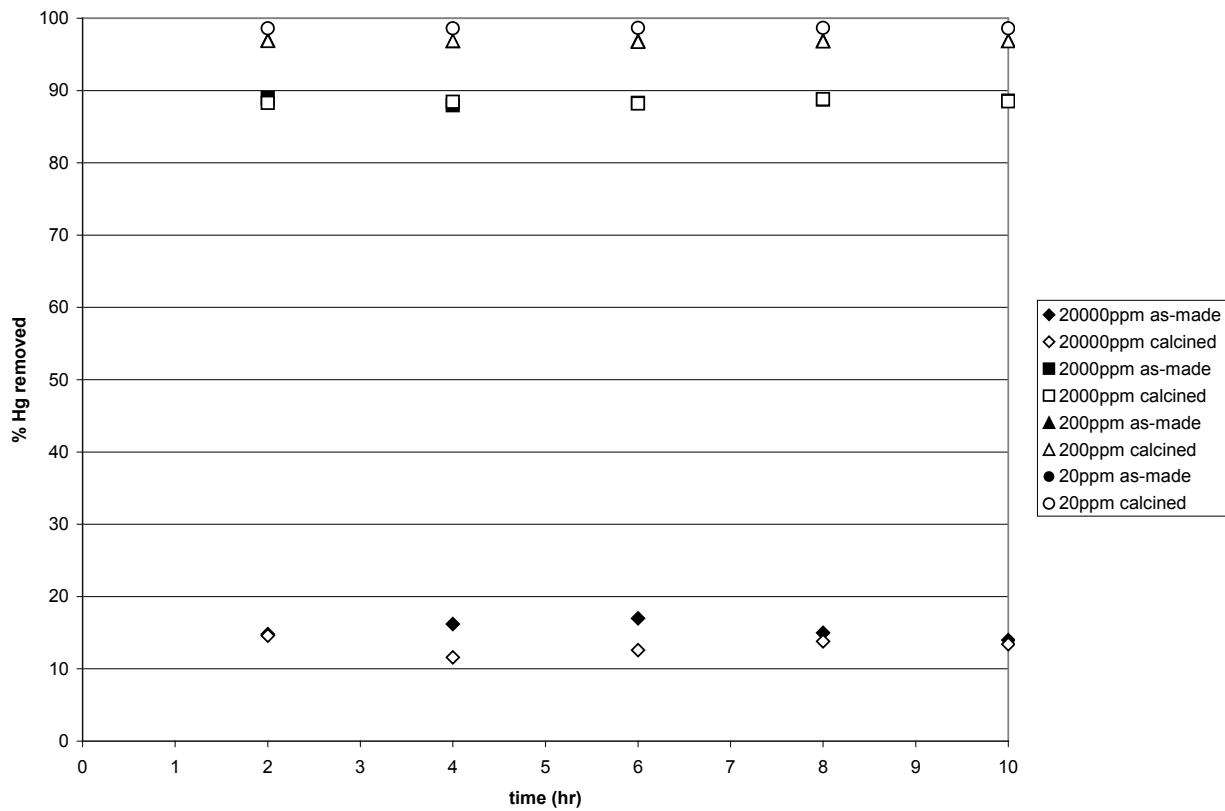


Figure 55 VPI-9 Mercury Ion Exchange Percent Removal as Function of Time

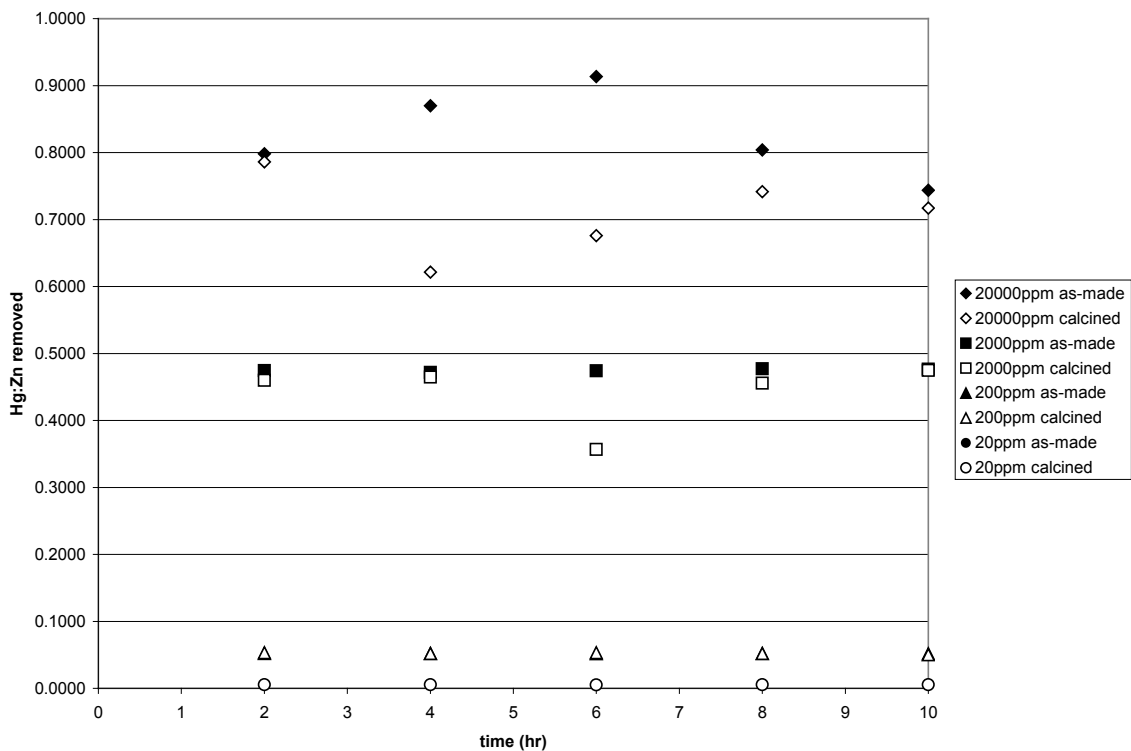


Figure 56 VPI-9 Ion Exchange Mercury:Zinc as Function of Time

Table 15 VPI-10 Mercury Ion Exchange Data and Calculations Part I

Zeolite Used	Mass Zeolite (g)	Calcined (y/n)	Volume (g)	Exchange Time (hr)	Time Error (hr)
VPI-10	0.1498	n	14.9906	10	0.1
VPI-10	0.1497	n	14.9871	8	0.1
VPI-10	0.1512	n	15.1184	6	0.1
VPI-10	0.1502	n	15.0211	4	0.1
VPI-10	0.1507	n	15.0771	2	0.1
VPI-10	0.1504	n	15.0533	10	0.1
VPI-10	0.15	n	15.0009	8	0.1
VPI-10	0.1493	n	14.9396	6	0.1
VPI-10	0.1492	n	14.9408	4	0.1
VPI-10	0.151	n	15.1042	2	0.1
VPI-10	0.1506	n	15.0543	10	0.1
VPI-10	0.1503	n	15.0337	8	0.1
VPI-10	0.1499	n	15.0061	6	0.1
VPI-10	0.1501	n	15.0122	4	0.1
VPI-10	0.1502	n	15.0322	2	0.1
VPI-10	0.1498	n	14.9869	10	0.1
VPI-10	0.1498	n	14.9858	8	0.1
VPI-10	0.1504	n	15.0477	6	0.1
VPI-10	0.1507	n	15.0766	4	0.1
VPI-10	0.1503	n	15.0219	2	0.1

Table 16 VPI-10 Mercury Ion Exchange Data and Calculations Part II

Initial Hg conc. (ppm)	AA conc. (ppb)	Dilution Factor	Actual conc.	Hg removed	Hg mass (mol)
20000	4.45	4000000	17800	11	1.6490E-04
20000	4.42	4000000	17680	11.6	1.7385E-04
20000	4.47	4000000	17880	10.6	1.6026E-04
20000	4.48	4000000	17920	10.4	1.5622E-04
20000	4.5	4000000	18000	10	1.5077E-04
2000	4.02	100000	402	79.9	1.2028E-04
2000	4.05	100000	405	79.75	1.1963E-04
2000	4.07	100000	407	79.65	1.1899E-04
2000	4.08	100000	408	79.6	1.1893E-04
2000	3.86	100000	386	80.7	1.2189E-04
200	4.05	8000	32.4	83.8	1.2616E-05
200	4.08	8000	32.64	83.68	1.2580E-05
200	4.1	8000	32.8	83.6	1.2545E-05
200	4.11	8000	32.88	83.56	1.2544E-05
200	4.14	8000	33.12	83.44	1.2543E-05
20	3.67	800	2.936	85.32	1.2787E-06
20	3.71	800	2.968	85.16	1.2762E-06
20	3.72	800	2.976	85.12	1.2809E-06
20	3.73	800	2.984	85.08	1.2827E-06
20	3.76	800	3.008	84.96	1.2763E-06

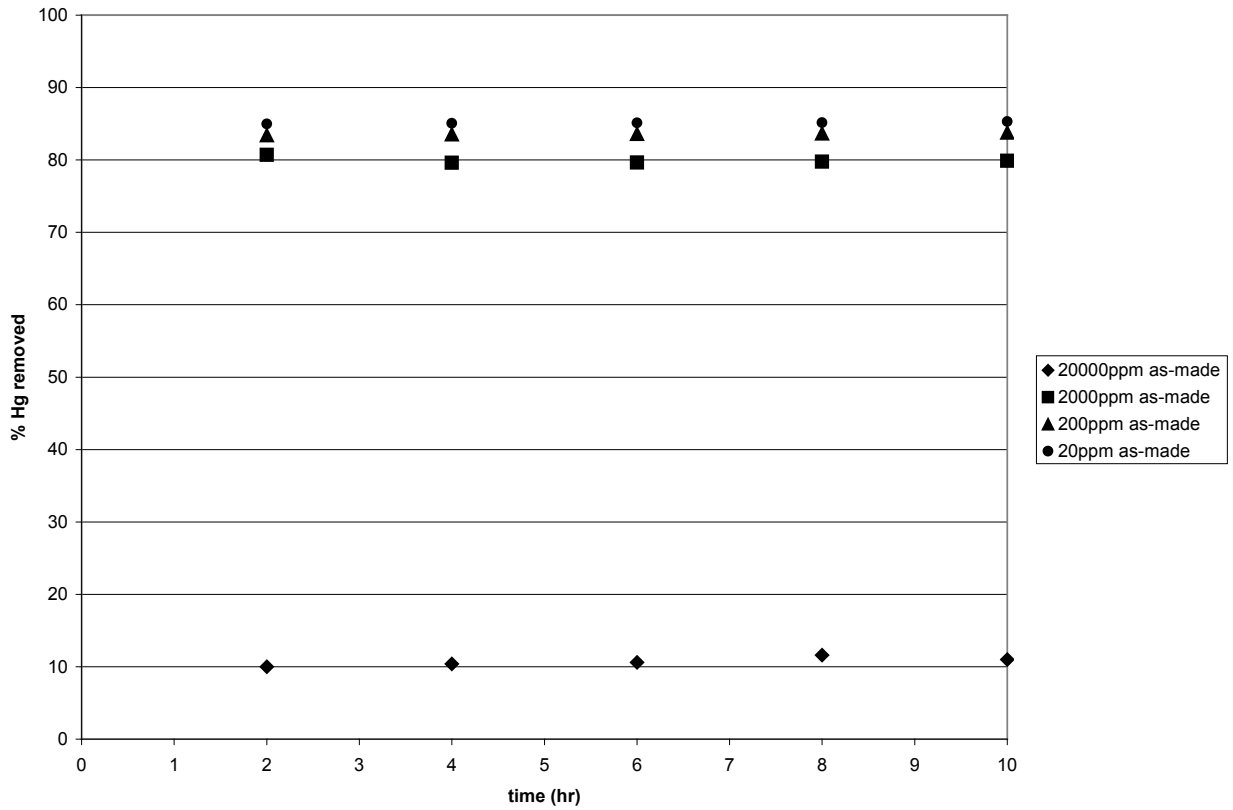


Figure 57 VPI-10 Mercury Ion Exchange Percent Removal as Function of Time

Table 17 Zincosilicate Temperature Exchange Experimental Results Part I

Zeolite Used	Mass Zeolite (g)	Volume (g)	Exchange Time (hr)	Temperature C	Init. Hg conc. (ppm)
VPI-7	0.1509	15.0087	24	25	20000
VPI-7	0.1522	15.0235	24	50	20000
VPI-7	0.1508	15.0192	24	60	20000
VPI-7	0.1507	15.0008	24	40	20000
VPI-9	0.1503	15.0143	24	25	20000
VPI-9	0.1503	15.0287	24	50	20000
VPI-9	0.1505	15.0189	24	60	20000
VPI-9	0.1502	15.0087	24	40	20000

Table 18 Zincosilicate Temperature Exchange Experimental Results Part II

AA conc. (ppb)	Dilution Factor	Actual conc. (ppm)	Hg removed	Hg mass (mol)	Zn (mol)	Hg:Zn
3.78	4000000	15120	24.4	3.662E-04	3.791E-04	0.966
4.03	4000000	16120	19.4	2.915E-04	3.824E-04	0.762
4.2	4000000	16800	16	2.403E-04	3.789E-04	0.634
3.99	4000000	15960	20.2	3.030E-04	3.786E-04	0.800
4.38	4000000	17520	12.4	1.862E-04	2.803E-04	0.664
4.52	4000000	18080	9.6	1.443E-04	2.803E-04	0.515
4.63	4000000	18520	7.4	1.111E-04	2.807E-04	0.396
4.41	4000000	17640	11.8	1.771E-04	2.801E-04	0.632

Table 19 Binary Selectivity Experimental Results Part I

Pb-Hg	Init. Zeolite mass (g)	Init. Solution Mass (g)	Init. Conc. Pb (ppm)	Init. Conc. Hg (ppm)
VPI-7	0.152	15.2023	5175	5015
VPI-9	0.152	15.1949	5175	5015

Pb-Na	Init. Zeolite mass (g)	Init. Solution Mass (g)	Init. Conc. Pb (ppm)	Init. Conc. Na (ppm)
VPI-7	0.1516	15.1718	5175	575
VPI-9	0.1509	15.0988	5175	575

Pb-K	Init. Zeolite mass (g)	Init. Solution Mass (g)	Init. Conc. Pb (ppm)	Init. Conc. K (ppm)
VPI-7	0.1504	15.0347	5175	978
VPI-9	0.1507	15.0723	5175	978

Pb-Ca	Init. Zeolite mass (g)	Init. Solution Mass (g)	Init. Conc. Pb (ppm)	Init. Conc. Ca (ppm)
VPI-7	0.1511	15.1165	5175	1000
VPI-9	0.1513	15.1402	5175	1000

Hg-Na	Init. Zeolite mass (g)	Init. Solution Mass (g)	Init. Conc. Hg (ppm)	Init. Conc. Na (ppm)
VPI-7	0.1507	15.0697	5015	575
VPI-9	0.1505	15.0533	5015	575

Hg-K	Init. Zeolite mass (g)	Init. Solution Mass (g)	Init. Conc. Hg (ppm)	Init. Conc. K (ppm)
VPI-7	0.1508	15.0811	5015	978
VPI-9	0.1505	15.0549	5015	978

Hg-Ca	Init. Zeolite mass (g)	Init. Solution Mass (g)	Init. Conc. Hg (ppm)	Init. Conc. Ca (ppm)
VPI-7	0.1507	15.0755	5015	1000
VPI-9	0.1506	15.0604	5015	1000

Table 20 Binary Selectivity Experimental Results Part II

Final Conc. Pb (ppm)	Final Conc. Hg (ppm)	Moles Pb Removed	Moles Hg Removed	Selectivity Pb:Hg
753	1428	3.248E-04	2.727E-04	2.31
319	928	3.565E-04	3.105E-04	3.40

Final Conc. Pb (ppm)	Final Conc. Na (ppm)	Moles Pb Removed	Moles Na Removed	Selectivity Pb:Na
740	213	3.251E-04	2.388E-04	2.07
551	213	3.373E-04	2.376E-04	2.91

Final Conc. Pb (ppm)	Final Conc. K (ppm)	Moles Pb Removed	Moles K Removed	Selectivity Pb:K
511	386	3.388E-04	2.282E-04	3.82
434	378	3.452E-04	2.319E-04	4.27

Final Conc. Pb (ppm)	Final Conc. Ca (ppm)	Moles Pb Removed	Moles Ca Removed	Selectivity Pb:Ca
477	290	3.431E-04	2.683E-04	4.02
403	273	3.490E-04	2.752E-04	4.45

Final Conc. Hg (ppm)	Final Conc. Na (ppm)	Moles Hg Removed	Moles Na Removed	Selectivity Hg:Na
1456	208	2.682E-04	2.405E-04	0.79
1505	88	2.642E-04	3.187E-04	0.08

Final Conc. Hg (ppm)	Final Conc. K (ppm)	Moles Hg Removed	Moles K Removed	Selectivity Hg:K
1433	424	2.701E-04	2.142E-04	1.46
992	396	3.028E-04	2.247E-04	1.88

Final Conc. Hg (ppm)	Final Conc. Ca (ppm)	Moles Hg Removed	Moles Ca Removed	Selectivity Hg:Ca
1467	317	2.674E-04	2.574E-04	1.13
1005	211	3.020E-04	2.971E-04	1.08

Table 21 Binary Selectivity Coefficient Calculations for VPI-7 Part I

System	osmotic pressure	ionic volume1	ionic volume2	pressure term	solid ion activity1	solid ion activity2
Pb:Hg	1.23E+05	5.93E-06	3.94E-06	9.99E-05	0.6017	0.2344
Pb:Na	1.23E+05	5.93E-06	8.86E-06	5.89E-04	0.5862	0.0343
Pb:K	1.23E+05	5.93E-06	3.94E-06	9.70E-05	0.6315	0.0197
Pb:Ca	1.23E+05	5.93E-06	3.74E-06	1.10E-04	0.6533	0.1837
Hg:Na	1.23E+05	3.94E-06	8.86E-06	6.89E-04	0.1916	0.0251
Hg:K	1.23E+05	3.94E-06	3.94E-06	1.97E-04	0.2087	0.0147
Hg:Ca	1.23E+05	3.94E-06	3.74E-06	1.00E-05	0.2053	0.2036

Table 22 Binary Selectivity Coefficient Calculations for VPI-7 Part II

System	solid activity term	solution ion activity1	solution ion activity2	solution activity term	Selectivity Coefficient
Pb:Hg	0.9427	0.2900	0.2899	0.0010	2.57
Pb:Na	2.8385	0.3435	0.7683	-2.1514	1.99
Pb:K	3.4675	0.3436	0.7666	-2.1417	3.77
Pb:Ca	1.2687	0.2799	0.2719	0.0870	3.88
Hg:Na	2.0325	0.3436	0.7684	-2.1511	0.89
Hg:K	2.6531	0.3438	0.7667	-2.1404	1.67
Hg:Ca	0.0083	0.2800	0.2720	0.0870	1.10

Table 23 Binary Selectivity Coefficient Calculations for VPI-9 Part I

System	osmotic pressure	ionic volume1	ionic volume2	pressure term	solidion activity1	solid ion activity2
Pb:Hg	1.23E+05	5.93E-06	3.94E-06	9.99E-05	0.6716	0.1878
Pb:Na	1.23E+05	5.93E-06	8.86E-06	5.89E-04	0.6588	0.0268
Pb:K	1.23E+05	5.93E-06	3.94E-06	9.70E-05	0.6949	0.0195
Pb:Ca	1.23E+05	5.93E-06	3.74E-06	1.10E-04	0.7116	0.1793
Hg:Na	1.23E+05	3.94E-06	8.86E-06	6.89E-04	0.2047	0.2270
Hg:K	1.23E+05	3.94E-06	3.94E-06	1.97E-04	0.2279	0.0130
Hg:Ca	1.23E+05	3.94E-06	3.74E-06	1.00E-05	0.2113	0.2004

Table 24 Binary Selectivity Coefficient Calculations for VPI-9 Part II

System	solid activity term	solution ion activity1	solution ion activity2	solution activity term	Selectivity Coefficient
Pb:Hg	1.2743	0.2900	0.2899	0.0010	3.58
Pb:Na	3.2020	0.3435	0.7683	-2.1514	2.86
Pb:K	3.5734	0.3436	0.7666	-2.1417	4.19
Pb:Ca	1.3785	0.2799	0.2719	0.0870	4.33
Hg:Na	-0.1034	0.3436	0.7684	-2.1511	0.11
Hg:K	2.8640	0.3438	0.7667	-2.1404	2.06
Hg:Ca	0.0530	0.2800	0.2720	0.0870	1.15

Appendix B - Adsorption Data

**Table 25 Loading of Selected Zeolite-Sorbate Systems on Gravimetric Microbalance
Calculations Part I**

Sorbent	Sorbate	Loading by Mass	Estimated Error	Loading by Surface Area	Estimated Error
4A	ethanol	1.103E-01	2.205E-05	9.188E-04	1.838E-07
13X	ethanol	1.585E-01	3.170E-05	1.016E-03	2.032E-07
ZSM-5	ethanol	7.827E-02	1.565E-05	6.748E-04	1.350E-07
VPI-7	ethanol	3.293E-02	6.586E-06	1.937E-03	3.874E-07
VPI-9	ethanol	4.734E-02	9.467E-06	1.155E-03	2.309E-07
MCM-41	ethanol	6.832E-02	1.366E-05	9.760E-05	1.952E-08
4A	DMMP	1.003E-01	2.006E-05	8.360E-04	1.672E-07
13X	DMMP	1.631E-01	3.262E-05	1.045E-03	2.091E-07
ZSM-5	DMMP	8.312E-03	1.662E-06	7.166E-05	1.433E-08
VPI-7	DMMP	-	-	-	-
VPI-9	DMMP	-	-	-	-
MCM-41	DMMP	8.443E-02	1.689E-05	1.206E-04	2.412E-08
4A	2-CEES	-	-	-	-
13X	2-CEES	-	-	-	-
ZSM-5	2-CEES	5.320E-01	1.064E-04	4.586E-03	9.172E-07
VPI-7	2-CEES	-	-	-	-
VPI-9	2-CEES	-	-	-	-
MCM-41	2-CEES	1.011E-01	2.023E-05	1.445E-04	2.889E-08
4A	n-butanethiol	7.553E-02	1.511E-05	6.294E-04	1.259E-07
13X	n-butanethiol	-	-	-	-
ZSM-5	n-butanethiol	-	-	-	-
VPI-7	n-butanethiol	-	-	-	-
VPI-9	n-butanethiol	4.811E-03	9.622E-07	1.173E-04	2.347E-08
MCM-41	n-butanethiol	9.660E-02	1.932E-05	1.380E-04	2.760E-08

Table 26 Loading of Selected Zeolite-Sorbate Systems on Gravimetric Microbalance

Calculations Part II

Sorbent	Sorbate	Uptake Rate by Mass	Estimated Error	Uptake Rate by Surface Area	Estimated Error
4A	ethanol	2.205E-02	4.410E-06	1.838E-04	3.675E-08
13X	ethanol	3.170E-02	6.340E-06	2.032E-04	4.064E-08
ZSM-5	ethanol	1.565E-02	3.131E-06	1.350E-04	2.699E-08
VPI-7	ethanol	6.586E-03	1.317E-06	3.874E-04	7.748E-08
VPI-9	ethanol	9.467E-03	1.893E-06	2.309E-04	4.618E-08
MCM-41	ethanol	1.366E-02	2.733E-06	1.952E-05	3.904E-09
4A	DMMP	4.090E-03	8.179E-07	3.408E-05	6.816E-09
13X	DMMP	4.544E-03	9.089E-07	2.913E-05	5.826E-09
ZSM-5	DMMP	8.840E-04	1.768E-07	7.620E-06	1.524E-09
VPI-7	DMMP	7.022E-04	1.404E-07	4.130E-05	8.261E-09
VPI-9	DMMP	5.887E-04	1.177E-07	1.436E-05	2.872E-09
MCM-41	DMMP	7.965E-04	1.593E-07	1.138E-06	2.276E-10
4A	2-CEES	3.898E-03	7.795E-07	3.248E-05	6.496E-09
13X	2-CEES	3.792E-03	7.583E-07	2.430E-05	4.861E-09
ZSM-5	2-CEES	4.290E-03	8.580E-07	3.698E-05	7.397E-09
VPI-7	2-CEES	8.573E-04	1.715E-07	5.043E-05	1.009E-08
VPI-9	2-CEES	9.863E-04	1.973E-07	2.406E-05	4.811E-09
MCM-41	2-CEES	8.156E-04	1.631E-07	1.165E-06	2.330E-10
4A	n-butanethiol	3.840E-03	7.680E-07	3.200E-05	6.400E-09
13X	n-butanethiol	5.280E-03	1.056E-06	3.385E-05	6.769E-09
ZSM-5	n-butanethiol	4.030E-03	8.060E-07	3.474E-05	6.948E-09
VPI-7	n-butanethiol	-	-	-	-
VPI-9	n-butanethiol	3.800E-04	7.600E-08	9.268E-06	1.854E-09
MCM-41	n-butanethiol	7.488E-04	1.498E-07	1.070E-06	2.139E-10

Table 27 Loading of Selected Zeolite-Sorbate Systems on QCM Calculations Part I

Sorbent	Sorbate	Loading by Mass	Estimated Error	Loading by Surface Area	Estimated Error
4A	ethanol	1.191E-01	1.191E-02	9.923E-04	9.923E-05
13X	ethanol	1.728E-01	1.728E-02	1.107E-03	1.107E-04
ZSM-5	ethanol	8.297E-02	8.297E-03	7.153E-04	7.153E-05
VPI-7	ethanol	3.524E-02	3.524E-03	2.073E-03	2.073E-04
VPI-9	ethanol	4.923E-02	4.923E-03	1.201E-03	1.201E-04
MCM-41	ethanol	7.174E-02	7.174E-03	1.025E-04	1.025E-05
4A	DMMP	9.831E-02	9.831E-03	8.192E-04	8.192E-05
13X	DMMP	1.680E-01	1.680E-02	1.077E-03	1.077E-04
ZSM-5	DMMP	7.980E-03	7.980E-04	6.879E-05	6.879E-06
VPI-7	DMMP	-	-	-	-
VPI-9	DMMP	-	-	-	-
MCM-41	DMMP	8.612E-02	8.612E-03	1.230E-04	1.230E-05
4A	2-CEES	-	-	-	-
13X	2-CEES	-	-	-	-
ZSM-5	2-CEES	5.852E-01	5.852E-02	4.586E-03	4.586E-04
VPI-7	2-CEES	-	-	-	-
VPI-9	2-CEES	-	-	-	-
MCM-41	2-CEES	9.607E-02	9.607E-03	1.445E-04	1.445E-05
4A	n-butanethiol	7.629E-02	7.629E-03	6.357E-04	6.357E-05
13X	n-butanethiol	-	-	-	-
ZSM-5	n-butanethiol	-	-	-	-
VPI-7	n-butanethiol	-	-	-	-
VPI-9	n-butanethiol	4.763E-03	4.763E-04	1.162E-04	1.162E-05
MCM-41	n-butanethiol	9.370E-02	9.370E-03	1.339E-04	1.339E-05

Table 28 Loading of Selected Zeolite-Sorbate Systems on QCM Calculations Part II

Sorbent	Sorbate	Uptake Rate by Mass	Estimated Error	Uptake Rate by Surface Area	Estimated Error
4A	ethanol	2.382E-02	2.382E-03	1.985E-04	1.985E-05
13X	ethanol	3.455E-02	3.455E-03	2.215E-04	2.215E-05
ZSM-5	ethanol	1.659E-02	1.659E-03	1.431E-04	1.431E-05
VPI-7	ethanol	7.047E-03	7.047E-04	4.145E-04	4.145E-05
VPI-9	ethanol	9.846E-03	9.846E-04	2.401E-04	2.401E-05
MCM-41	ethanol	1.435E-02	1.435E-03	2.050E-05	2.050E-06
4A	DMMP	4.008E-03	4.008E-04	3.340E-05	3.340E-06
13X	DMMP	4.681E-03	4.681E-04	3.000E-05	3.000E-06
ZSM-5	DMMP	8.486E-04	8.486E-05	7.316E-06	7.316E-07
VPI-7	DMMP	-	-	-	-
VPI-9	DMMP	-	-	-	-
MCM-41	DMMP	8.124E-04	8.124E-05	1.161E-06	1.161E-07
4A	2-CEES	4.131E-03	4.131E-04	3.443E-05	3.443E-06
13X	2-CEES	3.564E-03	3.564E-04	2.285E-05	2.285E-06
ZSM-5	2-CEES	4.719E-03	4.719E-04	4.068E-05	4.068E-06
VPI-7	2-CEES	-	-	-	-
VPI-9	2-CEES	-	-	-	-
MCM-41	2-CEES	7.748E-04	7.748E-05	1.107E-06	1.107E-07
4A	n-butanethiol	3.961E-03	3.961E-04	3.301E-05	3.301E-06
13X	n-butanethiol	5.110E-03	5.110E-04	3.276E-05	3.276E-06
ZSM-5	n-butanethiol	3.986E-03	3.986E-04	3.436E-05	3.436E-06
VPI-7	n-butanethiol	-	-	-	-
VPI-9	n-butanethiol	4.200E-04	4.200E-05	1.024E-05	1.024E-06
MCM-41	n-butanethiol	7.710E-04	7.710E-05	1.101E-06	1.101E-07

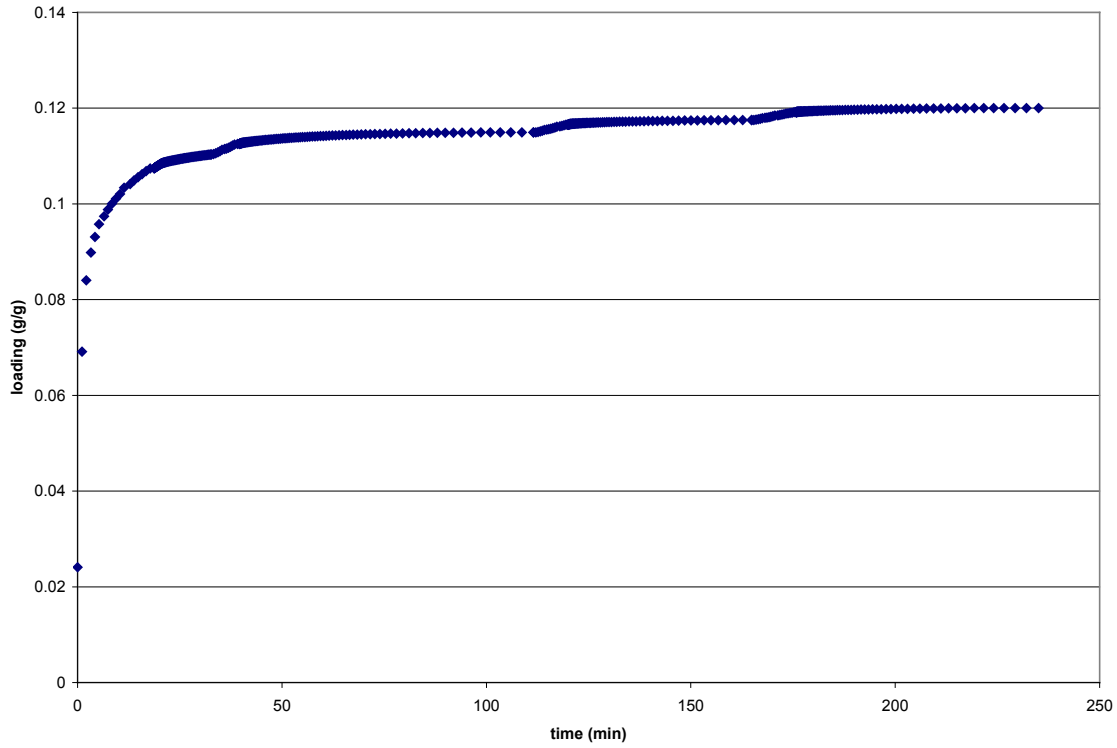


Figure 58 Kinetic Data for Ethanol Uptake onto Zeolite 4A

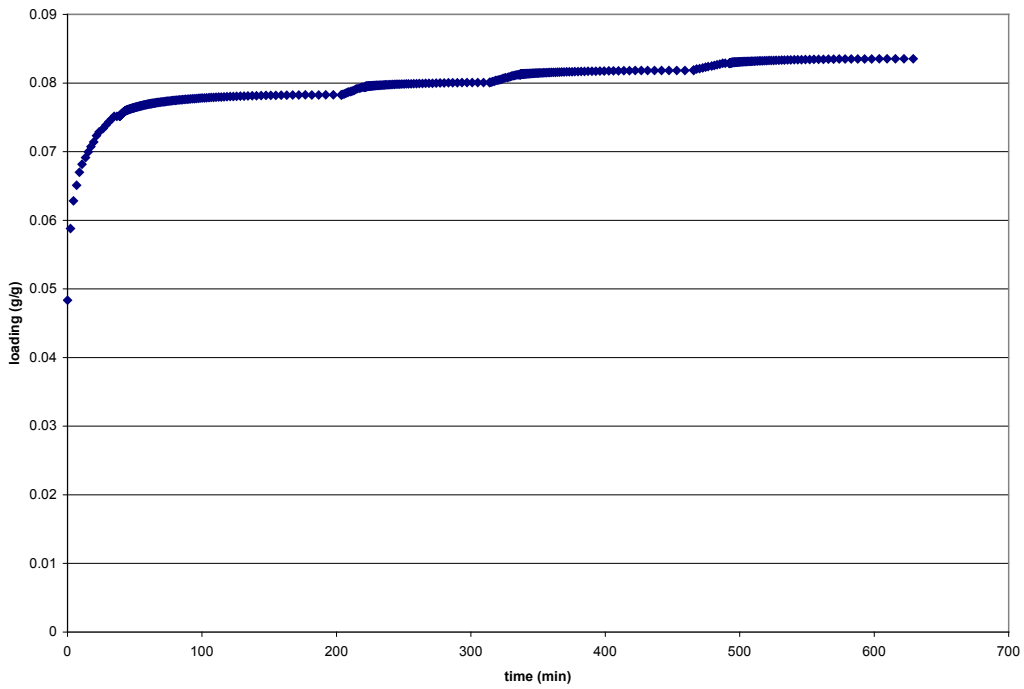


Figure 59 Kinetic Data for Ethanol Uptake onto ZSM-5

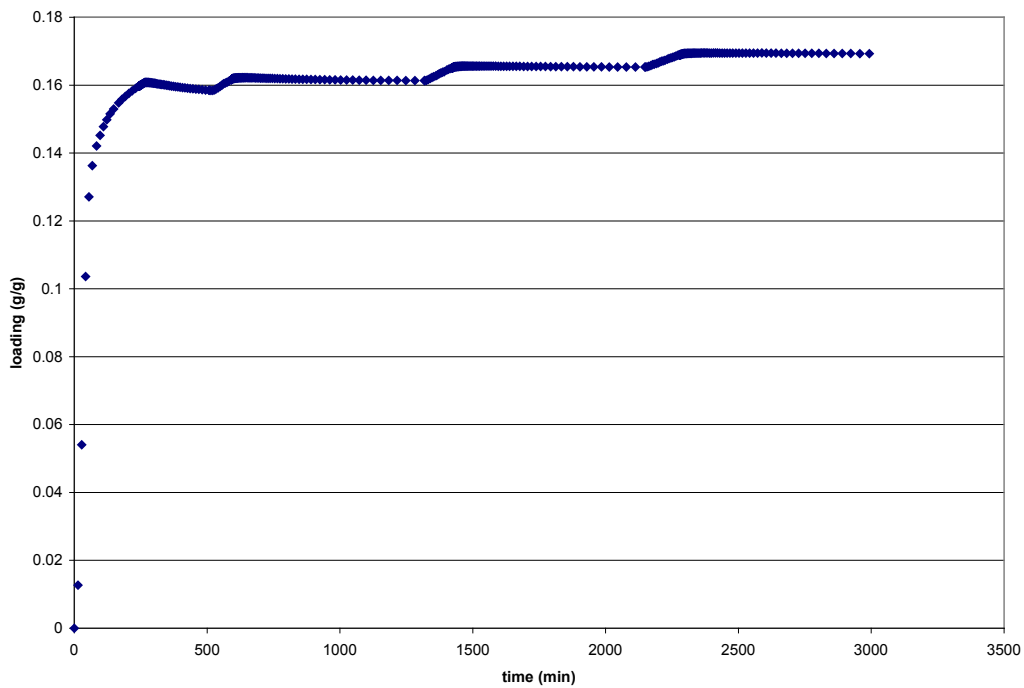


Figure 60 Kinetic Data for Ethanol Uptake onto Zeolite 13X

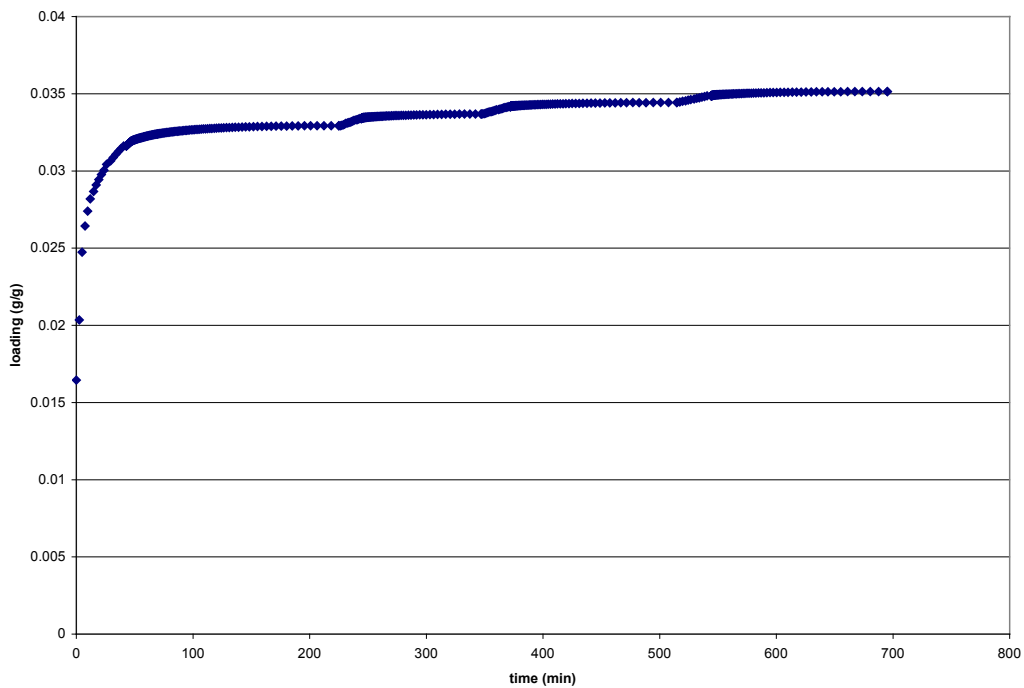


Figure 61 Kinetic Data for Ethanol Uptake onto Zeolite VPI-7

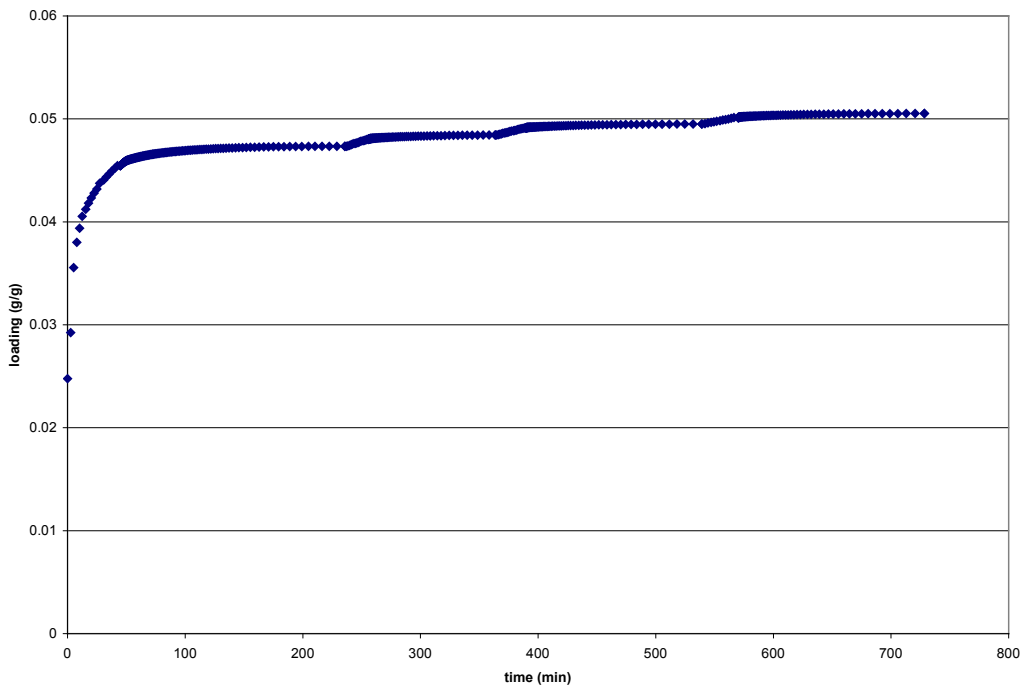


Figure 62 Kinetic Data for Ethanol Uptake onto Zeolite VPI-9

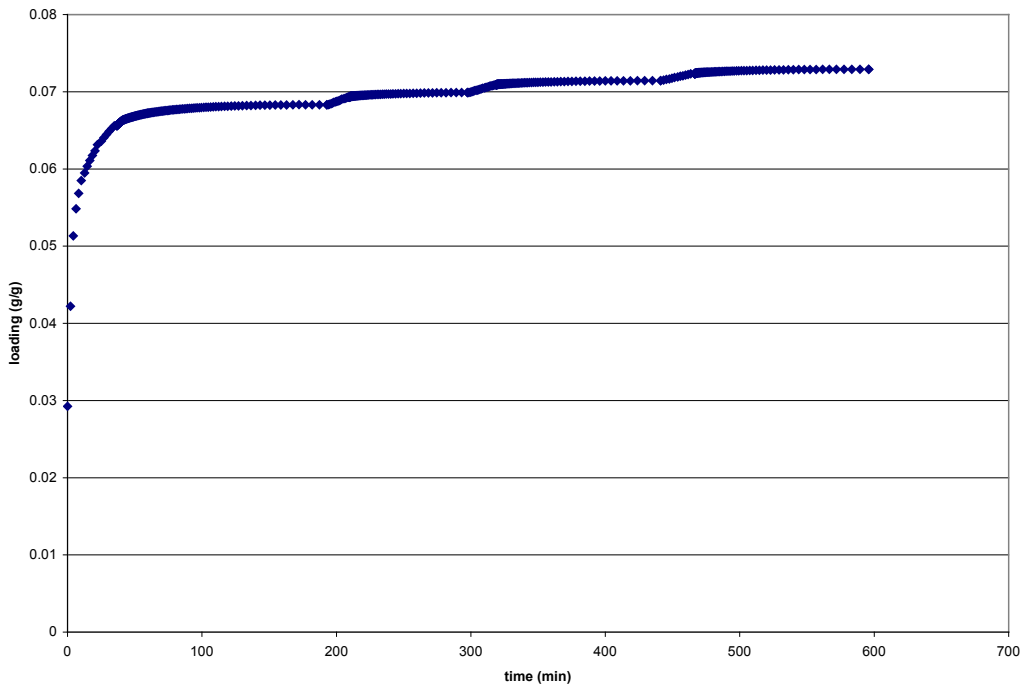


Figure 63 Kinetic Data for Ethanol Uptake onto MCM-41

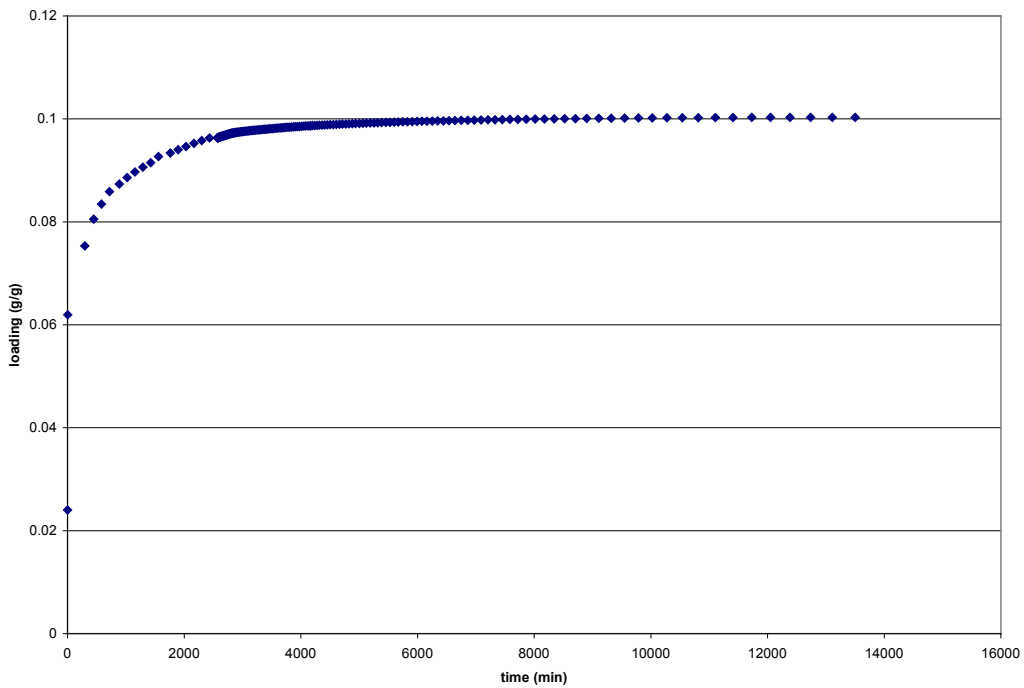


Figure 64 Kinetic Data for DMMP Uptake onto Zeolite 4A

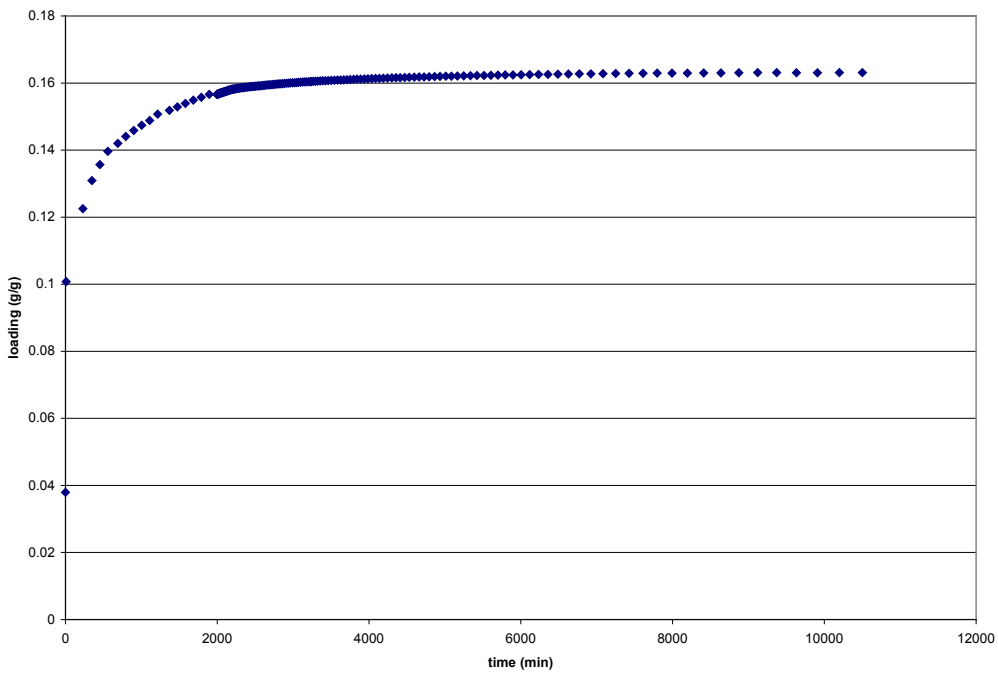


Figure 65 Kinetic Data for DMMP Uptake onto Zeolite 13X

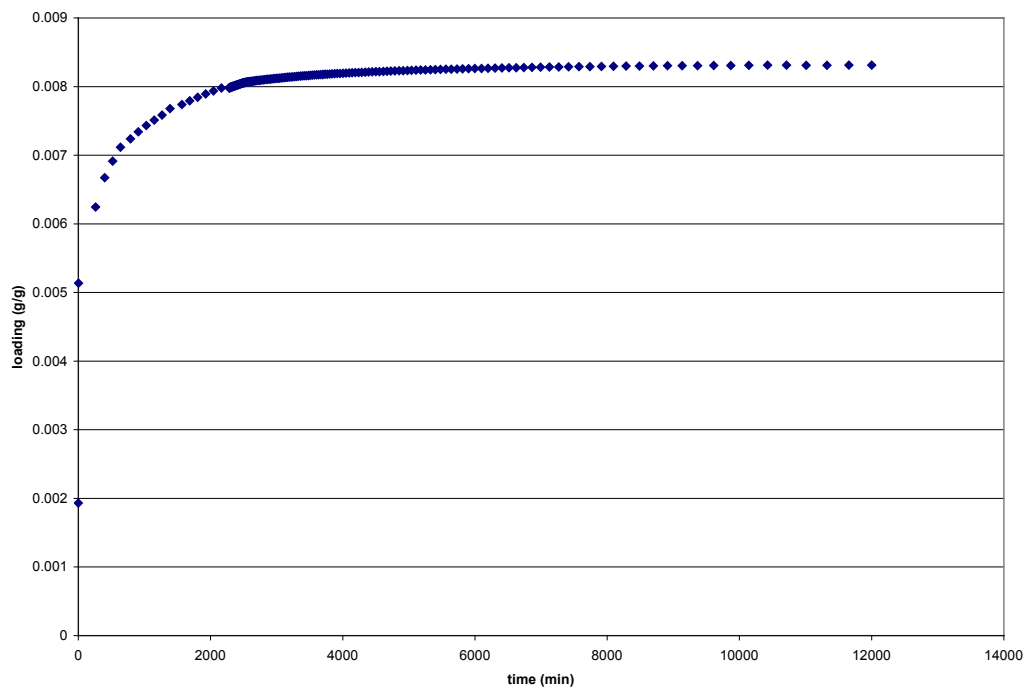


Figure 66 Kinetic Data for DMMP Uptake onto Zeolite ZSM-5

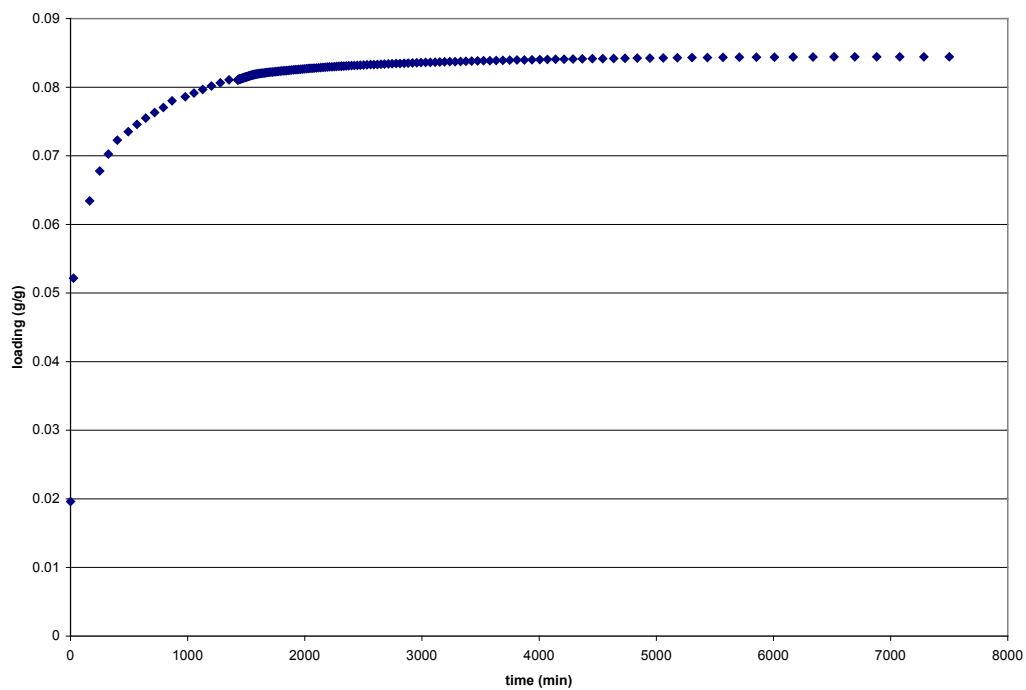


Figure 67 Kinetic Data for DMMP Uptake onto MCM-41

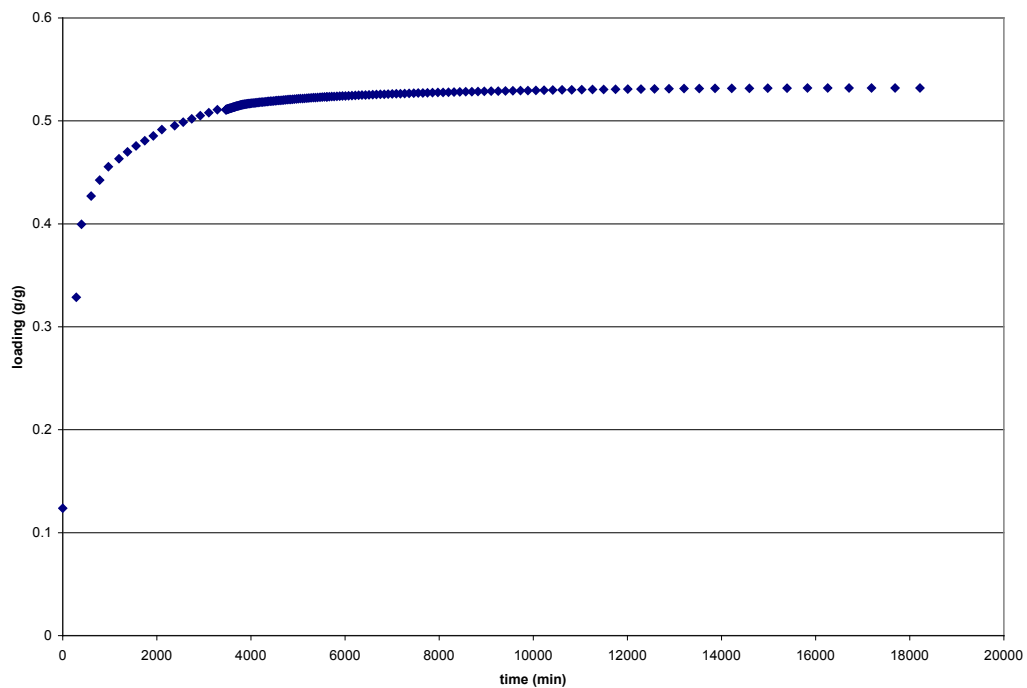


Figure 68 Kinetic Data for 2-CEES Uptake onto ZSM-5

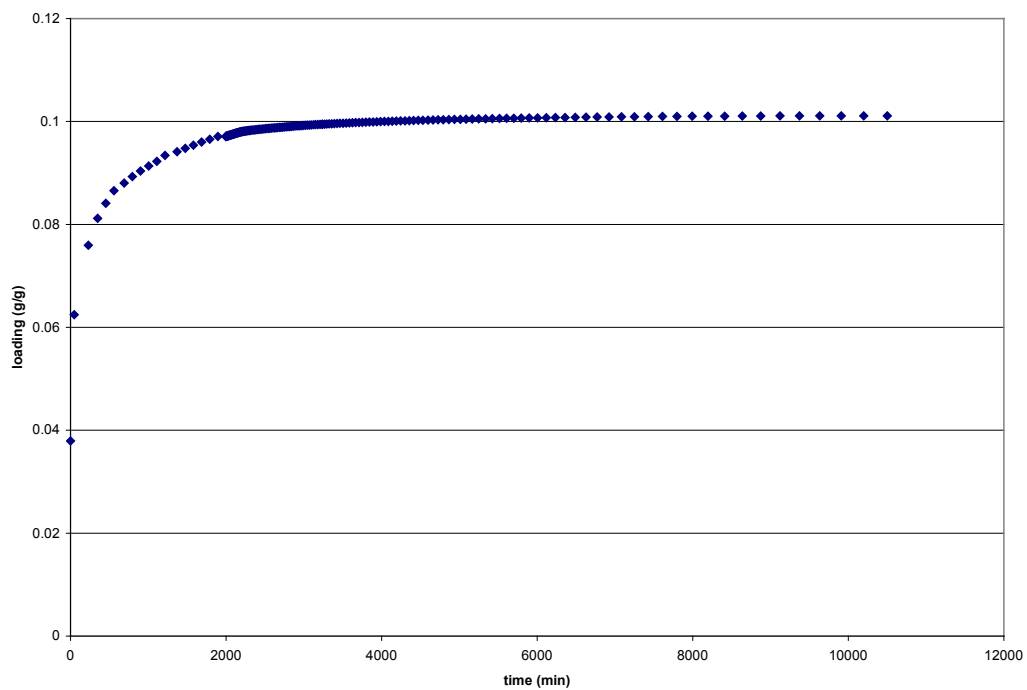


Figure 69 Kinetic Data for 2-CEES Uptake onto MCM-41

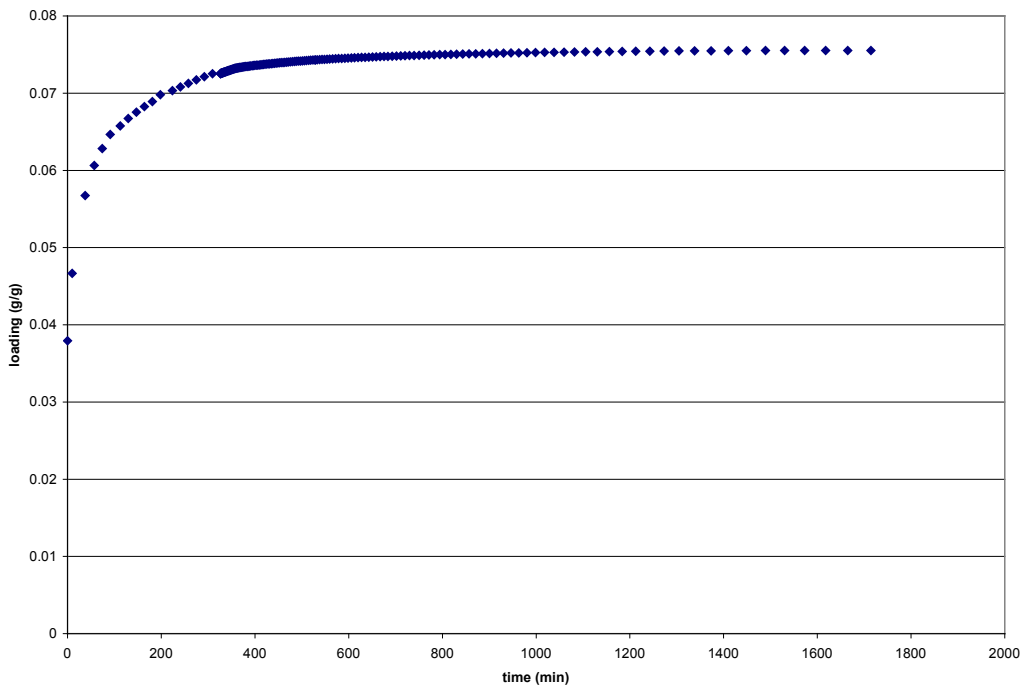


Figure 70 Kinetic Data for n-butanethiol Uptake onto Zeolite 4A

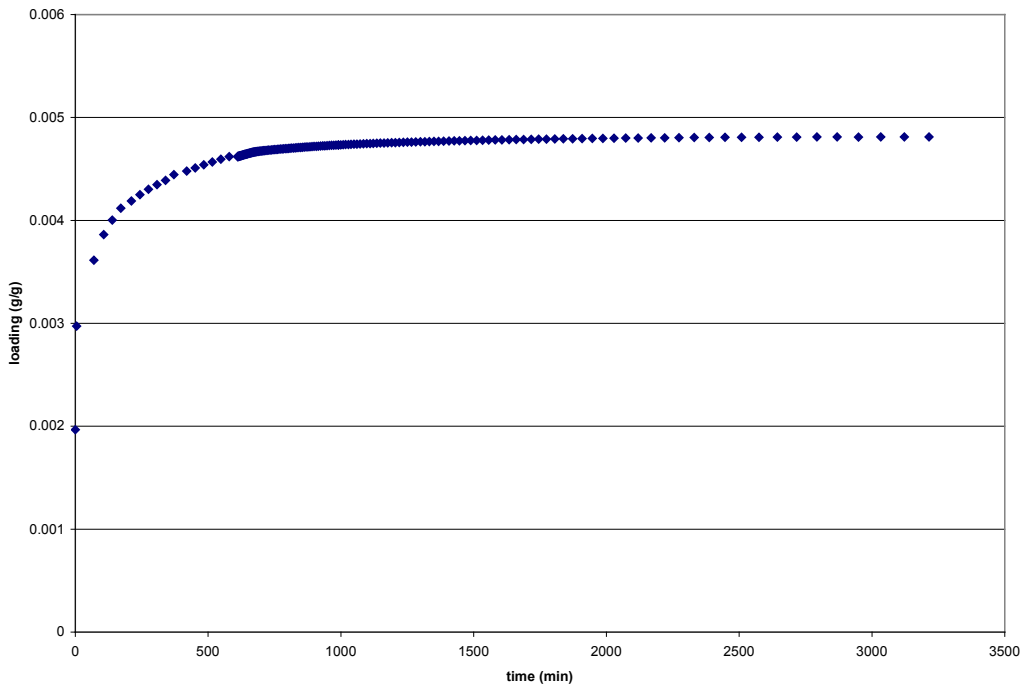


Figure 71 Kinetic Data for n-butanethiol Uptake onto Zeolite VPI-9

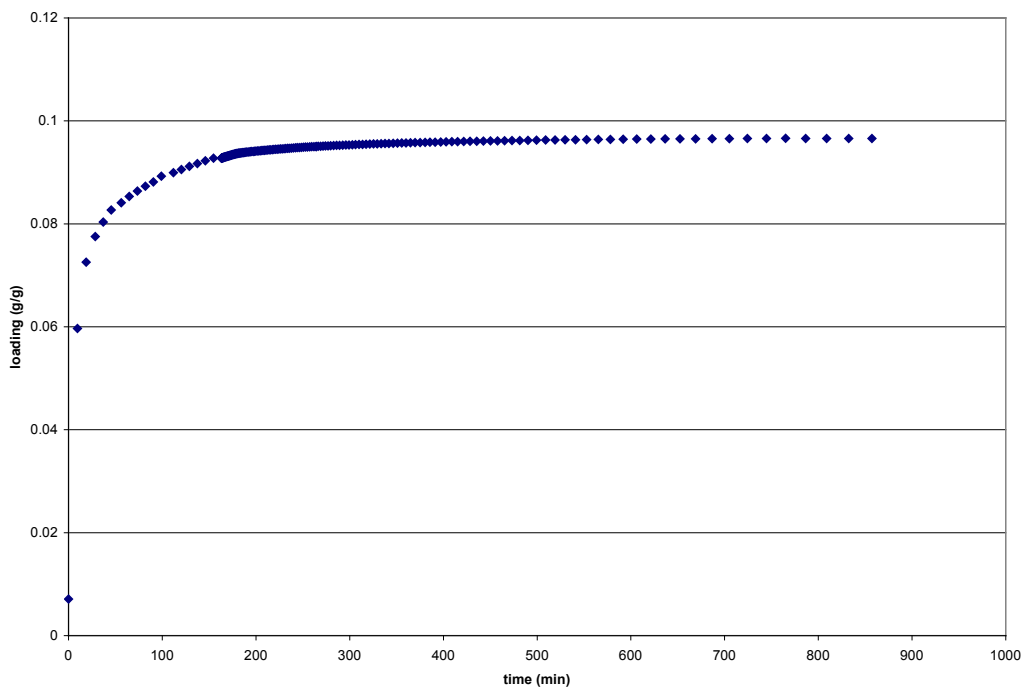


Figure 72 Kinetic Data for n-butanethiol Uptake onto MCM-41

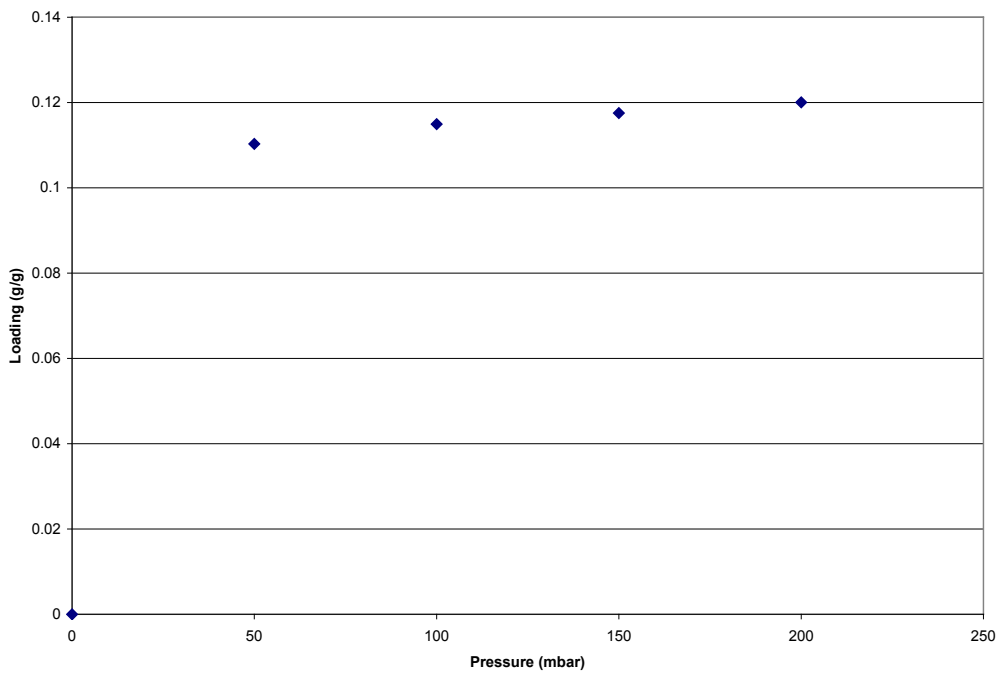


Figure 73 Equilibrium adsorption isotherm of ethanol onto zeolite 4A

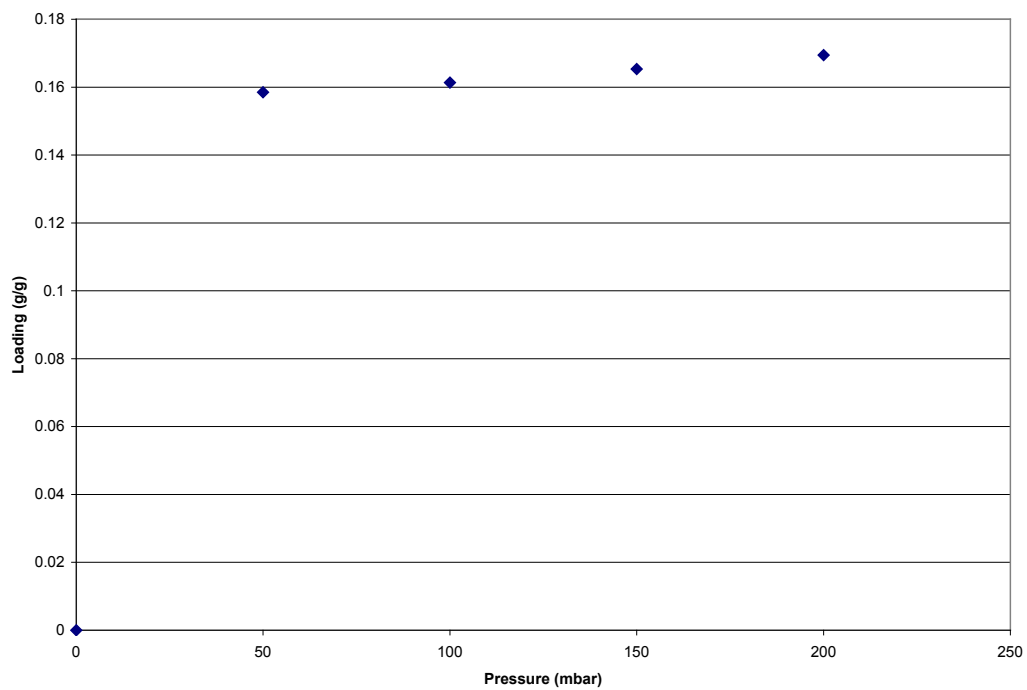


Figure 74 Equilibrium adsorption isotherm of ethanol onto zeolite 13X

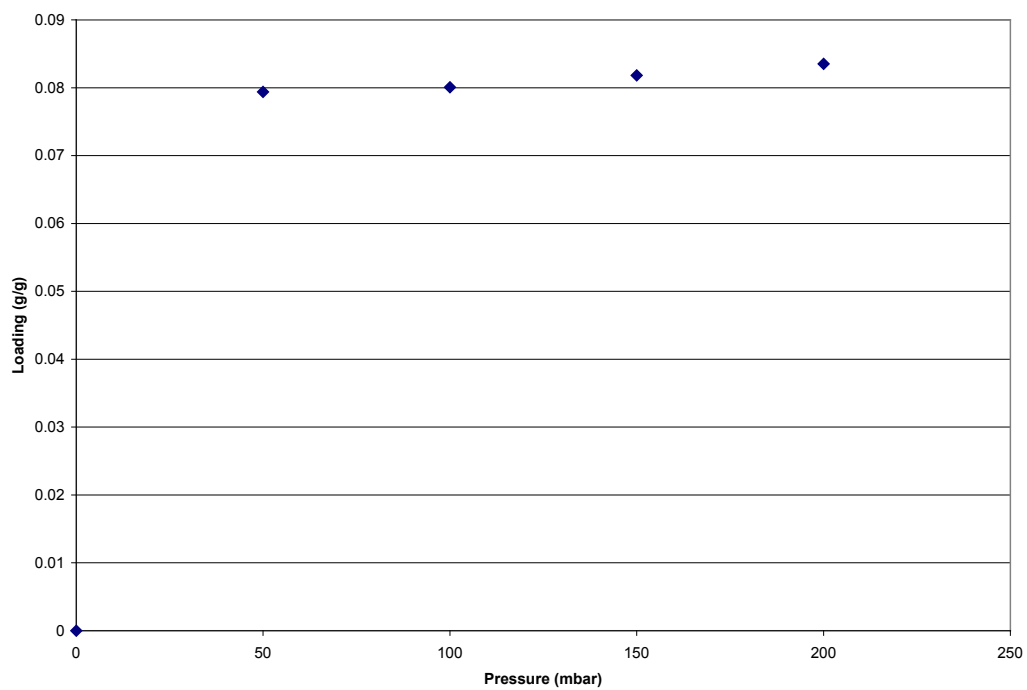


Figure 75 Equilibrium adsorption isotherm of ethanol onto zeolite ZSM-5

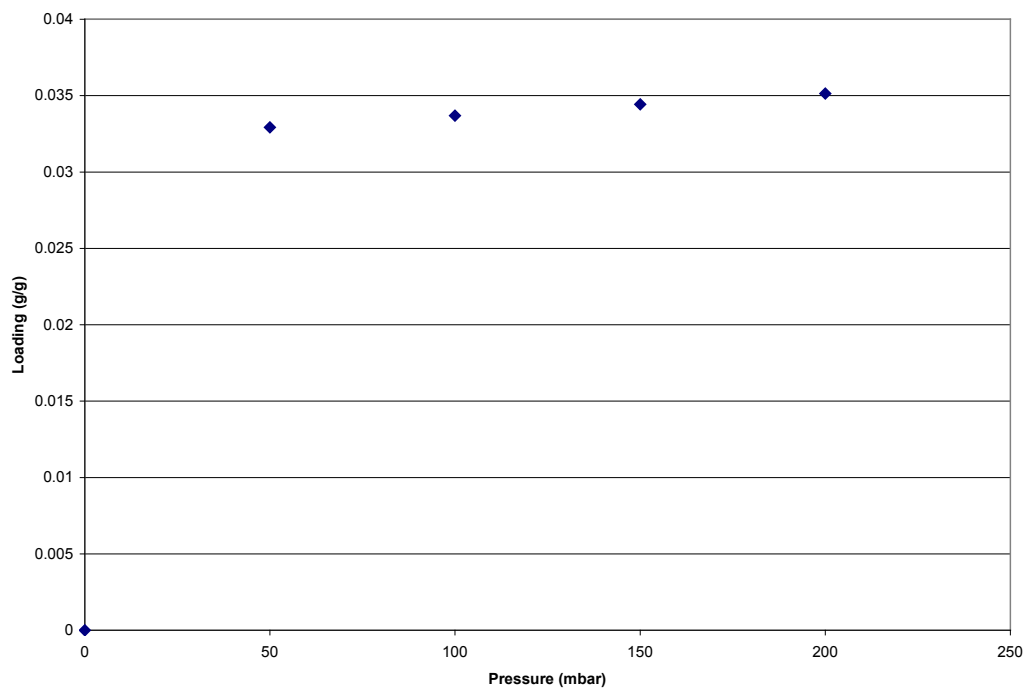


Figure 76 Equilibrium adsorption isotherm of ethanol onto zeolite VPI-7

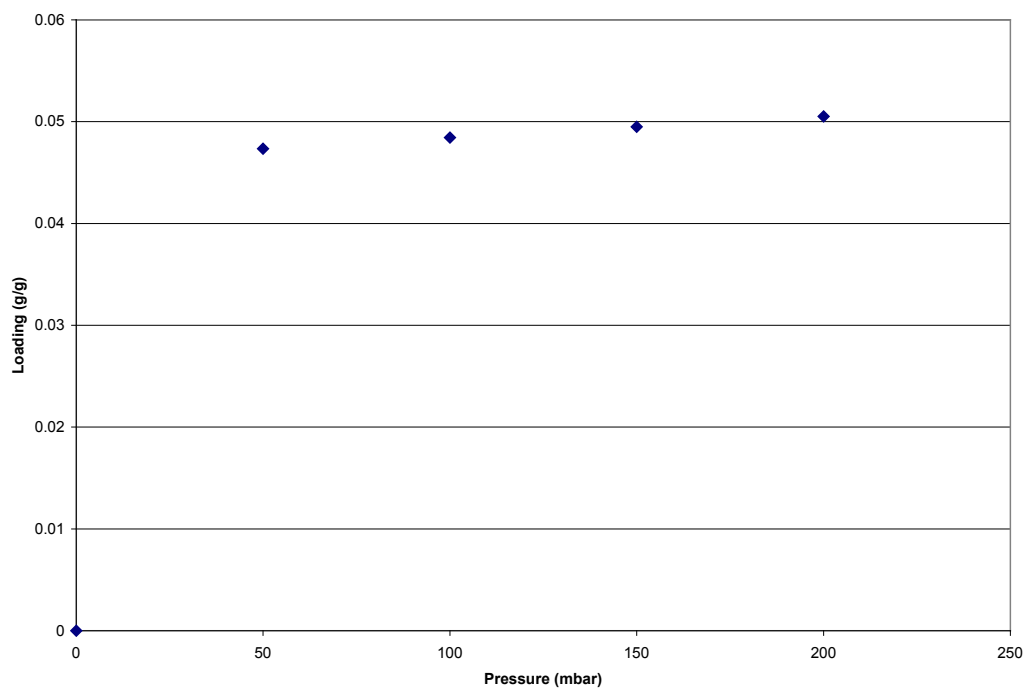


Figure 77 Equilibrium adsorption isotherm of ethanol onto zeolite VPI-9

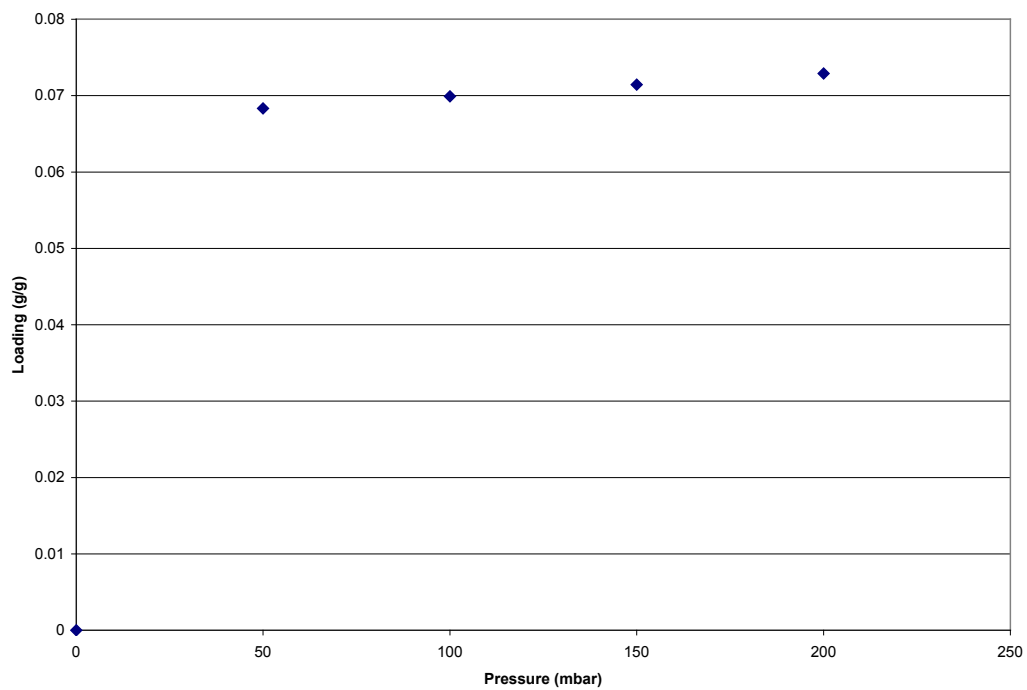


Figure 78 Equilibrium adsorption isotherm of ethanol onto MCM-41

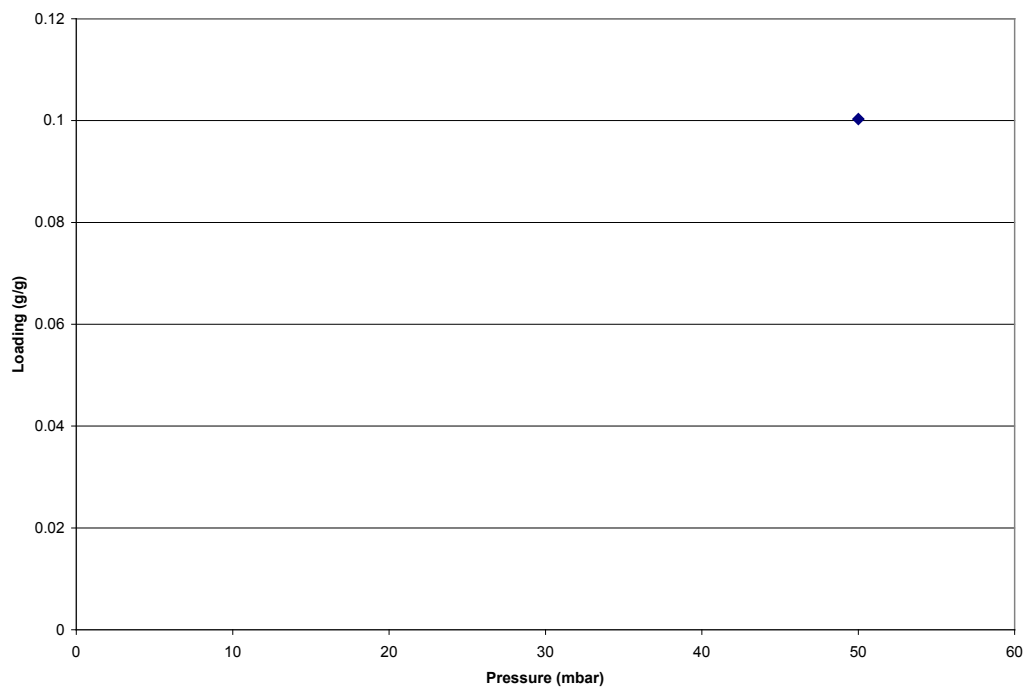


Figure 79 Equilibrium adsorption of DMMP onto zeolite 4A

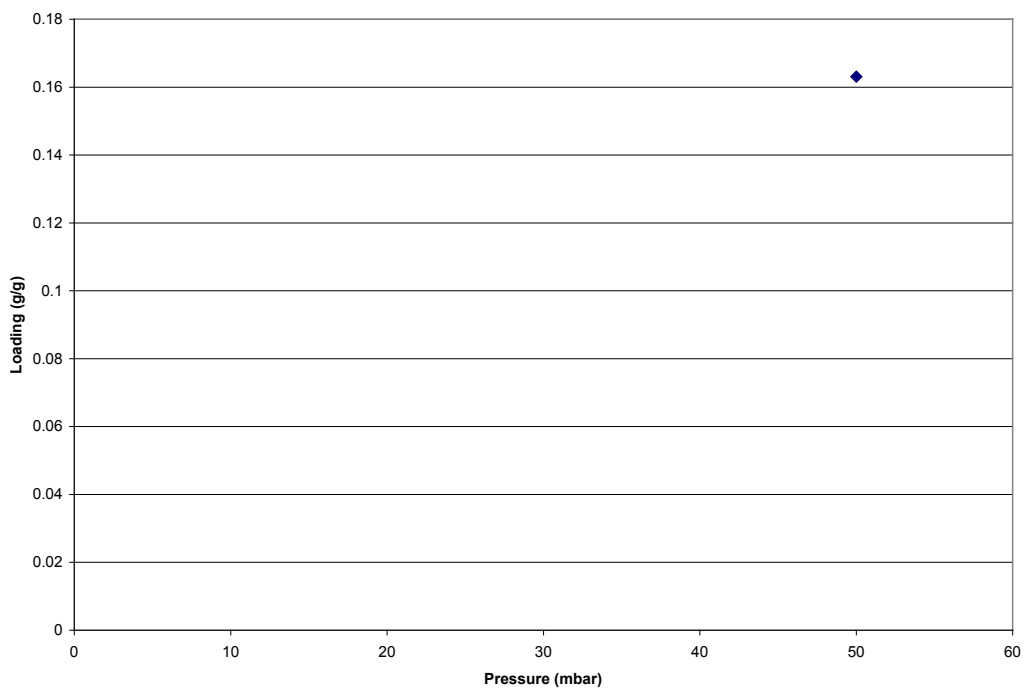


Figure 80 Equilibrium adsorption of DMMP onto zeolite 13X

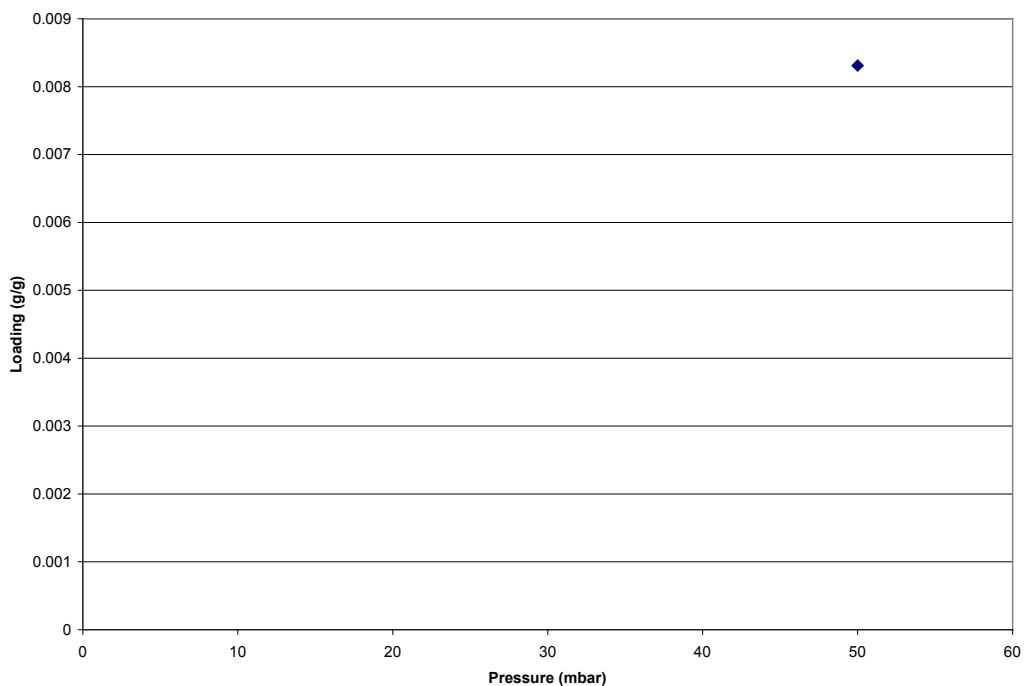


Figure 81 Equilibrium adsorption of DMMP onto zeolite ZSM-5

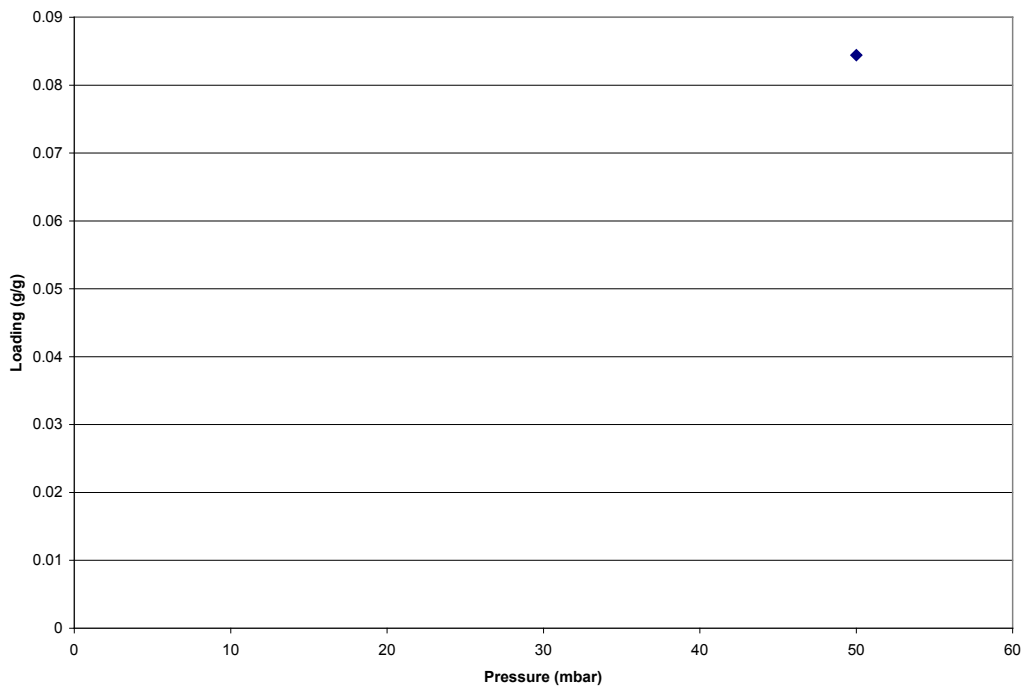


Figure 82 Equilibrium adsorption of DMMP onto zeolite MCM-41

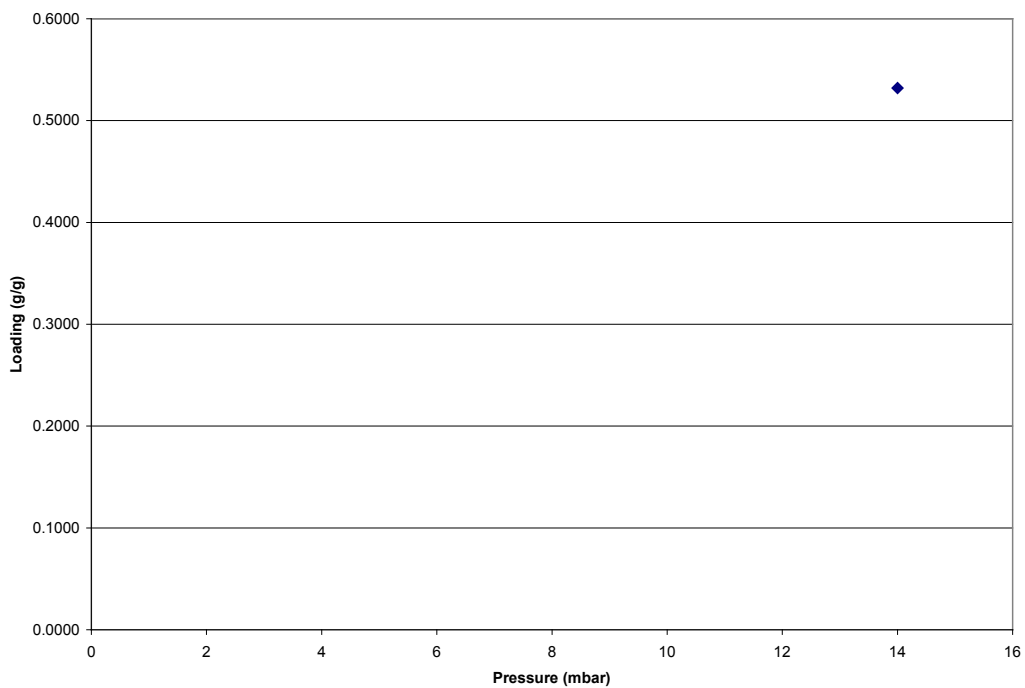


Figure 83 Equilibrium adsorption of 2-CEES onto zeolite ZSM-5

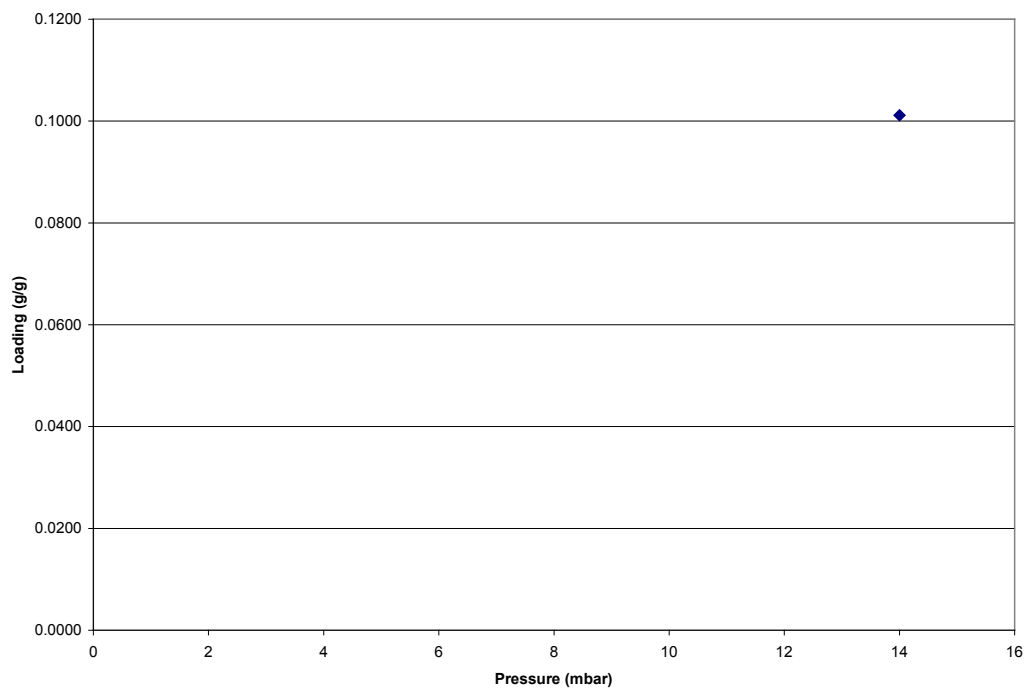


Figure 84 Equilibrium adsorption of 2-CEES onto zeolite MCM-41

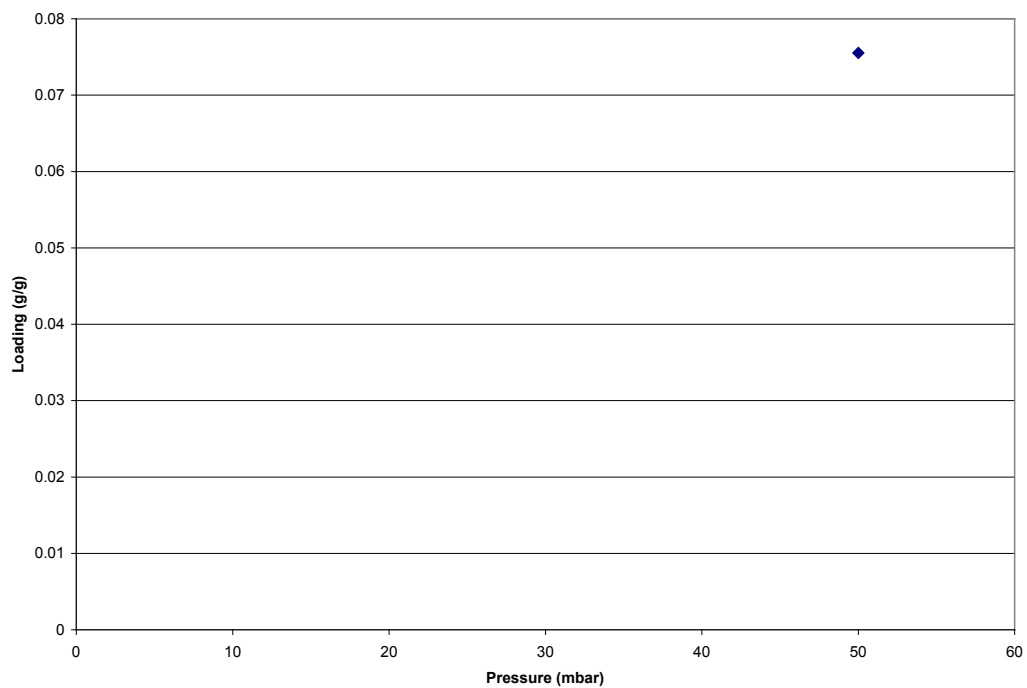


Figure 85 Equilibrium adsorption of n-butanethiol onto zeolite 4A

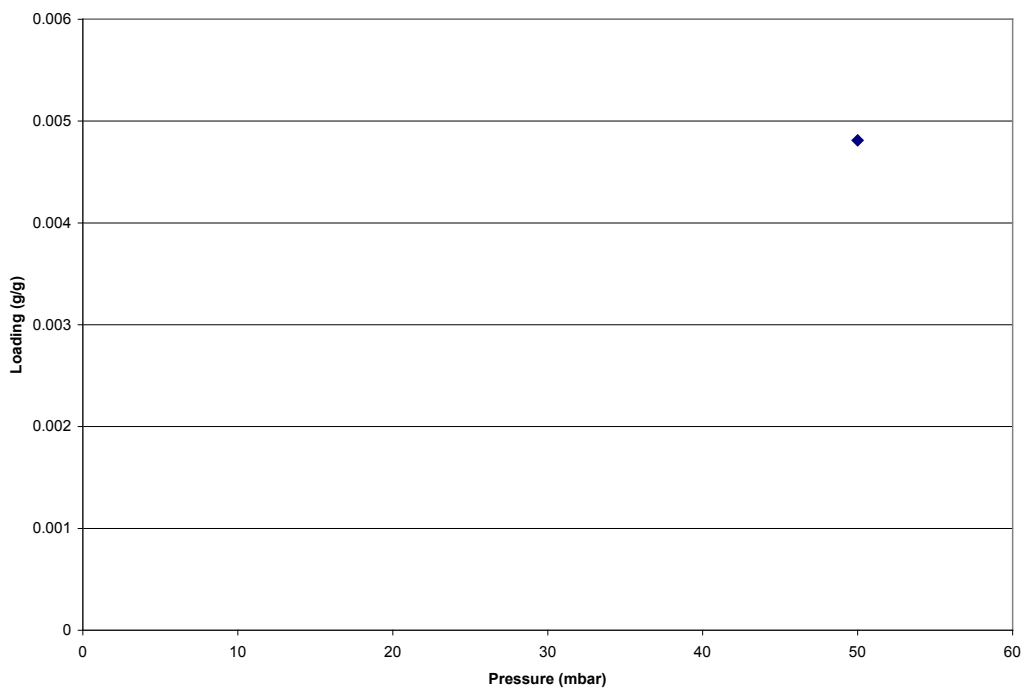


Figure 86 Equilibrium adsorption of n-butanethiol onto zeolite VPI-9

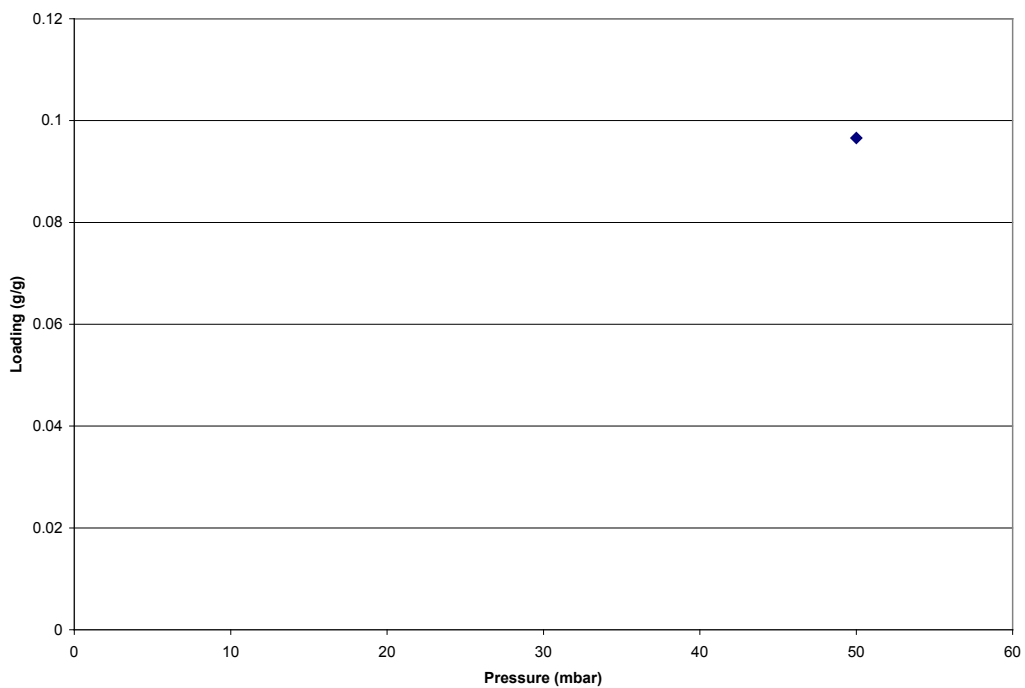


Figure 87 Equilibrium adsorption of n-butanethiol onto zeolite MCM-41